University of Cape Town

Department of Chemical Engineering

A Study of Configurational Alternatives of a Gas-To-Liquids Process based on Fischer-Tropsch Technology

Master's Dissertation by Ashcaan Tendo Khazali
Supervisor: Professor Klaus Möller
Co-supervisor: Professor Eric van Steen

October 2018

Acknowledgement

I would like to thank my supervisors, Professor Klaus Möller and Professor Eric van Steen, for their invaluable assistance and for the opportunity to work on this project, my family and friends for their unwavering support, the University of Cape Town for funding and the 4th year thesis students Veleshia Govender, Devin Marder, Mishka Slammang and Verona Moodley for their assistance in porting the models to Scilab.

"The steady drip of water wears away the stone"

Titus Lucretius Carus

PLAGIARISM DECLARATION

I know the meaning of plagiarism and declare that all the work in the document, save for that which is properly acknowledged, is my own. This thesis/dissertation has been submitted to the Turnitin module (or equivalent similarity and originality checking software) and I confirm that my supervisor has seen my report and any concerns revealed by such have been resolved with my supervisor.

Signed

Signed by candidate

Ashcaan Tendo Khazali

Contents

List of Figures

List of Tables

List of Abbreviations

ABCs	Asymptotic Behavior Correlations
AGR	Acid Gas Removal
ASF	Anderson-Schulz-Flory distribution
ASPEN	Advanced System for Process Engineering simulation software
ASU	Air Separation Unit
ATR	Auto-Thermal Reformer
BPD	Barrels Per Day
BTL	Biomass To Liquid
CCS	Carbon Capture and Storage
CCU	Carbon Capture and Usage
CFBR	Circulating Fluidised Bed Reactor
COCO	Cape Open to Cape Open
COD	Conversion of Olefins to Distillate
CPO	Catalytic Partial Oxidation
CTL	Coal To Liquid
EOS	Equation Of State
ERC	External Recycle
FBR	Fixed Bed Reactor
FT(S)	Fischer-Tropsch (Synthesis)
FTL	Fischer-Tropsch Liquids
GAMS	Generalized Algebraic Modeling System
GHG	Green House Gas
GTL	Gas To Liquids
HHV	Higher Heating Value
HTFT	Higher Temperature Fischer-Tropsch
HTS	High Temperature Shift
IG	Ideal Gas
IRC	Internal Recycle
LHV	Lower Heating Value
LNG	Liquid Natural Gas
LTFT	Low Temperature Fischer-Tropsch
LTS	Low Temperature Shift
MLR	Monolith Reactor
MR	Micro-Reactor
ODE	Ordinary Differential Equation
OT	Once-Through

PCD	Pure Component Database
PO	Partial Oxidation
PREOS	Peng Robinson Equation Of State
PSA	Pressure Swing Adsoprtion
RC	Recycle
RK	Redlich-Kwong equation of state
rWGS	reverse Water Gas Shift
SBCR	Slurry Bubble Column Reactor
SMDS	Shell Middle Distillate Synthesis
SMR	Steam Methane Reforming
SPD	Slurry Phase Distillate
SRK	Soave-Redlich-Kwong equation of state
WHC	Wax Hydrocracker

Abstract

Environmental concerns, associated legislation, limited oil reserves and fluctuating crude oil prices are some of the factors that highlight the need for alternative and environmentally friendly routes to fuels. One alternative is to use Fischer-Tropsch Synthesis (FTS) as the major technology in conversion of carbon containing feedstock to transportation fuels. The FTS product, called syncrude, can be refined to high quality transportation fuels in Coal, Gas or Biomass to liquid plants (denoted as CTL, GTL, and BTL, respectively, and collectively referred to as XTL). The economic viability of XTL processes is generally subject to the present price of crude oil and past studies show that traditional refining is generally more economically viable. However, XTL processes have been shown to be more economical and in some cases more environmentally friendly than conventional options when legislative measures aiming to curb traditional fossil fuel usage are considered. This study explores XTL process configurations that can improve plant carbon efficiency to diesel and liquids. The configuration encompasses technologies used, operating conditions, and layout of unit operations. A basic GTL process configuration consists of an Air Separation Unit (ASU), Auto-Thermal Reforming (ATR), syngas cleaning, full conversion Low Temperature Fischer-Tropsch (LTFT) and wax hydrocracking (WHC). These operations are modeled individually and combined to produce a plant model for study with the aim of determining the effects of configurational alternatives on the process efficiency to liquids and diesel. Furthermore, given that the ASU is a major contributor to costs the effect of using oxygen-enriched or pure air is investigated. Since production of heavy wax is prioritized, FTS represents the use of cobalt catalyst in LTFT operation. Where air is used, FTS is run to high conversion in once through mode to avoid the unfavorable economics of recycling nitrogen. After separation of the syncrude, the light fraction is reformed back to syngas in order to maximize carbon efficiency. The heavy wax is hydrocracked to maximize distillate range material. The light products from the WHC are combined with the lights from FTS and the heavy wax is recycled. Carbon efficiency, liquid selectivity and diesel yield are the means of assessing performance. The Scilab programming language is used along with physical properties estimated using the COCO/ChemSep pure component database as a starting point. Estimation of properties for alkanes and olefins of carbon chain length up to C_{200} has been carried out. The presence of 25% nitrogen in the ATR was found to beneficial to the $H_2 : CO$ ratio in the resulting syngas. Furthermore, in FTS the presence of 10-20% nitrogen produced the lowest reduction in carbon monoxide conversion and α_{FTS}. In general, the introduction of nitrogen resulted in decreased conversion of methane in the ATR and both decreased α_{FTS} and conversion in FTS. WHC performance was found to benefit from alpha being as high as possible; however, when the heavy wax recycle was inactive the optimal value was 0.92. The OOT80 configuration was found to have the highest liquid selectivity, while the efficiency to diesel was maximized for the OIRC40 configuration.

1. Introduction

1.1. Subject of Study

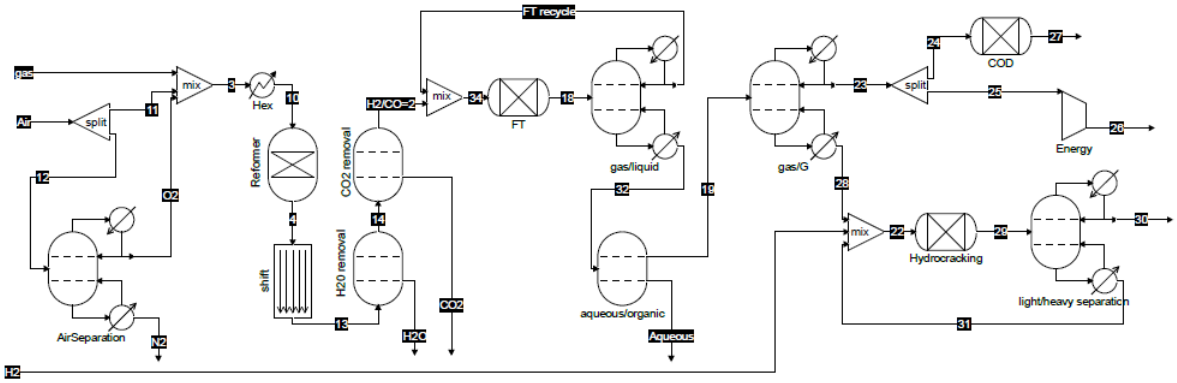

Figure 1.1: Process flow diagram for a gas to liquids process

The subject of this study is a GTL process based on Fischer-Tropsch Synthesis (FTS) which is tailored towards production of diesel. The example of this process is shown in Figure 1.1. It is fed by natural gas and air which is cryogenically separated to produce oxygen. The methane in the feedstock is converted to carbon monoxide through steam reforming after which the hydrogen to carbon monoxide ($H_2 : CO$) ratio is tuned in the water gas shift reactor. Syngas cleaning steps follow prior to FTS which produces an analog to crude oil called syncrude. Two successive separation steps follow where the the lighter gaseous hydrocarbons are recycled back to FTS and the heavy wax in the syncrude is routed to the Wax Hydrocracker (WHC). The heavy wax is hydrocracked to produce mainly diesel. The heavier products are recycled back to the WHC, while valuable lighter products are unutilized. The gaseous hydrocarbons leaving the second separation can be routed to the COD process or burned to produce energy. The most efficient configuration for this standard process has not been fully realized. Studies by (Tijmensen et al., 2002; Liu et al., 2010; Kreutz et al., 2008; Adams and Barton, 2011; Baliban et al., 2012; Bao et al., 2010; Choi et al., 1997; Floudas et al., 2012; Hao et al., 2008; Kaiser et al., 2013; Kim et al., 2009; de Klerk, 2008; Panahi et al., 2011; Prins et al., 2005; Sudiro and Bertucco, 2009; van Vliet et al., 2009) indicate that exploration of configurational alternatives has the potential to increase process efficiency and lower capital and operating costs. Any configuration must ensure that certain preexisting process constraints, such as product specifications and reactor process constraints are met. Alternatives can be weighed against each other using the operating cost and yield to desired product as measures. The process configurations result from combination and exclusion of process elements and stream routing. The standard configuration uses pure oxygen which is costly

to produce. There is a possibility of using air instead of cryogenically separated oxygen; however, adjustments must be made to downstream operations to compensate for the effects of nitrogen. Due to the large quantity of nitrogen in air, utility usage, equipment sizes and the volumetric flowrate of recycle streams are increased which has a major impact on cost. The Fischer-Tropsch product distribution for the Fischer-Tropsch process is defined by a probability parameter (α) which encompasses many kinetic phenomena, process parameters and technologies in FTS (Puskas and Hurlbut, 2003). The diesel yield is related to the alpha value through the WHC process which is influenced by the product distribution of the syncrude and therefore α. Promising options will be explored in this work in order to identify a strategy for optimizing the process to maximize the diesel yield and mitigate performance losses arising from the use of air.

1.2. Background

Compared with the traditional method of refining fuels from crude oil, FTS is more versatile. From fossil fuels and organic feedstocks, FTS can produce syncrude which may be further treated to produce synthetic transportation fuels (de Klerk, 2008). These synthetic fuels have favorable characteristics such as low sulphur content, high cetane number and good cold flow properties (Sie et al., 1991). Furthermore, switching to FTS transportation fuels does not require significant changes to the present fuels infrastructures because they are essentially equivalent to crude oil derived transportation fuels (Tijmensen et al., 2002; van Vliet et al., 2009; Kaiser et al., 2013; Knottenbelt, 2002; Ahlgren et al., 2008). There is a general consensus that global supplies of natural gas and coal will outlast crude oil; however, environmental concerns rather than availability of crude is the major driving factor in the shift away from oil (Kaiser et al., 2013). In certain configurations, FTS has the potential to reduce carbon dioxide emissions. The potential for reducing carbon emissions in moving from a fossil fuel based refining system to a FTS system has been demonstrated by van Vliet et al. (2009) who showed that when combined with CCS, BTL plants may actually have negative carbon emissions. GTL plants perform comparably to fossil fuel based options and in some cases have higher emissions, while CTL plants generally have higher emissions (van Vliet et al., 2009; Liu et al., 2010). Therefore FTS represents an attractive alternative for production of fuels in comparison to crude oil derived fuels.

The process is not a recent development but has not seen widespread commercial implementation due to oil prices being low enough to make refining of crude oil more economical (Sie et al., 1991). However, in certain scenarios traditional methods may be brought on a economical level with FTS. In the case of remote gas reserves, for example, where the construction of Liquefied Natural Gas (LNG) plant, pipelines and infrastructure may be impractical or more expensive compared with producing and transporting liquid fuels through FTS (Sie et al., 1991) or where restrictions on emissions may restrict flaring of gas (Prins et al., 2005). In some locations and political climates the additional overhead costs of importing crude-derived fuels can make FTS more economical.

FTS development began at the Kaiser-Wilhem-Institut für Kohlenforschung in the 1920s by Franz Fischer and Hans Tropsch (Sie et al., 1991). The first commercial plant was operated in 1935 by the Ruhrchemie AG company in Germany using a fixed bed reactor and Low Temperature Fischer Tropsch Synthesis (LTFT) (Steynberg and Dry, 2004). By the end of the Second World War, fourteen plants using LTFT in Fixed Bed Reactors (FBRs) were active in Germany (Basha et al., 2015). Since then commercial and research projects have produced the High Temperature Fischer-Tropsch (HTFT) process, multiplied catalyst options, developed new reactor options and broadened the understanding of the process. FTS facilities have been operated in the United States (Sie et al., 1991; Basha et al., 2015), France, Manchuria and Japan Steynberg and Dry (2004) but as of today these are no longer in operation. At present, large scale commercial operations exist in South Africa, Malaysia and Qatar. In South Africa, the low price of coal and its global positioning has made FTS a viable alternative to the traditional methods of producing fuels. The first plant in South Africa was opened in 1955 at Sasolburg by Sasol using ARGE Fixed Bed Reactors (FBRs) and Kellogg's Circulating Fluidized Bed Reactors (CFBR) with coal as feedstock and gasoline as the main product Steynberg and Dry (2004); Sie et al. (1991); Bub et al. (1980).

Today Sasol operates via both GTL and CTL routes using HTFT and LTFT with cobalt and iron catalysts (Basha et al., 2015). The Sasol Oryx GTL in Qatar operates with a capacity of 34000 bbl/day of liquid fuels with LTFT carried out in two parallel trains using Cobalt catalyst in Slurry Bubble Column (SBCR) reactors (17000 bbl/day) (Panahi et al., 2011). Another plant (Pearl GTL) operated by Shell with a capacity of 260000 bbl/day (140000 bbl/day GTL products) using 24 parallel FBRs (6000 bbl/day) has begun operations close to the Oryx GTL plant (Panahi et al., 2011). In South Africa, PetroSA operate a plant using iron catalysed HTFT in CFBRs (Basha et al., 2015) and have previously operated a pilot plant using cobalt catalysed LTFT in SBCRs. In Bintulu, Malaysia Shell operate a plant using LTFT in FBRs (Basha et al., 2015). The plant is based on the Shell Middle Distillate Synthesis where high quality distillates are produced through FTS and hydrocarbon cracking. The synergy between FTS and hydrocracking form the basis for the process (Sie et al., 1991).

FTS is essentially a polymerization reaction where carbon monomer units combine to form various compounds. The Fischer-Tropsch product is characterized by the carbon number of the product compounds and the alpha (α_{FTS}) value. The carbon number is the number of carbons present in the compound in question; for example, ethane and ethene both have a carbon number of 2 (C2). α_{FTS} is the carbon number independent probability of of chain growth between monomer units and it indicates the ratio of heavy products to light products; therefore, a high α_{FTS} value would indicate that the bulk of the material exists as high carbon number compounds. In the ideal case the carbon numbers present in the FTS product follow an Anderson-Schluz-Flory distribution where the logarithm of the relative molar quantity of polymer of each chain length (or carbon number) decreases linearly with

respect to carbon number. Given that FTS cannot be used to target a narrow range of carbon numbers, such as the range representing diesel for example, additional processing steps are required to maximize diesel production. Therefore, the broad significance of α_{FTS} is that a high value will lead to greater wax production which, through hydrocracking of heavy wax, leads to potentially more diesel and liquid fuel production.

1.3. Objectives

The objectives for this project are the following.

- Review of literature options for the process configurations and operating conditions
- Building a thermodynamic database up to C_{200}
- Development of a flexible XTL flowsheet using Scilab
- Analysis of the baseline operation
- Study of the effect of nitrogen on the system
- Study of the alpha value on the performance of the FTS-WHC reaction system
- Study of process configurations by case studies

1.4. Scope and Limitations

The reactor models are not sufficiently detailed to take into account the limitations imposed by catalyst deactivation or the effects of fluid dynamics and dimensional effects. No reactor sizings or costings are carried out. The simulation environment is the open source programming language, Scilab. Details of the composition and properties of intermediate streams from commercial processes are generally not divulged (de Klerk, 2008). In the absence of this information, the data required for modeling, verification or comparative purposes are sourced from literature, where available. The physical properties have been developed using the ChemSep Pure Component Database (PCD) which only includes paraffins up to C_{29} and olefins up to C_9 thus property estimation has been carried out for carbon numbers up to C_{200}. The properties are only developed for n-paraffins and $\alpha - olefins$ which are the main products of FTS. The FTS reactor model does not include the temperature dependence of the kinetic constants; therefore, analysis of the FTS reactor does not include a temperature sensitivity. The Conversion of Olefins to Distillate (COD) reactor modeling is not included in this project. Futhermore, this project is not concerned with the gasification operations or modeling of the ASU. In terms of vapor liquid equilibrium the Peng Robinson Equation of State (PREOS) is used with modified alpha functions. Where PREOS is used, the Binary Interaction Parameters are unavailable and

are therefore not used in the equations of state. This research has been carried out on various modestly powerful dual core computers; therefore, certain measures have been taken to decrease solution time at the expense of high precision and accuracy.

2. Literature Review

2.1. Upstream of Fischer-Tropsch

The section of the plant upstream of FTS can be referred to as the syngas production section. The purpose of this section is to produce syngas from carbon containing feedstocks. The syngas is a combination of hydrogen and carbon monoxide at the correct ratio and free of the impurities that would adversely affect downstream operations.

Three types of feedstock have been investigated by authors in this area of research, coal by Sudiro and Bertucco (2009), van Vliet et al. (2009), Liu et al. (2010) natural gas by Kim et al. (2009), Sudiro and Bertucco (2009), van Vliet et al. (2009), Liu et al. (2010) and the broad category of biomass feedstocks by Tijmensen et al. (2002), van Vliet et al. (2009), Liu et al. (2010). Facilities using coal, natural gas, and biomass for feedstock are referred to as Coal To Liquids (CTL), Gas To Liquids (GTL) and Biomass to Liquids (BTL), respectively, and generally they are referred to as XTL processes.

Biomass and coal feedstocks produce syngas with sub-optimal hydrogen to carbon monoxide ratios due to the low ratio of hydrogen to carbon atoms in their constituent compounds. This is in comparison to natural gas which primarily contains methane (4:1 ratio of hydrogen to carbon). The solid feedstocks require gasification in preparation for reforming while natural gas does not. In gasification the carbon in the feedstocks is partially converted to carbon monoxide, carbon dioxide and methane through some combination of pyrolysis, oxidation and thermal decomposition. The oxygen required for gasification and reforming may either be supplied by the energy intensive cryogenic ASU (Liu et al., 2010), which produces pure oxygen, or by air which is the more economical choice but remains untested commercially. If air is used directly, a large quantity of nitrogen is included in the syngas which, if not removed, would affect the downstream processes adversely.

The stream from gasification or the feedstock natural gas stream (GTL) must be processed in a reformer in order to adjust the quantity of hydrogen relative to carbon monoxide to the ratio suitable for FTS. In order to achieve the correct $H_2 : CO$ ratio, a separate WGS step may also be required. The WGS reactor may be run at low temperature (Low Temperature Shift or LTS) or high temperature (High Temperature Shift or HTS). Syngas produced from natural gas feedstock can contain an excess of hydrogen which can potentially negate the need for WGS altogether; however, certain process configurations, such as with carbon dioxide recycle, may require the inclusion of WGS (Basha et al., 2015). Coal and biomass feedstocks may require supplementary hydrogen in reforming in order to achieve the correct $H_2 : CO$ ratio. The FTS reactors approach a hydrogen to carbon monoxide usage ratio of 2:1 as the selectivity for higher carbon number compounds is increased (de Klerk, 2008); this is due to the 2:1 ratio of hydrogen to carbon in long chain FTS products.

Following gasification and reforming, a number of syngas cleaning steps may be required. Both iron and cobalt based FTS catalysts are susceptible to deactivation from sulphur and coke (Sudiro and Bertucco, 2009); therefore, desulphurization of the syngas is required for any sulphur containing feedstocks (gasified coal for example). Sulphur can be removed using the Claus process (Baliban et al., 2012). Acid gas removal can be achieved through amine based removal (Tijmensen et al., 2002; Baliban et al., 2012), combined Acid Gas Removal (AGR), Pressure Swing Absorption (PSA), Vacuum-Swing Absorption (VSA) or membrane separation (Baliban et al., 2012). AGR processes such as the methanol based Rectisol process may be used to remove carbon dioxide, sulphur dioxide, hydrogen sulphide, hydrogen and ammonia (Sudiro and Bertucco, 2009; Baliban et al., 2012; Kreutz et al., 2008). Water in syngas also has the effect of lowering the rate of FTS when present on the surface of the catalyst (van Steen and Schulz, 1999) which creates the need for water removal before FTS.

2.2. Methane Reforming

Several options exist for the reforming process, namely the use of Steam Methane Reforming (SMR) and Partial Oxidation (PO) or the combination of these (ATR) (Basha et al., 2015; Rowshanzamir et al., 2009). The preferred method in industry for plants fed by natural gas is the ATR (van Vliet et al., 2009) due to the fact that it is the most economical (Panahi et al., 2011).

Auto thermal reforming can be carried out in a two section catalytic bed consisting of Catalytic Partial Oxidation (CPO) prior to SMR or a two stage reactor (non catalytic partial oxidation PO and SMR) (Rowshanzamir et al., 2009). In the oxidation section the fuel is partiality oxidized (catalytically or non-catalytically (CPO and PO, respectively). Syngas with the targeted $H_2 : CO$ ratio may be produced in SMR, depending on the hydrogen to carbon ratio in the feed. If the ratio is sufficient to achieve the desired $H_2 : CO$ ratio the subsequent WGS step is not required. Carbon dioxide is a byproduct of the partial oxidation reaction and its production is accompanied by a large quantity of heat which is essential to SMR. The quantity of carbon dioxide in the ATR is reduced through CO_2 reforming.

At the conditions seen in GTL, SMR is endothermic and requires high temperatures ($\approx 1000^oC$) in order to achieve a high syngas yield (Rowshanzamir et al., 2009); therefore, it is usually necessary to preheat the feed before partial oxidation. When CPO is employed in the ATR lower feed temperatures may be used and the formation of soot and hot spots in the reactor are less likely (Rowshanzamir et al., 2009). As stated before the ATR is the most economical method; this is due to the fact that most of the necessary reaction heat is provided through oxidation of the feedstock in the PO/CPO section.

SMR is often carried out over nickel based heterogeneous catalysts (Biesheuvel and Kramer, 2003), while PO/CPO is usually carried out over nickel catalysts. Two mechanisms have been identified by which partial oxidation proceeds; total combustion of

methane followed by steam and carbon dioxide reforming (indirect route); and catalytic methane pyrolysis followed by hydrogen desorption and carbon oxidation (direct route) (Jin et al., 2000). The first mechanism has been shown to be favored over nickel catalysts (Dissanayake et al., 1991) and is used in studies by De Groote and Froment (1996); Jin et al. (2000) and Donazzi et al. (2008).

Biesheuvel and Kramer (2003) have developed an empirical correlation for the methane conversion or fuel utilization ratio (UT) in CPO. Figure 2.1 shows the contour map of the methane conversion as determined by applying the correlation to a 2D mesh built from a range of $PO\alpha$ (oxygen to feed carbon ratio) and $PO\gamma$ (steam to feed carbon ratio) values. There is a local maximum at low λ; however, the global maximum is at $PO\alpha = 0.8076834$ and $PO\gamma = 0.0000032$. Therefore the maximum methane conversion is expected for when the steam fraction of the feed is low and the $PO\alpha$ value is around 0.8. Considering the reaction on a global overall basis will result in poor prediction since the equation constants must vary significantly to account for the complexity of the reaction mechanism which often includes numerous radical species (Karim et al., 1993; Berger and Marin, 1999); therefore, reaction kinetics are recommended to model PO.

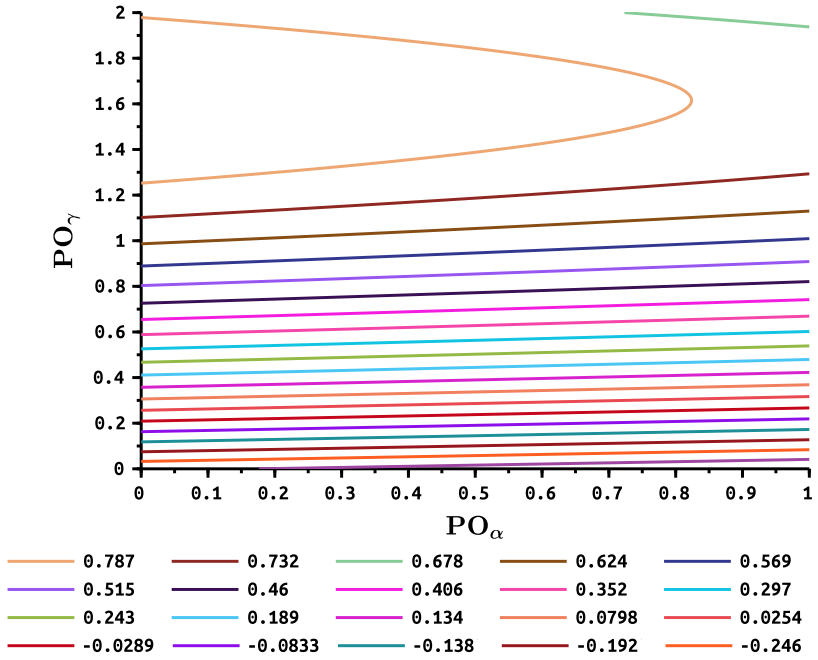

Figure 2.1: Methane conversion in reformer as a function of oxygen-to-methane and steam-to-methane rations, as determined from a correlation by Biesheuvel and Kramer (2003)

2.3. Fischer-Tropsch Synthesis

2.3.1. Hydrogen to Carbon Monoxide Ratio

The $H_2 : CO$ ratio in the syngas is an important process parameter which directly affects the distribution of FTS products amongst the different carbon numbers (product distribution). The required ratio depends upon the desired FTS product distribution, and the

catalyst in use. Over iron catalysts, WGS activity results in low H_2 usage (Atwood and Bennett, 1979); therefore, the $H_2 : CO$ ratio entering FTS may be lower than for cobalt catalysts because hydrogen will be produced within the FTS reactor. Low ratios result in greater paraffin wax production due to the role hydrogen plays in the reaction mechanism. Ratios lower than 1:1 are not recommended due to an increased potential for plugging of the reactor/catalyst pores by wax and carbon formation (Atwood and Bennett, 1979).

2.3.2. High and Low Temperature Fischer-Tropsch Synthesis

Two operating regimes have been distinguished for FTS, one in the range $290^oC \leq T \leq 360^oC$ (HTFT) and another in the range $180^oC \leq T \leq 260^oC$ (Basha et al., 2015; Tijmensen et al., 2002) (LTFT). HTFT produces more methane and short chain hydrocarbons than wax (Atwood and Bennett, 1979; Basha et al., 2015). In FBRs operating at HTFT conditions the accumulation of wax in the catalyst pores due to capillary condensation Wang et al. (2003); de Klerk (2008); Bub et al. (1980) may lead to defluidisation so the reactor is operated such that the chain growth probability factor (α_{FTS}) is limited to ≈ 0.7, whereas the LTFT α_{FTS} value may exceed 0.9 (de Klerk, 2008) which corresponds to greater quantities of longer carbon chain waxes.

2.3.3. Catalysts

At present cobalt and iron catalysts are the only catalysts used in large scale commercial projects (Basha et al., 2015). Ruthenium shows higher FTS activity than both iron and cobalt; however, cobalt and iron catalysts are more economical partially due to the relative scarcity of Ruthenium. Nevertheless, combined catalysts are under investigation. Cobalt catalysts have the next highest activity and iron has the lowest of the three (Basha et al., 2015). The iron catalysts have some WGS activity (de Klerk, 2008) which eliminates the need for, or reduces the load on, the WGS operation (Basha et al., 2015). Cobalt catalysts do not show any appreciable WGS activity under FTS conditions (Basha et al., 2015); therefore, control of the $H_2 : CO$ ratio in the syngas is important. Conventional iron catalysts are cheaper than cobalt catalysts (Basha et al., 2015; Bao et al., 2010). However, cobalt catalysts have higher wax yields (Atwood and Bennett, 1979; Bao et al., 2010) and longer lifetimes (Bao et al., 2010). Additionally, cobalt catalysts may be preferred due to the need for catalyst regeneration when iron catalysts are used in SBCR reactors (Basha et al., 2015).

2.3.4. Reaction Mechanism

The reactants in syngas diffuse from the bulk phase to the catalyst surface where they are adsorbed before reaction occurs. FTS produces a range of products through primary and secondary reactions. The primary reactions occur between the reactants on the surface of the catalyst, while the secondary reactions occur between primary products and other

species in the reaction mixture or readsorbed products and surface species. The primary FTS products are: n-paraffins, α-olefins, primary alcohols, carboxylic acids and aldehydes. Ketones, esters and secondary alcohols are secondary products and are formed in much smaller quantities (de Klerk, 2008).

The general formulae for FTS producing n-paraffins and α-olefins are shown in Equations 2.1 and 2.2, respectively.

$$(2n+1)H_2 + nCO \rightarrow C_nH_{2n+2} + nH_2O \tag{2.1}$$

$$(2n)H_2 + nCO \rightarrow C_nH_{2n} + nH_2O \tag{2.2}$$

The exact mechanism is under dispute but the Carbide, Enol/Oxygenate and CO-insertion mechanisms feature prominently throughout literature (Basha et al., 2015). These mechanisms cannot account for the entire product spectrum and must be used in combination for accurate representation (Basha et al., 2015). Figure 2.2 illustrates the carbide mechanisms of formation of paraffins and α-olefins. The mechanism can be divided into the following steps:

1. Adsorption of CO and H_2 species onto the catalyst surface
2. Chain initiation through the formation of the methylene monomer $-CH_2-$
3. Chain growth or polymerization by addition of methylene monomer units
4. Chain termination
5. Product desorption
6. Additional steps such as readsorption and continued reaction may also take place (van der Laan, 1999).

The role of hydrogen surface species in the reaction mechanism includes being responsible for triggering the termination of chain growth (Mthombeni, 2009). There is a direct relationship between the hydrogen surface species concentration and the $H_2 : CO$ ratio; a higher ratio will lead to greater production of long chain hydrocarbons.

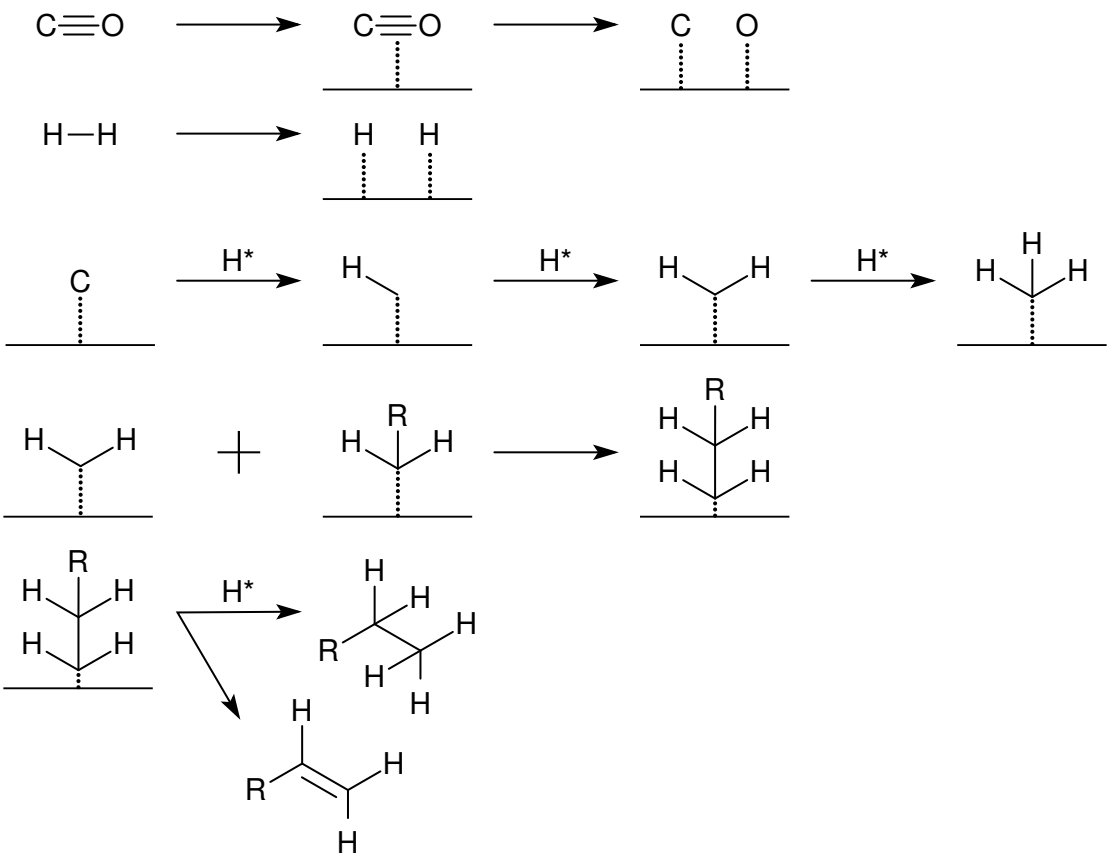

Figure 2.2: Carbide mechanism for the formation of paraffins and α-olefins, adapted from Mthombeni (2009)

2.3.5. Product Distribution

The formation of Fischer-Tropsch products could be regarded as a polymerization reaction with $-CH_2-$ or methylene monomer being the monomer unit. Equation 2.3 gives the probability of finding a polymer of length x monomer units (or x-mer) in the product. Equation 2.3 was published by R.B. Anderson, H. Schulz and P.J. Flory independently though it is given in the form derived by Flory (1936).

$$\Pi_x = x\alpha^{x-1}(1-\alpha)^2 \tag{2.3}$$

In the derivation of Equation 2.3 by Flory (1936), an assumption of a constant reactivity across all functional groups is made, the justification being that when the polymerization products are mostly long chain molecules the long carbon chains will attenuate any inter-functional group effects that would affect the rate of polymerization (Flory, 1936). This translates to a fixed probability of reaction (or chain growth) α between monomer units regardless of chain length. The probability of chain growth is related to kinetics in that alpha is the ratio of the propagation rate relative to the rate at which all reactions including termination occur. Monomer units are imagined to be laid out end to end to end with each gap between them representing a potential covalent bond between monomers as shown in Figure 2.3. Henceforth, the covalent bond between $-CH_2-$ monomers and $-CH_2$ or

$-CH_3$ endpoints shall be referred to as a linkage. There is a fixed probability of linkage at any of the potential bond locations. For any segment C_S to be part of a polymer chain there must be linkages on one or both sides of C_S (L3 or L4, L3 and L4). In addition, there may be linkages extending further up or down from the chain from the position of C_S. Taking C_3 as an example, (three monomers linked together $\Longleftrightarrow$ propene/propane), there are three configurations that will produce a C_3 polymer containing C_S, these are the set of linkages; L2 and L3; L3 and L4; L4 and L5. An example of an invalid linkage set is L1 and L2 because it excludes segment C_S; by the same consideration L5 and L6 are not valid. Therefore, 3 possible linkage sets will produce a C_3 polymer containing C_S and each set will always contain only 2 linkages. By considering chains of different lengths, a general set of rules become apparent. For any carbon chain containing x carbons the number of linkage configurations that will result in any segment C_S being part of a chain of length x will be equal to x. Another rule is that any carbon chain of length x will contain $x-1$ linkages and no linkages at the two endpoints. Regarding the possible states of a potential linkage, there are only two possibilities: linkage or no linkage; the corresponding probabilities are α and $1-\alpha$, respectively. Given the fixed probability of linkage at any potential linkage site α (and correspondingly, no linkage), the probability of existence of a polymer chain containing x carbons will be the product of the number of configurations that such a polymer chain may exist in x, the probability of the $x-1$ linkages required to form such a chain α^{x-1} and the probability that no linkage occurs at either end of the chain $(1-\alpha)^2$ resulting in Equation 2.3.

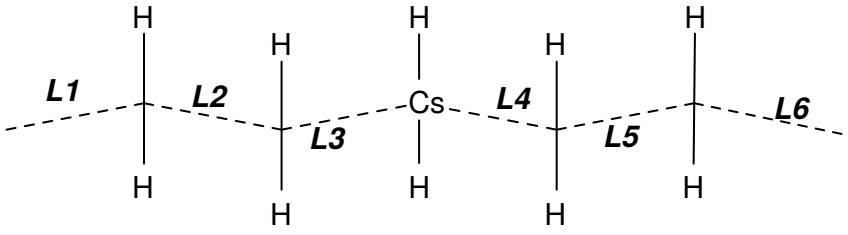

Figure 2.3: Linkage schematic showing potential methylene monomer units ($-CH_2-$) laid end to end, where ***LN*** are potential linkage points where covalent bonds (between carbon atoms) may be formed

Π_x may be calculated from the real product distribution by dividing the number of monomer units belonging to a carbon chain of length x by the total number of monomer units in the product. The weight of x-mer product may be determined by computing the product of the number of polymer units (in moles) by number of monomer units and the molecular weight of a single unit. The total weight of atomic species will be conserved between the reactants and products and if no elimination occurs then the total weight of monomer units in the polymer product will equal to the total weight of potential monomer units in the reactant. Thus, provided these assumptions hold, Π_x is equivalent to the mass fraction.

An ideal product distribution given by Equation 2.3 is illustrated in Figure 2.4. It is a well established fact that real product distributions deviate from the ideal ones (Puskas and Hurlbut, 2003; Dictor and Bell, 1983). The y axis in Figure 2.4 is the natural logarithm of

the weight fraction of carbon chains of length x (W_x) in the product divided by the number of carbons in the chain (x). In reality the product distribution remains close to ideal in the C_4 to C_{12} region (Puskas and Hurlbut, 2003) with negative deviation (i.e. less product than is predicted by the ideal distribution) for carbon numbers lower than C_{10} (Dictor and Bell, 1983) and positive deviation for the higher carbon numbers. In order to adequately model real product distributions, it may be necessary to use two alpha values to form two successive ASF distributions; as may be the case with the modeling the products from slurry phase reactors (van Vliet et al., 2009; Fernandes, 2006).

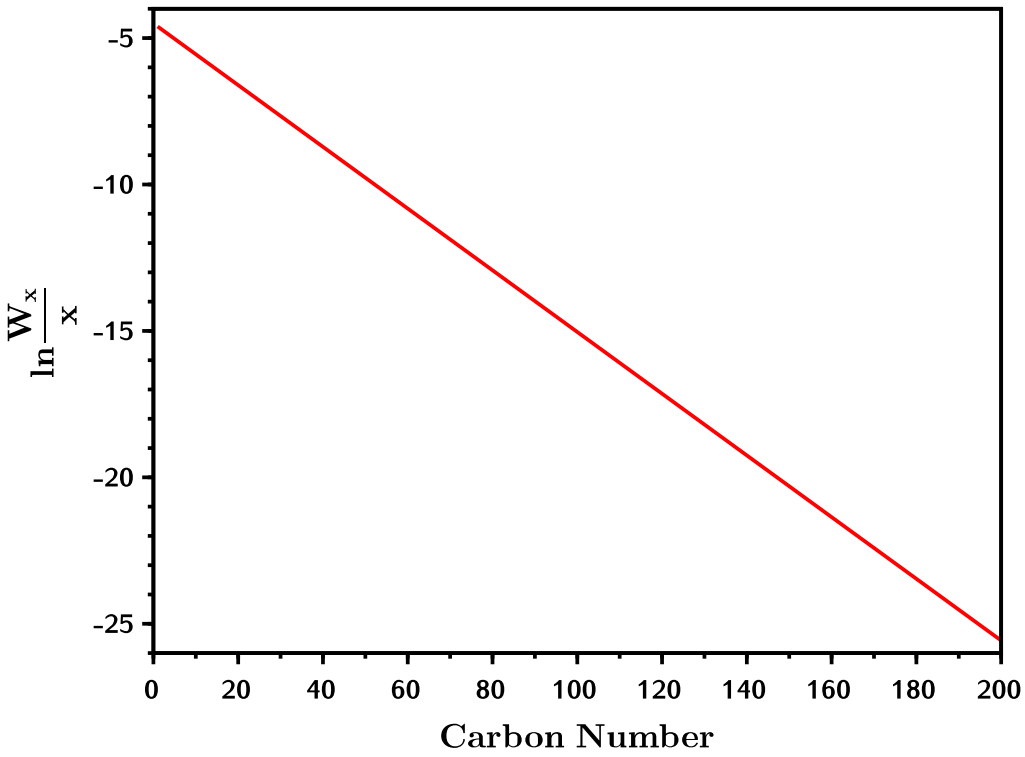

Figure 2.4: An ideal ASF distribution

Table 2.1 shows process parameters for two commercial FTS based XTL operations, the Shell Middle Distillate Sythesis (SMDS) and the Slurry Phase Distillate process by Sasol. As shown in Table 2.1, commercial processes are targeting high α values and correspondingly greater wax production. The production of heavy wax is beneficial if products such as middle distillates or diesel are targeted. This is due to the fact that FTS cannot target a narrow range of carbon numbers in syncrude product such as diesel (e.g. C_{10} to C_{20}). However, production of heavy wax along with additional processing steps achieve selective production of hydrocarbons belonging to a narrow carbon number range.

Table 2.1: Fischer-Tropsch Synthesis process information for SMDS and the Slurry Phase Distillate (SPD) process, adapted from (van Vliet et al., 2009; Eilers et al., 1990)

FT process	SMDS	SPD
α (Inferred)	0.93 $C14 - C40$	0.92
$H_2 : CO$ ratio	2.15	2.10
Operating temperature $[^oC]$	230	230
Operating pressure $[bar]$	40.0	25.2
Syngas conversion [%]	92	92
Diesel selectivity $[wt\%]$	85	70

2.3.6. Reactor Type

Three categories of reactor have been identified for LTFT, slurry reactors (such as the SBCR), Fixed Bed Reactors (FBR and Fluidized Bed Reactors); and the more recently developed Micro- and Monolith Reactors (MR & MLR) (Basha et al., 2015) which have not yet been implemented commercially.

The Fischer-Tropsch process is highly exothermic; therefore, cooling tubes are needed in order to keep the reactor isothermal. Since FTS is highly exothermic, heat transfer and reactor temperature are essential considerations. Excessively high temperature in FBRs will result in carbon formation and subsequently plugging at hot spots in the reactor (Basha et al., 2015). Additionally, temperature differentials greater than 1^oC between the bulk and catalyst phases may lead to catalyst overheating (Atwood and Bennett, 1979). Higher temperatures lead to higher methane selectivities and decreased C_{5+} selectivities and therefore decreased wax production (Wang et al., 2003). Increasing the reactor diameter will increase the heat transfer load per unit area resulting in a higher temperature at the hotspot (Atwood and Bennett, 1979; Wang et al., 2003) and therefore reduced C_{5+} selectivity. Higher reactor pressure is accompanied by higher temperatures in the FBR (Wang et al., 2003) and enhanced adsorption due to the increased driving force for mass transfer to the catalyst surface. In recycle configurations, increasing the recycle ratio to the FBR produces a flatter axial temperature profile due to the presence of non-reabsorbing, and therefore, chemically inert products (Wang et al., 2003). The lack of a pronounced hotspot is beneficial to the C_{5+} selectivity since the reactants are not exposed to high temperatures that favor methane production. Such hot spots will be absent in slurry reactors due to the bulk phase being mixed.

FBRs require larger catalyst particle diameters in comparison to slurry reactors and particle diameters on the order of a $200\,\mu m$ to $5000\,\mu m$ are typical for FBRs (Basha et al., 2015; Wang et al., 2003). Smaller catalyst particles ($\leq$2 mm) produce better heat transfer characteristics allowing for reduced heat transfer areas (Atwood and Bennett, 1979); however, the pressure drop across the bed will increase as the particle diameter is decreased. As has been stated in Section 2.3.2, FBRs are prone to defluidisation at high α values due to plugging of the reactor by wax and excessive pressure drops; therefore, slurry reactors are favored for heavy wax production.

Although the presence of significant quantities of inerts acting as a large heat sink may be beneficial to reactor heat transfer characteristics in the FBR (Jess et al., 1999), the effect on conversion is detrimental, while in the SBCR the effect on conversion is less pronounced (Tijmensen et al., 2002). The SBCR has been found to have the best performance with respect to catalyst and reactor specific productivity (Guettel and Turek, 2009); furthermore, heat transfer performance is better (Basha et al., 2015). The capital cost of SBCRs is 20% to 40% lower than for FBRs (Basha et al., 2015). Where low down time is prioritized, the SBCR is most suitable, however, unlike for the FBR, scale-up of lab and pilot plant data presents a challenge (Tijmensen et al., 2002). Given all this information it seems clear that slurry reactors offer the greatest advantages for maximising heavy wax and subsequently diesel production.

2.3.7. Slurry Reactors

In the SBCR liquid and catalyst slurry are fed at low velocities into the bottom of the reactor and continuously withdrawn at the top. These are the defining features of continuous operation. In semi-batch mode, no liquid is withdrawn from the reactor. Synthesis gas is fed from the bottom and bubbles up through the reactor exchanging mass with the liquid phase.

In addition to what has been stated in the previous section, the SBCR has the following advantages over the FBR: nearly isothermal operation; ability to handle smaller catalyst particles (typically between 1 and 200 μm (Basha et al., 2015)); good mixing characteristics; low pressure drop; low construction and operation costs and good temperature control.

Few studies have covered slurry reactors at industrial conditions (Basha et al., 2015). Table 2.2 shows the parameters investigated by modeling studies and an experimental study dealing with industrial conditions.

Table 2.2: Summary of slurry reactor parameters for studies dealing with industrial conditions

Author	**Fernandes (2006)**	**Wang et al. (2008)**	**van der Laan et al. (1999)**	**Woo et al. (2010)**
Catalyst	Fe	Fe	Fe	Co & Ru
Temperature $[^oC]$	270	250 –> 300	250	210 –> 250
Pressure $[bar]$	10 –> 30	15 –> 35	30	10 –> 30
$H_2 : CO[]$	0.5 –> 2.0	0.53 –> 0.65		
Length of reactor $[m]$	30	30	24	1.5
Diameter of reactor $[m]$	7	5	8	0.05
Superficial gas velocity $[ms^{-1}]$	0.25 –> 0.45	0.1 –> 0.4	0.15 –> 0.4	0.017 –> 0.136
Superficial slurry velocity $[ms^{-1}]$	0.01			
Solids holdup []	0.1 –> 0.25			
Catalyst apparent density kgm^{-3}	647		{varying voidage}*1957	
Wax Type				Squalane and parrafin wax

All studies assume that: the reactor is isothermal, is in steady-state, the location of the gas-liquid mass transfer limitation is in the liquid phase, that large bubbles are in plug flow, that liquid is perfectly mixed and that the hydrocarbon products in the gas and liquid phases are in equilibrium at the reactor outlet. In their study, van der Laan et al. (1999) also assume that catalyst distribution is uniform due to upflow of the slurry phase and that the effectiveness factor of catalyst particles is equal to unity. Wang et al. (2008) assumed the system is isobaric and we can infer that Fernandes (2006) and van der Laan et al. (1999) have made the same assumption from their respective methods of calculating the partial pressures. Both Fernandes (2006) and van der Laan et al. (1999) state that they assume that the superficial slurry velocity is constant. The mass transfer resistance between the liquid and catalyst can be neglected due to the large interfacial area (Basha et al., 2015); therefore, there will be no concentration gradients in the catalyst particles. The liquid can be assumed to be perfectly mixed if the reactor is operating in the churn turbulent regime; therefore, the mass transfer resistance in the bulk liquid can also be neglected (Basha et al., 2015). The bulk gas (in the bubbles) to liquid film resistance can also be neglected due to the low vapor pressure of FTS products (Basha et al., 2015).

In general, as the pressure increases the carbon monoxide conversion and heavy hydrocarbon yield and selectivity increases as evidenced by the results of Fernandes (2006) and Wang et al. (2008). Physically speaking, higher pressure will produce more small bubbles and will result in greater gas density leading to greater gas holdup in the reactor (Basha et al., 2015). Additionally, higher pressure will produce greater concentration gradients between the bulk gas phase and the adsorbed phase on the catalyst surface. This will be reflected in the VLE separation factors and reaction kinetics through the dependence on partial pressure, activity or some analogue. At low superficial gas velocities of 0.2, the results of Wang et al. (2008) show a maximum in the gasoline yield at 20 bar. In the diesel and waxes selectivity curves of Fernandes (2006), we see greater yield of diesel and waxes at higher pressure. The results of Fernandes (2006) indicate that the yield of gasoline increases almost linearly with increasing pressure but the selectivity will be low since the increase of the diesel and waxes yield is far more rapid.

As temperature is increased, the selectivity towards heavy hydrocarbons decreases, while that of light hydrocarbons and methane increases as evidenced by the results of both Wang et al. (2008) and Woo et al. (2010). Increased rate of reaction on the catalyst surface is expected which would likely tend to increased chain termination. Additionally, increased mass transfer in the catalyst particles will prevent the hydrocarbons from staying on the catalyst surface long enough to attain high molecular weight. Woo et al. (2010) report high selectivity to heavy hydrocarbons at low temperature. There is a maximum in the yield profile for C_2 to C_4 hydrocarbons and, correspondingly, a maximum is also expected for diesel and gasoline.

The results of Fernandes (2006) indicate that lower $H_2 : CO$ ratios will result in higher yields of diesel and gasoline. Wang et al. (2008) also find higher selectivity towards gasoline rather than diesel. The yield of heavy hydrocarbons is highest at low $H_2 : CO$

ratios. This may be attributed to the role hydrogen plays in the termination of chain growth in the Fischer-Tropsch mechanism. The results of van der Laan et al. (1999) indicate low conversion at high superficial gas velocity. This is intuitive because higher superficial gas velocity will result in lower residence time and therefore lower conversion.

2.4. Hydrocracking and Product Upgrading

The design of the product upgrade section is informed by the products of choice. When diesel production is prioritized, the products from FTS are mainly high carbon number n-paraffin waxes with a small amount of lighter compounds. This is due to the fact that highly selective production of diesel from FTS is not possible with present commercial technology; therefore, the production of wax is favored which is later cracked back into the diesel range through hydrocracking (Le Grange, 2009). Figure 2.5 shows the variation in the split across the various syncrude fractions with changing FTS α; diesel lies within the distillate range and the fraction of products other than diesel is always sizable. However, at high FTS α values the majority of the syncrude will take the form of wax. Therefore, if selective wax product is prioritized an alternative process such as hydrocracking can be employed to process most of the FTS product and to target the narrow product range which diesel occupies. Waxes would be the main elements of the organic phase but as can be seen from Equations 2.1 and 2.2 water is also a major component produced creating an aqueous phase in the product which must be removed before further processing. The waxes are routed to the WHC where the carbon chains are cracked by addition of hydrogen resulting in lighter and less aromatic compounds (de Klerk, 2008). Diesel produced by through FTS and hydrocracking has favorable characteristics such as low sulphur content and high cetane number (Prins et al., 2005). Another function of hydrocracking is to remove heteroatoms by hydrotreating (de Klerk, 2008). A more detailed upgrade section could follow a Bechtel design with a wax hydrocracker; distillate, kerosene and naphtha hydrotreaters; naptha reformer; C_4 isomerizer; C_5/C_6 isomerizer; C_3/C_4 alkylation unit; and a saturated gas plant (Baliban et al., 2012).

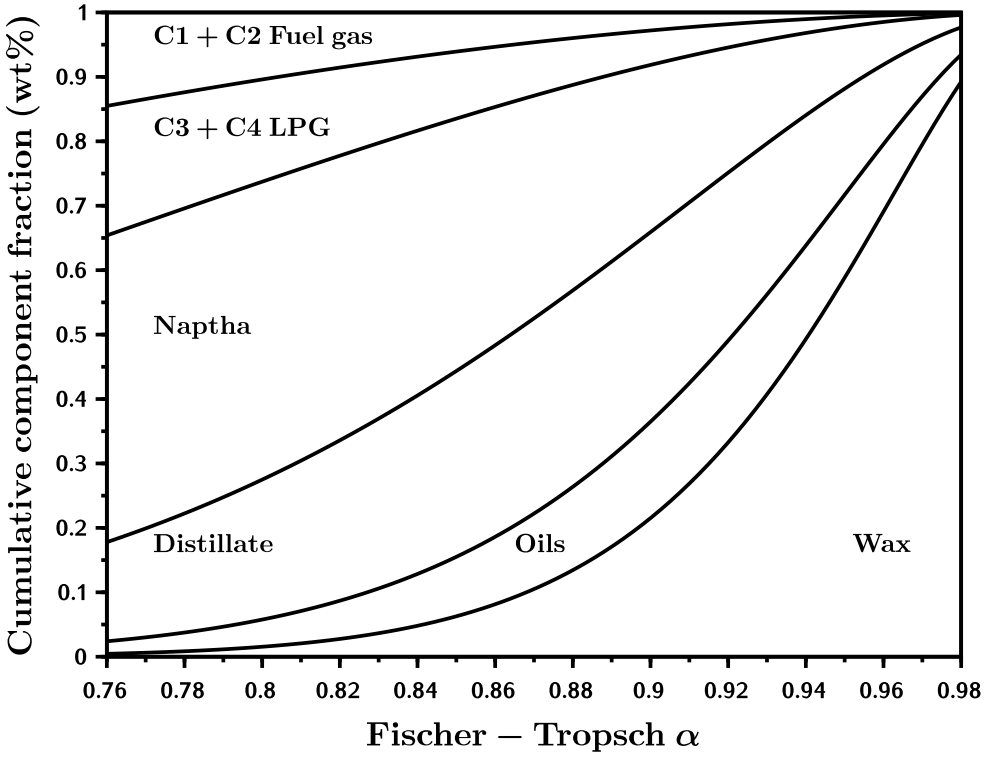

Figure 2.5: Cumulative component fractions (from wax to fuel gas) as a function of the Fischer-Tropsch Synthesis chain growth probability, adapted from Sie et al. (1991)

Hydrocracking of Fischer-Tropsch waxes occurs on platinum catalysts at temperatures in the range $300^oC \leq T \leq 400^oC$ and pressures in the range $30\,bar \leq P \leq 150\,bar$ (de Klerk, 2008) and has the potential to double the diesel yield (Le Grange, 2009). WHCs are traditionally fixed bed reactors configured in trickle bed mode (Le Grange, 2009). Hydrocracking requires a stream of hydrogen which could be purchased or produced in the process at an alternative unit. SMR of natural gas can produce a $H_2 : CO$ ratio of 3 : 1 (Le Grange, 2009) at fairly high methane conversion and the excess hydrogen may be separated out through PSA or membrane separation in order to supply hydrogen to hydrocracking. In hydrocracking, the long chain wax molecules are broken up into shorter chain molecules and the product distribution is shifted towards the lighter compounds. The cracking occurs in a cascading fashion with long chains cracking to short chains stepwise; therefore, the products from hydrocracking will still contain the heavy waxes but in reduced quantities. These waxes are separated out through distillation and recycled back to the hydrocracker to undergo further cracking till they leave the process in the desired carbon number range.

There are five distinct types of hydrocracker models: heuristic models, discrete pseudo-component lumped models, continuum lumping models, single events kinetic models and hybrid models (Le Grange, 2009). Building on the work of Accolla (2006) (Model A), Le Grange (2009) developed what are essentially one parameter hydrocracker models

dubbed Model B and Model C. These models are developed from the observation of a constant activation energy of the cracking reaction for the different hydrocarbons which is indicative of a single kinetic step being rate limiting. The mechanistic description of the reaction is improved in Model B and the model shows the correct dependence on the partial pressure of hydrogen as compared with Model A. Model C includes isomer species but limited data on the isomers led the parameters to converge to incorrect values; therefore, Model B is recommended by Le Grange (2009). Model B is able to accurately predict middle distillate yield and selectivity; however, it does not differentiate between isomers so it may be classified as a carbon number lumped model. Model B may also be classified as a single event kinetic model; therefore, it falls under the hybrid category. Discrete pseudo component lumping (Stangeland, 1974) is often used but the model parameters are feedstock specific and new ones must be calculated for changing feedstocks making these models unsuitable for this project. For the same reason, continuum lumping models are unsuitable. These models are normally feedstock independent but require a large number of parameters. Both Le Grange (2009) and Accolla (2006) have used a system where the a $\phi - \phi$ method VLE solver is embedded in the reactor function along with the kinetics.

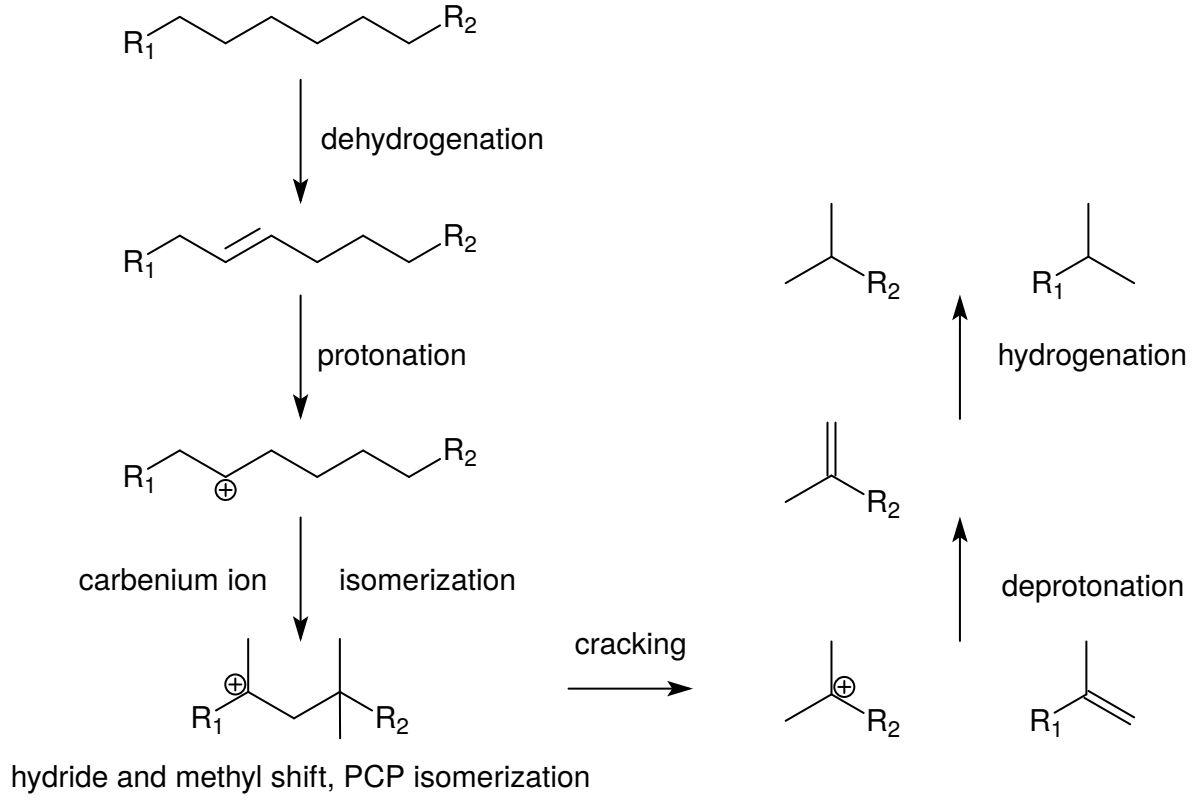

Figure 2.6: Hydrocracking mechanism, adapted from Le Grange (2009)

The reaction mechanism may be divided into the following steps (Le Grange, 2009):

1. Dehydrogenation of alkanes to olefins on the metal sites of the bi-functional catalyst
2. Protonation of the olefins to the carbenium ions on the acid catalyst sites

3. Hydroisomerisation of the carbenium ions to the precursor species specific to the succeeding β-scission type
4. Cracking via β-scission
5. Deprotonation of the carbenium ions to olefins on the acid catalyst sites
6. Hydrogenation of the olefins to alkanes

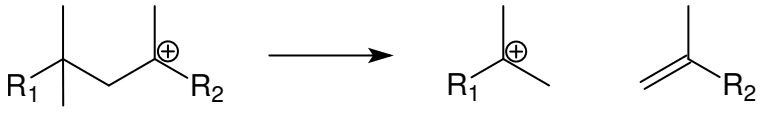

Figure 2.7: Type A β-scission, adapted from Le Grange (2009)

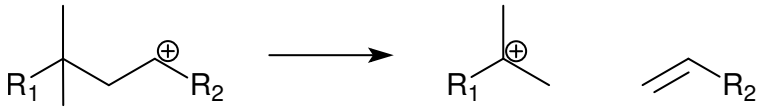

Figure 2.8: Type B1 β-scission, adapted from Le Grange (2009)

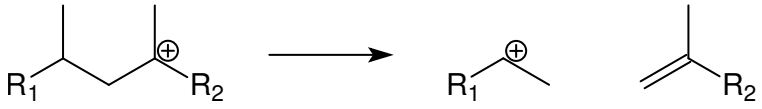

Figure 2.9: Type B2 β-scission, adapted from Le Grange (2009)

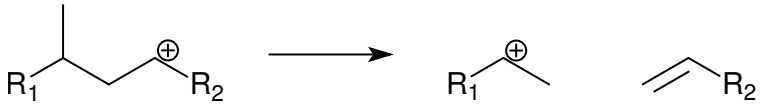

Figure 2.10: Type C β-scission, adapted from Le Grange (2009)

The cracking step proceeds according to the β-scission mechanism. The mechanism may be divided into types A1, B1, B2 , C and D scission, as shown in Figures 2.7, 2.8, 2.9 and 2.10. Type D scission is significantly slower than the other forms (Le Grange, 2009), hence it is not accounted for in Model B. In addition to these steps, the reactants and products may be further hydrogenation to unbranched alkanes either prior or subsequent to reaction on the catalyst surface.

2.5. Process Synthesis

The process topology is the specific process technologies in use, stream routing between units, and conditions in the process units themselves. A system of related process topologies may be referred to as a superstructure (Baliban et al., 2012). The process topologies are usually implemented in a process simulation software such as ASPEN Plus which seems to be the most popular simulation tool (Bao et al., 2010; Baliban et al., 2012; Prins et al., 2005; Kreutz et al., 2008; Adams and Barton, 2011; Choi et al., 1997; Hao et al.,

2008; Lee et al., 2008; Tijmensen et al., 2002). However, in some cases it is only used in part (i.e. for only calculating the mass and energy balances). Alternatives such as gPROMs (van der Laan et al., 1999), UniSIM (Panahi et al., 2011), the Cape Open to Cape Open (COCO) simulation environment and DWSIM are rarely used.

Most studies use a component database consisting of compounds between C_1 and C_{30} (Bao et al., 2010; Baliban et al., 2012; Adams and Barton, 2011) and it is often unclear whether paraffins and olefins are considered separately. A common technique to account for hydrocarbons beyond C_{30} is to lump these together into pseudo components. Some studies lump the sub C_{30} components as well (Bao et al., 2010; Adams and Barton, 2011) which is beneficial from a performance standpoint. The use of a large number of compounds would increase the solution time and make convergence of the simulation difficult to attain (Bao et al., 2010). This is intuitive because, for example, mass-energy balances and property calculations would need to be evaluated for a greater number of species. To the authors knowledge, the trade-off between accuracy and the number of species has not been quantified and most studies seem to be limited by the number of compounds in the available property databases rather than the computational difficulty of using a large set of compounds.

An XTL process based around FTS may generally be divided into three sections: syn-gas generation and cleaning, syngas conversion and product upgrading. However, these boundaries become blurred when recycle, heat and utility streams are incorporated. The objective of syngas generation is to produce syngas at a specific $H_2 : CO$ ratio. Without external recycle, this section may be modeled independently from the rest of process.

In terms of reactor modeling, several approaches can be taken. Extents of reaction or specification of the product stream may be used (Baliban et al., 2012) if the reaction conditions are fixed and the feed stream concentrations are unchanging. Furthermore, the process should be static in the variables affecting the product streams. Such an approach simplifies the overall modeling and solution of the model system. The accuracy of this approach will depend upon the static variable assumption being correct and how representative the extent of reaction values actually are. The reactors can also be modeled as equilibrium reactors (Bao et al., 2010; Baliban et al., 2012; Kreutz et al., 2008; Hao et al., 2008) which take into account, and respond to changes in, thermodynamically relevant variables such as temperature and pressure. The solution time will be higher compared with the extent of reaction method. The major drawback with this method is the assumption that the system is at equilibrium which may introduce errors depending upon how far from equilibrium the real system operates. Steady state reactor design equations can be employed with kinetics and including/excluding effects from mass and heat transfer and fluid dynamics. In the case of plug flow reactors, this method usually requires the solution of a system of ODEs or PDEs with solution time being generally much higher than the previous methods. In the case of perfectly mixed reactors, solution of a system of algebraic equations is usually required, the accuracy of which is highly sensitive to the initial guess. These approaches may push the boundaries of what simulation software

is capable of. Furthermore, interfacing with programming languages such as FORTRAN may be required in order to fully implement the model. The final category of models are otherwise similar to the aforementioned models except that the reactor equations are dynamic and unsteady state models. In the case of slurry reactors, these are less sensitive to the initial guess as the solution is approached gradually and from the correct region in solution space. However, the solution time will generally be much higher than all other methods covered here.

A common analysis approach is to use case studies (Baliban et al., 2012) which entails generation and comparison of performance figures from different process topologies. This style of analysis can usually be carried out in standard simulation software. Another more rigorous approach is to perform an optimization on the topology or even the whole superstructure. Although, the difficulty will likely be compounded by the presence of discrete (on/off) variables resulting in non differentiable objective functions. An example may be a variable which determines whether air is routed to the ASU or not. This is a complex task that often requires significant time to formulate and to compute. One solution to these issues is to approximate the objective function using methods like collocation and software such as GAMS (Adams and Barton, 2011) or to reduce the solution space through additional assumptions and constraints.

The optimal process configurations are subject to potentially volatile market conditions (such as crude oil prices, electricity prices and feedstock prices) and the most profitable design can change on a month to month basis (Adams and Barton, 2011). Interestingly, the feedstock price often has a greater effect on the best choice of product than the product price (Lee et al., 2008). Feedstock prices can vary significantly over time making it difficult to set upon a future-proof process design. Moreover, all that can be stated is that under some specific set of conditions, such a process configuration is most economical, or otherwise shows the best performance. Coal and natural gas feedstocks present the most technically and economically viable alternatives for liquid fuel production due to the maturity of conversion technologies. Additionally, coal and natural gas are naturally consolidated in large quantities; whereas, biomass sources are generally dispersed and in comparatively small quantities.

Plant capacities can range from 10,000 Barrels Per Day (BPD) to 200,000 BPD with 50,000 BPB being regarded as medium capacity (Baliban et al., 2012). Note that the BPD unit may be defined according to the Fischer-Tropsch Liquid (FTL) volumetric flow rates or according to the equivalent volume of crude oil products on a Higher (HHV) or Lower Heating Value (LHV) basis (Kreutz et al., 2008). The latter would provide a better comparison with petroleum based fuels. Small plants producing only liquid fuels tend to have higher normalized investment costs (Baliban et al., 2012). GTL processes have the lowest capital costs due to the lack of the capital intensive gasification step; however, the profitability of GTL in particular is sensitive to different factors based on the plant capacity. Additionally, a medium to large sized plant has been reported to be sensitive to the cost of natural gas feedstock (Bao et al., 2010). Since GTL is economical where natural

gas supply is cheap and requires less processing steps, it becomes particularly useful for valorization of remote gas reserves (Choi et al., 1997). Additionally, liquid fuels have a higher energy density than both biomass and natural gas; therefore, it is more economical to convert these feedstocks to liquids before transportation over long distances. In the case of valorization of remote natural gas, it may be more economical to maximise the production of a single stable pumpable liquid rather than to produce an array of products (Choi et al., 1997).

It is expected that approximately 40% of the Higher Heating Value (HHV) of the feedstock ends up in the liquid fuels product (Prins et al., 2005). On a carbon weight basis figures of 15% have been quoted (Prins et al., 2005). In terms of the LHV cost per unit of energy, coal is the cheapest followed by natural gas and then biomass (Baliban et al., 2012). Cobalt based FTS shows higher plant-wide overall thermal efficiency and carbon efficiency (Hao et al., 2008). In terms of reactor setup, CSTRs in series have been found to show better thermal efficiency than PFRs Hao et al. (2008). The greatest energy losses occur in the gasification section, the shift and reforming sections, the FT section and combined cycle sections (cogeneration) in that order (Tijmensen et al., 2002).

BTL can be carbon neutral or negative if CCS is employed (Liu et al., 2010). In general, GTL and CTL processes produce either equivalent or significantly more CO_2 emissions compared to production of crude oil based fuels. CTL in particular can produce double the emissions of traditional methods (Kreutz et al., 2008; Liu et al., 2010). CCS schemes are often proposed to combat this. In the case of CTL-CSS, the resulting emissions would be roughly equivalent to petroleum based refining without CSS; however, CO_2 capture costs are lower than for stand-alone coal power plants (Kreutz et al., 2008) due to the fact that XTL processes generally produce relatively pure streams of CO_2 as a byproduct making capture far more efficient than if the CO_2 were captured at the stack. Generally, the long term effects of CCS on the environment are not covered in XTL studies; however, the emissions may be incorporated into carbonate deposits in the long term. Furthermore, there may be a risk of leakage back into the atmosphere (Kaiser et al., 2013). Cofeeding biomass with coal can result in zero emissions (Kreutz et al., 2008) and capitalize on low CTL investment costs. Other alternatives are to utilize the carbon dioxide through Carbon Capture and Utilization (CCU) where, for example, the reverse Water Gas Shift (rWGS) can be employed to produce more syngas or the carbon dioxide may be used in agriculture. CTL-OT emissions can be reduced below Recycle (RC) systems by incorporating ATR and CCS but the operating costs would be higher unless the emissions penalty is high (Kreutz et al., 2008).

While CCS is attractive for emissions reduction, the carbon efficiency of the process may suffer due to diversion and loss of feedstock carbon into the waste CO_2 that could otherwise be converted to product (Adams and Barton, 2011; Liu et al., 2010), hence a high emissions penalty is needed to offset this effect. Typical CTL carbon conversion to liquid product is between 20% and 35% but higher conversions can be achieved through recycle of CO_2 at the expense of greater capital costs (Floudas et al., 2012). The removal of carbon

dioxide from syngas affects FTS by increasing the partial pressure of carbon monoxide leading to a greater selectivity to hydrocarbons Baliban et al. (2012); Kreutz et al. (2008); however, the increase in selectivity is small and may not be worth the high energy costs associated with carbon dioxide removal (Baliban et al., 2012; Adams and Barton, 2011; Tijmensen et al., 2002). In the case of cobalt catalysed FTS, it may be beneficial to avoid CO_2 removal in full conversion configurations (Hao et al., 2008) since the cobalt based catalyst is not affected by the presence of CO_2 (Floudas et al., 2012; Espinoza et al., 1999). Conversely for iron based catalysts, OT configurations with multiple reactors in series including CO_2 removal can yield better carbon efficiency (Hao et al., 2008). This is may be due to CO_2 pushing the WGS equilibrium towards CO and lowering the $H_2 : CO$ ratio yielding more wax.

In terms of hydrogen production for the WHC or other uses, supplementary hydrogen should be avoided if it is sourced from a carbon based fuel, as opposed to carbonless sources such as electrolysis of water, since this would lead to greater overall emissions (Adams and Barton, 2011). Carbon conversions of 100% can be achieved if hydrogen is supplied from a non carbon based source and rWGS is employed (Floudas et al., 2012) (the later would be classified as CCU if the carbon dioxide needed for rWGS is supplied from the process). Alternatively, a portion of the syngas may be diverted to hydrogen production upstream of FTS (Kreutz et al., 2008). The isolation of pure hydrogen can be accomplished through hydrogen pressure swing adsorption or hydrogen selective membranes (Adams and Barton, 2011).

Using natural gas, the required $H_2 : CO$ ratio can more readily be attained than for coal and biomass (Floudas et al., 2012) since natural gas has a higher hydrogen to carbon ratio than coal or biomass. Moreover, an external source of hydrogen may not be required (Baliban et al., 2012) since $H_2 : CO$ ratios around 3 should be achievable (Adams and Barton, 2011). Furthermore, the the $H_2 : CO$ ratio can be obtained without the need for further carbon losses through production of hydrogen from carbon based fuel sources (Floudas et al., 2012) and can be obtained with a higher carbon efficiency than coal or biomass (Dry, 2002). Consequently, the carbon conversion for GTL-RC processes is usually on the order of 65%-75% (Floudas et al., 2012; Hao et al., 2008), which is higher than similar CTL and BTL processes. Additionally, the load on the ASU is reduced due to fact that gasification is not needed for GTL. Considering that syngas gasification and cleaning can account for up to 70% of costs (Dry, 2002), the use of natural gas presents a significant cost saving opportunity over coal and biomass. The $H_2 : CO$ ratio to FTS is mainly controlled in the reforming section. The ratio can be controlled by adjusting the oxygen and steam feed rates to the reformer (Bao et al., 2010). The ATR shows better economies of scale Floudas et al. (2012); Lee et al. (2008) than steam reforming making it the preferred reforming method in GTL (Floudas et al., 2012) . The ATR may be operated with pure oxygen or oxygen enriched air (Choi et al., 1997). Using natural gas with associated CO_2 could eliminate the need for the CO_2 recycle and potentially allow the use of an air blown ATR (Choi et al., 1997). However, CO_2 removal prior to reforming

has a positive effect on the energy efficiency of the ATR (Hao et al., 2008).

Increasing the oxygen to methane ratio beyond the value of 0.6 may result in diminishing increases to the $H_2 : CO$ ratio (Bao et al., 2010). Ratios beyond 0.7 can result in undesirable adiabatic flame temperatures (Choi et al., 1997). The steam to carbon inlet ratio showed diminishing returns beyond a value of 1.3 (Bao et al., 2010).

Running FTS at high conversions ($\geq$80%) leads to low partial pressure of carbon monoxide in the reactor which leads to decreased yield of liquid products Prins et al. (2005); Tijmensen et al. (2002). Moreover, the decreased rate of reaction results in larger reaction volumes (for the same performance) and greater investment costs (Prins et al., 2005). At high conversions, the economic benefit of tail gas utilization becomes more significant due to its increased production of light compounds in FTS. Prins et al. (2005) have recommended a maximum conversion of 80% in FTS in order to maximise the yield to liquids. These high conversions are not possible in FBRs where maximum achievable conversions are around 40% which may be due to the increasing partial pressure of steam lowering the catalyst activity (Kaiser et al., 2013). In contrast, slurry reactors can reach conversions of 80% (Kreutz et al., 2008). Running FTS using nitrogen diluted syngas has been covered by Prins et al. (2005) who predicted α values in the range of 0.930–0.949 for 80% conversion in OT LTFT with 50% nitrogen in syngas. The presence of a large quantity of inerts without commensurate increase in the overall pressure will lead to decreased liquid selectivity as a result of the lowered partial pressure of hydrogen and carbon monoxide (Tijmensen et al., 2002). There is potential for cost saving in routing the large quantity of water (can be up to 56% by weight) (Hao et al., 2008) in the FTS syncrude product to water treatment (by reverse osmosis for example) and subsequently steam generation (Bao et al., 2010). The tail gas from FTS can either be recycled back to FTS (internal recycle) or to the ATR (external recycle) where the light hydrocarbons will be converted back to syngas. The C_1 to C_4 tail gas can also be burned for energy (as a means of heat integration or otherwise) or used to generate electricity (cogeneration) (Tijmensen et al., 2002). The FTS tail gas has such a low heating value that it may not be viable for use in a gas turbine; therefore, a combined cycle or steam-rankine cycle can be used (Prins et al., 2005). If CO_2 is present in the tail gas, removing it will benefit the heating value (Liu et al., 2010). External recycle ratios of 25% have been reported in literature (Bao et al., 2010). A trade-off between the cost of recycle and the benefit of increased liquid products is likely due to compression costs and increased reactor size in the ATR and FTS. OT, with coproduction of electricity, has been reported to have lower operating costs compared to RC due to the cost of production of liquid fuels being offset by the income from the sale of energy; however, emissions are higher (Kreutz et al., 2008; Floudas et al., 2012; Liu et al., 2010). OT configurations will also produce a much greater quantity of heat than RC configurations due to the higher conversion (Kreutz et al., 2008); therefore, the economic effect of heat integration will be more significant.

2.6. Key Questions

The key questions for this project are based on the objectives of investigating the potential use of air (nitrogen diluted syngas) instead of pure oxygen as a means to reduce operating costs and exploring process configurations that lead to greater yield of diesel and liquids. These objectives are interlinked in that when air is used the process configuration will need to be changed in order to mitigate any loss of performance resulting from the use of nitrogen diluted syngas. Therefore it is valuable to highlight process configurations that will maximize the diesel yield as potential candidates for further exploration in regard to the use of nitrogen diluted syngas. It is not immediately clear how FTS should be operated such that diesel yield can be maximized in the WHC; therefore, investigation of the effect of α_{FTS}on the WHC is necessary. Furthermore, evaluating configurations using pure oxygen and FTS recycle is useful for the sake of comparison with once-through configurations using nitrogen diluted syngas in FTS.

1. What is the effect of using air on the diesel yield?
2. What is the optimal value of α_{FTS} that will maximize the diesel yield?
3. Which process configuration maximizes diesel yield?

3. Theory and Methodology

After considering the complexities of this research and the time constraints, a deliberate effort has been made to reduce the scope of work to a sufficiently detailed but manageable level with the aim of accomplishing the goals of this study using a simple framework that can be built upon in subsequent research. The key aspects of the modeling approach used herein are: the use of elementary reactor models in the FTS and WHC reactors, accounting for VLE using PREOS and accounting for an extensive range of carbon numbers. The variables of interest in this study are the process wide diesel yield, carbon efficiency, α_{FTS} and those variables affected by theN_2 content. Given that this study is focused on diesel yield and carbon efficiency it is not necessary to include reactor sizings, separator sizings and utility usage. In order to perform a meaningful study on the effect of α_{FTS} on hydrocracking (at high values of α_{FTS}) it is necessary to account for a wide range of carbon numbers. From the standpoint of studying process configurations in the general sense, economic analysis would be more relevant; however, economic constraints are always changing with new market conditions and technologies. Studies such as this valuable because they show what is possible given no economic constraints.

3.1. General

All modeling is done within the Scilab 5.5.2 programming language as supplied by the Ubuntu 16.04 package manager. However, the standard libblas and liblapack libraries have been substituted with their OpenBlas equivalents for performance reasons. The physical property data and light gases correlations are sourced from ChemSep v7.15.

The vector used to represent all material streams and their temperature and pressure is shown in Equation 3.1. This is used throughout the plant model. The first seven species are referred to as the light gases. The flows denoted by F_{Pi} and F_{Oi} are the n-paraffins and α-olefins, respectively, of carbon number i. Temperature and pressure are included in the flow vector. The ^{T} here is denoting the transpose of this vector (the vector orientation is important for any vectorized operations).

$$F = (F_{CO}, F_{H_2}, F_{H_2O}, F_{CO_2}, F_{N_2}, F_{O_2}, F_{CH_4}, F_{P2}, F_{P3}, \ldots F_{PN}, F_{O2}, F_{O3}, \ldots F_{ON}, T, P)^T \tag{3.1}$$

Any stream separations are accomplished through the use of basic stream splitting. This method is used for the syngas cleaning steps; removal of CO_2 and water; product upgrade separations such as separation of tail gas and aqueous phase from the syncrude; and fractionation of the upgraded products. Mass and energy balances are always checked across units in order to determine whether the system is operating correctly. The energy balances across streams are determined using standard heats of formation and the ideal gas heat capacities according to Equations 3.2 and 3.3. The liquid enthalpy is based on the assumption of saturated liquid in equilibrium with the vapor phase. The definite

integral in Equation 3.2 is calculated from the heat capacity polynomials for all species. For the supercritical species, the vapor and liquid enthalpies are assumed to be equal.

$$H_V(T) = \sum^{species} \left(H^{\Theta}_{f,i} + \int_{T=298}^{T} Cp_i \, dT \right) y_i F_V \tag{3.2}$$

$$H_L(T) = \sum^{species} \left(H_V(T) - \Delta H_i^{vap} \right) x_i F_L \tag{3.3}$$

The reactor energy requirement is determined by the difference between the enthalpy of the feed and product streams as shown in Equation 3.4. For each stream the vapor and liquid enthalpies are determined as shown in Equations 3.2 and 3.3. The major assumption here is that the vapor and liquid phases are in equilibrium in these streams and throughout the reactor; therefore, any liquid will be saturated liquid and the same will be true for the vapor phase.

$$Q = H_{Feed} - H_{Product} \tag{3.4}$$

Table 3.1 shows the classification of carbon numbers by cut used in this project.

Table 3.1: Syncrude cuts

Cut	**Range**
Lights	C1-C4
Naptha	C5-C9
Diesel	C10-C20
Wax	C21+

3.2. Vapor Liquid Equilibrium

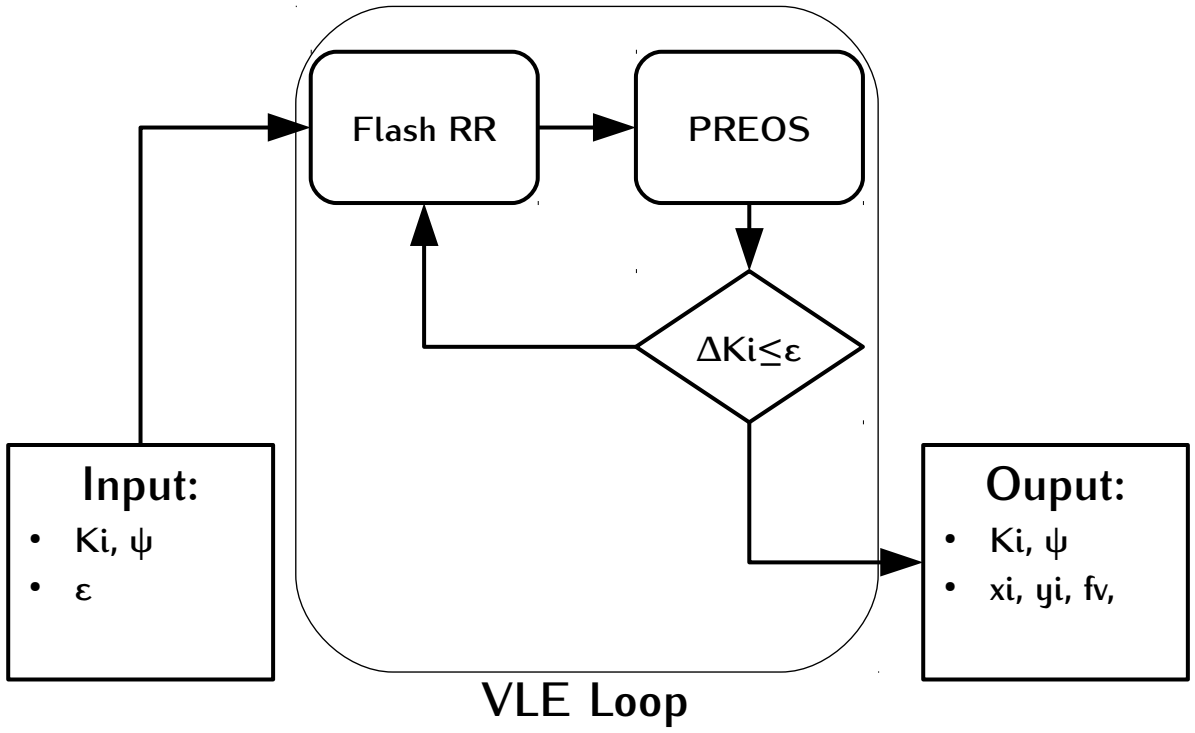

Figure 3.1: $\phi - \phi$ algorithm

3.2.1. Rachford Rice Isothermal Flash

A diagram of the VLE procedure is given in Figure 3.1. The input to the procedure is a guess for the separation factor and psi. The separation factor guesses are determined by the correlation described in Appendix 9.3 and the guess for ψ is determined by guessing the vapor liquid split and solving the Rachford Rice method. The Rachford-Rice isothermal flash method shown in Equation 3.5 reduces the number of equations necessary for a flash calculation to one. This is highly beneficial from a solution time perspective. The input is the separation factor guess K_i, the total mole fractions z_i and a guess for the vapor fraction over the feed on a molar basis. The root of Equation 3.5 is found using Brent's root finding method which is taken from Fortran's FZERO and has been implemented in Scilab. Once the root of the equation has been found Equations 3.6 and 3.7 can be used to determine the mole fractions of each species. Within the VLE loop, the Rachford Rice method is used in the same fashion to update the value of ψ and to determine the new mole fractions using the new K_i value (which is updated by PREOS).

$$\sum_{i=1}^{N} \frac{(K_i - 1)\, z_i}{\psi\,(K_i - 1) + 1} = 0 \tag{3.5}$$

$$x_i = \frac{z_i}{1 + \psi\,(K_i - 1)} \tag{3.6}$$

$$y_i = K_i x_i \tag{3.7}$$

The isothermal flash is also used to determine whether the system is at the dew point or the bubble point by evaluating the flash function at ψ values of zero and 0.99999. If Equation 3.5 is positive or zero when ψ is zero we know the system contains saturated liquid at its bubble point. If 3.5 is negative or zero when ψ is close to one then we can deduce the system contains saturated vapor at the dew point.

3.2.2. Peng Robinson Equation Of State

Zabaloy and Vera (1998) have shown that PREOS Equation of State (EOS) is superior to the Soave-Redlich-Kwong (SRK) EOS and van der Waal (vdW) EOS for non polar molecules. However, PREOS 1976 does not extrapolate well to heavy paraffinic waxes reaching a maximum value at C_{70} then decreasing on a PREOS-alpha probability vs carbon number plot. Modifications to the alpha function usually employ polynomials which do not extrapolate well. Twu et al. (1994) have developed a correlation (Equation 3.8) for the PREOS-alpha parameter which is a linear function of the accentric factor. Twu et al. (1997) recommend calculation of the binary interaction parameters using Gibbs Excess Models; however, this is beyond the scope of this project. Therefore, the interaction parameters are assumed to be equal to zero. In Equation 3.8, ω is the accentric factor and T_r is the ratio of the system temperature to the critical temperature for that component (the reduced temperature).

$$\begin{aligned} \alpha_i\left(\omega_i, T_{r,i}\right) &= \alpha_i^0 + \omega_i\left(\alpha_i^1 - \alpha_i^0\right) \\ \alpha_i^0 &= T_{r,i}^{-0.171813} exp\left[0.125282\left(1 - T_{r,i}^{1.77634}\right)\right] \\ \alpha_i^1 &= T_{r,i}^{-0.607352} exp\left[0.511614\left(1 - T_{r,i}^{2.20517}\right)\right] \end{aligned} \tag{3.8}$$

In order to determine K_i using PREOS, the fugacity coefficients are determined according to Equation 3.10, where Ω denotes the phase (either vapor or liquid). In the vapor phase $Z_{mix}^{\Omega} \equiv Z_{mix}^{V}$ is the maximum positive real root of Equation 3.9, while when in the liquid phase $Z_{mix}^{\Omega} \equiv Z_{mix}^{L}$ is the minimum positive real root of Equation 3.9. The separation factor can be determined by the ratio of the liquid and vapor fugacity coefficients as shown in Equation 3.11. Equation 3.10 has been given in a vectorized form so multiplication and division are element wise and in this case $\left(z_i^{\Omega}\right)^T$ denotes the transpose (to a row vector) of the mole fractions for phase Ω. The other parameters are given in Appendix 9.3.

$$\left(Z_{mix}^{\Omega}\right)^3 + \alpha_{mix}^{\Omega}\left(Z_{mix}^{\Omega}\right)^2 + \beta_{mix}^{\Omega} Z_{mix}^{\Omega} + \gamma_{mix}^{\Omega} = 0 \tag{3.9}$$

$$ln\overline{\phi}_i^{\Omega}(T,P,z_i) = \frac{B_i}{B_{mix}^{\Omega}}\left(Z_{mix}^{\Omega}-1\right) - ln\left(Z_{mix}^{\Omega}-B_{mix}^{\Omega}\right)\ldots \\ \ldots - \frac{A_{mix}^{\Omega}}{2B_{mix}^{\Omega}\sqrt{2}}\left[2\frac{\left(z_i^{\Omega}\right)^T A_{ij}}{A_{mix}^{\Omega}} - \frac{B_i}{B_{mix}^{\Omega}}\right] ln\left[\frac{Z_{mix}^{\Omega}+\left(1+\sqrt{2}\right)B_{mix}^{\Omega}}{Z_{mix}^{\Omega}+\left(1-\sqrt{2}\right)B_{mix}^{\Omega}}\right] \tag{3.10}$$

$$K_i = \frac{\overline{\phi}_i^L}{\overline{\phi}_i^V} \tag{3.11}$$

3.3. Reforming

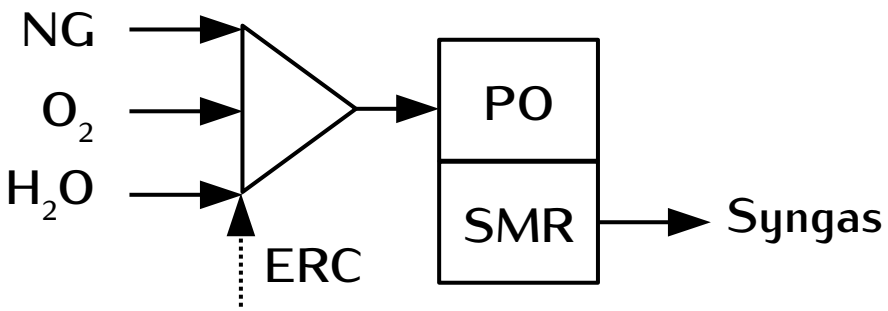

Figure 3.2: Reformer flow diagram

Figure 3.2 illustrates the flows into and out of the ATR section. The reformer consists of a PO and a SMR section both described by adiabatic plug flow reactors. When the external recycle stream is active the tail gas from FTS is routed back to the ATR and mixes with the feed prior to PO. It is assumed that only methane is reformed in the ATR.

3.3.1. Partial Oxidation

The purpose of the PO section is to react some of the methane to carbon dioxide and water through total combustion. Additionally PO provides the reaction heat to bring the temperature to that needed in the steam reforming stage ($\approx 1000^oC$). The temperature out of PO and conversion of methane is controlled by changing the $PO\lambda$ and $PO\gamma$ parameters. The parameters $PO\lambda$ and $PO\gamma$ are defined in Equations 3.12 and 3.13. They are the oxygen to feed carbon ratio and the steam to feed carbon ratio. The feed carbon is equivalent to the moles of methane.

$$\lambda = \frac{F_{O_2,0}}{F_{C,0}} \tag{3.12}$$

$$\gamma = \frac{F_{H_2O,0}}{F_{C,0}} \tag{3.13}$$

In non catalytic combined methane reforming, the total combustion step (or partial oxidation step) precedes the SMR step (De Groote and Froment, 1996); however, some degree of reforming is accounted for in PO. It is assumed that the reactions indicated in Table 3.2 (De Groote and Froment, 1996; Jin et al., 2000; Donazzi et al., 2008) are taking place in the PO section; reaction 1 is the exothermic total combustion of methane; reaction 2 is the endothermic steam reforming of methane ; and reaction 3 is the carbon dioxide reforming reaction. It is assumed that carbon formation due to the Boudouard reaction and methane cracking do not occur. The combustion kinetics have been sourced from Donazzi et al. (2008). The steam reforming and carbon dioxide reforming kinetics have been sourced from Jin et al. (2000).

Table 3.2: Partial oxidation reactions from Donazzi et al. (2008) and Jin et al. (2000)

No	Reaction	Heat of reaction [J mol^{-1}]
1	$CH_4 + 2O_2 \longrightarrow CO_2 + 2H_2O$	-804.3
2	$CH_4 + H_2O \longleftrightarrow CO + 3H_2$	204.1
3	$CH_4 + CO_2 \longleftrightarrow 2CO + 2H_2$	245.3

$$r_1 = k_1 \frac{p_{CH_4} p_{O_2}}{(p_{O_2} + 10^{-6})\,(1 + k_A p_{H_2O})} \tag{3.14}$$

$$r_2 = k_2 p_{CH_4} p_{H_2O} \left(1 - \frac{p_{CO} p_{H_2}^3}{K_{E,2} p_{CH_4} p_{H_2O}}\right) \tag{3.15}$$

$$r_3 = k_3 p_{CH_4} p_{CO_2} \left(1 - \frac{p_{CO_2}^2 p_{H_2}^2}{K_{E,3} p_{CH_4} p_{CO_2}}\right) \tag{3.16}$$

Table 3.3: Partial oxidation rate constants from Donazzi et al. (2008) and Jin et al. (2000)

Parameter	Value	Units	Activation Energy [kJ mol^{-1}]
$k_1(873K)$	1.03×10^{-1}	$\frac{mol}{atm\, g_{cat}\, s}$	92.0
k_2	4.19×10^{-9}	$\frac{mol}{Pa^2\, g_{cat}\, s}$	29.0
k_3	2.42×10^{-9}	$\frac{mol}{Pa^2\, g_{cat}\, s}$	23.7

Table 3.4: Partial oxidation equilibrium constants

Parameter	Formula	Units
K_2	$exp\left\{-\frac{1}{RT}\left(-G^{\theta}_{f,CH_4} - G^{\theta}_{f,H_2O} + G^{\theta}_{f,CO} + 3G^{\theta}_{f,H_2}\right)\right\}$	bar^2
K_3	$exp\left\{-\frac{1}{RT}\left(-G^{\theta}_{f,CH_4} - G^{\theta}_{f,CO_2} + 2G^{\theta}_{f,CO} + 2G^{\theta}_{f,H_2}\right)\right\}$	bar^2

Table 3.5: Partial oxidation adsorption constants from Donazzi et al. (2008)

Species	$K_{ads}\,[atm^{-1}]$	$\Delta H_i\,[kJ\ mol^{-1}]$
H_2O	3.90×10^2	-16

The partial oxidation section is modeled as an adiabatic PFR. This assumption is based on the fact that the PO section only accounts for a small part of the ATR volume and the reaction is extremely rapid (Biesheuvel and Kramer, 2003); therefore, it is assumed that heat losses will be negligible. The stoichiometric matrix for the three reactions in Table 3.2 is shown in Equation 3.17. The product of the stoichiometric matrix and the rate vector is determined to give the PFR Ordinary Differential Equation (ODE) shown in Equation 3.18. Equations 3.14, 3.15 and 3.16 are used to determine the rates r_i.

$$
\nu_{PO} = \begin{array}{ccccc}
R_1 & R_2 & R_3 & & \\
\downarrow & \downarrow & \downarrow & & \\
0 & 1 & 2 & \leftarrow & CO \\
0 & 3 & 2 & \leftarrow & H_2 \\
2 & -1 & 0 & \leftarrow & H_2O \\
1 & 0 & -1 & \leftarrow & CO_2 \\
0 & 0 & 0 & \leftarrow & N_2 \\
-2 & 0 & 0 & \leftarrow & O_2 \\
-1 & -1 & -1 & \leftarrow & CH_4 \\
0 & 0 & 0 & \leftarrow & P2 \equiv C_2H_6 \\
0 & 0 & 0 & \leftarrow & P3 \\
\vdots & \vdots & \vdots & \leftarrow & \vdots \\
0 & 0 & 0 & \leftarrow & PN \\
0 & 0 & 0 & \leftarrow & O2 \equiv C_2H_4 \\
0 & 0 & 0 & \leftarrow & O3 \\
\vdots & \vdots & \vdots & \leftarrow & \vdots \\
0 & 0 & 0 & \leftarrow & ON
\end{array} \tag{3.17}
$$

$$
\frac{dF}{dW} = \nu_{PO} \begin{bmatrix} r_1 \\ r_2 \\ r_3 \end{bmatrix} \frac{1}{3600} \tag{3.18}
$$

3.3.2. Steam Reforming

Table 3.6 shows the main reactions occurring in SMR and their heats of reactions. The rate equations developed by Xu and Froment (1989) are numbered correspondingly and are shown in Equations 3.19, 3.20, 3.21 and 3.22. Rowshanzamir et al. (2009) have used effectiveness factors from De Groote and Froment (1996) and these are shown in Table 3.6.

Table 3.6: Steam Methane Reforming reactions from Xu and Froment (1989) with effectiveness factors from De Groote and Froment (1996)

No	Reaction	Heat of reaction [J mol^{-1}]
1	$CH_4 + H_2O \longleftrightarrow CO + 3H_2$	−206100
2	$CO + H_2O \longleftrightarrow CO_2 + H_2$	+41150
3	$CH_4 + 2H_2O \longleftrightarrow CO_2 + 4H_2$	−165000

$$DEN = 1 + K_{CO}p_{CO} + K_{H_2}p_{H_2} + K_{CH_4}p_{CH_4} + K_{H_2O}p_{H_2O}\left(p_{H_2}\right)^{-1} \tag{3.19}$$

$$r_1 = \frac{k_1}{p_{H_2}^{2.5}}\left(p_{CH_4}p_{H_2O} - \frac{p_{H_2}^3 p_{CO}}{K_1}\right)\frac{1}{DEN^2} \tag{3.20}$$

$$r_2 = \frac{k_2}{p_{H_2}}\left(p_{CO}p_{H_2O} - \frac{p_{H_2}p_{CO_2}}{K_2}\right)\frac{1}{DEN^2} \tag{3.21}$$

$$r_3 = \frac{k_3}{p_{H_2}^{3.5}}\left(p_{CH_4}p_{H_2O}^2 - \frac{p_{H_2}^4 p_{CO_2}}{K_3}\right)\frac{1}{DEN^2} \tag{3.22}$$

Table 3.7: Steam reforming rate constants adapted from Rowshanzamir et al. (2009)

Parameter	Value	Units	Activation Energy [J mol^{-1}]
k_1	1.955×10^{06}	bar	67130
k_2	1.020×10^{15}	$bar^{0.5}$	243900
k_3	5.852×10^{17}	$bar^{-1.5}$	204000

Table 3.8: Steam reforming equilibrium constants from Rowshanzamir et al. (2009)

Parameter	Formula	Units
K_1	$5.75 \times 10^{12} exp\left\{-\frac{11476}{T}\right\}$	bar^2
K_2	$1.26 \times 10^{-2} exp\left\{\frac{4639}{T}\right\}$	-
K_3	$7.24 \times 10^{10} exp\left\{-\frac{21646}{T}\right\}$	bar^2

Table 3.9: Steam reforming adsorption constants from Rowshanzamir et al. (2009) where $K_i = K_{oi} exp\left(\frac{-\Delta H_i}{RT}\right)$

Species	K_{oi} [bar^{-1}]	ΔH_i [J mol^{-1}]
CH_4	6.65×10^{-4}	−38280
CO	8.23×10^{-5}	−70650
H_2	6.12×10^{-9}	−82900
H_2O	$1.77 \times 10^{5}\ bar$	+88680

The steam reforming section is assumed to be an adiabatic PFR. Three steam reforming reactions are accounted for as shown in Table 3.6. The stoichiometric matrix is shown in Equation 3.23. Equations 3.19, 3.20, 3.21 and 3.22 are used to determine the rate r_i. The effective rate is used in the PFR design equation as shown in Equation 3.24 which is an ODE and may be solved as such.

$$
\begin{array}{cccccc}
 & R_1 & R_2 & R_3 & & \\
 & \downarrow & \downarrow & \downarrow & & \\
 & 1 & -1 & 0 & \leftarrow & CO \\
 & 3 & 1 & 4 & \leftarrow & H_2 \\
 & -1 & -1 & -2 & \leftarrow & H_2O \\
 & 0 & 1 & 1 & \leftarrow & CO_2 \\
 & 0 & 0 & 0 & \leftarrow & N_2 \\
 & 0 & 0 & 0 & \leftarrow & O_2 \\
\nu_{SMR} = & -1 & 0 & -1 & \leftarrow & CH_4 \\
 & 0 & 0 & 0 & \leftarrow & P2 \equiv C_2H_6 \\
 & 0 & 0 & 0 & \leftarrow & P3 \\
 & \vdots & \vdots & \vdots & \leftarrow & \vdots \\
 & 0 & 0 & 0 & \leftarrow & PN \\
 & 0 & 0 & 0 & \leftarrow & O2 \equiv C_2H_4 \\
 & 0 & 0 & 0 & \leftarrow & O3 \\
 & \vdots & \vdots & \vdots & \leftarrow & \vdots \\
 & 0 & 0 & 0 & \leftarrow & ON
\end{array}
\tag{3.23}
$$

$$
\frac{dF}{dW} = \nu_{SMR} \begin{bmatrix} r_1 \\ r_2 \\ r_3 \end{bmatrix} \frac{1}{3600} \tag{3.24}
$$

3.3.3. Energy Balance

The energy balance for both PO and SMR is formulated as shown in Equation 3.25.

$$
\frac{dT}{dW} = \frac{1}{3600} [r_1, r_2, r_3] \begin{bmatrix} \Delta H_1^{rxn} \\ \Delta H_2^{rxn} \\ \Delta H_3^{rxn} \end{bmatrix} \frac{1}{\sum_{i=1}^{N} z_i F \, Cp(T)} \tag{3.25}
$$

3.4. Fischer-Tropsch Synthesis

3.4.1. Carbon Number Range

Figure 3.3 shows the effect of increasing FT α on the sum of the mole fractions predicted by the ASF distribution (Equation 2.3) for changing maximum carbon number. As shown, a sum of the mole fractions equaling one is not always guaranteed. The sum of the mole

fractions only truly equals to one when the maximum carbon chain length is infinite i.e the whole range is accounted for. However, a sum close to the limit of machine precision will be treated as equal to one by the computer. When accounting for a small range of carbon numbers, one is effectively truncating the ASF plot, resulting in a greater portion of the species being excluded and thus a mole fraction that does not sum close enough to the machine value of 1. Low alpha values favor greater material distribution among the lighter compounds; therefore, the mole fraction summation is nearer to 1 even if a small subset of the FTS products is considered. When alpha is close 1, most of the product will be distributed amongst the heavier carbon numbers; therefore, the effect will be more pronounced as shown in Figure 3.3. Where very high alpha values are sought, adjustments must be made to in order to counteract this material loss.

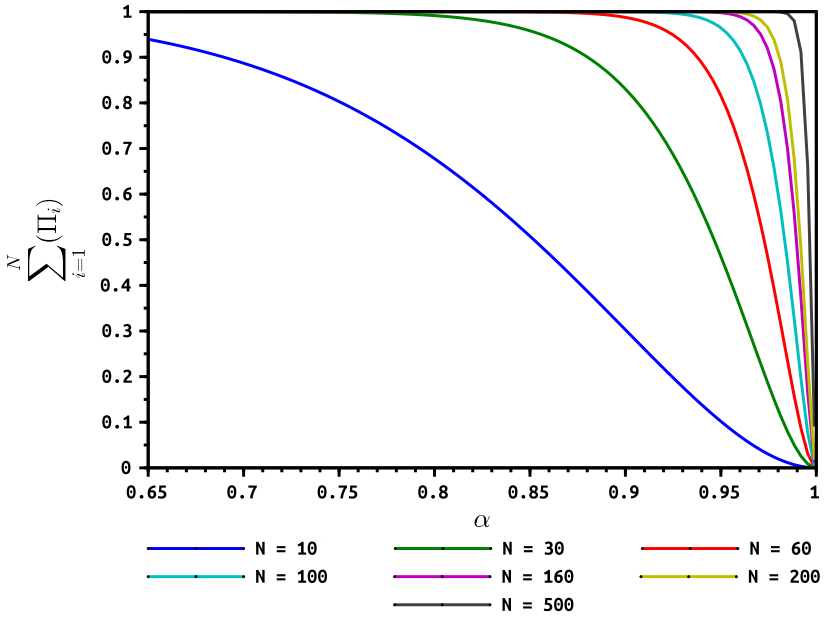

Figure 3.3: Sum of the mole fractions as a function of FTS α and the maximum carbon number

One solution is to normalize the ASF distribution, forcing the summation to unity, but this would produce a different distribution (by changing the slope of the ASF distribution); represented by a different value of FT α. Referring to Figure 3.3 again, note that the summation may also be pushed towards unity by increasing the maximum carbon number and thereby the carbon number range. This would preserve the distribution as defined by alpha; only adding more to the tail end of the curve. As shown in Figure 3.3, carbon numbers up to C_{30} are sufficient to describe alpha values below 0.68 if 4 decimal places of precision are required. Setting the limit at C_{60} will allow description of alpha values up to 0.82 with 4 decimal precision. At C_{160} and C_{200}, respectively, the alpha value limits are 0.93 and 0.94 for 4 decimal places of precision.

Any method where the solution is dependent upon an ASF distribution is susceptible to this kind of error. Moreover, given a product distribution that is ASF distributed,

truncating the polymer size range by considering too 'small' a subset of carbon numbers may result in a sizable portion of polymer being unaccounted for.

3.4.2. FTS Reactor Model

Modeling studies considering reaction kinetics together with phase equilibrium in FTS are scarce with studies by Visconti (2013), Mthombeni (2009), Visconti et al. (2007), Ahon et al. (2005) and van der Laan (1999) being the only ones identified. Mthombeni (2009) studied the effect of VLE on FTS through the development of a two phase, elementary, continuous slurry reactor model which was adapted from the work of Visconti et al. (2007) and van der Laan (1999). This model is able to account for real product distributions observed in FTS through elementary reaction kinetics and accounting for VLE using an embedded $\phi - \phi$ method; moreover, it does not depend upon ASF.

The reactor is assumed to be isothermal, isobaric and perfectly mixed with no heat or mass transfer limitations. Additionally, the vapor and liquid phase are assumed to be in thermodynamic equilibrium. Furthermore, heat and mass transfer limitations are ignored. VLE is coupled with kinetics by using the component activities rather than partial pressures in the elementary rate equations. This formulation is advantageous because the liquid and vapor fugacities will be equal at equilibrium and therefore the reaction kinetics will be phase independent. In the two phase model, Mthombeni (2009) defines the activity as shown in Equation 3.27.

The kinetic model is based on the carbide mechanism for the formation of products and the alkyl insertion mechanism for chain growth. The rate equations (Table 3.10) are formulated from elementary steps; so called because there is only a single transition state between the reactant and the product.

In reality there are at least four phases present in the slurry reactor: vapor, hydrocarbon liquid, aqueous and adsorbed phases. The model accounts for VLE between the vapor and a combined hydrocarbon-aqueous phase. The adsorbed phase which resides in the catalyst is accounted for via surface reactions. The kinetic model is independent of the number of phases present because the component fugacities at equilibrium are assumed to be the same for all phases.

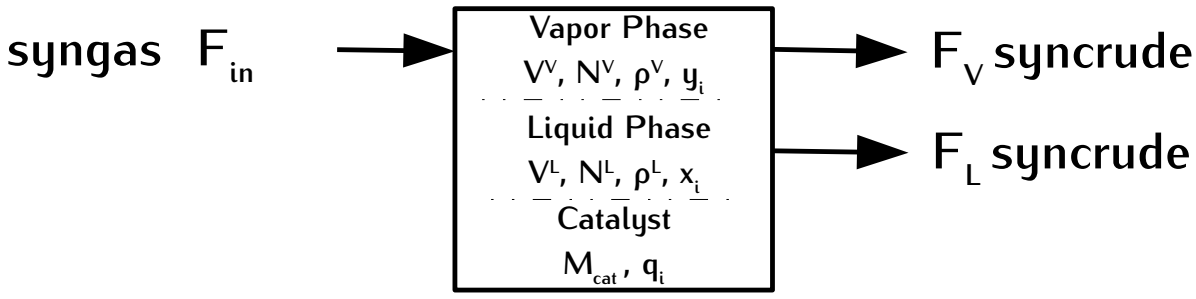

Figure 3.4: Fischer-Tropsch Synthesis reactor phase diagram, adapted from Mthombeni (2009)

The presence of water makes the liquid phase highly non-ideal which rules out the use of Raoult's Law. Phase equilibrium is handled using the $\phi - \phi$ method with PREOS and corrections for the alpha value by Twu et al. (1995) as described in Section 3.2. As a step towards truly multiphase operation the activity is used in the kinetics rather than concentration. The activity arises from the chemical potential for a mixture of ideal gases as shown in equation 3.26, where μ_i^0 is the chemical potential at a reference pressure p^0 (1 bar) and f_i is the species fugacity. The quotient in the log term of equation 3.26 is defined as the species activity α_i. Equation 3.27 shows an equivalent formulation where the activity is determined by taking the ratio of the component fugacity in the mixture with the pure component fugacity at 1 bar which will be close to unity. Equation 3.27 has been used to determine the activity. The fugacity can be determined from the fugacity coefficient as given by PREOS (Section 3.2) as shown in Equation 3.28.

$$\mu_i^{\Omega} = \mu_i^{\Omega,0} + RT\, ln\left(\frac{\bar{f_i}^{\Omega}(T,P,z)}{p^0}\right) \tag{3.26}$$

$$\bar{a_i}^{\Omega} = \frac{\bar{f_i}^{\Omega}(T,P,z_i)}{f_i^{\Omega}(T,P=1bar)} \tag{3.27}$$

$$\bar{f_i}^{\Omega} = z_i \overline{\phi}_i^{\Omega} P \tag{3.28}$$

The method used by Mthombeni (2009) involves assuming the initial vapor-liquid distribution and ramping up the feed from zero to the steady state flowrate. The contents of the reactor at the first time step are assumed to be an equimolar mixture of syngas, water and an ASF distributed series of paraffins and olefins. Henceforth, this will be referred to as the initial guess within this same context. The equations used by Mthombeni (2009)

Table 3.10: Fischer-Tropsch reaction mechanisms and rate equations, adapted from Mthombeni (2009).

Description	Reaction	Rate Equation
Surface reactions	$CO + 4H\theta \rightarrow H_2O + CH_2\theta + 3\theta$	$r_1 = k_1 \bar{a}_{CO} \theta_{H*}$
H_2 adsorption	$H_2 + 2\theta \rightarrow 2H\theta$	$r_2 = k_2 \bar{a}_{H_2} \theta^2$
Chain initiation	$CH_2\theta + H\theta \rightarrow CH_3\theta + \theta$	$r_3 = k_3 \theta_{CH_2} \theta_{H*}$
Methanation	$CH_3\theta + H\theta \rightarrow CH_4 + 2\theta$	$r_4 = k_4 \theta_{CH_3*} \theta_{H*}$
Chain growth (n=1,199)	$CH_2\theta + C_nH_{2n+1}\theta \rightarrow C_{n+1}H_{2n+3}\theta + \theta$	$r_5 = k_5 \theta_{CH_2*} \theta_{C_nH_{2n+1}*}$
β-dehydrogenation to olefins (n=2,200)	$C_nH_{2n+1}\theta \leftrightarrow C_nH_{2n} + H\theta$	$r_6 = k_{6f} \theta_{C_nH_{2n+1}*} - k_{6r} \bar{a}_{C_nH_{2n+1}} \theta_{H*}$
Hydrogenation to paraffins (n=2,200)	$C_nH_{2n+1}\theta + H\theta \rightarrow C_nH_{2n+2} + 2\theta$	$r_7 = k_7 \theta_{C_nH_{2n+1}*} \theta_{H*}$

took the form of a Differential Algebraic (DAE) system. As of Scilab 5.5.2, the language does not provide an interface to the DASPK 3.1 DAE system solver. The DASSL solver is available but struggles with problems of index greater than 1 such as the one tackled herein. A steady state assumption is made as shown in Equations 3.29 and 3.30. All time derivatives fall away due to the steady state assumption; the surface species equations reduce to Equation 3.33 which is based upon a pseudo steady state hypothesis (i.e. it is assumed that the active intermediates have a short lifetime due to their high reactivity and that they are present in low concentrations on the catalyst surface; therefore, the rate of formation of any surface species is perfectly balanced by the rate of reaction to other species); and finally, the volume balance is incorporated into the material balances and VLE Equation. This reduces to a system of $1 + 2*(2*N+5) + 1 + (N+2) + 1 = 5N+15$ equations. One overall material balance (Equation 3.30), $N+5$ species material balances, $N+5$ species VLE equations, 1 combined mole fraction summation, $N+2$ surface species rate balances and one site balance. This totals to $5N + 15$ equations with $5N + 15$ unknowns (x_i,y_i,q_j,$\dot{F}^V$,$\dot{F}^L$,θ_v).

$$0 = \dot{F}_{i,in} - x_i \dot{F}^L - y_i \dot{F}^V - \left(\sum_{k=1}^{NR} v_{i,k} r_k \right) M_{cat} \tag{3.29}$$

$$0 = \sum_{i=1}^{NS} \dot{F_{i,in}} - \dot{F}^L - \dot{F}^V - \sum_{i=1}^{NS} \left(\sum_{k=1}^{NR} v_{i,k} r_k \right) M_{cat} \tag{3.30}$$

$$y_i = \frac{\bar{\phi}_i^L}{\bar{\phi}_i^V} x_i = K_i x_i \tag{3.31}$$

$$0 = \sum y_i - \sum x_i \tag{3.32}$$

Table 3.11: Fischer-Tropsch Synthesis rate constants from Mthombeni (2009)

Constant	Value [$\mathbf{mol\ s^{-1}\ g_{cat}^{-1}}$]
k_1	0.1
k_2	$7.00k_1 \times 10^{-2}$
k_3	$2.42k_1 \times 10^{2}$
k_4	$2.18k_1 \times 10^{3}$
k_5	$1.56k_1 \times 10^{3}$
k_{6f}	$4.00k_1 \times 10^{0}$
k_{6r}	$6.00k_1 \times 10^{-7}$
k_7	$9.71k_1 \times 10^{1}$

$$r_j = \left(\sum_{k=1}^{NR} v_{i,k} r_k \right) \tag{3.33}$$

$$1 = \theta_v + \sum \theta_{j*} \tag{3.34}$$

This system of equations is solved using a Newton Method solver as supplied by Scilab's *fsolve* which requires a good initial guess in order to give meaningful answers. The solution is verified by checking the elemental balances. Instead fo embedding the VLE loop in the reactor function, a loop is used to iterate through gradually increasing conversions and the VLE is updated within this loop.

Since the rate constants are catalyst specific and the development of high conversion catalysts is still underway, the rate constants should not be regarded as fixed. The rate constants are adapted by Mthombeni (2009) from Visconti et al. (2007). The model developed by Mthombeni (2009) is capable of producing a dual alpha product distribution as well as the spectrum of positive and negative deviations seen in literature; however, it does not capture the C_2 anomaly commonly seen in real FTS product distributions. A sensitivity analysis of the rate constants led Mthombeni (2009) to conclude that high conversion and alpha values may be achieved with increased k1 and k5 rate constants which represent the rate of carbon monoxide adsorption (rate limiting step for surface reactions) and the rate of chain growth.

Table 3.12: Fischer-Tropsch Synthesis pseudo steady state rate balances

Active Intermediate	Rate of Reaction
$H\theta$	$0 = 4r_1 + 2r_2 - r_1 - r_4 + r_6 - r_7$
$CH_2\theta$	$0 = r_1 - r_3 - r_5$
$CH_3\theta$	$0 = r_3 - r_4$
$C_nH_{2n+1}\theta$ / $C_{n+1}H_{2n+3}\theta$	$0 = \sum_{n=1}^{198} r_{5,n} - \sum_{n=2}^{199} r_{5,n} - \sum_{n=1}^{198} r_{6,n} - \sum_{n=1}^{198} r_{7,n}$
$C_{200}H_{399}\theta$	$0 = \sum_{n=2}^{199} r_{5,n} - \sum_{n=1}^{198} r_{6,n} - \sum_{n=1}^{198} r_{7,n}$

In order to determine the surface concentrations for the initial guess an initial reactor state

is assumed. The reactor is assumed to contain wax and unreactive catalyst. The total number of moles in the reactor is assumed, from which the quantities of all species are calculated according to the following procedure. The mole fraction of carbon monoxide is specified and used to determine the hydrogen flow from a specified $H_2 : CO$ ratio (same as feed if available). The nitrogen composition in the reactor is assumed to be equal to that present in the feed that will be added to the reactor later. The remaining moles of feed are assumed to comprise of all the syncrude compounds and are distributed amongst the carbon numbers according to ASF with some specified alpha value (this value does not constrain the syncrude alpha value as shown in Section 5.3.1). Finally, for each carbon number, the moles of paraffins and olefins are determined using an assumed carbon-number-specific paraffin to olefin ratio. The variables in the Reactor function are expanded in Table 3.13. The reactor contents are flashed in order to give the vapor and liquid quantities, then the reactor is then solved with these contents assuming no catalyst activity. Then the initial surface concentrations θ_i are determined.

Table 3.13: Reactor function variables

Variable	Description	Scope
y_i	vapor phase mole fractions	$CO, H_2, H_2O, N_2, CH_4, C_nH_{2n+2}, C_nH_{2n}$
x_i	liquid phase mole fractions	$CO, H_2, H_2O, N_2, CH_4, C_nH_{2n+2}, C_nH_{2n}$
V	vapor phase total moles	-
L	liquid phase total moles	-
θ_i	surface concentrations	$\theta_H, \theta_{CH_2}, \theta_{CH_3}, \theta_{C_nH_{2n+1}}, \theta_V$

3.4.3. Product Distribution

It is necessary to calculate the chain growth probability from the product because the reactor model does not depend on ASF. Mthombeni (2009) noted that two alpha values were sufficient to describe the product distribution. The slope of the semi-logarithmic plot of the weight fraction of carbon in each component divided by the number of monomer units in a single component against carbon number will give the logarithm of the chain growth probability as can be seen in Equation 3.35. Equation 3.35 can be reformulated for ease of linear regression as shown in Equation 3.36. In order to determine the the alpha value between carbon numbers i and n the least squares fit can be performed ($x = A\backslash b$). This can also be done using mole fractions as the slope of the semi-logarithmic plot of the mole fraction of each components in the hydrocarbon product will also give the logarithm of the chain growth probability.

$$\frac{w_n}{n} = \alpha^{n-1}(1-\alpha)^2 \qquad \frac{d\, ln\left(\frac{w_n}{n}\right)}{dn} = ln\,(\alpha) \tag{3.35}$$

$$\begin{bmatrix} i & 1 \\ i+1 & 1 \\ i+2 & 1 \\ \vdots & \vdots \\ n & 1 \end{bmatrix} \begin{bmatrix} ln(\alpha) \\ intercept \end{bmatrix} = ln\left(\begin{bmatrix} \frac{w_i}{i} \\ \frac{w_{i+1}}{i+1} \\ \frac{w_{i+2}}{i+2} \\ \vdots \\ \frac{w_n}{n} \end{bmatrix} \right) \equiv Ax = b \tag{3.36}$$

3.5. Hydrocracker Model

For the WHC, the model by Le Grange (2009), specifically Model B, is used. Model B is based upon the following assumptions:

1. The reactor is isothermal and isobaric
2. There is no preferential absorption of hydrocarbons from liquid phase to the catalyst surface
3. The catalyst is always homogeneously wetted which ensures that the reaction always happens in pseudo reactive liquid phase with no reaction in gaseous phase
4. The vapor and liquid phases are always in equilibrium
5. There is no mass transfer limitations across the vapor-liquid phase boundary or in the catalyst pores
6. The β-scission cracking step is rate controlling
7. All the other kinetic steps are assumed to be fast or at equilibrium
8. All the reactions are first order with respect to the liquid phase

In the formulation used by Le Grange (2009), the liquid concentrations are used in the kinetics; however, as a step towards a truly multiphase model the kinetics have been defined in terms of the species activities α_i which are always defined even if there is no liquid present in the reactor. The activity is defined as the ratio of the liquid fugacity to the pure component fugacity at the reactor temperature which is the same as the formulation used in FTS (Equation 3.27).

$$K1 = k_{B1} + k_{B2} + 2k_C \tag{3.37}$$

$$K2 = k_A + k_{B1} + k_{B2} + k_C \tag{3.38}$$

The Model B kinetics are given in Table 3.14. Carbon numbers C_1 and C_2 do not crack because they fall below the minimum length required for β-scission to occur and since the minimum required carbon number for any type of β-scission (of the types accounted for: A, B1, B2, C) is C_7, C_2 or C_1 will not be formed during hydrocracking. Furthermore, C_3 is the smallest carbon chained formed through β-scission of C_6 which is reflected in the $2k_C$ term in the $j = 3$ rate equation in Table 3.14. Other than this, all carbon numbers from C_7 to C_N can form C_3 (and C_{i-3}) which is reflected in the $K1 \sum_{i=7}^{n} a_i$ term. To produce C_4 the

carbon number must at minimum be greater than 4 by 1 carbon (i.e. C_5); moreover, C_4 may also be produced from type A β-scission, hence the use of the K2 rate; and finally, C_4 may be produced through cracking at either end of the chain, hence the 2 in the $K2\sum_{i=j+4}^{n} a_i$ term. This same logic applies for all rates from j=8 to j=n. The $K1a_{j+3}$ term arises from the fact that only one C_4 can be produced from cracking of C_7 and this again applies to rates j=4 to j=n. The j=6 rate contains the negative term $-k_C a_j$ because C_6 can be cracked through type C β-scission to C_3 (note that only 1 unit of C_6 is cracked). The $-K1a_j$ in the j=7 rate equation is due to loss of C_7 from cracking to C_3 and C_4 and this same term is applied for rates from j=7 to j=n. In the case of C_8, the algebraic term $-((j-7)K2+K1)a_j$ captures the loss of C_8 through cracking to C_3, C_4 and so on for j=9 through to j=n.

Table 3.14: Hydrocracking Rates

Carbon Numbers	Rate
$j = 1, 2$	$r_j = 0$
$j = 3$	$r_j = K1\sum_{i=7}^{n} a_i + 2k_C a_6$
$j = 4, 5$	$r_j = 2K2\sum_{i=j+4}^{n} a_i + K1a_{j+3}$
$j = 6$	$r_j = 2K2\sum_{i=j+4}^{n} a_i + K1a_{j+3} - k_C a_j$
$j = 7$	$r_j = 2K2\sum_{i=j+4}^{n} a_i + K1a_{j+3} - K1a_j$
$j = 8 \rightarrow n-4$	$r_j = 2K2\sum_{i=j+4}^{n} a_i + K1a_{j+3} - ((j-7)K2 + K1)a_j$
$j = n-3$	$r_j = K1a_{j+3} - ((j-7)K2 + K1)a_j$
$j = n-2 \rightarrow n$	$r_j = -((j-7)K2 + K1)a_j$

Le Grange (2009) has provided a number of different sets of constants for different catalysts; however, these constants are concentration specific. When activities are used, the definition of the rate constants change and the values need to be adjusted accordingly. Instead of relating the rate constants to activity, it is simpler to find the rate constants that produce the desired product distribution by means of regression.

Figure 3.5 shows the algorithm for solving the WHC system. The main difference from the procedure used by Le Grange (2009) is the pre-hydrocracker which converts the olefins in the wax to paraffins (hydrogenation). In reality, this reaction occurs rapidly as wax enters the WHC. The procedure is also convenient because the Model B algorithm lumps all isomers into a single carbon number. The hydrogen requirement is determined and subsequently the pure paraffins enter into the hydrocracker reactor. The feed to the reactor is combined with the recycle stream (RC) if it is active. The VLE loop is equivalent to that described in Section 3.2. Using the fugacity coefficients from PREOS (Section 3.2),

the the activity is determined according to Equations 3.28 and 3.27. Following this, the kinetics from Table 3.14 are used to determine the rates R_i and then the ODE shown in Equation 3.39 is solved.

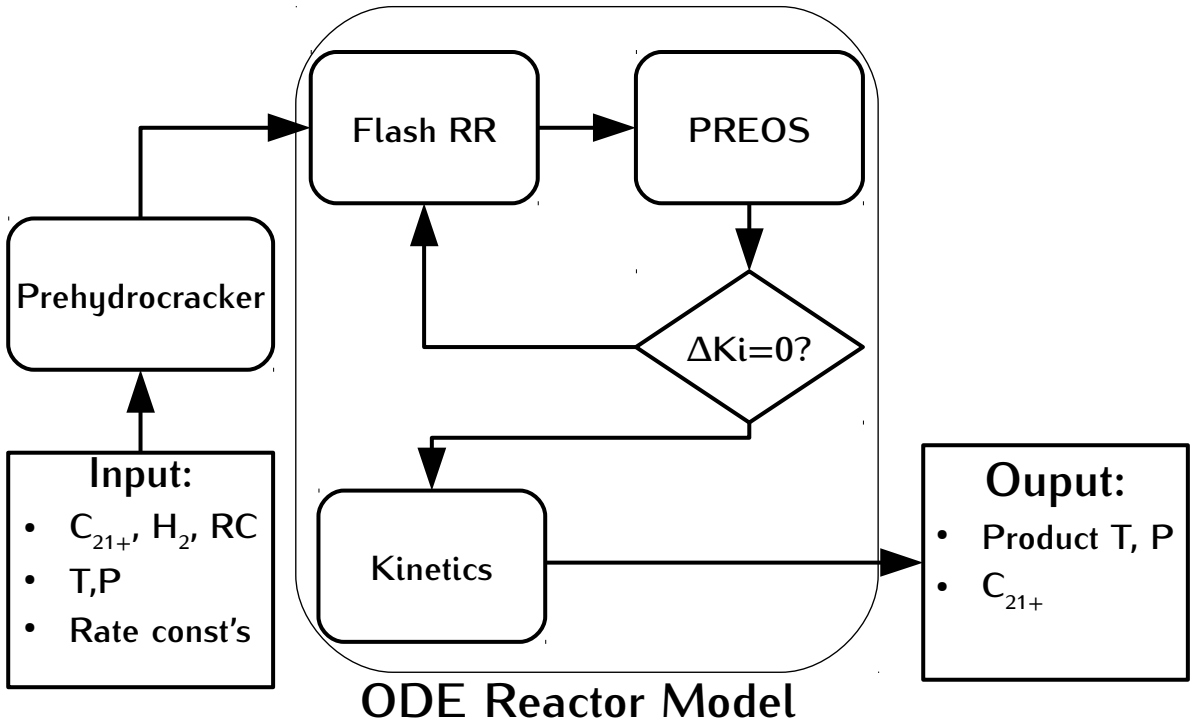

Figure 3.5: Model-B modified algorithm, adapted from Le Grange (2009)

$$dF = R_i M_{cat} \tag{3.39}$$

Two performance measures are used for the hydrocracker, the diesel yield and the $C_{23}+$ conversion, these are defined in Equations 3.40 and 3.41.

The diesel yield is defined as:

$$Y = \frac{\sum(Product\,carbon\,in\,diesel) - \sum(Feed\,carbon\,in\,diesel)}{\sum(Feed\,carbon\,in\,Cn > diesel)} \tag{3.40}$$

The $C_{23}+$ conversion is defined as:

$$Y = \frac{\sum(Carbon\,in\,Cn > C23\,in\,product) - \sum(Carbon\,in\,Cn > C23\,in\,feed)}{\sum(Carbon\,in\,Cn > C23\,in\,feed)} \tag{3.41}$$

3.6. Thermophysical Property Estimation

3.6.1. Group Contribution Method of Constantinou and Gani (1994)

Constantinou and Gani (1994) have introduced a thermophysical property estimation

method based on contributions by molecular groups. All the alkanes except methane can be described by the first order groups CH_3 and CH_2, so the method becomes relatively simple in application. The original method can predict; the normal boiling and melting points; critical temperature, pressure and volume; enthalpy of formation and vaporization; and the standard Gibbs Energy. Equation 3.42 shows the method for the first-order approximation. Refer to Appendix 9.1 for the contribution parameters and the correlations used. Experimental data is preferred for regression purposes since data generated by other methods may carry systemic bias Constantinou and Gani (1994). In terms of the Group Contribution Methods, the parameters are used as given in the original paper (Constantinou and Gani, 1994).

$$f(X) = \sum_i N_i C_i \tag{3.42}$$

3.6.2. Asymptotic Behavior Correlations

The n-paraffins and α-olefins can be referred to as a homologous series of compounds because, effectively, each member of the series differs from the others only in the number of monomer units. Given that the physical properties arise from the functional groups, the properties of a homologous series will become more similar as the number of monomer units increases for compounds containing the same number of monomer units (or equivalently, having the same carbon number). Therefore, the properties are interrelated and can be correlated as a function of carbon number. Furthermore, as the carbon number becomes large the degree of similarity will increase (Marano and Holder, 1997a).

Marano and Holder (1997a) have proposed generalized Asymptotic Behavior Correlations (ABCs) (Equations 3.43, 3.44 and 3.45) for the calculation of temperature independent properties of a homologous series of hydrocarbon compounds. These correlations are able to represent sigmoidal, linear and exponential dependencies (Marano and Holder, 1997a). They distinguish two types of behavior for hydrocarbon physical properties, Type I and Type II. Type I properties approach a finite property value as the number of monomer units in the molecules become large (a horizontal asymptote). Type II properties increase with carbon number by fixed increments and have different limiting values for different compounds of the same carbon number; however, the increment at the limit will be the same (Marano and Holder, 1997a) (neither horizontal nor vertical asymptote). Further justification arises from considering the difference between say a C_{100} and C_{101} paraffin which differ by a single $-CH_2-$ monomer unit; whose contribution will be small in comparison to the other 98 $-CH_2-$ monomers. Furthermore, the difference between a C_{100} alkane and alkene will be negligible because the vast majority of the molecule will be made up of $-CH_2-$ monomers. Therefore as the chain length increases it is expected that all isomers and chain lengths will give either the same value for the physical property or a value differing from the previous compound by the effect of a single monomer unit. This is the basis for the Type I and Type II properties. This limiting value or asymptote is the

same for all compounds of the same carbon number. This phenomenon was demonstrated experimentally for the normal boiling point of n-paraffins and α-olefins by Kreglewski and Zwolinski (1961). Table 3.15 shows the limiting behavior of some of the main physical properties of interest (Marano and Holder, 1997a,b,c).

$$Y = Y_\infty - \Delta Y_0 exp\left(-\beta\left(n \pm n_0\right)^\gamma\right) \tag{3.43}$$

$$Y_\infty = Y_{\infty,0} - \Delta Y_\infty \left(n - n_0\right) \tag{3.44}$$

$$n \geq n_0, \quad \beta > 0, \quad \gamma > 0 \tag{3.45}$$

Equation 3.43 gives the general formula for a Type I or II property Y or alternatively, a property function defined by Y. For Type I properties, Y_∞ is constant and ΔY_0 equals $Y_\infty - Y_0$ leaving n_0, Y_0, Y_∞, β and γ as adjustable parameters. Equation 3.44 is used for Type II properties where the limiting value Y_∞ is a linear function of carbon number. The sign in the $n \pm n_0$ term is negative unless the property increases with carbon number and exhibits positive curvature. In most cases, n_0 is less than 1 and it is the only parameter that differs between paraffins and olefins (or other members of the homologous series). The constraints given by equation 3.45 are necessary for convergence and asymptotic behavior (Marano and Holder, 1997a).

$$\begin{aligned} \triangle Y_0\left(p\right) &= \triangle Y_0\left(o\right) \\ Y_{\infty,0}\left(p\right) &= \triangle Y_{\infty,0}\left(o\right) \\ \triangle Y_\infty\left(p\right) &= \triangle Y_\infty\left(o\right) \\ \beta\left(p\right) &= \beta\left(o\right) \\ \gamma\left(p\right) &= \gamma\left(o\right) \end{aligned} \tag{3.46}$$

In general, temperature dependent properties for a specific compound are expressed by equations of the form shown in Equation 3.47. These equations provide poor estimates when extrapolated out of the temperature range for which they are correlated (Marano and Holder, 1997a). This is due to the fact that they are polynomials and may change concavity or inflect to produce all the graphical features native to such polynomials but not native to the properties they are attempting to describe. For example, if a cubic is used to describe a temperature dependent property that is only ever positive then it will extrapolate poorly outside the range it is correlated for because a cubic will always be negative for some value of T.

$$Y = A_1 f_1\left(T\right) + A_2 f_2\left(T\right) + \ldots + A_r f_r\left(T\right) \tag{3.47}$$

Marano and Holder (1997a) extend the method shown in Equation 3.47 to include carbon number by taking the parameters $Y_{\infty,0}$, ΔY_∞ and ΔY_0 to be functions of temperature

with dependence described by Equation 3.47. These correlations will certainly produce incorrect behavior if extrapolated outside of their region of applicability on the temperature scale; however, they should extrapolate relatively well on the carbon number scale.

$$Y = Y_{\infty,0}(T) - \Delta Y_{\infty}(T)(n - n_0) - \Delta Y_0(T)\, exp\left(-\beta (n \pm n_0)^{\gamma}\right) \tag{3.48}$$

$$\begin{aligned} Y_{\infty,0} &= A_{1\infty,0} f_1(T) + A_{2\infty,0} f_2(T) + \ldots + A_{r\infty,0} f_r(T) \\ \Delta Y_{\infty} &= A_{1\infty,0} f_1(T) + A_{2\infty,0} f_2(T) + \ldots + A_{r\infty,0} f_r(T) \\ \Delta Y_0 &= A_{10} f_1(T) + A_{20} f_2(T) + \ldots + A_{r0} f_r(T) \end{aligned} \tag{3.49}$$

$$\begin{aligned} A_1 &= A_{1\infty,0} - \Delta A_{1\infty}(n - n_0) - \Delta A_{10} exp\left(-\beta (n \pm n_0)^{\gamma}\right) \\ A_2 &= A_{2\infty,0} - \Delta A_{2\infty}(n - n_0) - \Delta A_{20} exp\left(-\beta (n \pm n_0)^{\gamma}\right) \\ &\vdots \\ A_r &= A_{r\infty,0} - \Delta A_{r\infty}(n - n_0) - \Delta A_{r0} exp\left(-\beta (n \pm n_0)^{\gamma}\right) \end{aligned} \tag{3.50}$$

The parameters n_0, β, γ, $A_{1\infty,0}$, $\Delta A_{1\infty}$, ΔA_{10}, ... , ΔA_{r0} 3.50 must be determined for the n-paraffins and α-olefins separately, while the remaining parameters are equal for paraffins and olefins. Where these equations are used, they are regressed against data from multiple temperatures over the temperature range of interest. Regarding the limits of Equations 3.47, Marano and Holder (1997a) constrained the first and second derivatives of the asymptote with respect to temperature to not change sign within the temperature range of interest. However, in this work the correlations of the form 3.47 have not been regressed outside of the range of applicability (the range is given in the ChemSep PCD data).

Table 3.15: Limiting behavior of the physical properties

Type I	**Type II**
Critical Temperature	Molar Volume
Critical Pressure	Molar Enthalpy
Normal Boiling Point	Molar Entropy
Surface Tension	Molecular Weight
Heat of Vaporization	Critical Volume
	Liquid Molar Volume
	Vapor Pressure
	Ideal Gas Enthalpy
	Free Energy of Formation
	Ideal Gas Heat Capacity
	Liquid Heat Capacity

The properties are regressed by taking the sum of the squares of the relative error between the calculated value and the value determined by the ChemSep PCD method as shown in Equation 3.51 (the objective function). The correlation constants are solved

for in order to minimize the objective function using a Quasi-Newton Method with the Broyden–Fletcher–Goldfarb–Shanno algorithm as supplied by Scilabs *optim* solver.

$$\sum_{i=1}^{N} (Y_{PCD} - Y)^2 \tag{3.51}$$

4. Process Synthesis

4.0.1. Process Configurations

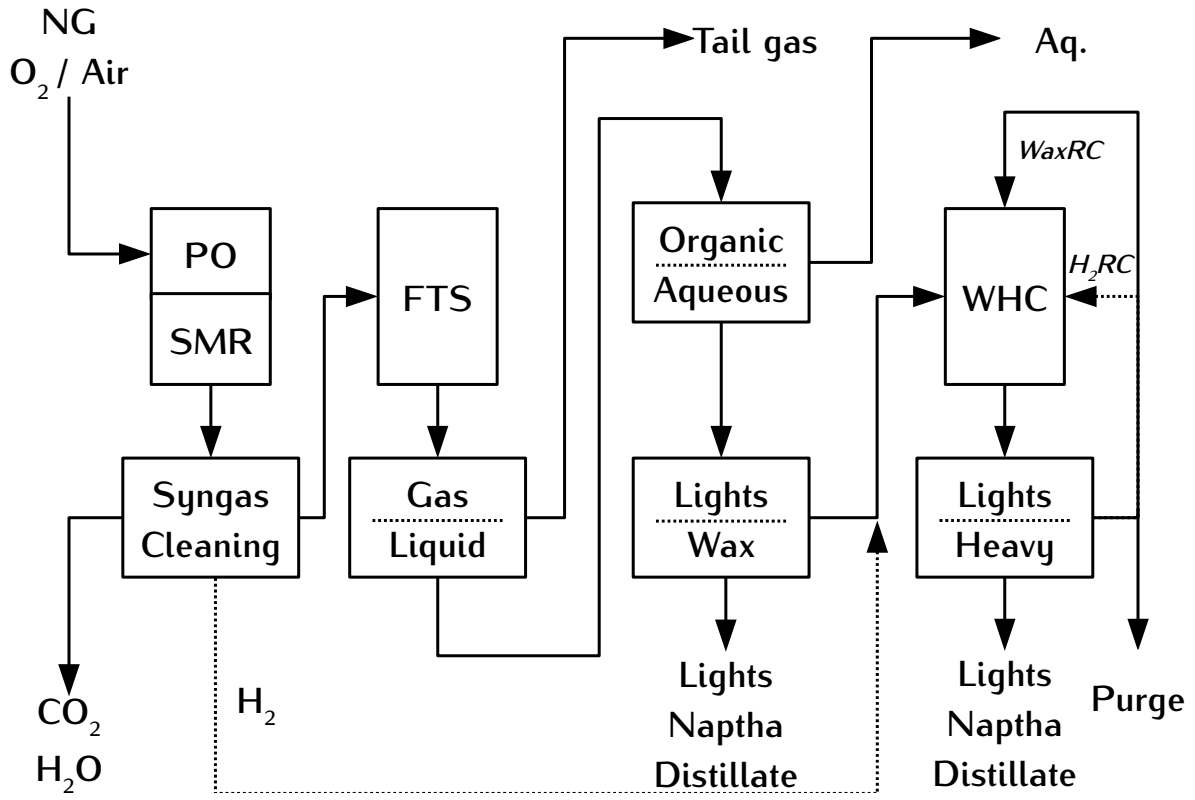

Figure 4.1: OOT/AOT configuration

Figure 4.1 shows the oxygen or air once through in FTS configuration ($OOT80$ or $AOT80$). Natural gas mixed with either oxygen (from the ASU) or air enters the ATR where it is converted to syngas at the correct $H_2 : CO$ ratio. The syngas is then stripped of the carbon dioxide, water and any acid gases before being routed to FTS. FTS is carried out through a single reactor in once-through mode. After FTS, the vapor and liquid are separated in a knockout stage, following which the organic and aqueous liquid phases are separated. Subsequently, the C_{21+} wax is separated from the light organic liquids. The wax is routed to the WHC where it is cracked to lighter compounds, the products from hydrocracking are separated into unreacted hydrogen, tail gas, light liquids, naptha and the primary product, distillate. The remaining C_{21+} wax bottoms from the separator is recycled back to hydrocracking with a fraction sent to the purge stream. The dotted line streams denote possible sources of hydrogen for the WHC; the unreacted hydrogen from the hydrocracker can be recycled back to the to WHC; additionally, excess hydrogen can be produced in the ATR by adding more steam.

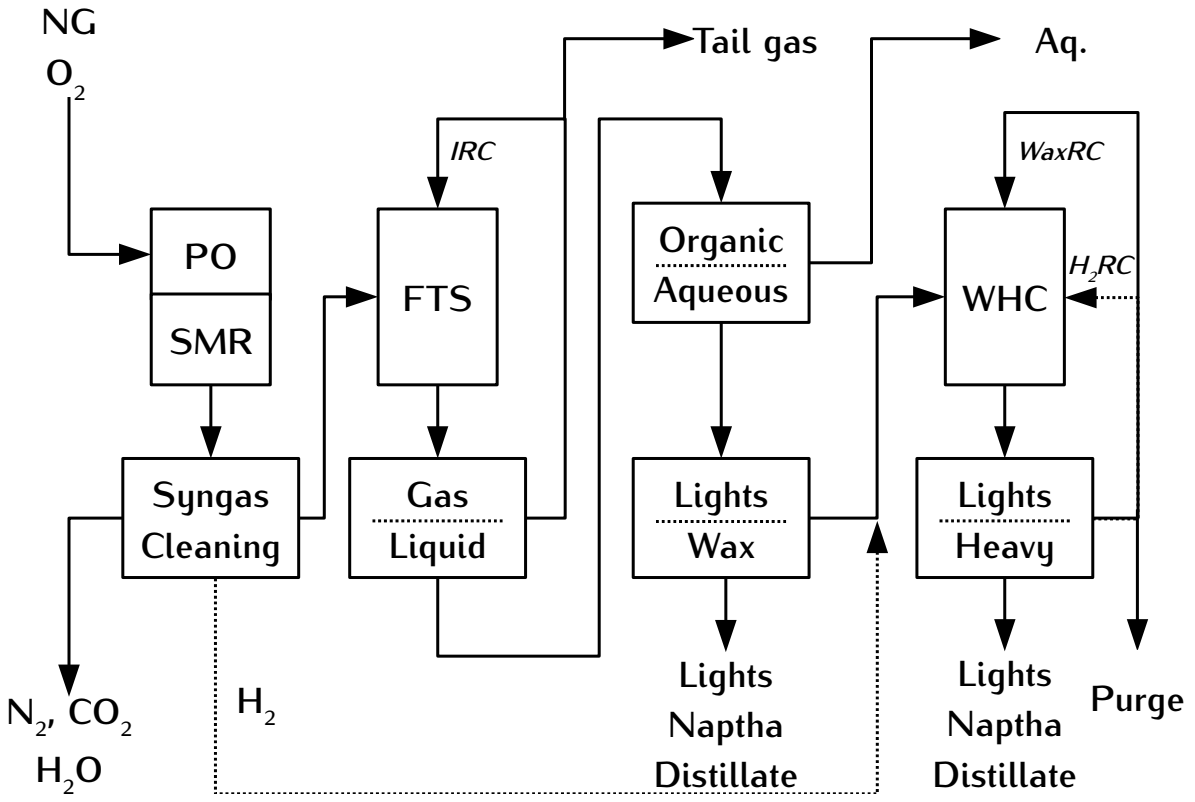

Figure 4.2: OIRC configuration with FTS tail gas recycle

Figure 4.2 shows the general flowsheet for the *OIRC*40 and *OIRC*60 configurations. Where *RC* stands for recycle and the preceding letter *I* signifies that the inter nal recycle is active and the succeeding number denotes the conversion in FTS. The conversion in FTS is taken to be 40% or 60% which is representative of conversions seen in literature. Using air instead of oxygen is not considered due to the high compression costs of recycling the nitrogen.

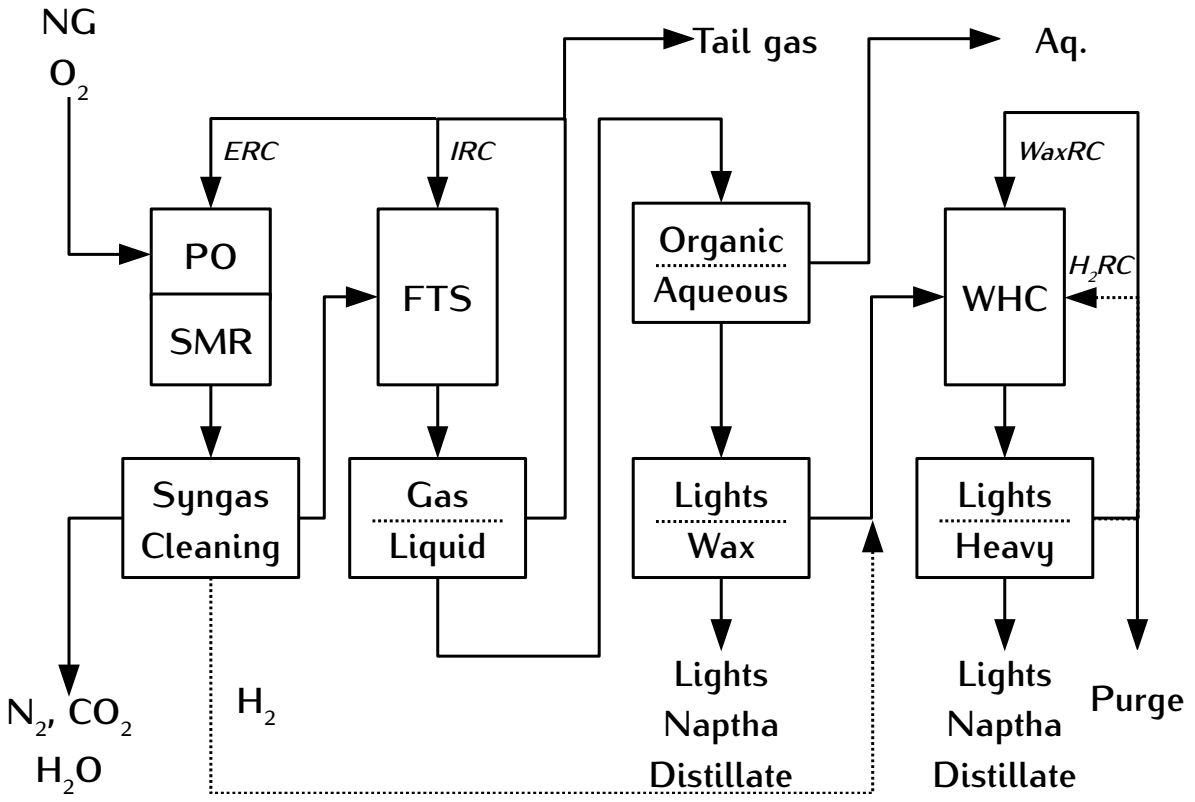

Figure 4.3: OERC configuration with tail gas recycle to FTS and the ATR

Figure 4.2 shows the general flowsheet for the *OERC*40 and *OERC*60 configurations. This configuration is the same as the previous general configuration except for the presence of the external tail gas recycle stream (ERC) from the Gas/Liquid separator to the ATR.

4.0.2. Recycle Streams

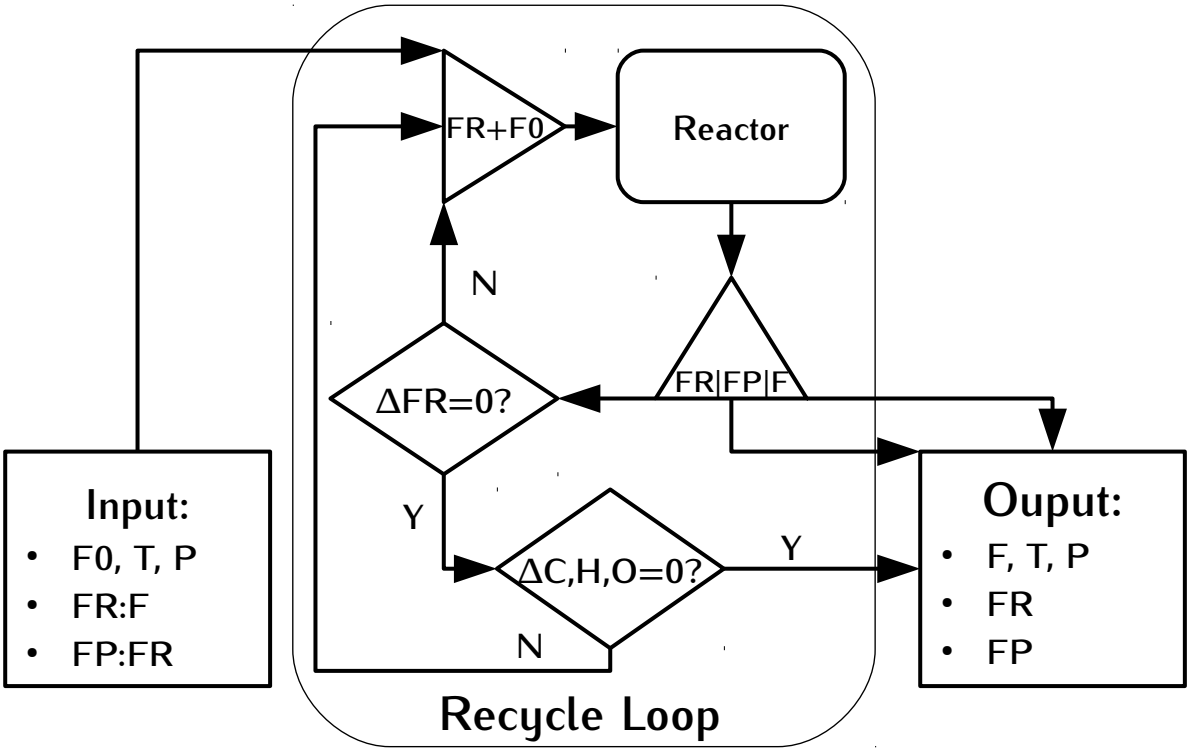

Figure 4.4: Recycle algorithm

There are three recycle streams in the process, the external FTS recycle (FTS-ERC), the internal FTS recycle (FTS-IRC) and the heavy wax recycle stream (WHC-RC). The algorithm for the recycle streams is shown in Figure 4.4. The FTS-IRC and the WHC-RC loops are converged as follows: the recycle stream is initialized as the feed stream multiplied by zero (or the cached stream from the previous solution), thereafter it is combined with the feed stream. The reactor model is then solved after which the product is partitioned into the recycle stream and another product stream by the recycle ratio. If there is a purge on the recycle it is partitioned off from the main recycle at this point. Subsequently, the partitioned recycle stream is checked against the old recycle stream to see if the change in total flowrate is greater than the tolerance, if this is not the case, the recycle stream is combined with the feed to restart the procedure. If the difference between the old and new total recycle flows is below the tolerance, then the overall elemental balances are checked between the original feed stream, the purge stream and the product stream after partitioning. If each balance falls below the tolerance, then the recycle loop is considered to have converged. The method of converging the FTS external recycle stream is the same except that the procedure is nested within itself, as if the reactor in Figure 4.4 were replaced with the internal recycle loop.

5. Model Validation and Sensitivity

5.1. Thermophysical Properties

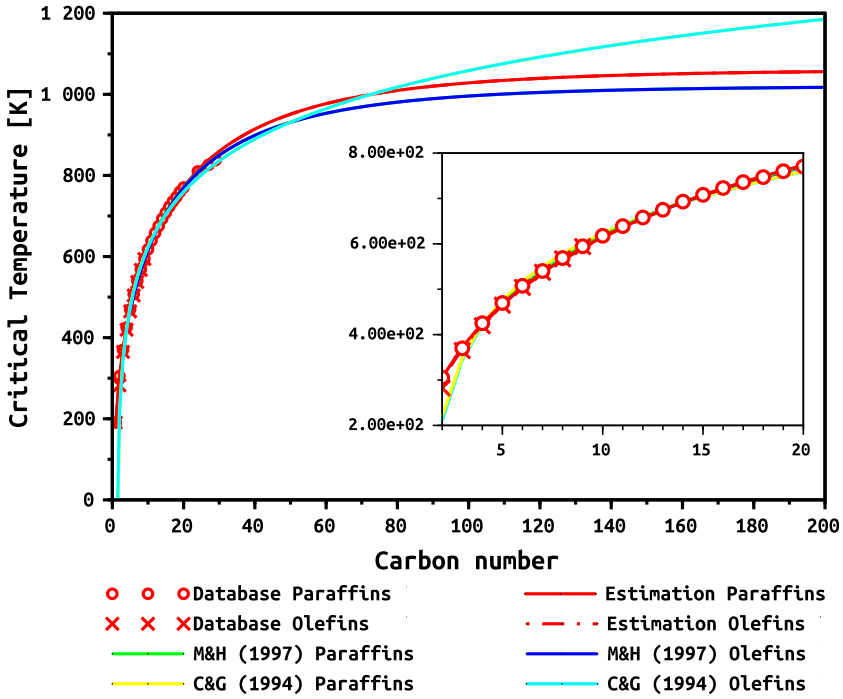

Figure 5.1: Critical Temperature

Table 5.1: Legend key for Figure 5.1

Legend Item	Definition
M&H 1997	Marano and Holder (1997)
C&G 1994	Constantinou and Gani (1994)

The results of the property estimation for critical temperature are shown in Figure 5.1 along with the results of the critical temperature estimation by Marano and Holder (1997b), the Group Contribution Methods of Constantinou and Gani (1994) and the Chem-Sep PCD data. With regard to the legend, the 'Database' curves are for the PCD data. The 'Estimation' curves are for the results of the estimation carried out using the ABCs and the PCD data and as shown in the Table 5.1, the 'M&H (1997)' curves represent the critical temperature estimations carried out by Marano and Holder (1997a). The 'C&G 1994' curves represent the application of the Group Contribution Method of (Constantinou and Gani, 1994). The Group Contribution Method has been applied according to Equations 5.1 and 5.2 where $tc0 = 181.128$, $t_{c1,CH_3} = 1.6781$, $t_{c1,CH_2} = 3.4920$ and $t_{c1,CH_2=CH} = 5.0146$ (Constantinou and Gani, 1994). Both the paraffin and olefin data are plotted for all curves in Figure 5.1; however, due to the overlap of the curves it may not

be possible to distinguish one from another (the same applies to all succeeding figures in this section).

$$T_{c,P} = tc0\, log\,[2t_{c1,CH_3} + (n-2)t_{c1,CH_2}] \tag{5.1}$$

$$T_{c,O} = tc0\, log\,[t_{c1,CH_2=CH} + t_{c1,CH_3} + (n-3)t_{c1,CH_2}] \tag{5.2}$$

The critical temperature of both paraffins and olefins approaches the same finite value as the carbon number is increased which is characteristic of a Type I property (Marano and Holder, 1997a). This is reflected in 'Estimation' and 'M&H (1997)' curves in Figure 5.1. However, due to the mathematical formulation of the Group Contribution Method the critical temperature increases indefinitely as a byproduct of applying a logarithmic function dependent on an ever increasing carbon number. This is a major obstacle to applying the Group Contribution Method in its current state. As carbon number approaches C_∞, the same critical temperature is approached (the limiting value) for both paraffins and olefins since they are part of the same homologous series. The ABCs in Equation 3.43, have been applied in both the 'Estimation' and M&H (1997) cases. The PCD data serve in the place of experimental data in the regression of the parameters for the ABCs. It is recognized that the PCD data may sometimes be derived from other property estimation methods but given that Marano and Holder (1997a) have a used a comparably limited dataset (limited in terms of carbon number range: C_1 to C_{18} paraffins), the estimations carried out in this work are favored for further use. The PCD dataset displayed unexpected deviations in the C_{21} to C_{29} paraffin data. These discrepancies may be attributed to the inclusion of data derived by different methods and have been removed. All the methods provide a good fit with the PCD data for carbon numbers less than C_{20}. The accuracy of the correlation for low carbon numbers is not necessarily indicative of the accuracy of the extrapolated values because the correlations allow for some freedom in the value of the asymptote, while still maintaining a good fit in the low carbon number region Marano and Holder (1997a). This is exemplified by Figure 5.1 where all correlations give a good fit for the available PCD data but show a appreciable difference in asymptotes. The discrepancy in the limiting value between the two ABCs cases can be attributed to differing experimental datasets. Siepmann et al. (1993) report a critical temperature of 930±10K for a C_{48} paraffin from molecular simulations. In comparison, the estimated values are 945K, 926K and 924K for (the Estimation, M&H and C&G paraffins, respectively).

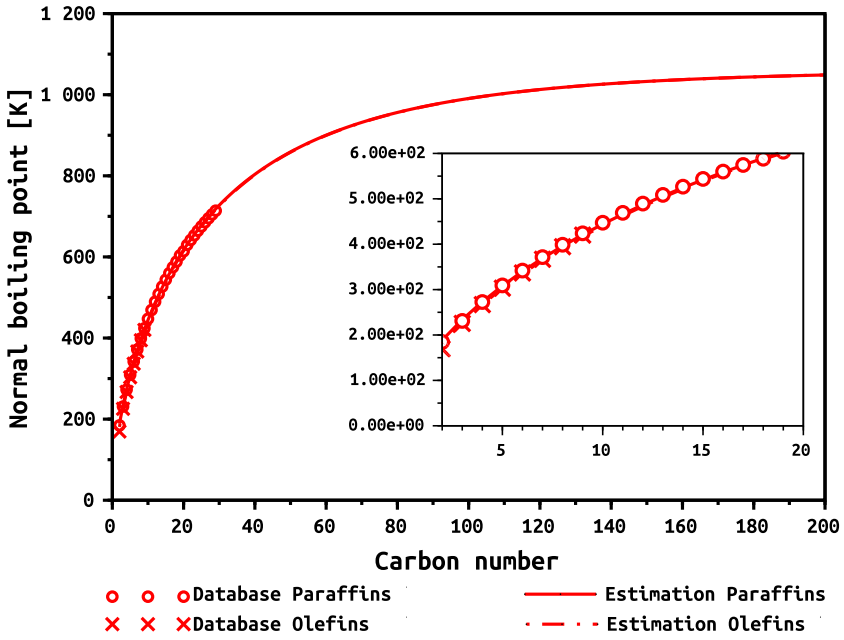

Figure 5.2: Normal Boiling Point

Critical Temperature is expected to approach the normal boiling point (Figure 5.2) for high carbon numbers Marano and Holder (1997a). The critical temperature shows a maximum of 1060K and normal boiling point shows a maximum value of 1061K (both as given by Y_∞). Since the parameter determining the asymptote, Y_∞ in Equation 3.43 is unknown, the regression procedure could be carried out for both critical temperature and normal boiling point concurrently with the constraint that Y_∞ be the same for both; however, this was not done in this case. The fit for the Normal Boiling point estimation in Figure 5.2 is good in the low carbon number range and given that the asymptote matches closely with that for the critical temperature, these estimations are regarded as accurate over the the carbon number range C_1 to C_{200}.

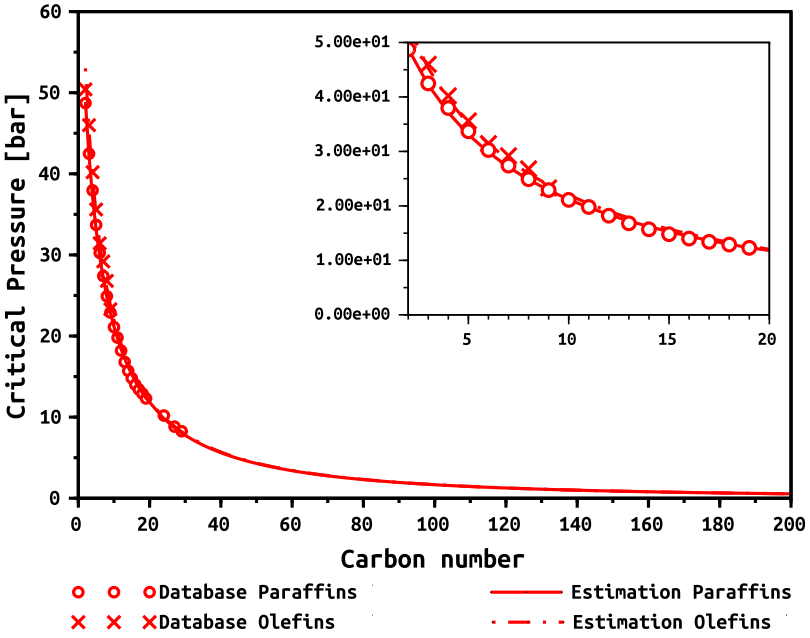

Figure 5.3: Critical Pressure

The critical pressure estimations are shown in Figure 5.3. When Y_∞ is unfixed the limiting value is 4.8 bar as opposed to the value of 0 derived from Lattice Fluid Theory (Marano and Holder, 1997b). Marano and Holder (1997b) have constrained the critical pressure to 1.01 bar at the carbon number where the critical temperature and normal boiling point curves intersect. This is an example of ensuring self consistency in the estimated value through forcing correct interrelations of properties as dictated by theory. However, these two properties are only expected to really intersect at C_∞. In the case of the Estimations, the limiting value has been constrained to zero in line with the aforementioned prediction by Lattice Fluid Theory.

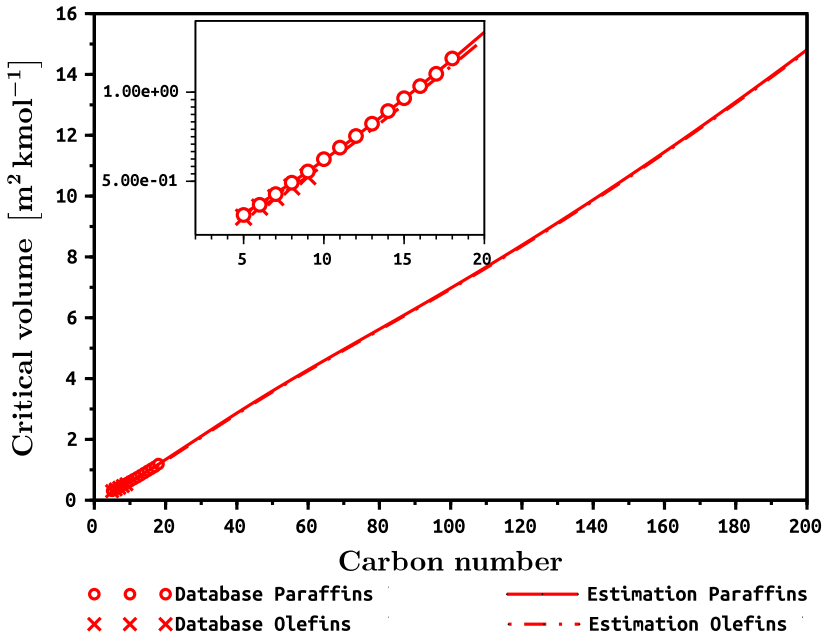

Figure 5.4: Critical Volume

Figure 5.4 shows the results of the critical volume estimation. Marano and Holder (1997a) have used the Type II correlation with the sign of the ± term in Equation3.43 as negative. The Estimation has been constrained to approach the same limiting value as that determined by Marano and Holder (1997a) which is informed by recommended critical density values from literature and molecular simulation.

The critical compressibility factor provides some insight into the validity of the other critical properties since it may be related to the critical temperature and critical pressure through Equation 5.3. If experimental data for Z_C is available, the compressibility factor may be regressed using ABCs; however, this alone does not ensure self consistency in the correlations.

$$Z_{c,i} = \frac{p_{c,i} V_{c,i}}{R T_{c,i}} \tag{5.3}$$

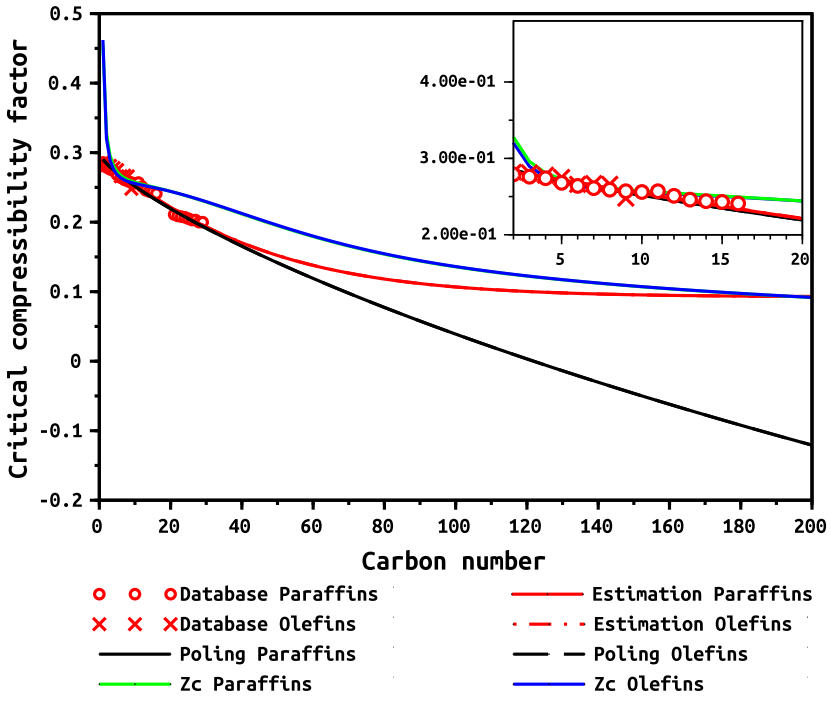

Figure 5.5: Critical Compressibility

Figure 5.5 shows the results of applying equation 5.3 with the critical properties supplied by the Estimations. Major deviations are observed in the sub C_4 region. The large starting value is due to the inaccuracy of these methods for predicting the properties of methane. In all the property database used in the plant modeling, the PCD data for methane has been used instead. Due to the fact that the critical pressure approaches zero, the critical compressibility factor should have an asymptote at zero making it a Type I property. However, according to lattice fluid theory the limiting value of the critical compressibility factor should be 1/3 Marano and Holder (1997b). This limiting value raises questions about the accuracy of the data used here (Database/PCD data) since even the low carbon number compounds show critical temperatures exceeding this value.

The theoretical formulation of the accentric factor suggests that the critical compressibility factor should be less than 0.291 for compounds with $T_c > 100\,K$ Poling et al. (2001). The critical temperature of methane is $187\,K$ according to the Estimations; therefore, this rule is expected to apply for all paraffins and olefins. It does indeed apply for the PCD database values for the Estimations and for Equation 5.4, but not for those calculated from Equation 5.3 because of methane and the C_2 compounds. Poling et al. (2001) recommend checking the critical compressibility factor against Equation 5.4. This check seems to show valid estimations for sub C_{25} compounds; however, for higher carbon numbers it quickly trails off and becomes negative beyond C_{100} which is unacceptable. It is likely that Equation 5.4 is not derived for long chain hydrocarbons. However, if 5.4 were accurate for high carbon numbers, it could be used to constrain the limiting accentric factor. The Z_c predicted would be Type I property because the accentric factor is also Type I property. If it is assumed that Z_c in Equation 5.4 is zero for large n, this would yield a maximum

accentric factor of 3.6375. If Z_c for large n is 1/3 (as predicted by Lattice Fluid Theory), the maximum accentric factor would be -0.53 which does not make sense. Given these difficulties, Equation 5.4 has not been used to constrain the accentric factor.

$$Z_c = 0.291 - 0.080w \tag{5.4}$$

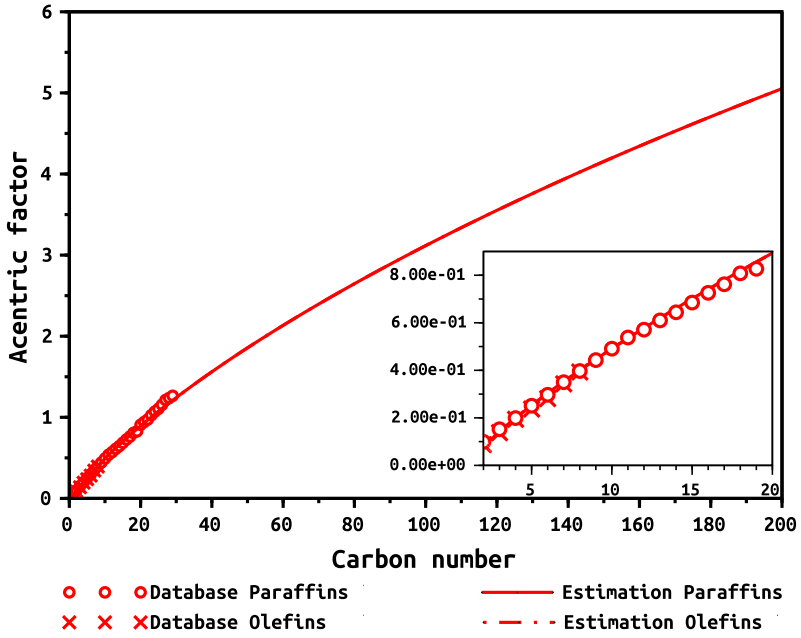

Figure 5.6: Accentric Factor

The definition of the accentric factor is given in Equation 5.5. Where T_r is the reduced temperature and $P_{vap,r}$ the reduced vapor pressure, relative to the critical values. Since the vapor pressure can be directly measured, the accentric factor is nominally calculated using Equation 5.5. However, in the Estimations the accentric factor has been directly correlated from the PCD data using the ABCs as shown in Figure 5.6.

$$\omega = -log_{10}\left[lim_{(T/T_c)=0.7}\left(P_{vap}/P_c\right)\right] - 1.000 \tag{5.5}$$

Figure 5.6 will go on to yield a maximum accentric factor of ~ 18. Due to the formulation of the accentric factor used by Marano and Holder (1997b) as shown by Equation 5.6, the accentric factor would increase indefinitely and be neither Type I nor Type II since the the curve would neither approach a horizontal asymptote nor a constant slope with increasing carbon chain length. Judging by the formulation of the accentric factor given in 5.5, a logarithmic increase would be expected since P_c approaches a finite value and P_{vap} approaches zero for this homologous series.

$$\omega = \Delta\omega_0 + \beta(n - n_0)^\gamma \tag{5.6}$$

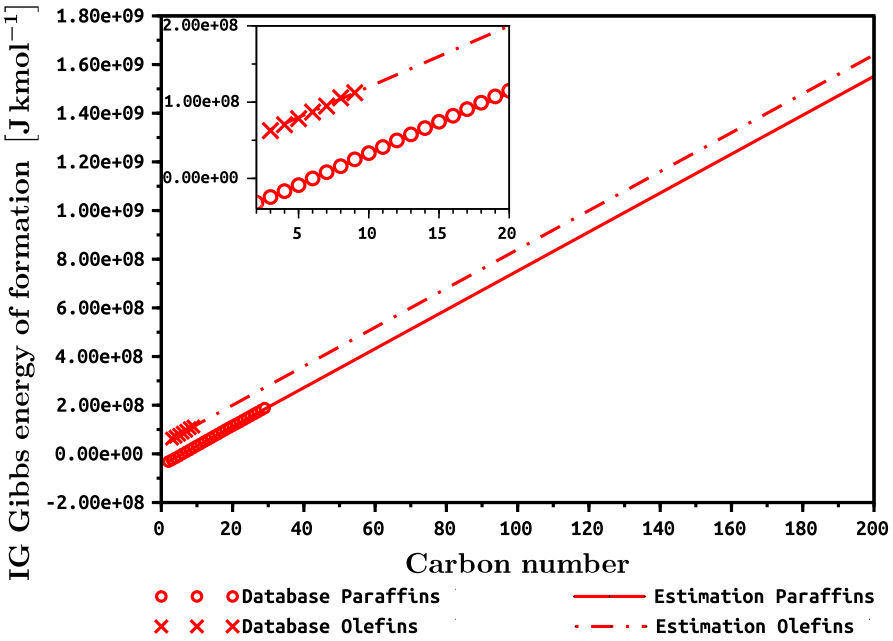

Figure 5.7: Ideal Gas Gibbs Energy of Formation

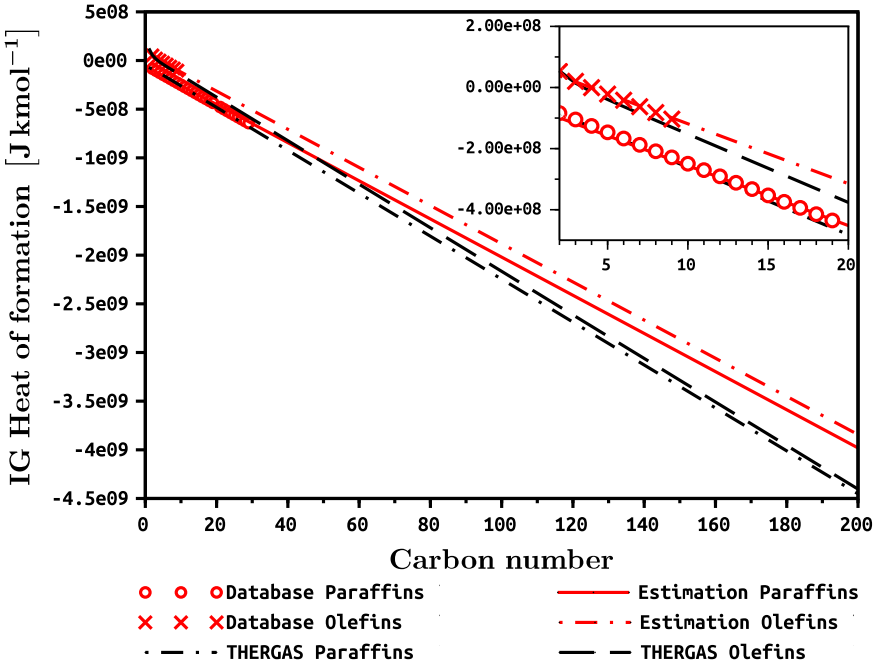

Figure 5.8: Ideal Gas Heat of Formation

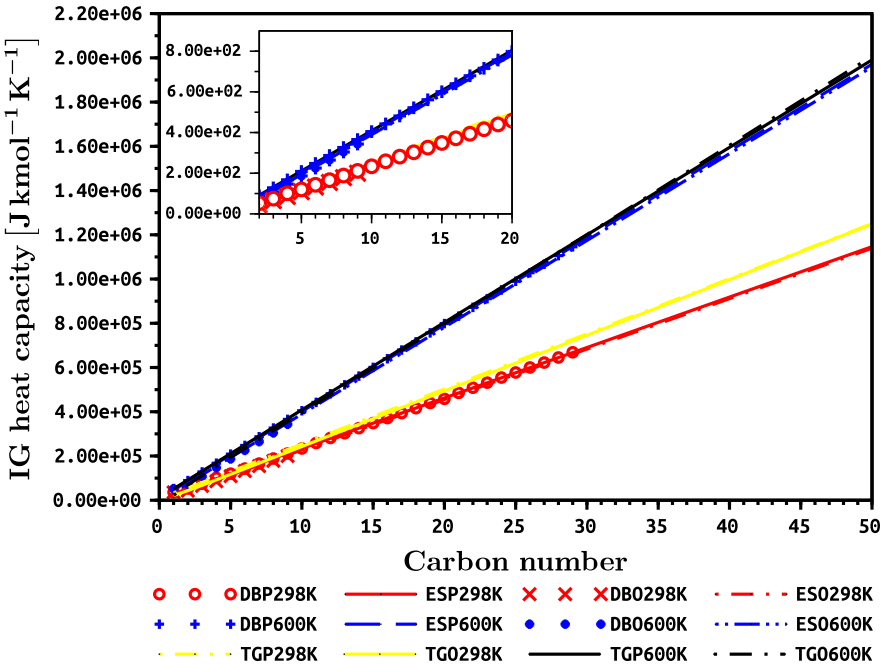

Figure 5.9: Ideal Gas Heat Capacity

Table 5.2: Legend key for Figure 5.9

Legend Item	Definition
DBP<temperature>	Database property value for parafins at <temperature>
DBO<temperature>	Database property value for olefins at <temperature>
ESP<temperature>	Estimated property value for parafins at <temperature>
ESO<temperature>	Estimated property value for olefins at <temperature>
TGP<temperature>	THERGAS property value for parafins at <temperature>
TGO<temperature>	THERGAS property value for olefins at <temperature>

The ideal gas properties are expected to all be Type II properties Marano and Holder (1997c). With regard to Figures 5.7 and 5.8, it is noted that in all cases, the difference between the paraffin and olefin curve appears to diminish with increasing carbon number; however, this is only the case for the estimations made using information from THERGAS (T paraffins and olefins). The justification for no diminishing difference can also be derived conceptually since the paraffin and olefin data will always be separated by the difference between the heat of formation of the $-H_2C = CH-$ group and the $CH_3 - CH_2-$ group which is constant.

The ideal gas heat capacity Estimations and THERGAS estimations are in close agreement over the given range for sub C_{20} carbon numbers but deviation is seen at high temperature. The results are compared in Figure 5.9 for temperatures 298K and 600K which demonstrate a good fit over a temperature range applicable to conditions seen in XTL processes.

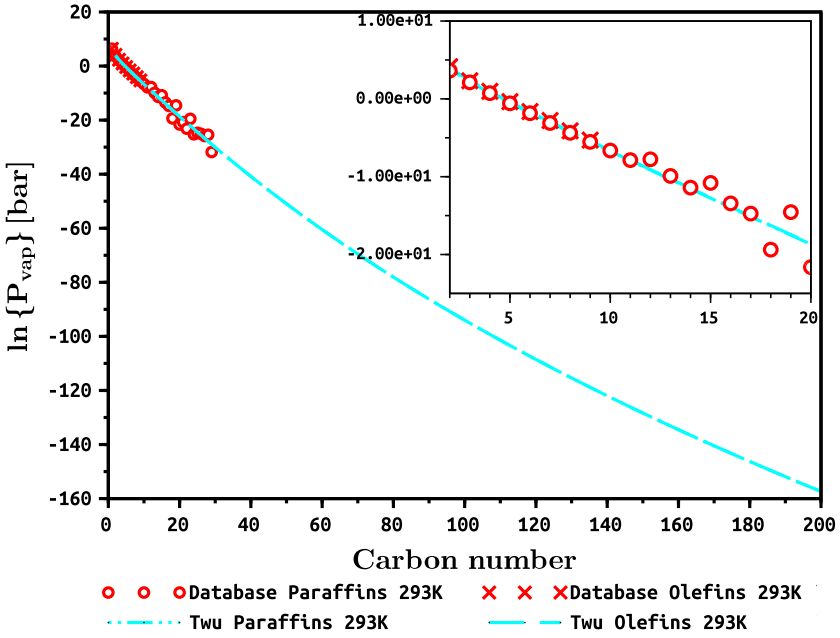

Figure 5.10: Vapor Pressure

Table 5.3: Legend key for Figure 5.10

Legend Item	Definition
Twu <compound> <temperature>	Twu et al. (1994)

The results of the vapor pressure estimation are shown in Figure 5.10. The vapor pressure follows a trend of exponential decay; therefore, its logarithm can be represented by the Type II correlation.

Twu et al. (1994) have proposed a vapor pressure equation capable of accurate estimation over a wide range of reduced temperatures. The correlation is a modification of a correlation by Pitzer (1955); Pitzer et al. (1993); Pitzer and Curl Jr (1957) and the Wagner equation and is given in Equations 5.7, 5.8 and 5.9. The results of applying this correlation are shown in Figure 5.10 and even though there is no relation between the PCD data (as far as is evident), the correlation shows a good fit.

$$ln\ P_r = ln\ P_r^{(0)} + \omega ln\ P_r^{(1)} \tag{5.7}$$

$$ln\ P_r^{(0)} = \frac{1}{T_r}\left[-5.96346\,(1-T_r) + 1.17639\,(1-T_r)^{1.5} - 0.559607\,(1-T_r)^3 - 1.31901\,(1-T_r)^6\right] \tag{5.8}$$

$$ln\ P_r^{(1)} = \frac{1}{T_r}\left[-4.78522\,(1-T_r) + 0.413999\,(1-T_r)^{1.5} - 8.91239\,(1-T_r)^3 - 4.98662\,(1-T_r)^6\right] \tag{5.9}$$

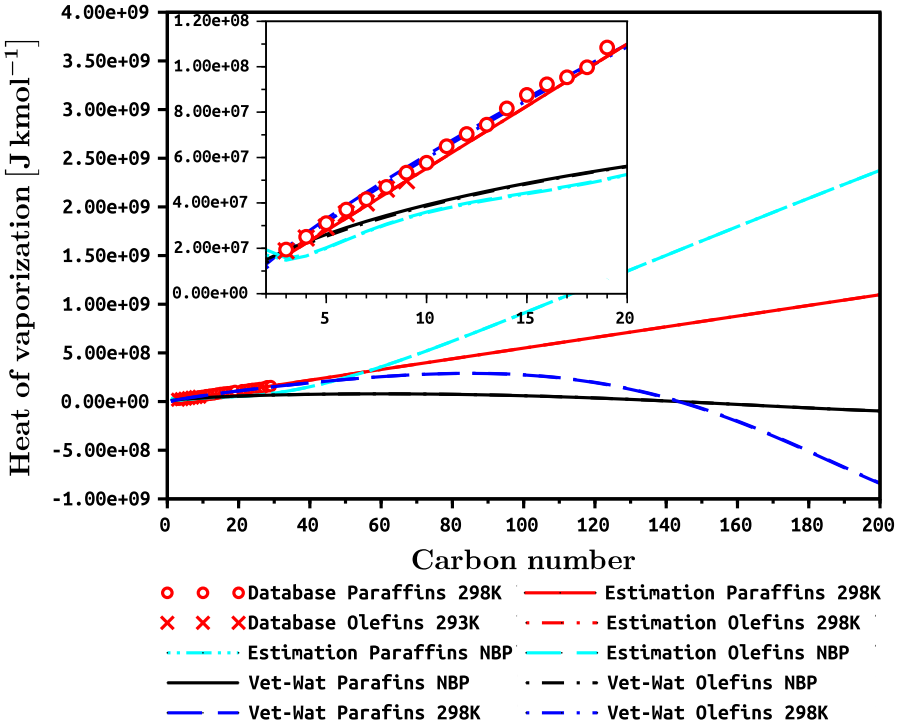

Figure 5.11: Heat of Vaporization at 298K and at the normal boiling point with comparison to Marano and Holder (1997c)

Table 5.4: Legend key for Figure 5.11

Legend Item	Definition
Vet-Wat <compound> NBP	Vetere (1995) and Watson relation at normal boiling point
Vet-Wat <compound> 298K	Vetere (1995) and Watson relation at 298K

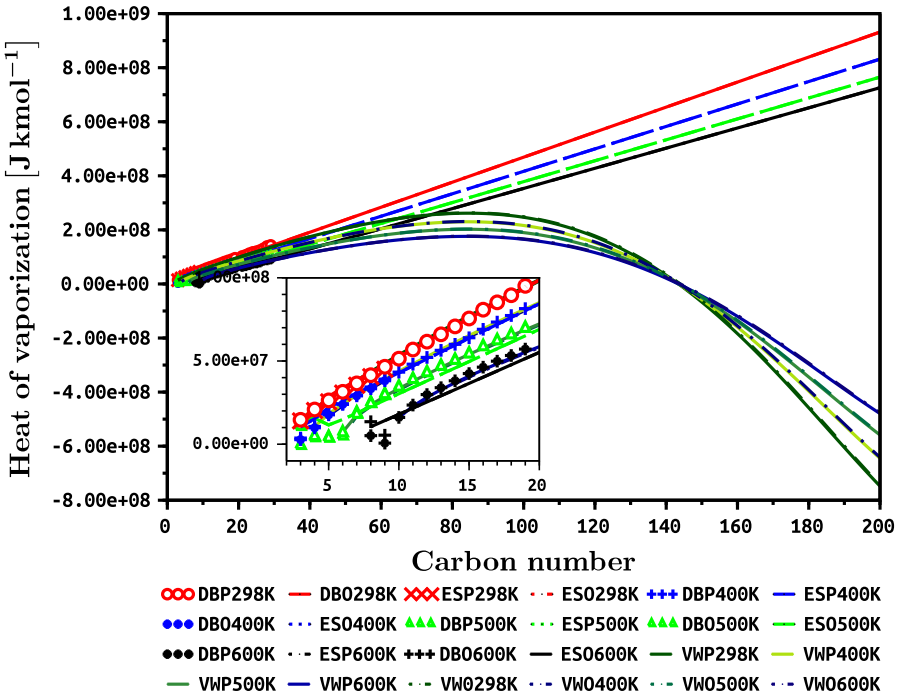

Figure 5.12: Heat of Vaporization at various temperatures

Table 5.5: Legend key for Figure 5.12

Legend Item	Definition
DBP<temperature>	Database property value for parafins at <temperature>
DBO<temperature>	Database property value for olefins at <temperature>
ESP<temperature>	Estimated property value for parafins at <temperature>
ESO<temperature>	Estimated property value for olefins at <temperature>
VWP<temperature>	Vetere (1995) and Watson for parafins at <temperature>
VWO<temperature>	Vetere (1995) and Watson for olefins at <temperature>

Figures 5.12 and 5.11 show the results of the estimation of the heat of vaporization at $298K$ and at the normal boiling point. Judging by Figure 5.12, the fit to the PCD data is good over a wide range of temperatures; however, when compared with the regressions of Marano and Holder (1997c), there are some discrepancies. The heat of vaporization at the normal boiling point is expected to show the same limiting trend observed by Marano and Holder (1997c). Estimations have been carried out using Equation 5.10 and Equation 5.11. The Type II relations did not produce the correct behavior at the normal boiling point as shown in Figure 5.11 and therefore the estimations of Equation 5.10 are used.

The enthalpy of vaporization at the normal boiling point may be determined using the correlations from Vetere (1979, 1995) shown in Equation 5.10. The latent heat of vaporization is zero at the critical point Poling et al. (2001).

$$\Delta H_{vb} = RT_b \left(1 - T_{br}\right)^{0.38} \frac{\left(ln\ P_c - 0.513 + 0.5066/\left(P_c T_{br}^2\right)\right)}{1 - T_{br} + \left(1 - \left(1 - T_{br}\right)^{0.38}\right) ln\ T_{br}} \tag{5.10}$$

The Watson relation show in Equation 5.11 is then used to determine the heat of vaporization at other temperatures by regressing the a and b values in the power. The value of the power term is usually taken as 0.38. However, more complex relationships are commonly required for an accurate fit such as the one shown here.

$$\Delta H_{v2} = \Delta H_{v1} \left(\frac{1 - T_{r2}}{1 - T_{r1}}\right)^{a + b(1 - T_{r2})} \tag{5.11}$$

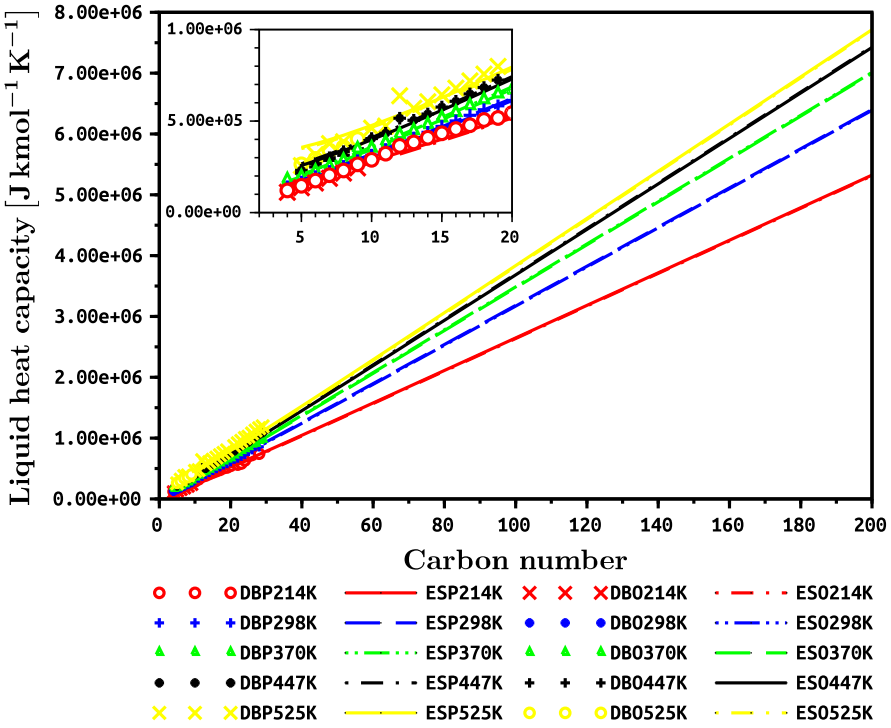

Figure 5.13: Liquid Heat Capacity

Table 5.6: Legend key for Figure 5.13

Legend Item	Definition
DBP<temperature>	Database property value for parafins at <temperature>
DBO<temperature>	Database property value for olefins at <temperature>
ESP<temperature>	Estimated property value for parafins at <temperature>
ESO<temperature>	Estimated property value for olefins at <temperature>

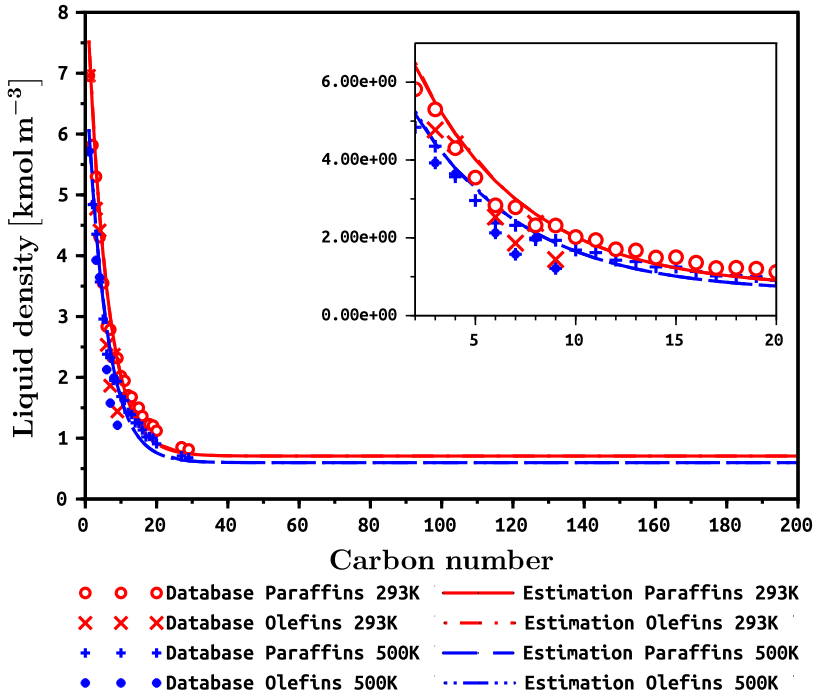

Figure 5.14: Liquid Density

Figure 5.13 shows the results of the estimation of liquid heat capacity for various temperatures. As with the ideal gas heat capacity, we expect the liquid heat capacity to follow a linear trend.

Figure 5.14 shows the results of the estimation of liquid density. Since Liquid Molar Volume is a Type II property, density is therefore a Type I property so a horizontal asymptote is expected. Furthermore, since the liquid volume is a Type II property that increases indefinitely with increase in carbon number, the density is expected to approach a limiting value of zero.

5.2. Reformers

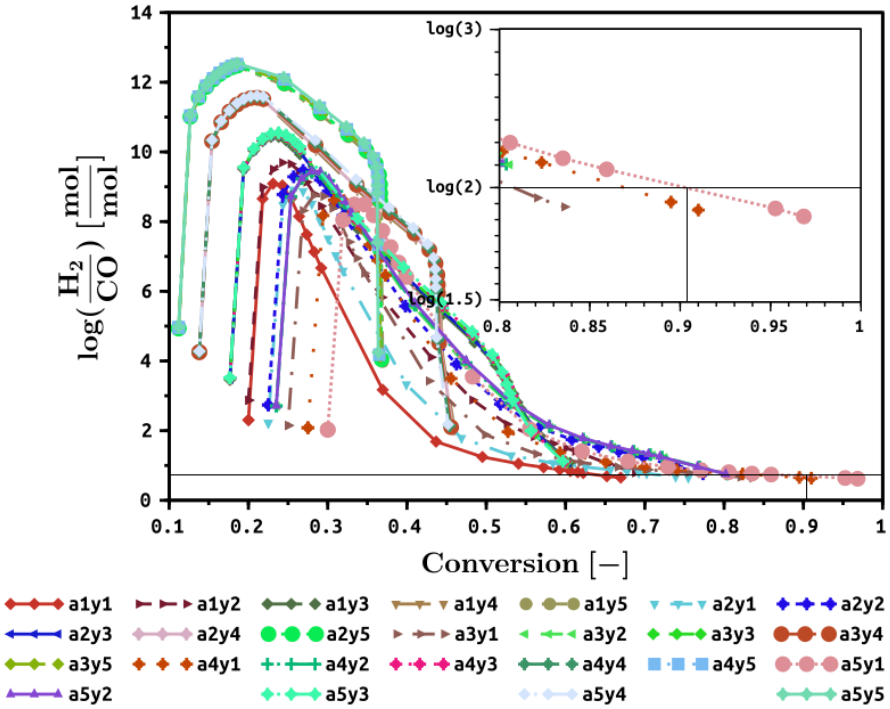

Figure 5.15: Reformer $H_2 : CO$ ratio as a function of methane conversion for changing $PO\gamma$ and $PO\alpha$, where $T_{inlet} = 400^oC$, $P = 30\,bar$ and the air fraction is zero

Table 5.7: Legend key for Figure 5.15

Legend Item	$\frac{O_2}{C}$	Legend Item	$\frac{H_2O}{C}$
a1	PO alpha = 0.40	y1	PO gamma = 0.00
a2	PO alpha = 0.45	y2	PO gamma = 0.25
a3	PO alpha = 0.50	y3	PO gamma = 0.50
a4	PO alpha = 0.55	y4	PO gamma = 0.75
a5	PO alpha = 0.60	y5	PO gamma = 1.00

Figure 5.15 shows the effect of changing alpha and gamma on the $H_2 : CO$ ratio in the syngas leaving the reformer. The meaning of the legend codes are given in Table 5.7. The graph does not show zero conversion data because the $H_2 : CO$ ratio is undefined at this point. There is a large variation in the $H_2 : CO$ ratio with peak values far in excess of what is required in FTS; however, these peaks occur at low methane conversions in the range of 25% to 45%. Of the values tested, the highest methane conversion at a $H_2 : CO$ ratio of 2 will occur when $PO\alpha = 0.6$ and $PO\gamma = 0$. In the partial oxidation section an increase in the partial pressure of oxygen will not drive the combustion reaction forward because of the pressure terms are balanced in the rate equation of the combustion reaction, Equation 3.14. However, an increase in the partial pressure of oxygen will lower the partial pressure of the other species which will in turn cause a decrease in the rates of reactions 2 and 3 (Table 3.2). These reactions are endothermic and therefore there would be an increase

in the top temperature exiting the partial oxidation section which overcomes the decrease in temperature that would arise out of the oxygen behaving as a heat sink. The higher temperature feeds back into all the reactions with the general effect of increasing the reaction rate. Subsequently, in the steam reforming section the quantity of CO_2 and H_2O entering will increase and the quantity of CH_4 will decrease. Through SMR reactions 1 and 3, the production of hydrogen and carbon monoxide will increase due to the increased quantity of water. The increased feed carbon dioxide and increased rate of reaction 3 will drive the reverse reaction 2. All this will lead to greater production of syngas and higher conversion of methane which is reflected in Figure 5.15. The increasing top temperature will raise the forward rate constants of all the other reactions in SMR. Additionally, all the equilibrium constants will increase except for reaction 2 which decreases. For each reaction in both PO and SMR, a maximum rate is expected at stoichiometric quantities of the reactants; therefore, it is expected that a net maximum $H_2 : CO$ exists which is reflected in the results shown in Figure 5.15.

As the quantity of H_2O is increased, the effects of increasing the oxygen partial pressure diminish and a less rapid response is observed in the H_2CO ratio manifesting in a broader peak. Additionally, the maximum conversion decreases. Moreover, the H_2CO ratio out of partial oxidation increases along with that out of steam reforming. In partial oxidation, an increase in the partial pressure of steam will lower the rate of the combustion reaction, while driving forward reaction 2. This will lower the top temperature out of PO and increase the H_2CO ratio due to the $3 : 1$ stoichiometry in reaction 2. A decrease in the top temperature will lower the forward rate of all reactions in SMR, while the equilibrium constant of reaction 2 will increase (which will drive the reaction futher forward). The net effect will be a decreased conversion with a higher H_2CO ratio. The dampening of the response to increases in the oxygen partial pressure is caused by the reduced rate of the combustion reaction, Equation 3.14.

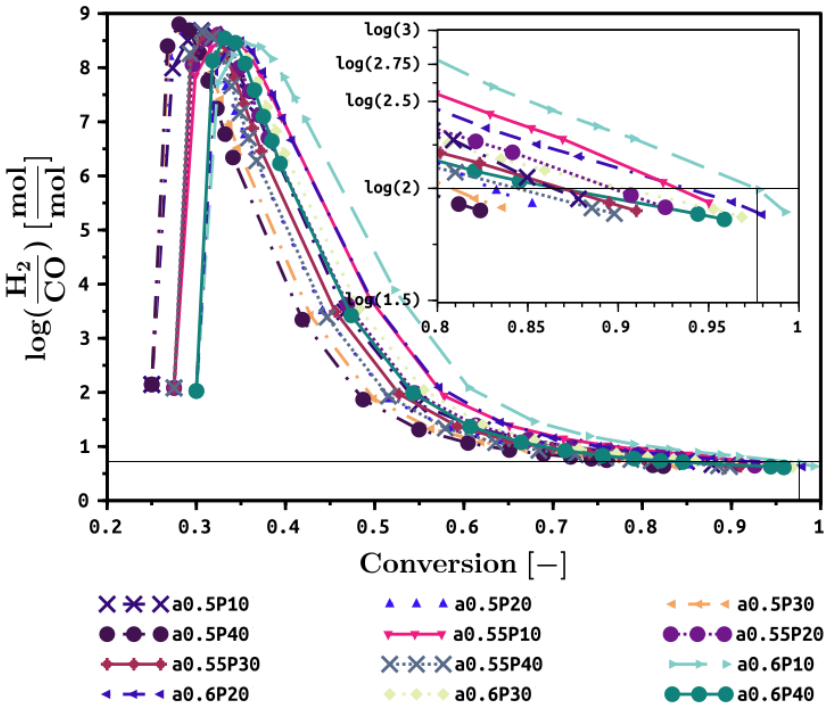

Figure 5.16: Reformer $H_2 : CO$ ratio as a function of methane conversion for changing pressure and $PO\alpha$, where $PO\gamma = 0$, $T_{inlet} = 400^oC$ and the air fraction is zero

Table 5.8: Legend key for Figure 5.16

Legend Item	Definition
a<num>	<num> = the value of PO alpha
P<num>	<num> = Pressure in bar

Figure 5.16 shows the effect of changing pressure, $PO\alpha$ and conversion on the $H_2 : CO$ ratio in the outlet syngas. The legend codes are given in Table 5.8. The highest conversions are seen at the low end of the pressure range, 10 bar in this case. Of the tested values a $PO\alpha$ value of 0.6 gives the highest conversion at an $H_2 : CO$ ratio of 2. Within the partial oxidation section, a rise in pressure will not affect the combustion reaction because the partial pressures in Equation 3.14 will remain within the same ratios. In accordance with Le Chatelier's principle, reactions 2 and 3 will favor the reverse reaction which will result in lower methane conversion to CO and H_2 in PO and a higher top temperature. Subsequently, in SMR a higher pressure would favor the reverse of reactions 1 and 3. Reaction 2 would be suppressed through the increase in partial pressures which would increase DEN. Overall, a lower conversion is expected along with a reduction in the $H_2 : CO$ ratio (comparing the same at a specific conversion) and this is what is observed in Figure 5.16.

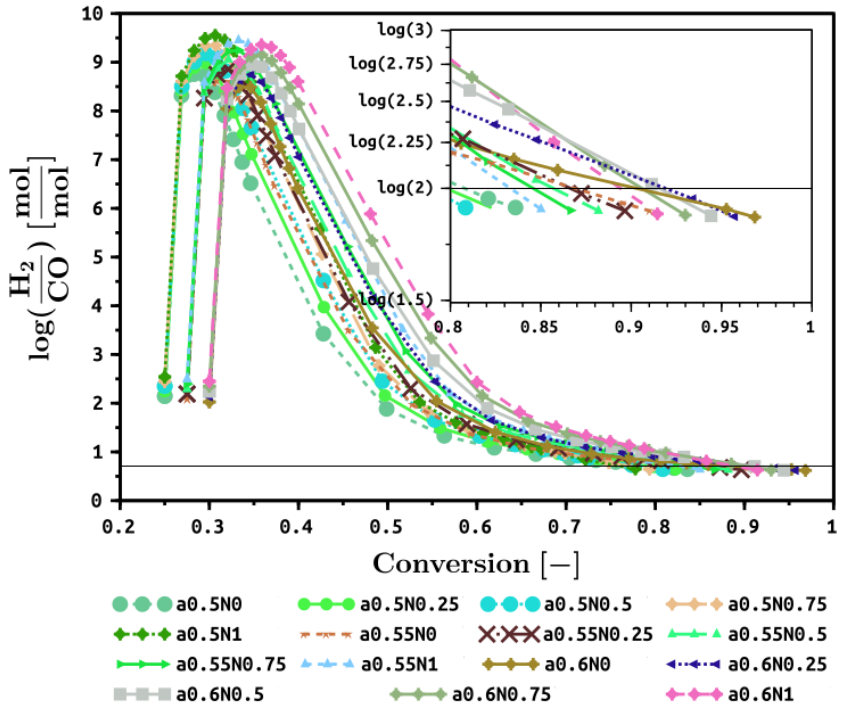

Figure 5.17: Reformer $H_2 : CO$ ratio as a function of methane conversion for changing nitrogen concentration (fraction of oxygen supplied by air) and $PO\alpha$, where $PO\gamma = 0$, $T_{inlet} = 400^oC$, $P = 30\,bar$ and the air fraction is zero

Table 5.9: Legend key for Figure 5.17

Legend Item	Definition
a<num>	<num> = the value of PO alpha
N<num>	<num> = fraction of oxygen supplied by air

Figure 5.17 shows the effect of increasing nitrogen concentration on the $H_2 : CO$ ratio out of the reformer. The legend codes are given in Table 5.8. The nitrogen concentration is changed indirectly through x_{air} which is the fraction of oxygen supplied by air. Given a certain $PO\alpha$, the amount of nitrogen is calculated according to Equation 5.12. At 100% air usage, the quantity of nitrogen is the amount that would be associated with the oxygen (determined by $PO\alpha$ and F_{CH_4}) provided all the oxygen is supplied by air.

$$F_{N_2} = x_{air} \frac{0.79}{0.21} PO\alpha \, F_{CH_4} \tag{5.12}$$

A $H_2 : CO$ ratio of 2 can be achieved with the highest methane conversion when $PO\alpha$ is 0.6 and pure oxygen is used. Increasing the air fraction will have a similar effect to lowering pressure due to the fact that the partial pressure will be lowered for the reacting species. As the air fraction and nitrogen concentration are increased in tandem, there is a slight increase in the quantities of the product species due to the aforementioned reason. The top temperature out of partial oxidation decreases significantly. Jess et al.

(1999) have noted that a large quantity of nitrogen in syngas has major implications on the temperature profile of the reactors due to nitrogen acting as a heatsink. This is not ideal for the reformers since SMR requires a high inlet temperature and is endothermic under these conditions. In order to counter this effect, a greater quantity of fuel must be converted in PO to maintain the SMR feed temperature. This causes a reduction in conversion in SMR and produces a lower $H_2 : CO$ ratio at high conversion as can be seen in Figure 5.17. However, at low conversion the $H_2 : CO$ ratio is higher for higher nitrogen concentration which is attributed to the reduction in partial pressures producing the same effect as if the pressure were lowered. The reason for the $H_2 : CO$ ratio displaying the opposite effect at high conversion is because steam reforming is endothermic and the temperature drops along the reactor length. Lower temperatures will favor production of CO over H_2 which will lead to reduced $H_2 : CO$ ratios.

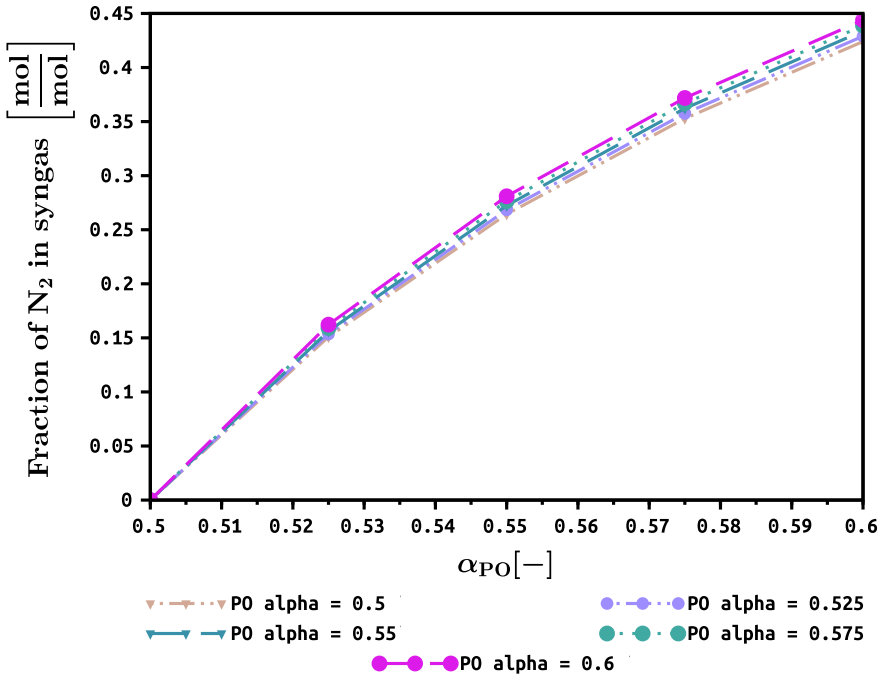

Figure 5.18: Percentage of nitrogen in syngas out of reformers with varying α_{PO}, where oxygen is wholly supplied by air

Figure 5.18 shows the effect of increasing the oxygen to methane ratio on the percentage of nitrogen in the syngas leaving the reformer when only air is used to supply the oxygen. The syngas contains over 45% nitrogen when $PO\alpha = 0.6$, this in in agreement with the maximum values quoted in literature (Jess et al., 1999).

5.3. Fischer-Tropsch Synthesis

5.3.1. Model Validation

Figure 5.19 shows the initial guess and calculated product distributions (natural logarithm of the normalized carbon mass distribution from C_1 to C_{60}). The product distribution shows

the characteristically high selectivity of methane; however, the C_2 selectivity does not reflect the trends seen in real product distributions where C_2 shows negative deviation from ASF (Dictor and Bell, 1983). Presently, the C_2 production is modeled according to the same rules as C_3 to C_N, namely hydrogenation to paraffins and β dehydrogenation to olefins). This could be remedied by using a separate chain growth rate constant for of C_2 rather than k3 (refer to Table 3.10). When alpha is fitted over the range C_{14} to C_{60}, the sub C_{22} mole fractions show positive deviation from ASF. The trends appear to be in line with expectations for cobalt catalysts as can be observed in the experimental results of Patzlaff et al. (1999). The carbon numbers are only taken to C_{60} in order to illustrate the effect of using small carbon number ranges on the system.

Due to the model formulation, the carbon numbers must be taken to N+1 where N is the desired carbon number, in order to avoid overestimation of the quantity of the carbon number N+1. This last carbon number has a tendency to accumulate because it is effectively acting as a barrier in a reaction scheme where material cascades towards larger and larger carbon numbers. If carbon number N+1 is included, there will be a raised tail end of the curve indicating a high mole fraction of C_{61} (in this case) which is attributed to the fact that the last carbon number is not consumed by chain growth in the kinetics since addition to CN would produce CN+1 which is not accounted for. In order to mitigate any associated error, the carbon number range must be increased.

In this instance C_{61} accounts for 0.60% of the total mass and 0.05% of the total moles of non-methane-product. Increasing the carbon number range will not reduce the error substantially. The carbon numbers C_{31} to C_{61} contain 35.08% and 13.51% of the total mass and total moles of non-methane-product, respectively, which are both substantial quantities. The range C_2 to C_{30} accounts for 64.92% of the total mass of non-methane-product. Therefore there appears to be considerable merit in accounting for carbon numbers beyond C_{30} in such analyses.

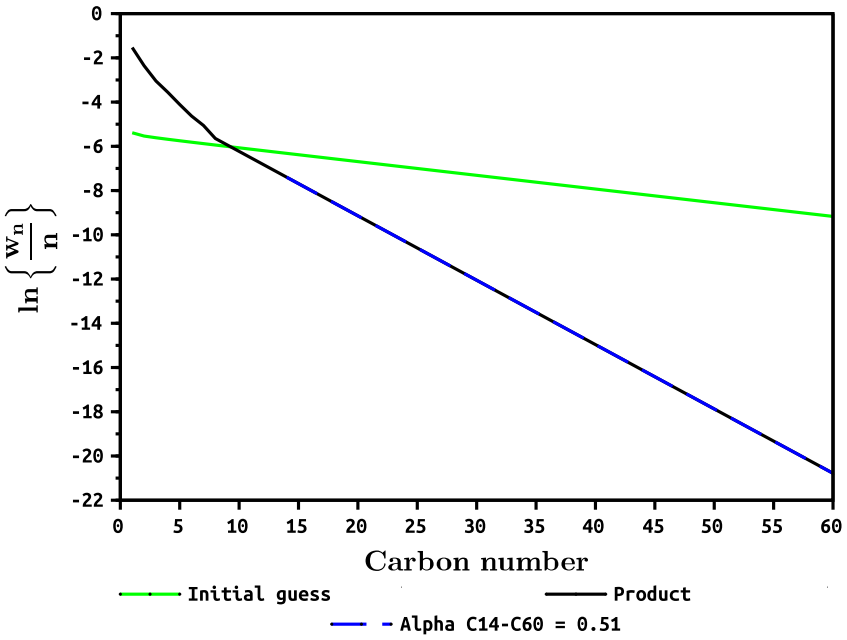

Figure 5.19: ASF distribution of once-through Fischer-Tropsch Synthesis product C_1 to C_{60}, $X_{CO} = 64\%$, $T = 230^oC$, $P = 35\,bar$, syngas $xN_2 = 0$.

Increasing the maximum carbon number to C_{160} (C_{161} in actual fact) increases the solution time by a factor of ~11. The product distribution is shown in Figure 5.20. The peak at C_{161} accounts for 0.04% and 0.34% of the moles and mass of product, respectively, a significant reduction from those when the carbon numbers are truncated at C_{60}. The range C_{31} to C_{160} accounts for 41.99% of the mass of product, while C_{31} to C_{60} accounts for 31.34%. This fraction is not equivalent to when only 60 carbon numbers are accounted for in the model. This can be attributed to the effect of the extra compounds on the VLE and surface concentrations.

The paraffin to olefin ratio for cobalt catalysts is expected to increase exponentially with carbon number (Shi and Davis, 2005; Yao et al., 2012). Mthombeni (2009) observed a nearly constant olefin to paraffin selectivity for the two phase model with two distinct regions. In the liquid rich hydrocarbon mixture, a ratio of 8.2 was observed. The olefin to paraffin ratio produced from running the reactor at the same conditions is approximately equal for all species at 2.0. The discrepancy can be attributed to the different method of handling VLE.

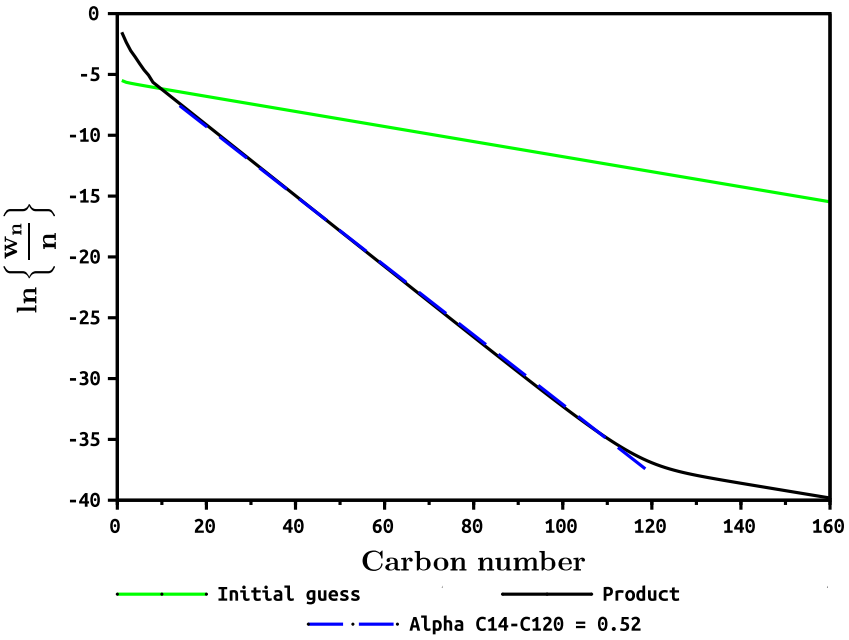

Figure 5.20: Anderson Schulz Flory distribution of once-through Fischer-Tropsch Synthesis product C_1 to C_{160}, $X_{CO} = 64\%$, $T = 230^oC$, $P = 35\,bar$, syngas $xN_2 = 0$.

5.3.2. Fischer-Tropsch Sensitivity

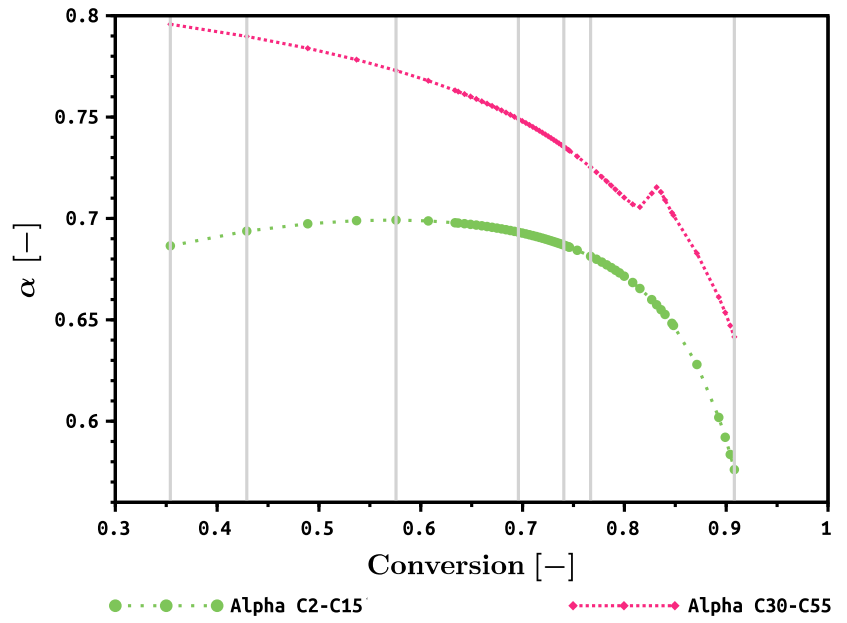

Figure 5.21: Fischer-Tropsch Synthesis chain growth probability (α) versus conversion for $H_2 : CO = 2$, $N = 160$, $xN_2 = 0$, $T_{FTS} = 230^oC$, $P_{FTS} = 40\ bar$.

Figure 5.21 shows the effect of increasing conversion on alpha (as effected by increasing catalyst weight). In this case, alpha is taken between C_{30} and C_{55} as was done by Mthombeni (2009). Similar trends have been reported by Mthombeni (2009) where the CO conversion increased and the lower carbon range alpha values decreased with an increase in catalyst loading and the higher carbon range alpha decreased and then began to increase with increasing catalyst loading. The product distribution includes both the liquid and vapor products and also paraffins and olefins lumped together. The chain growth probability is strongly related to the process conditions rather than the conversion with which it shows a complex relationship (van der Laan, 1999). In reality, the product would be withdrawn as liquid from the slurry reactor.

An increase in conversion will increase the catalyst independent rates of all reactions. The vapor fraction continuously decreases as conversion is increased. Initially, the liquid fraction increases until a conversion of 60% beyond which it decreases. There is a decrease in the activities of carbon monoxide and hydrogen which is initially due to the increasing conversion but further driven by the decreasing liquid fraction. The decrease in the liquid fraction is caused by the decreasing activities of hydrogen and carbon monoxide which decrease the surface concentration of hydrogen and methylene monomer surface species. The surface concentration of all species decreases approximately quadratically with increasing conversion except for the paraffin and olefin precursors whose surface concentrations may increase with increasing conversion beyond a certain crossover carbon number. Beyond this point, the surface concentrations increase with increasing conversion. This eventually raises the alpha value of the heavy species as can be seen in Figures 5.22 and 5.23.

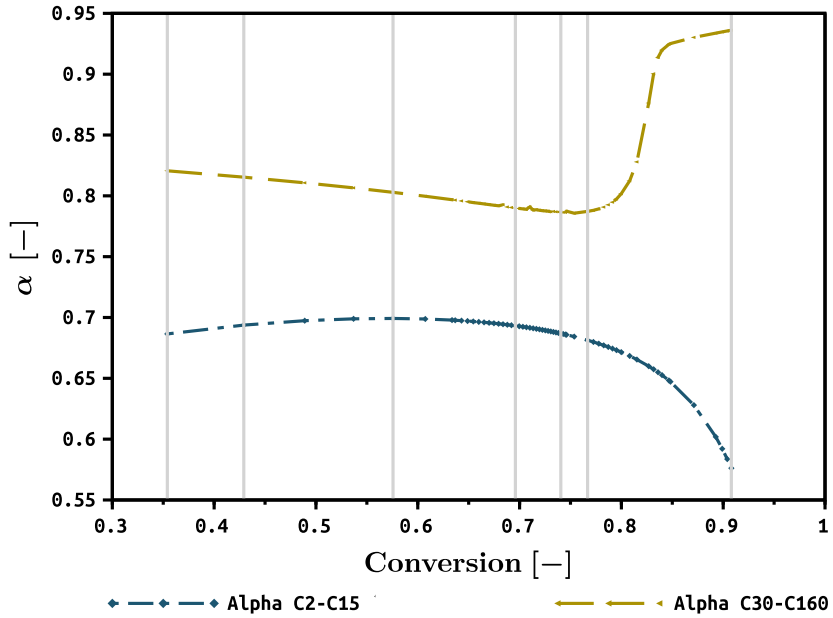

Figure 5.22: Fischer-Tropsch Synthesis chain growth probability (α) versus conversion for $H_2 : CO = 2$, $N = 160$, $xN_2 = 0$, $T_{FTS} = 230^oC$, $P_{FTS} = 40\ bar$.

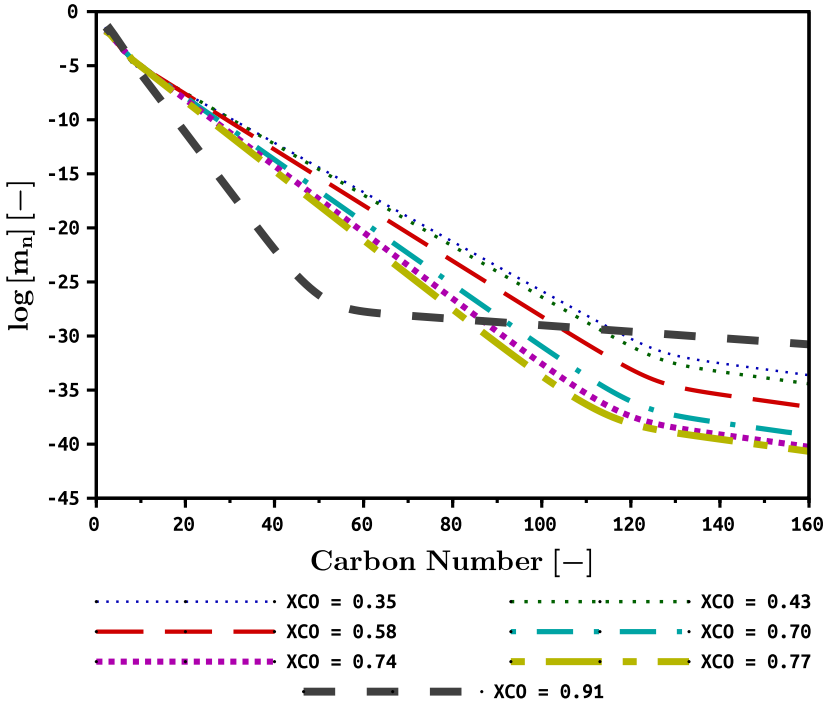

Figure 5.23: Fischer-Tropsch Synthesis syncrude ASF distribution for carbon monoxide conversions indicated by the gray vertical lines in Figure 5.21 and 5.22, where $H_2 : CO = 2$, $N = 160$, $xN_2 = 0$, $T_{FTS} = 230^oC$ and $P_{FTS} = 40\ bar$.

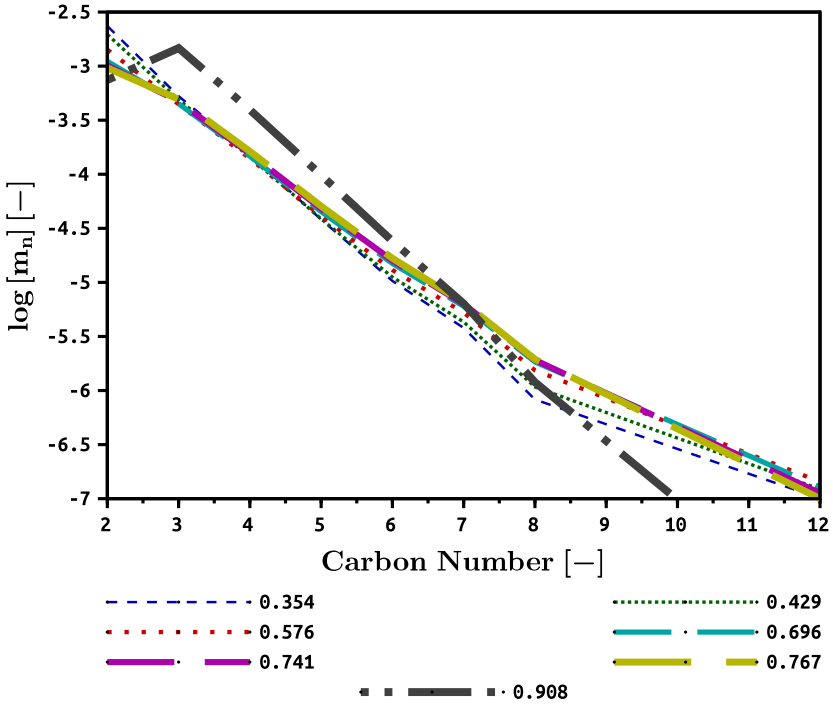

Figure 5.24: Fischer-Tropsch Synthesis syncrude ASF distribution for carbon monoxide conversions indicated by the gray vertical lines in Figure 5.21 and 5.22, where $H_2 : CO = 2$, $N = 160$, $xN_2 = 0$, $T_{FTS} = 230^oC$ and $P_{FTS} = 40\ bar$.

Figure 5.22 shows the same plot as Figure 5.21 except that now the second alpha value

has been taken to C_{160}. In this case, the alpha value rises beyond a conversion of 77% before beginning to flatten off. All that has changed here is that the carbon number range (over which alpha is fitted) has been increased and a much different trend results. The reason for these differences can be elucidated by plotting the ASF distribution.

Figure 5.23 shows the ASF distributions for the conversions marked by the gray vertical lines in Figures 5.21. These non-ideal ASF distributions can be described by two alpha values. However, if the alpha value range is fixed without regard to the the point of inflection on the curve then the alpha values may accurately describe the distribution. For example, if the range over which alpha is fitted was taken as C_{40} to C_{100} at a conversion of 91% then the alpha value would be determined from the slope of a straight line between C_{40} and C_{100} which would be highly inaccurate. In order to use the two alpha value method, one would need to determine the range over which to fit both alpha values on the fly.

In terms of the trend itself, as the final carbon number approaches the maximum, there is a tendency for the distribution to flatten beyond a certain inflection point. As the conversion increases, the carbon number of the inflection point will decrease and correspondingly the carbon number range of the flatter section will increase. Moreover, the average carbon weight fraction in a particular carbon number will increase with increasing conversion in the flatter tail, whereas the opposite is observed in the preceding linear section. This indicates that the choice of the carbon number range that alpha is regressed from will determine the trend of the alpha with conversion for non-ideal product distributions.

As shown in Equation 3.35, the derivative of the logarithm of the carbon number weight fraction in an n-mer with respect to n will equal the logarithm of alpha. This also applies when ASF Equation is given in molar form. In other words, the slope of the ASF plot will equal to the logarithm of alpha. Furthermore, given that the slope of the ASF plot is negative, a more negative slope would give a lower value of alpha. In the case of an ideal ASF distribution, described by a single alpha value, an increase in alpha would result in a decreased slope accompanied by a decrease in the intercept.

Iglesia et al. (1991) have reported that as the carbon monoxide conversion is increased, the molecular weight of products increases. This was attributed to the increase in the formation of C_2 to C_{25} hydrocarbons predominantly rather than $C_{25}+$ hydrocarbons which were found to be insensitive to the residence time (and therefore conversion). Over a wide range of operating parameters the chain growth probability is insensitive to the conversion (van der Laan, 1999). Figure 5.23 seems to be displaying the opposite trend; however, this is not the case. Figure 5.24 displays the same plot over the carbon numbers C_2 to C_{12}. As shown the chain growth probability increases with increasing carbon monoxide conversion up until a point where the curves cross over each other and the opposite trend is displayed. Figure 9.25 shows the same plot when the k5 rate constant is increased by a factor of 22. This results in a shift of the crossover region to heavier carbon numbers. The expected trend is seen here until the region of C_{30} where crossover occurs. Additionally, the terminal carbon numbers do not display a major difference in chain growth probability

from the rest as was the case with Figure 5.23. This feature is attributed to the solver struggling with the resolution of values approaching the limit of floating point precision which should occur around $ln(10^{-16}) = -34.5$.

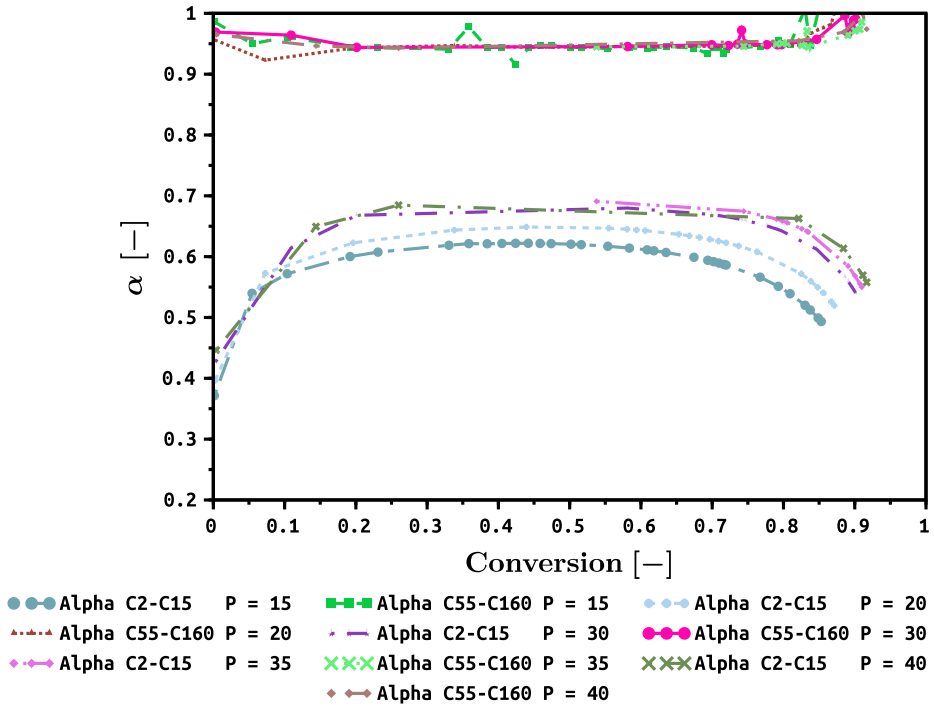

Figure 5.25: Fischer-Tropsch Synthesis chain growth probability (α) versus conversion of carbon monoxide for changing pressure and $H_2 : CO = 2$, $N = 160$, $xN_2 = 0$ and $T_{FTS} = 230^oC$.

As pressure increases, the partial pressure of all species would increase which would drive material into the liquid phase. The increased liquid fugacity would increase the activity of each species in the liquid phase which would increase the surface concentrations of each species and the reaction rate. The rates of adsorption of hydrogen and carbon monoxide are directly affected through the activity terms as can be seen in Table 3.10. The high pressure would reduce the concentration gradient between the liquid and the adsorbed phase on the catalyst which would promote chain growth and thereby cause the alpha value to increase. With regard to Table 3.10 and specifically the β-dehydrogenation to olefins, an increase in the activity of the olefin species would drive the reverse reaction and promote chain growth as opposed to desorption to olefins; therefore, as pressure is increased the paraffin to olefin ratio will decrease.

Figure 5.25 shows the effect of varying pressure on the alpha values. As expected the α_{C2-C15} value increases with increasing pressure; however, there is some overlap between conversions of 5% and 85% where pressures of 30 and 35 bar show greater alpha values. The $\alpha_{C15-C160}$ value remains relatively constant except for conversions above 85% where it is difficult to determine the behavior as stated before, alpha values taken over fixed ranges can be misleading.

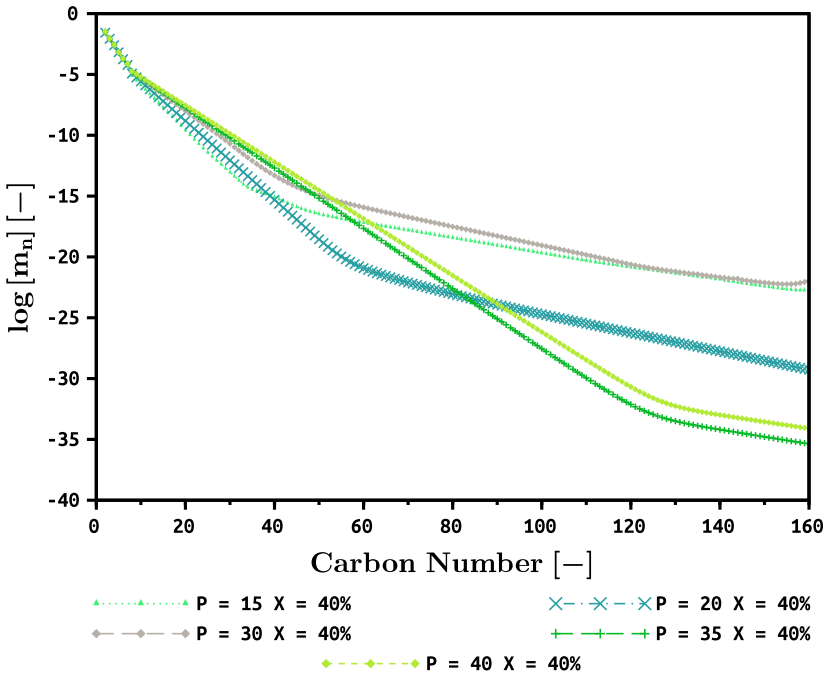

Figure 5.26: Fischer-Tropsch syncrude ASF distribution for varying pressure at a carbon monoxide conversion of 40%, where $H_2 : CO = 2$, $N = 160$, $xN_2 = 0$ and $T_{FTS} = 230^oC$.

The ASF distributions are taken at 3 representative conversions; 40%, 60% and 80%. The first two conversions are within the range of per pass conversions seen in commercial operations, while the last is taken to represent high conversion. The specific value of 80% is chosen so as to prevent any extrapolation outside the range of calculated values and is a realistically high conversion based on studies by Prins et al. (2005) and Kreutz et al. (2008). Since the change in conversion is effected by changing the catalyst loading, the model does not directly determine the products at a specific conversion, this can be seen through the spacing of data points in Figures 5.21, 5.22 and 5.25. Therefore, it is necessary to interpolate between the data points to get the value at a specific conversion. To clarify, supposing the conversion at 40% was desired, the model would search for the two nearest neighbors (e.g. 38.2% and 40.8%) and interpolate between those to give the value at 40% conversion. This leads to Figure 5.26 where the ASF distributions are plotted for each pressure at a conversion of 40%. Here the mole fractions have been interpolated. The first section of the ASF distribution shows an increase in alpha as the pressure is increased. The change from 20 to 30 bar is the greatest, while that from 30 to 35 to 40 bar is much less. In the second half of the curve the trend is not so clear. A maximum in alpha is seen for a pressure of 30 bar followed by 15 bar. Depending on what carbon number range in wax is desired, 20 bar or 35 bar could be the least beneficial.

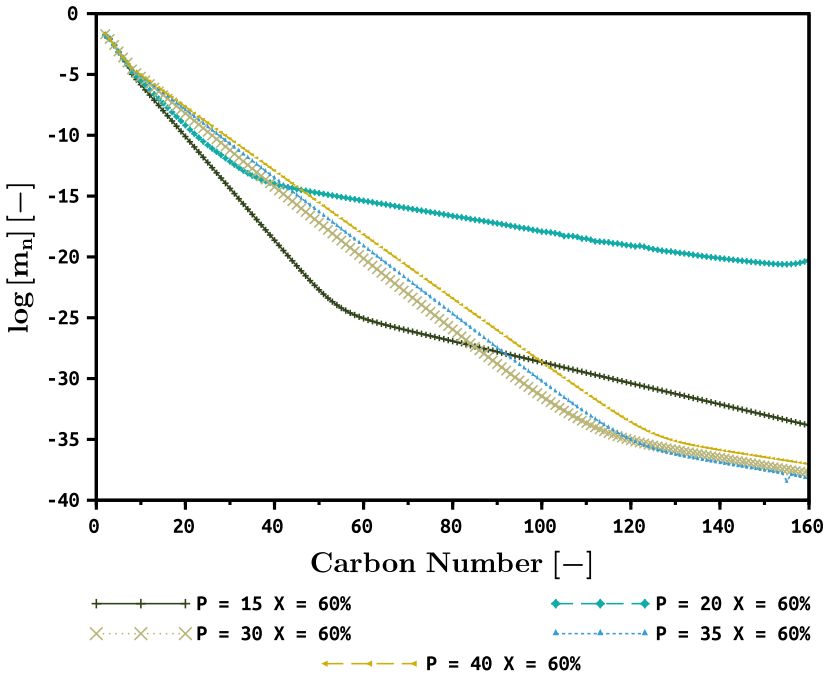

Figure 5.27: Fischer-Tropsch syncrude ASF distribution for varying pressure at a carbon monoxide conversion of 60%, where $H_2 : CO = 2$, $N = 160$, $xN_2 = 0$ and $T_{FTS} = 230^oC$.

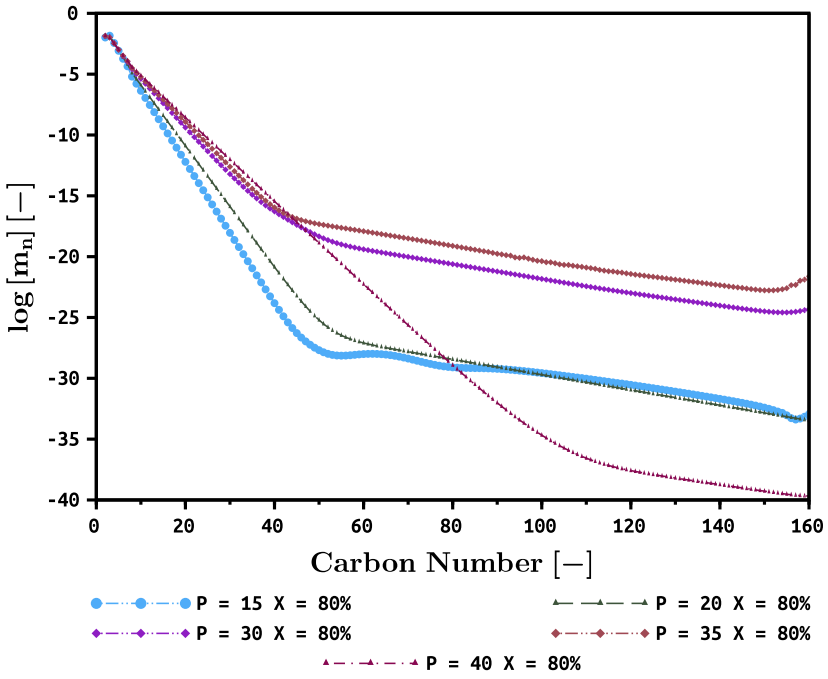

Figure 5.28: Fischer-Tropsch Synthesis syncrude ASF distribution for varying pressure at a carbon monoxide conversion of 80%, where $H_2 : CO = 2$, $N = 160$, $xN_2 = 0$ and $T_{FTS} = 230^oC$.

Figures 5.27 and 5.28 show ASF distributions for FTS syncrude at conversions of 60% and 80%, respectively. The first section of the distributions behave as expected showing

steadily increasing alpha values with increasing pressure. However, in the second section of the curve the highest alpha value is seen for a pressure of 20 bar and 35 bar for conversions of 60% and 80%, respectively. What determines which pressure will produce the most wax is the point of inflection where the two alpha values transition between one another. The earlier the inflection point, the greater the heavy wax production.

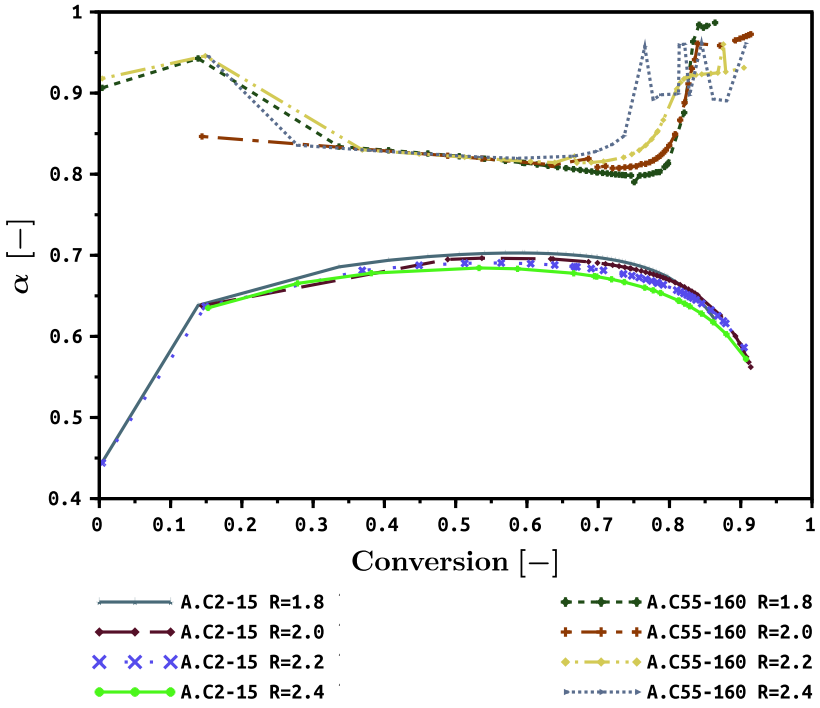

Figure 5.29: Fischer-Tropsch Synthesis chain growth probability (α) versus conversion of carbon monoxide for changing $H_2 : CO$ ratio in syngas and $N = 160$, $T_{FTS} = 230^oC$, $xN_2 = 0$ and $P_{FTS} = 40\ bar$.

Increasing the $H_2 : CO$ ratio will increase the activity and surface concentration of hydrogen and hydrogen surface species, respectively. Additionally, the activity and surface concentration of carbon monoxide and carbon monoxide surface species would decrease. The increase in the concentration of hydrogen surface species would promote chain termination and the decrease in the carbon monoxide activity would result in a decrease of the methylene monomer ($-CH_2-$) surface species which would also limit chain growth. Therefore, increasing the syngas $H_2 : CO$ ratio should be associated with a decrease in the alpha value. Figure 5.29 shows the effect of conversion and the $H_2 : CO$ ratio on α_{C2-C15} and $\alpha_{C55-C160}$. Between conversions of 50% and 80%, the aforementioned effect is observed, where α_{C2-C15} decreases with increasing $H_2 : CO$ ratio. However, at high conversion, the $H_2 : CO$ ratio of 2.0 produces the highest alpha value. The second $\alpha_{C55-C160}$ shows erratic variation below conversions of 30% and above conversions of 75%. However, between these conversions the alpha value increases with increasing $H_2 : CO$ ratio.

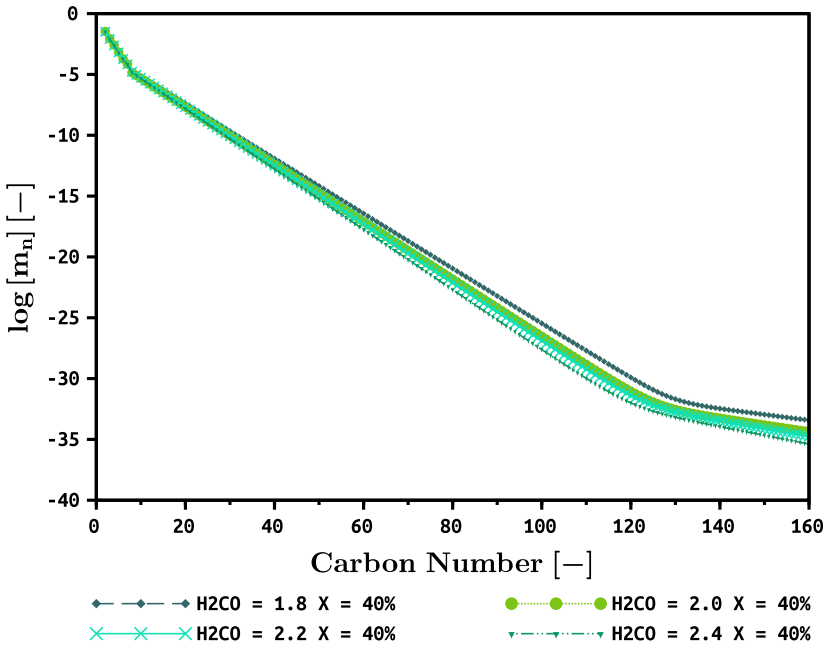

Figure 5.30: Fischer-Tropsch Synthesis syncrude ASF distribution for varying $H_2 : CO$ ratio at a carbon monoxide conversion of 40%, where $N = 160$, $T_{FTS} = 230^oC$, $xN_2 = 0$ and $P_{FTS} = 40\ bar$.

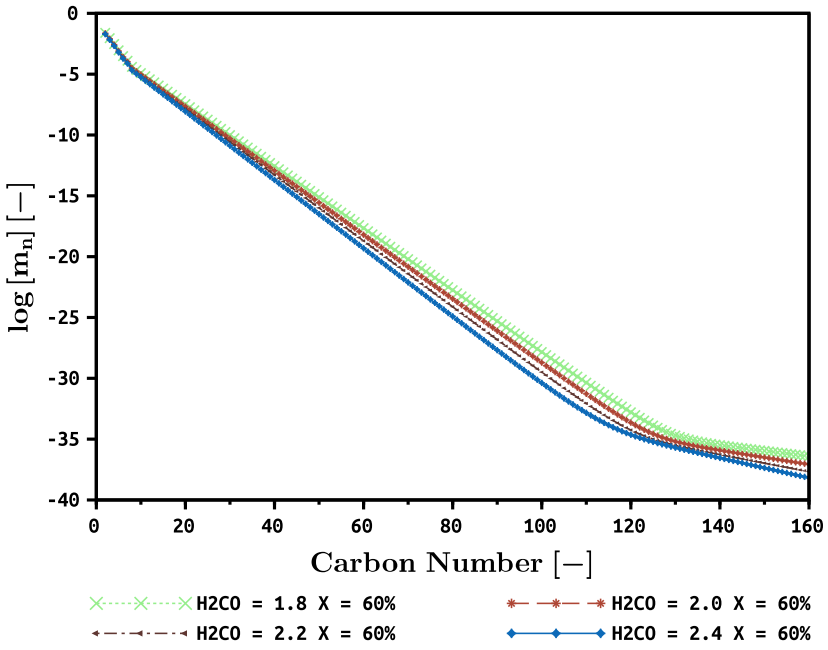

Figure 5.31: Fischer-Tropsch Synthesis syncrude ASF distribution for varying $H_2 : CO$ ratio at a carbon monoxide conversion of 60%, where $N = 160$, $T_{FTS} = 230^oC$, $xN_2 = 0$ and $P_{FTS} = 40\ bar$.

Figures 5.30 and 5.31 show the ASF distributions of the total FTS product at interpolated conversions of 40% and 60%, respectively. The expected behavior is observed throughout

the distribution. Of the values tested, an $H_2 : CO$ ratio of 1.8 appears to be best for maximising wax production. The distributions themselves are well behaved, hence the clear trends seen in Figure 5.29; however, the second alpha value is being fitted over a region with a point of inflection around C_{120}. This will cause an overestimate of the value of alpha but since there is no crossing of the ASF plots, the same conclusions can be drawn from Figure 5.29.

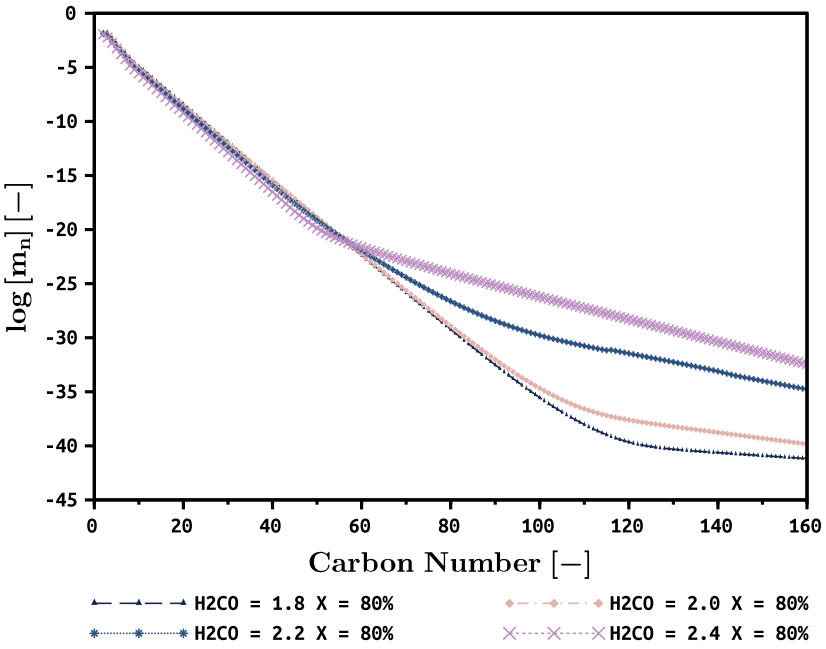

Figure 5.32: Fischer-Tropsch Synthesis syncrude ASF distribution for varying $H_2 : CO$ ratio at a carbon monoxide conversion of 80%, where $N = 160$, $T_{FTS} = 230^oC$, xN_2 and $P_{FTS} = 40\ bar$.

Figure 5.32 shows the ASF distribution of total FTS product at an interpolated conversion of 80%. The expected behavior is not observed beyond C_{30} as the 2.4 $H_2 : CO$ ratio inflects and crosses over the other distributions. At carbon numbers between C_{40} and C_{110}, the opposite behavior is observed, where alpha increases with increasing $H_2 : CO$ ratio.

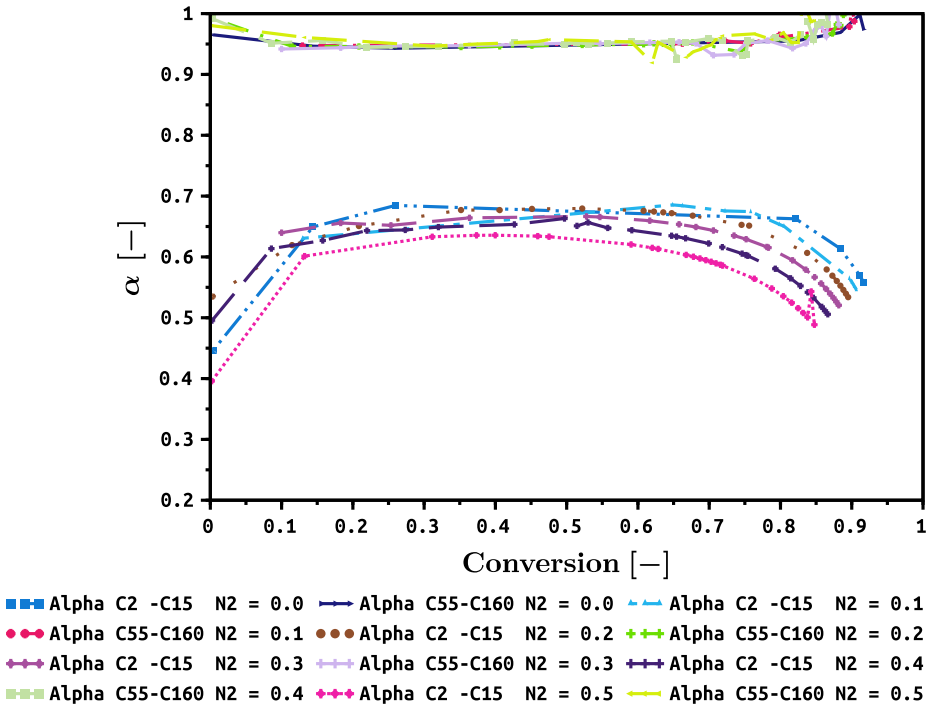

Figure 5.33: Fischer-Tropsch Synthesis chain growth probability (α) versus conversion of carbon monoxide for changing nitrogen concentration in syngas and $H_2 : CO = 2$, $N = 160$, $T_{FTS} = 230^oC$ and $P_{FTS} = 40\ bar$.

Nitrogen in syngas will lower the partial pressure of both hydrogen and carbon monoxide which will lower the activity of the hydrogen and carbon monoxide fluid species. In theory, lowering the activity of hydrogen should lower the surface concentration and promote chain growth; however, a quadratic increase in the surface concentration of hydrogen is observed which is driven by the increase in the void fraction of surface sites as can be seen in Table 3.10. The increasing surface hydrogen concentration would drive the adsorption of carbon monoxide and the formation of methylene monomer surface species but the effect is counteracted by the decrease in the activity of carbon monoxide. The decreasing methylene monomer concentration causes a decrease in the surface concentration of all paraffin and olefin precursors on the catalyst surface which produces an overall effect of lowering of alpha. Moreover, this feeds back into the hydrogen surface species concentration by increasing the void fractions on the surface.

Figure 5.33 shows the effect of conversion and nitrogen concentration in syngas on α_{C2-C15} and $\alpha_{C55-C160}$. In general, there is a clear decrease in α_{C2-C15} for increasing nitrogen concentration; however, at low nitrogen concentrations of 10% and 20% and between conversions of 50% and 60% the alpha value is higher than for zero nitrogen content. At high conversion (80%+), the expected trend is displayed. In order to maximize conversion, the nitrogen concentration must be minimized as can be seen from both alpha values. The $\alpha_{C55-C160}$ remains relatively constant with increasing nitrogen concentration.

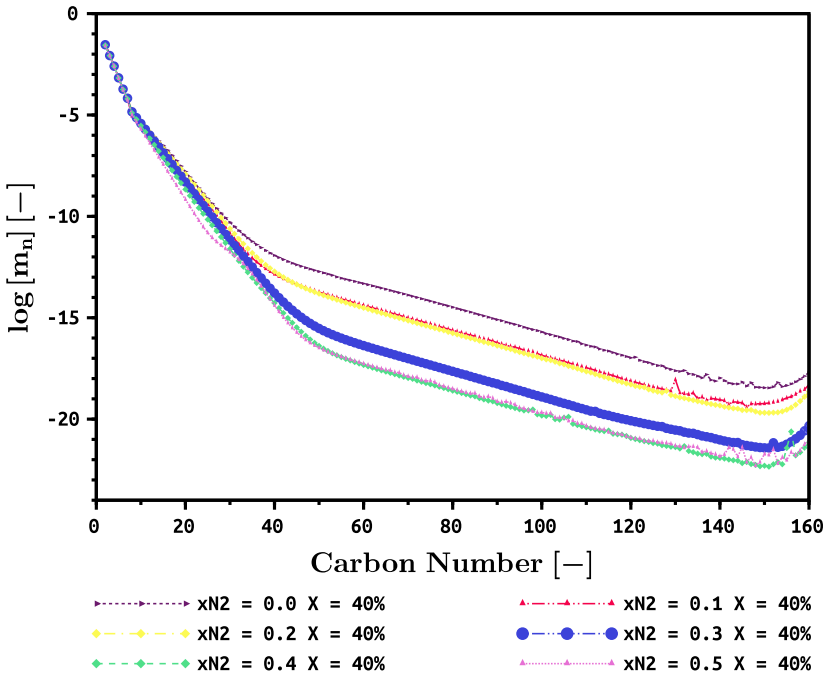

Figure 5.34: Fischer-Tropsch Synthesis syncrude ASF distribution for varying nitrogen concentration at carbon monoxide conversions of 40%, where $H_2 : CO = 2$, $N = 160$, $T_{FTS} = 230^oC$ and $P_{FTS} = 40\ bar$.

In Figure 5.34, the reason for the $\alpha_{C55-C160}$ remaining constant becomes clear. The slope of the ASF distribution in the second section of the curve remains relatively constant. However, there is a decrease in the average wax fraction for increasing nitrogen fraction. This decrease is not caused by nitrogen dilution since these fractions only include the FTS hydrocarbon products but is caused by a reduction in the surface reaction rates due to the reduction in partial pressure of hydrogen and carbon monoxide.

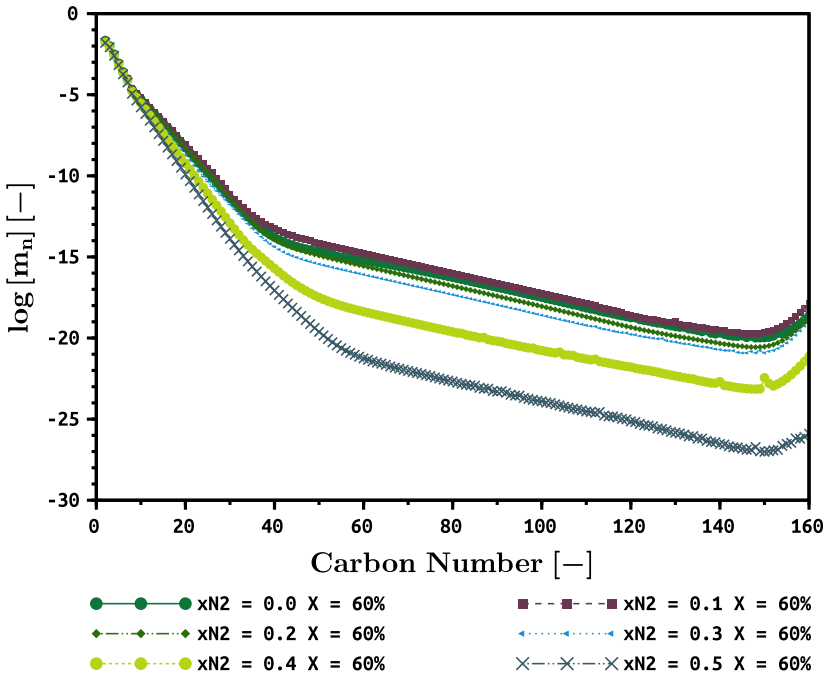

Figure 5.35: Fischer-Tropsch Synthesis syncrude ASF distribution for varying nitrogen concentration at carbon monoxide conversions of 60%, where $H_2 : CO = 2$, $N = 160$, $T_{FTS} = 230^oC$ and $P_{FTS} = 40$ bar.

As discussed for Figure 5.33, at a conversion of 60% the inclusion of 10% nitrogen in syngas seems to be beneficial as here is a slight increase in the alpha value over having no nitrogen. The reason for this is that a peak is observed in the $CH_3\theta$ surface species at a nitrogen concentration of 10%. This is caused by the opposing forces of the increasing surface hydrogen concentration due to the increasing void fraction (which is due to the decreasing surface concentrations of all species) and the decreasing methylene monomer surface species concentration. Depending on the conversion, this effect may be enough to cause a benefit to having a small quantity of nitrogen in the syngas as was seen in Figure 5.33.

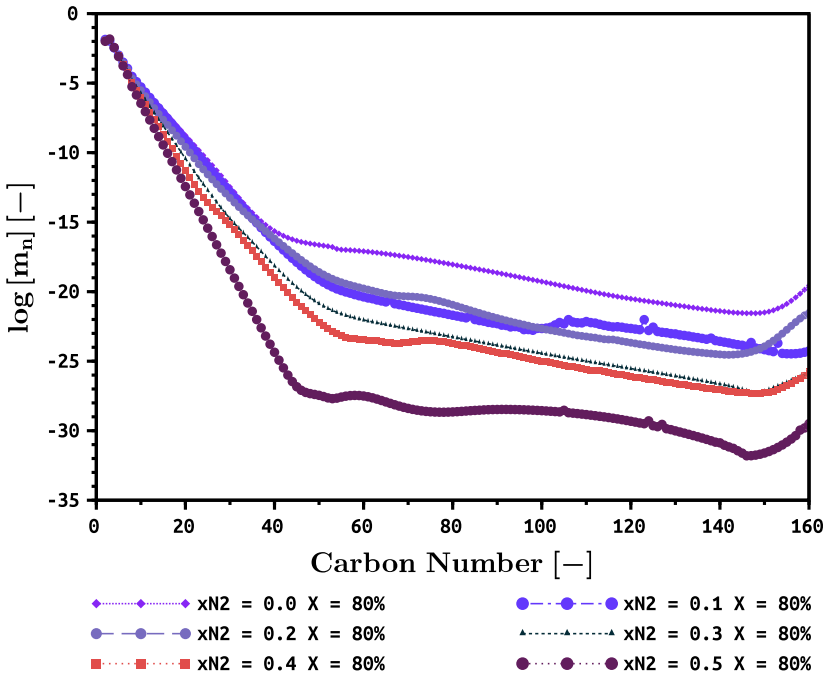

Figure 5.36: Fischer-Tropsch Synthesis syncrude ASF distribution for varying nitrogen concentration at carbon monoxide conversions of 80%, where $H_2 : CO = 2$, $N = 160$, $T_{FTS} = 230^oC$ and $P_{FTS} = 40$ bar.

Figure 5.36 shows the ASF distributions for increasing nitrogen concentration at a conversion of 80%. Here the aforementioned benefit of nitrogen is far more pronounced. Syngas without nitrogen produces the most wax but interestingly 30% nitrogen produces more wax than any other configuration. This is attributed to the peak in the $CH_3\theta$ surface species arising from the opposition between the increasing surface hydrogen concentration and decreasing methylene monomer surface species concentration.

The variation with temperature only affects the separation factors since the temperature dependence of the rate constants has not been included. Varying the temperature from 180^oC to 240^oC produced no significant change in either the alpha value or the conversion of carbon monoxide.

5.4. Hydrocracker

5.4.1. Model Validation

Figure 5.37 shows an attempt to reproduce the same validation carried out by Le Grange (2009) using the same kinetic constants. Model B was used to model hydrocracking of experimental data reported by Leckel (2005) who used a feed of Sasol iron catalysed FT wax and a $NiMo$ on SiO_2/Al_2O_3 catalyst. The fit is almost identical to that produced by Le Grange (2009). Le Grange (2009) has noted that the product distribution may be inaccurate due to the analysis technique. The peak at C_4 is attributed to an unknown mechanism which is not accounted for in the kinetics (Le Grange, 2009). However, this suffices to show that the model is operating correctly with the new kinetic constants.

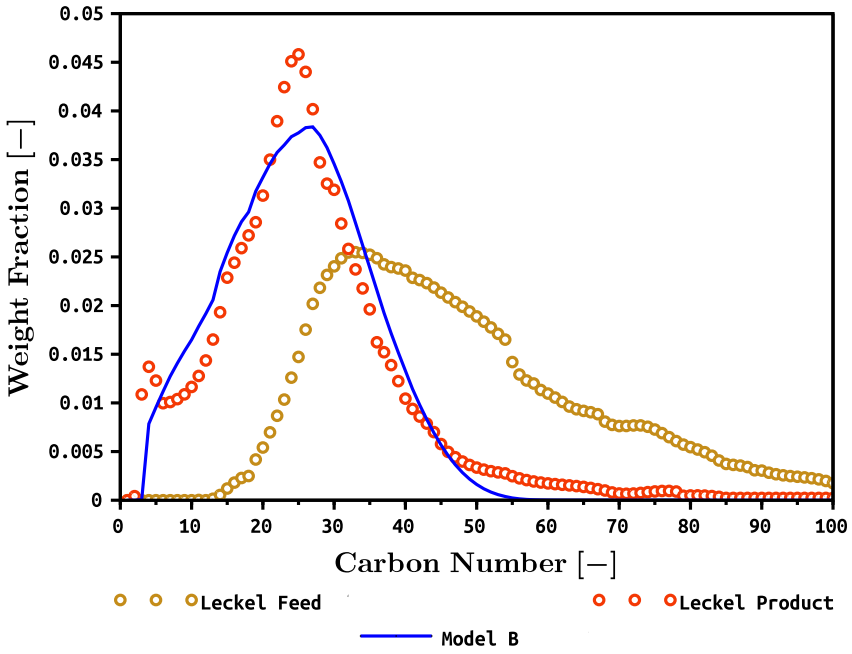

Figure 5.37: Once through hydrocracking of Fischer-Tropsch Synthesis slurry wax (Leckel, 2005) showing experimental product (Leckel, 2005) and the Model B (Le Grange, 2009) prediction, 35 bar, 350^oC, H_2 : $Hydrocarbons = 38:1$, $X_{C23+} = 39.24\%$

Table 5.10: Hydrocracker operating conditions for model validation

Operating Conditions	Value	Units
Temperature	365	^oC
Pressure	70	bar
Conversion C23+	37	%
H_2 : $Hydrocarbons$ ratio	38:1	-

Table 5.11: Hydrocracker kinetic constants

Kinetic Constant	Value [mol s^{-1} g_{cat}^{-1}]
k_{H_2}	3
k_A	1.17×10^{-4}
k_B1	1.56×10^{-4}
k_B2	55.4
k_C	1

5.4.2. Hydrocracker Sensitivity

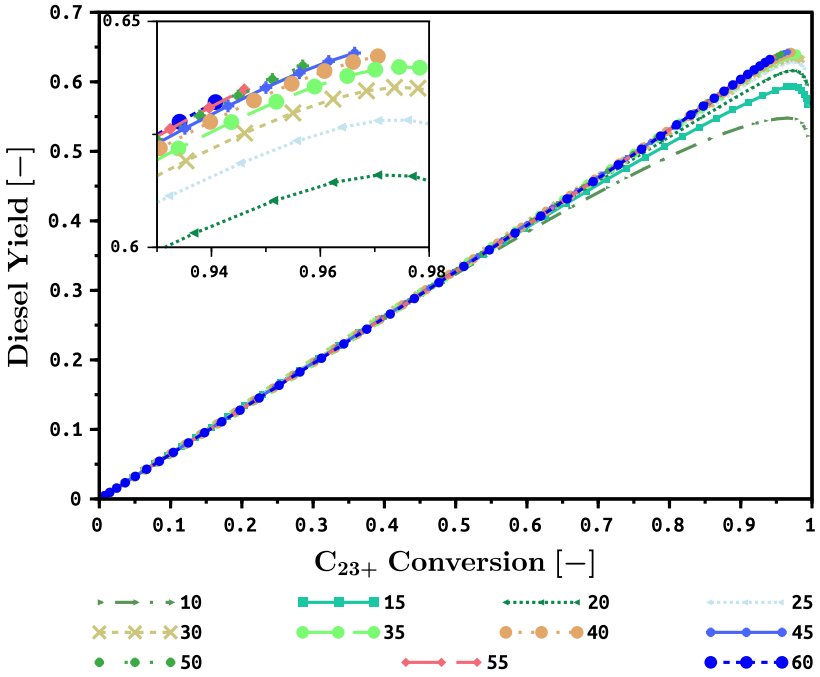

Figure 5.38: Once through hydrocracking of Fischer-Tropsch Synthesis C_{23+} wax $\alpha = 0.94$, $T = 350^oC$, $P = 35\ bar$ showing the sensitivity of the diesel yield to C_{23+} conversion and the $H_2 : Hydrocarbons$ ratio

Figure 5.38 shows the sensitivity of the diesel yield to the $H_2 : Hydrocarbons$ ratio for changing C_{23+} conversion. The change in yield with respect to the $H_2 : Hydrocarbons$ ratio is small up until a conversion of around 50%. As the C_{23+} conversion increases, the diesel yield increases as more wax is cracked into the diesel carbon number range. However, beyond a certain conversion it is expected that the diesel yield will begin to decrease as the bulk of the wax is cracked into sub diesel ranges. This can easily be seen at $H_2 : Hydrocarbons$ ratios of 10, 15 and 20 in Figure 5.38. In all other cases, the reactor ran out of liquid before the final time step could be solved. The rates are inversely proportional to the hydrogen activity; therefore, it is expected that an increase in the $H_2 : Hydrocarbons$ ratio will cause the rate of cracking to decrease. This is reflected in the decrease in the maximum C_{23+} conversion (before the liquid runs out). Of the values tested, the best $H_2 : Hydrocarbons$ ratio is 64.3% which is determined at an $H_2 : Hydrocarbons$ ratio of 45:1. However, given the slope of the curves, if the time step in the ODE solver were adjusted such that the conversion at the last time step were higher the $H_2 : Hydrocarbons$ ratio of 60 would give the highest diesel yield. Furthermore, out of a set of $H_2 : Hydrocarbons$ ratios, the one giving the highest yield at very high conversion will give the lowest yield at very low conversion.

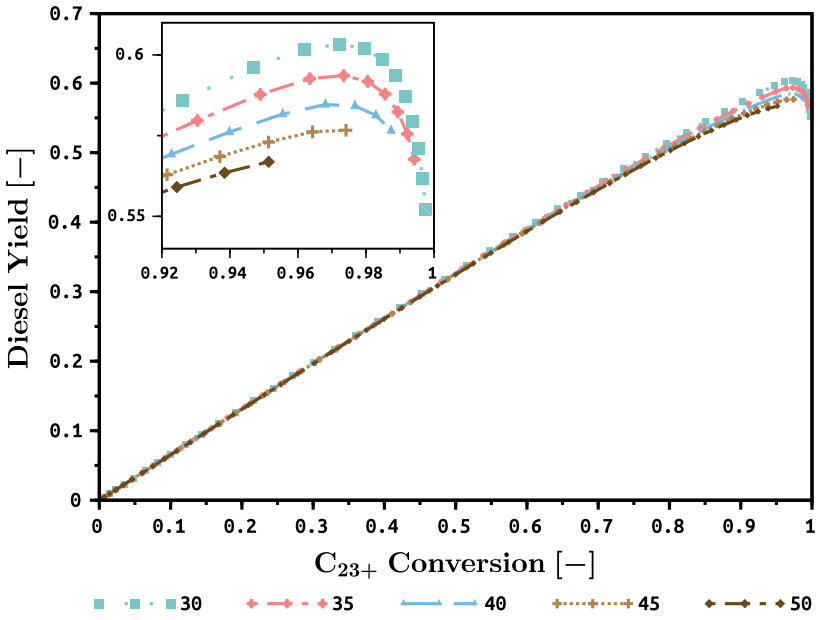

Figure 5.39: Once through hydrocracking of Fischer-Tropsch Synthesis C_{23+} wax $\alpha = 0.94$, $T = 350^{o}C$, $H_2 : Hydrocarbons = 15 : 1$ showing the sensitivity of the diesel yield to C_{23+} conversion and pressure

Figure 5.39 shows the sensitivity of the diesel yield to operating pressure for changing C_{23+} conversion. The change in yield with respect to pressure is small up until a conversion of about 70%. Of those tested, the best pressure with regard to maximizing diesel yield appears to be 35 bar, where a once through conversion greater than 97.2% can be obtained at a diesel yield of 60.3%. As pressure increases, the activity of all species will increase, this will increase the rate of cracking of wax. With a high rate of cracking, there is a possibility of overshooting the diesel range quicker and thereby having a high conversion but a low diesel yield. This can be seen in the increase of the downward curvature at high conversion for increasing pressure.

5.5. Plant Model Validation

In the preceding sections it has been shown that the individual reactor models are capable of producing realistic trends and therefore are assumed to be valid. Furthermore, it was shown that the physical property estimation produced reasonable results. Therefore, given that the plant model is composed of the reactor models and the property estimations, it is assumed that that the plant model is valid in those respects.

When the models are combined to produce the plant model some changes are expected. In regard to the ATR, when the external recycle is active, the ATR feed will contain some light hydrocarbons as well as the compounds assumed in the model validation. Apart from methane, the rest of the light hydrocarbons are inert because it has been assumed that only methane reacts in the ATR; therefore, these compounds act as a diluent and

heat sink. When any recycle is active, the feed to FTS differs from the feed used in the model validation because it will contain all the gaseous hydrocarbons instead of just syngas. This will affect the species activities and furthermore, the $H_2 : CO$ ratio will be expected to reduce. Reduction in the $H_2 : CO$ ratio has been covered in the Fischer-Tropsch sensitivity section. With reduction in the species activities, the rate of reaction will reduce and lower conversion results in FTS. The hydrocracker operation will differ from that used in the model validation in that the wax will not be distributed according to an ideal ASF distribution. On an OIRC run with 60% conversion in FTS, a plantwide carbon efficiency to liquids of 67.6% is achievable. This is within the expected range of 65%-75% (Floudas et al., 2012; Hao et al., 2008).

6. Results and Discussion

6.1. Optimal Value of FT α

Given that the separations succeeding FTS have been modeled using assumed split ratios the product distribution of the syncrude can be varied without attendant changes in the separation requirements. The α values are therefore varied independently of the FTS reactor altogether which is equivalent to assuming that FTS produces an ideal product distribution and then only the wax is hydrocracked. This approach highlights what α value should be targeted in FTS in order to maximise the diesel and liquids yield from the WHC.

6.1.1. Without WHC Heavy Wax Recycle

Given a full ASF distribution, one can seemingly produce diesel by changing α_{FTS}. In order to avoid confusion arising from this effect, the ASF distribution below a cutoff greater than the highest carbon number in diesel is regarded as zero. To clarify, if the cutoff is C_{10} then everything from C_1 to C_{10} is zero. The remaining compounds are summed up to give a total moles of hydrocarbons which are used to calculate the amount of hydrogen using the H2:Hydrocarbons ratio; finally, the mole fractions of all compounds are recalculated and multiplied with a fixed total molar flowrate to determine the true compound molar flows. Consequently, varying the $H_2 : Hydrocarbon$ ratio will distribute the same total molar flow between hydrogen and hydrocarbons heavier than diesel.

If only a small amount of catalyst is used, the feed to the hydrocracker cannot fully react; therefore, one finds that the optimal value of alpha will be the one that produces the most diesel-like compounds that fall outside of the cutoff range. To counteract this, one might try using a large quantity of catalyst to ensure that the amount of feed converted to diesel is maximized; however, the product distribution may overshoot the targeted diesel range and produce more sub-diesel compounds. Therefore the approach taken here is to steadily increase the catalyst loading and reinitialize the ODE with the results of the last iteration. This approach has been verified to produce the same result as taking the

ODE over the entire range of steps. If a single iteration fails due to lack of liquid, then the results will not be included.

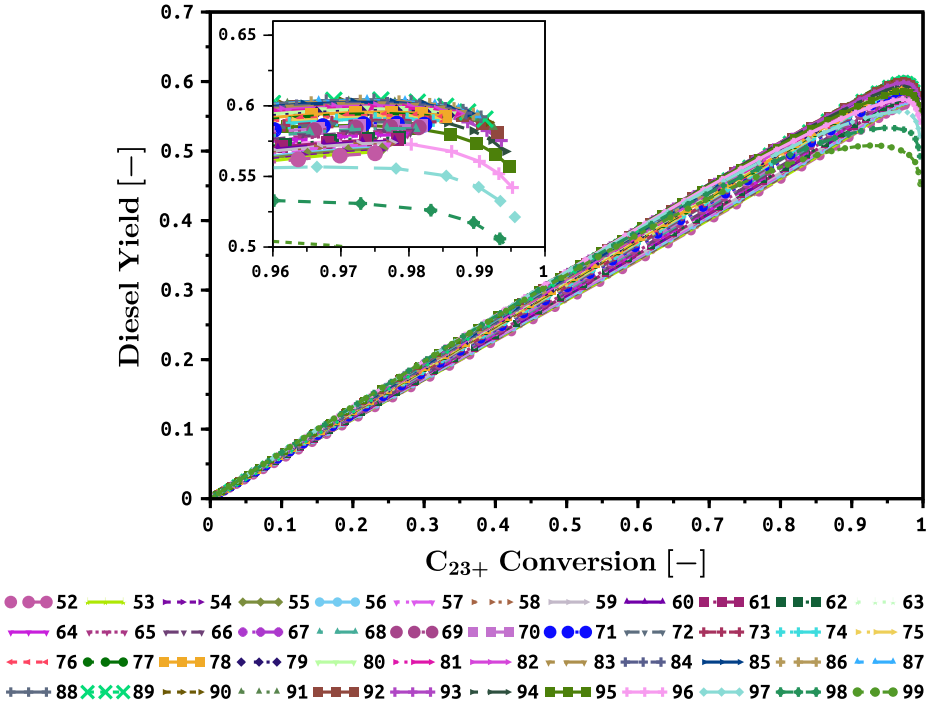

Figure 6.1: Once through hydrocracking of Fischer-Tropsch Synthesis C_{23+} wax, $T = 350^{o}C$, $P = 35\,bar$, $H_2 : Hydrocarbons = 15 : 1$ showing the sensitivity of the diesel yield to C_{23+} conversion and Fischer-Tropsch Synthesis α

Figure 6.1 shows the effect of increasing FTS α and conversion on the diesel yield in once through hydrocracking. The catalyst loading is fixed and chosen such that the conversion at an alpha value of 0.99 is highest. In reality, the maximum conversion will be reached when the reactor runs out of liquid and will always be 1 (i.e. all $C_{23}+$ material converted). However, in the case of this simulation, the maximum conversion will occur at the last time step and will decrease as the alpha value is decreased due to the fact that the last ODE time interval will be responsible for cracking a smaller and smaller quantity of the remaining wax (due to the fact that the amount of wax is decreasing because alpha is decreasing). The stipulation that both the C_{23+} conversion should be maximized along with the diesel yield leads to an optimal value of alpha. This optimum is due to the fact that the diesel range lies within the carbon number range (not at the end points) and therefore it is possible to over- or under-shoot this range in cracking. Too much cracking, and correspondingly, too high a conversion will result in a low diesel yield and too little will result in the same. Therefore there exists an optimum conversion under which the diesel yield will be maximized. The results in Figure 6.1 indicate that an alpha value of 0.88 is optimal for the diesel yield. If the carbon number range were to be changed, then the optimum alpha value might be expected to drift due to the presence of greater quantities of heavier wax compounds; however, the optimum remains the same when the carbon number range is reduced to 141 as shown in Figure 9.26.

6.1.2. With WHC Heavy Wax Recycle

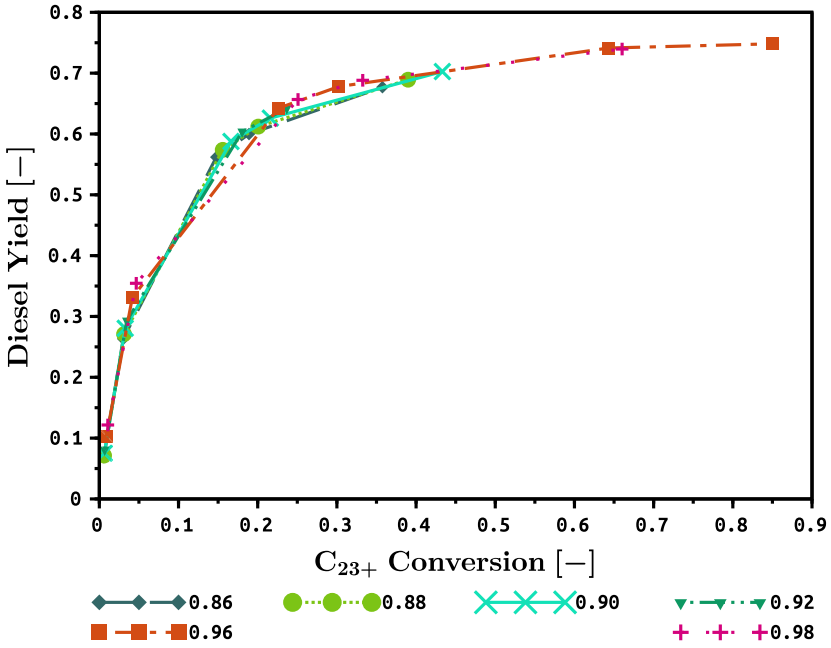

Figure 6.2: Once through hydrocracking of Fischer-Tropsch Synthesis C_{23+} wax $T = 350^oC$, $P = 35\,bar$, $H_2 : Hydrocarbons = 10 : 1$ showing the sensitivity of the diesel yield to C_{23+} conversion and Fischer-Tropsch Synthesis α with the heavy wax recycle active where the purge ratio is 5%

Figure 6.2 shows the effect of changing alpha value on the diesel yield and $C_{23}+$ conversion when the recycle is active with a 5% (total molar) purge ratio. The number of data points have been reduced in order to decrease solution time and the purge ratio is chosen also to decrease solution time while being as small as possible. Using the technique described in Section 4.0.2, it was difficult to obtain convergence at high conversion. However, the results show a definite shift from the case without recycle, where now an alpha value of 0.96 appears to be optimal. Given the slope of the curve for $\alpha = 0.88$, it is possible that the diesel yield will go on to be higher

Figure 9.27 shows a comparison between $\alpha = 0.88$ and $\alpha = 0.99$ for changing $C_{21}+$ conversion at a 45:1 $H_2 : Hydrocarbons$ ratio. At high per-pass conversions convergence of the recycle loop was not attainable. Comparing the two cases, at a conversion of 20% for $\alpha = 0.88$, the diesel yield is 61.2% for Figure 9.26 and 58.3% for Figure 9.27. This is the opposite of the expected effect for once through operation as the $H_2 : Hydrocarbons$ ratio has increased from 10:1 to 45:1.

The maximum diesel yield drops from 68.9% to 66.2% for $\alpha = 0.88$. In spite of the fact that the reactor was not solved for high conversion it is clearly illustrated in Figure 9.27 that at high conversion the diesel yield would remain below that of $\alpha = 0.99$.

6.2. Process Synthesis

Table 6.1: Gas-To-Liquids case studies where pure oxygen is supplied by the ASU

Configuration:	OOT80	OIRC40	OIRC60	OERC40	OERC60
α_{PO}	0.60	0.60	0.60	0.60	0.60
γ_{PO}	0.00	0.00	0.00	0.00	0.00
$(X_{CH_4})_{ATR}$	96.0%	96.0%	96.0%	96.1%	96.1%
$(H_2 : CO)_{ATR}$	2.04	2.04	2.04	2.04	2.04
$(H_2 : CO)_{FTS}$	2.04	1.79	1.59	2.05	2.04
$(x_{N_2})_{syngas}$	0.00%	0.00%	0.00%	0.00%	0.00%
$(X_{CO})_{FTS,pp}$	80.6%	40.2%	60.4%	40.3%	60.3%
α_{FTS}	0.93	0.91	0.88	0.94	0.94
$\left(S_{C_{10+}}\right)_{FTS}$	70.4%	46.6%	49.2%	44.3%	53.5%
$\left(X_{C_{21+}}\right)_{WHC,pp}$	66.8%	64.2%	59.5%	70.7%	68.4%
$(Y_{C10-C20})_{WHC}$	74.4%	74.3%	73.8%	74.5%	74.5%
$(\eta_{C10-C20})_{plant}$	36.6%	43.6%	42.2%	34.7%	41.2%
$\left(\eta_{liquids}\right)_{plant}$	79.1%	67.3%	67.6%	53.9%	62.9%

Table 6.1 shows the results of the case studies for the various configurations. It was found that in the OERC40 and OERC60 cases, that it was not possible to achieve $\alpha_{FTS} > 0.9$; therefore, the k_5 rate constant was increased by a factor of 22. The reformers are operated with $\alpha_{PO} = 0.6$ and at a pressure of 10 bar in order to maximize the $H_2 : CO$ ratio at high methane conversion. Consequently, an $H_2 : CO$ ratio close to 2.0 is achievable at a methane conversion of 96%. The $H_2 : CO$ ratio entering the FTS reactor is dependent upon whether the internal and external recycles are active. For the internal recycle case, the reformer operation would need to be adjusted in order to produce a higher $H_2 : CO$ ratio to compensate for the effect of combining the fresh syngas with the recycle. However, $H_2 : CO$ ratios below 2.0 are beneficial to wax formation but should not fall below a 1:1 ratio where plugging is a potential risk (Atwood and Bennett, 1979). In the OIRC40 and OIRC60 cases, the $H_2 : CO$ ratios drop to 1.79 and 1.59, respectively. This is mitigated by the low conversion in the OIRC40 case, since the heavy wax alpha value generally decreases with conversion provided the conversion is low as has been shown in Section 5.3.2. In the OIRC60 case, the effect of the increased conversion on alpha is more pronounced. The OERC40 and OERC60 cases show that the 25% external recycle is able to maintain the $H_2 : CO$ ratio around 2.0. Additionally, the highestα_{FTS} values seen in the ERC cases are comparable to the OT case since the $H_2 : CO$ ratio is practically unchanged. The diesel and wax selectivity of the syncrude is highest in the OOT80 case, which is attributed to the tendency for the wax production to increase with conversion for $X_{CO} \geq 80\%$ as shown in Section 5.3.2. In all cases, the WHC is operated such that recycle converges and the conversion is maximized without the VLE procedure failing. However, the conversion in hydrocracking does not have a significant effect on the diesel yield (from wax feed to wax product) as shown in Table 6.1 which remains around 74% in all cases. In terms of the plantwide carbon efficiencies, the efficiency to diesel is highest

for the OIRC40 case and lowest for the OERC40 case. This may be due to the effect of the tail gas on FTS diesel production, as in the ERC40 case the least amount of tail gas is recycled. In the OOT80 case, the efficiency to diesel is lower than all except the OERC40 case, which is attributed to the lack of stream integration. The plantwide carbon efficiency to liquids is highest for the OOT80 case, which results directly from the high liquid selectivity in FTS highlighting the potential for such a configuration to be utilized if the production of stable pumpable liquid is desired.

Table 6.2: Gas-To-Liquids case studies where oxygen is partially or fully supplied by air

Configuration:	**A25OT80**	**A50OT80**	**A100OT80**
α_{PO}	0.60	0.60	0.60
γ_{PO}	0.00	0.00	0.00
$(X_{CH_4})_{ATR}$	95.4%	94.4%	92.5%
$(H_2 : CO)_{ATR}$	2.04	2.04	2.04
$(H_2 : CO)_{FTS}$	2.04	2.04	2.04
$(x_{N_2})_{syngas}$	16.8%	28.9%	45.4%
$(X_{CO})_{FTS,pp}$	80.2%	80.5%	80.4%
α_{FTS}	0.91	0.90	0.88
$\left(S_{C_{10+}}\right)_{FTS}$	69.1%	68.0%	65.7%
$\left(X_{C_{21+}}\right)_{WHC,pp}$	64.5%	62.6%	60.2%
$(Y_{C10-C20})_{WHC}$	74.3%	74.1%	73.9%
$(\eta_{C10-C20})_{plant}$	35.4%	34.3%	31.8%
$\left(\eta_{liquids}\right)_{plant}$	78.8%	78.4%	76.9%

The plantwide effects of the introduction of nitrogen as determined in Sections 5.2 and 5.3.2 are as follows, a reduction in the methane conversion in the ATR, an increase in the $H_2 : CO$ ratio out of the ATR, a reduction in the conversion of carbon monoxide in FTS and a reduction in α_{FTS}. The catalyst loading in ATR was increased in order to increase the conversion and to lower the $H_2 : CO$ ratio back to approximately 2:1. Furthermore, the FTS catalyst loading was increased in order to keep the conversion around 80%. The k_5 rate constant was not changed in order to capture the effect of the presence of nitrogen in FTS on α_{FTS}. Table 6.2 shows the results of the case studies for 25%, 50% and 100% of oxygen supplied by air in the ATR, A25OT80, A50OT80, A100OT80, respectively. The conversion of methane in the ATR at which a $H_2 : CO$ ratio of 2:1 will be achieved decreases with increasing air fraction. At an air fraction of 25%, the methane conversion is 95.4% and subsequently decreases to 94.4% for an air fraction of 50% and 92.5% for 100% air fraction. In the sensitivity analysis, two operating regimes were identified where the addition of nitrogen could be beneficial or the detrimental effect minimal. These were at 25% nitrogen in the feed to the ATR, where there is benefit to the $H_2 : CO$ ratio, and 30% nitrogen fraction in the syngas, where the second highest α_{FTS} was observed. These two scenarios are reproduced in the A25OT80 and the A50OT80 cases, respectively. As shown in Table 6.2, at 50% air fraction the nitrogen fraction in syngas is close to 30%. As mentioned previously, the catalyst loading in the ATR (specifically SMR) has been

increased in order to bring down the $H_2 : CO$ ratio to the benefit of the conversion. In the A50OT80 case, α_{FTS} decreased to 0.90 from approximately 0.93 (OOT80). The selectivity to liquids heavier than diesel reduced by less than 3% in going from OOT to AOT configurations. The plantwide carbon efficiency to diesel reduced by 1.2% and 2.3% for A25OT80 and A50OT80, respectively. However, the decrease in liquid selectivity is 4.7% for the A100OT80 case. The overall efficiency to liquids reduced by 0.3%, 0.7% and 2.2% between the OOT and three AOT cases. In the former two cases, the effect on the operation of the hydrocracker is minimal due to the small changes in α_{FTS} and the $S_{C_{10+}}$ selectivity.

7. Conclusions and Recommendations

7.1. Outcomes

The physical properties for the paraffins and α-olefins were regressed for carbon numbers from C_1 to C_{200}. In all cases, large extrapolations were required and the asymptotes at the limit were generally uncertain. However, in the case of Critical Temperature and Normal Boiling Point, self consistency was demonstrated in that both approached the same limiting value. The group contribution methods were found to be unsuitable for large extrapolations in estimating the properties of paraffins and olefins due to the formulation of the correlations causing infinite increase in the property values.

In reforming, the optimal oxygen to methane (or to feed carbon) ratio was 0.6, while the optimal ratio of steam to carbon was 0. Increasing the oxygen to methane ratio resulted in an increased top temperature out of partial oxidation which was beneficial to the rates of reaction in the steam reforming section. However, increasing the oxygen to methane ratio beyond stoichiometric quantities for combustion resulted in decreased performance.

Increasing the steam to methane (or carbon) ratio led to an increase in the $H_2 : CO$ ratio in the syngas out of the reformer and a decrease in the overall conversion of methane. A decrease in the top temperature was also observed which drove the increase in the $H_2 : CO$ ratio.

Low pressure in reforming led to higher top temperature and higher conversion. Additionally, the $H_2 : CO$ ratio was found to decrease with increasing pressure.

At baseline conditions in the FTS product distribution, the carbon numbers C_{31} to C_{61} contained 35.1% and 13.5% of the total mass of product where the maximum carbon number was C_{61}, and 31.3% of the total mass of product where the maximum carbon number was C_{161}. The range C_{31} to C_{161} contained 42.0% of the mass of product. Therefore, it is concluded that accounting for carbon numbers only up to C_{30} will lead to a substantial misrepresentation of the product distribution. For alpha values up to 0.94 the benefit of accounting for carbon numbers beyond C_{200} will be far less than the benefit for accounting for carbon numbers beyond C_{30}, as incremental increases in the maximum carbon number always see diminishing improvements in accounting for all the material.

The product distribution produced by the FTS reactor model changed appreciably with system conditions complicating the description of the product by one or two alpha values. Therefore, it is recommended that a dynamic system of fitting alpha be applied to real product distributions where the number of alpha values is unspecified and the range over which alpha is fitted is calculated for each product distribution specifically.

In FTS, an increase in pressure led to an increased chain growth probability in the first alpha value and a decrease in the paraffin to olefin ratio. The second alpha value which is more representative of heavy wax showed a maximum alpha value at a pressure of 30 bar, 20 bar and 35 bar at carbon monoxide conversions of 40%, 60% and 80%, respectively.

This resulted from an inflection in the product distribution which occurred earliest in the carbon number range for these pressures.

Increasing the $H_2 : CO$ ratio resulted in a decrease in alpha consistently for conversions of 40% and 60%; however, at 80% conversion this trend was only seen in the first alpha value. The product distribution displayed an inflection point early in the distribution resulting in a higher than expected second alpha value. This meant the alpha value was maximized at an $H_2 : CO$ ratio of 2.0 where the point of inflection occurred earliest in the carbon number range.

Increasing the nitrogen fraction in the syngas had the effect of lowering the alpha value as a result of the increasing surface concentration of hydrogen. However, at 60% conversion the presence of 10% (mol) nitrogen in the syngas led to a maximum in the alpha value resulting from a maximum in the $H\theta$ and $CH_2\theta$ surface species concentrations.

The maximum achievable once through C_{23+} conversion (before liquid ran out) was observed at $H_2 : Hydrocarbons$ ratio of 10, while the maximum diesel yield was observed for a ratio of 20. A reduction in maximum conversion was observed for increasing $H_2 : Hydrocarbons$ ratio due to the inverse proportional relationship between the species rates and the hydrogen activity. The peak in diesel yield was attributed to the balance between over cracking at excess conversion and under cracking at low conversion.

A once through $C_{23}+$ conversion of 95% was achievable at a pressure of 35 bar. This pressure also produced the maximum diesel yield (60%). This was attributed to the proportional relationship between pressure and activity which is tied to the rate of cracking. Moreover, because a specific carbon range (in the middle of the whole range) is being targeted an optimum between over-cracking and under-cracking must exist.

The maximum achievable $C_{23}+$ conversion was found to increase with increasing FTS chain growth probability; however, when the heavy wax recycle stream was inactive a maximum in the diesel yield was observed for an alpha value of 0.92.

In the plantwide analyses, using air instead of pure oxygen was found to result in significant decreases in the conversion in FTS and considerable decrease in the chain growth probability. The performance changes could not be reversed by merely increasing the catalyst loading. Instead, the catalyst performance itself needed to be adjusted, specifically the ability of the catalyst to promote chain growth and conversion (k_5 rate constant, (Mthombeni, 2009)). It was found that increasing the k_5 rate constant by a factor of 4 would be sufficient to reverse the performance loss resulting from the use of nitrogen diluted syngas (35% mol N_2).

The chain growth probability was found to have a significant effect on the diesel yield in hydrocracking. As the chain growth probability increased, the diesel yield increased significantly and the $C_{23}+$ conversion decreased to a lesser extent. Therefore, it is concluded that for the case of hydrocracking of wax with wax recycle, in order to maximize diesel yield the alpha value in FTS should be as high as possible.

Of the process configurations investigated, the OT80 configuration produced the highest liquid selectivity (79.1%), while the plantwide efficiency to diesel was highest for the recycle configurations OIRC40 (43.6%) and OIRC60 (42.2%). When air was used to supply oxygen to the reformers, the A25OT80 and A50OT80 configurations were found to show similar performance to the OOT80 configuration with a maximum reduction in efficiency to diesel of 2.3% and a maximum reduction in plantwide efficiency to liquids of 0.7%.

7.2. Model Improvements

The following points address some of the most immediate shortcomings of the process model or represent interesting and relevant (in the context of the literature) additions. The following are recommended:

- Modeling the FTS slurry reactor as a three phase system (vapor-organic-aqueous)
- Incorporation of the temperature dependence into the FTS rate constants
- Expansion of physical properties to include all FTS primary products
- The use of Model C (Le Grange, 2009) in the WHC
- Implementation of an elementary combustion reactor model in the ATR
- Economic analysis and optimization of the process

8. References

Carlo Accolla. A reactor model for ft wax hydrocracking. Master's thesis, University of Cape Town, 2006.

Thomas A Adams and Paul I Barton. Combining coal gasification and natural gas reforming for efficient polygeneration. *Fuel Processing Technology*, 92(3):639–655, 2011.

Serina Ahlgren, Andras Baky, Sven Bernesson, Åke Nordberg, Olle Norén, and P-A Hansson. Future fuel supply systems for organic production based on fischer–tropsch diesel and dimethyl ether from on-farm-grown biomass. *Biosystems Engineering*, 99(1): 145–155, 2008.

Victor R Ahon, Esly F Costa, Jorge EP Monteagudo, Carlos E Fontes, Evaristo C Biscaia, and Paulo LC Lage. A comprehensive mathematical model for the fischer–tropsch synthesis in well-mixed slurry reactors. *Chemical engineering science*, 60(3):677–694, 2005.

Harvey E Atwood and Carroll O Bennett. Kinetics of the fischer-tropsch reaction over iron. *Industrial & Engineering Chemistry Process Design and Development*, 18(1):163–170, 1979.

Richard C Baliban, Josephine A Elia, Vern Weekman, and Christodoulos A Floudas. Process synthesis of hybrid coal, biomass, and natural gas to liquids via fischer–tropsch synthesis, zsm-5 catalytic conversion, methanol synthesis, methanol-to-gasoline, and methanol-to-olefins/distillate technologies. *Computers & Chemical Engineering*, 47: 29–56, 2012.

Buping Bao, Mahmoud M El-Halwagi, and Nimir O Elbashir. Simulation, integration, and economic analysis of gas-to-liquid processes. *Fuel Processing Technology*, 91(7): 703–713, 2010.

Omar M Basha, Laurent Sehabiague, Ahmed Abdel-Wahab, and Badie I Morsi. Fischer–tropsch synthesis in slurry bubble column reactors: Experimental investigations and modeling–a review. *International Journal of Chemical Reactor Engineering*, 13(3):201–288, 2015.

RJ Berger and GB Marin. Investigation of gas-phase reactions and ignition delay occurring at conditions typical for partial oxidation of methane to synthesis gas. *Industrial & engineering chemistry research*, 38(7):2582–2592, 1999.

P Maarten Biesheuvel and Gert Jan Kramer. Two-section reactor model for autothermal reforming of methane to synthesis gas. *AIChE journal*, 49(7):1827–1837, 2003.

G Bub, M Baerns, B Bussemeier, and C Frohning. Prediction of the performance of catalytic fixed bed reactors for fischer-tropsch synthesis. *Chemical Engineering Science*, 35(1-2):348–355, 1980.

Gerald N Choi, Sheldon J Kramer, Samuel S Tam, Joe M Fox, Norman L Carr, and Geoffrey R Wilson. Design/economics of a once-through natural gas fischer-tropsch plant with power co-production. In *Coal Liquefaction & Solid Fuels Contractors Review Conference*, 1997.

Leonidas Constantinou and Rafiqul Gani. New group contribution method for estimating properties of pure compounds. *AIChE Journal*, 40(10):1697–1710, 1994.

Ann M De Groote and Gilbert F Froment. Simulation of the catalytic partial oxidation of methane to synthesis gas. *Applied Catalysis A: General*, 138(2):245–264, 1996.

Arno de Klerk. *Fischer-Tropsch Refining*. PhD thesis, University of Pretoria, 2008.

Ronald A Dictor and Alexis T Bell. An explanation for deviations of fischer-tropsch products from a schulz-flory distribution. *Industrial & Engineering Chemistry Process Design and Development*, 22(4):678–681, 1983.

Dhammike Dissanayake, Michael P Rosynek, Karl CC Kharas, and Jack H Lunsford. Partial oxidation of methane to carbon monoxide and hydrogen over a ni/al2o3 catalyst. *Journal of Catalysis*, 132(1):117–127, 1991.

Alessandro Donazzi, Alessandra Beretta, Gianpiero Groppi, and Pio Forzatti. Catalytic partial oxidation of methane over a 4% rh/α-al2o3 catalyst: Part i: Kinetic study in annular reactor. *Journal of Catalysis*, 255(2):241–258, 2008.

Mark E Dry. High quality diesel via the fischer–tropsch process–a review. *Journal of Chemical Technology and Biotechnology*, 77(1):43–50, 2002.

J Eilers, SA Posthuma, and ST Sie. The shell middle distillate synthesis process (smds). *Catalysis Letters*, 7(1-4):253–269, 1990.

RL Espinoza, AP Steynberg, B Jager, and AC Vosloo. Low temperature fischer–tropsch synthesis from a sasol perspective. *Applied Catalysis A: General*, 186(1):13–26, 1999.

Fabiano AN Fernandes. Modeling and product grade optimization of fischer-tropsch synthesis in a slurry reactor. *Industrial & engineering chemistry research*, 45(3):1047–1057, 2006.

Paul J Flory. Molecular size distribution in linear condensation polymers1. *Journal of the American Chemical Society*, 58(10):1877–1885, 1936.

Christodoulos A Floudas, Josephine A Elia, and Richard C Baliban. Hybrid and single feedstock energy processes for liquid transportation fuels: A critical review. *Computers & Chemical Engineering*, 41:24–51, 2012.

Robert Guettel and Thomas Turek. Comparison of different reactor types for low temperature fischer–tropsch synthesis: a simulation study. *Chemical Engineering Science*, 64 (5):955–964, 2009.

Xu Hao, Martina Elissa Djatmiko, YY Xu, YI Wang, Jie Chang, and YW Li. Simulation analysis of a gtl process using aspen plus. *Chemical engineering & technology*, 31(2): 188–196, 2008.

Enrique Iglesia, Sebastian C Reyes, and Rostam J Madon. Transport-enhanced α-olefin readsorption pathways in ru-catalyzed hydrocarbon synthesis. *Journal of Catalysis*, 129 (1):238–256, 1991.

A Jess, R Popp, and K Hedden. Fischer–tropsch-synthesis with nitrogen-rich syngas: fundamentals and reactor design aspects. *Applied Catalysis A: General*, 186(1):321–342, 1999.

W Jin, X Gu, S Li, P Huang, N Xu, and J Shi. Experimental and simulation study on a catalyst packed tubular dense membrane reactor for partial oxidation of methane to syngas. *Chemical Engineering Science*, 55(14):2617–2625, 2000.

Philipp Kaiser, Rajabhau Bajirao Unde, Christoph Kern, and Andreas Jess. Production of liquid hydrocarbons with co2 as carbon source based on reverse water-gas shift and fischer-tropsch synthesis. *Chemie Ingenieur Technik*, 85(4):489–499, 2013.

GA Karim, AS Hanati, and G Zhou. A kinetic investigation of the oxidation of low heating value fuel mixtures of methane and diluents. *Journal of energy resources technology*, 115(4):301–306, 1993.

Yong Heon Kim, Ki-Won Jun, Hyunku Joo, Chonghun Han, and In Kyu Song. A simulation study on gas-to-liquid (natural gas to fischer-tropsch synthetic fuel) process optimization. *Chemical Engineering Journal*, 155(1-2):427 – 432, 2009. ISSN 1385-8947. doi: http://dx.doi.org/10.1016/j.cej.2009.08.018. URL http://www.sciencedirect.com/science/article/pii/S1385894709005919.

Cyril Knottenbelt. Mossgas "gas-to-liquid" diesel fuels-an environmentally friendly option. *Catalysis Today*, 71(3):437–445, 2002.

Aleksander Kreglewski and Bruno J Zwolinski. A new relation for physical properties of n-alkanes and n-alkyl compounds1. *The Journal of Physical Chemistry*, 65(6):1050–1052, 1961.

Thomas G Kreutz, Eric D Larson, Guangjian Liu, and Robert H Williams. Fischer-tropsch fuels from coal and biomass. In *25th annual international Pittsburgh coal conference*, volume 29, 2008.

Philip Le Grange. Models for the hydrocracking of fischer-tropsch derived waxes. Master's thesis, University of Cape Town, 2009.

Dieter Leckel. Hydrocracking of iron-catalyzed fischer-tropsch waxes. *Energy & fuels*, 19 (5):1795–1803, 2005.

Chul-Jin Lee, Youngsub Lim, Ho Soo Kim, and Chonghun Han. Optimal gas-to-liquid product selection from natural gas under uncertain price scenarios. *Industrial & Engineering Chemistry Research*, 48(2):794–800, 2008.

Guangjian Liu, Eric D Larson, Robert H Williams, Thomas G Kreutz, and Xiangbo Guo. Making fischer- tropsch fuels and electricity from coal and biomass: performance and cost analysis. *Energy & Fuels*, 25(1):415–437, 2010.

John J Marano and Gerald D Holder. General equation for correlating the thermophysical properties of n-paraffins, n-olefins, and other homologous series. 1. formalism for developing asymptotic behavior correlations. *Industrial & engineering chemistry research*, 36(5):1887–1894, 1997a.

John J Marano and Gerald D Holder. General equation for correlating the thermophysical properties of n-paraffins, n-olefins, and other homologous series. 2. asymptotic behavior correlations for pvt properties. *Industrial & engineering chemistry research*, 36(5):1895–1907, 1997b.

John J Marano and Gerald D Holder. A general equation for correlating the thermophysical properties of n-paraffins, n-olefins, and other homologous series. 3. asymptotic behavior correlations for thermal and transport properties. *Industrial & engineering chemistry research*, 36(6):2399–2408, 1997c.

Bongani Mthombeni. *Modeling Fischer Tropsch Synthesis in Two-phase, Continuous, Well-mixed Slurry Reactors*. PhD thesis, University of Cape Town, 2009.

Mehdi Panahi, Ahmad Rafiee, Sigurd Skogestad, and Magne Hillestad. A natural gas to liquids process model for optimal operation. *Industrial & Engineering Chemistry Research*, 51(1):425–433, 2011.

J Patzlaff, Y Liu, C Graffmann, and J Gaube. Studies on product distributions of iron and cobalt catalyzed fischer–tropsch synthesis. *Applied Catalysis A: General*, 186(1): 109–119, 1999.

Kenneth S Pitzer. The volumetric and thermodynamic properties of fluids. i. theoretical basis and virial coefficients1. *Journal of the American Chemical Society*, 77(13):3427–3433, 1955.

Kenneth S Pitzer and RF Curl Jr. The volumetric and thermodynamic properties of fluids. iii. empirical equation for the second virial coefficient1. *Journal of the American Chemical Society*, 79(10):2369–2370, 1957.

Kenneth S Pitzer, David Z Lippmann, RF Curl Jr, Charles M Huggins, and Donald E Petersen. The volumetric and thermodynamic properties of fluids.: Ii. compressibility factor, vapor pressure and entropy of vaporization. In *Molecular Structure And Statistical Thermodynamics: Selected Papers of Kenneth S Pitzer*, pages 303–310. World Scientific, 1993.

Bruce E Poling, John M Prausnitz, John P O'connell, et al. *The properties of gases and liquids*, volume 5. Mcgraw-hill New York, 2001.

Mark J Prins, Krzysztof J Ptasinski, and Frans JJG Janssen. Exergetic optimisation of a production process of fischer–tropsch fuels from biomass. *Fuel Processing Technology*, 86(4):375–389, 2005.

I Puskas and R.S Hurlbut. Comments about the causes of deviations from the anderson-schulz-flory distribution of the fischer-tropsch reaction products. *Catalysis Today*, 84(1-2):99 – 109, 2003. ISSN 0920-5861. doi: http://dx.doi.org/10.1016/S0920-5861(03)00305-5. URL http://www.sciencedirect.com/science/article/pii/S0920586103003055. Syngas Generation and Conversion to Fuels and Chemicals, {AIChE} Spring Meeting.

S Rowshanzamir, MH Eikani, et al. Autothermal reforming of methane to synthesis gas: Modeling and simulation. *international journal of hydrogen energy*, 34(3):1292–1300, 2009.

Buchang Shi and Burtron H Davis. Fischer–tropsch synthesis: the paraffin to olefin ratio as a function of carbon number. *Catalysis today*, 106(1):129–131, 2005.

ST Sie, MMG Senden, and HMH Van Wechem. Conversion of natural gas to transportation fuels via the shell middle distillate synthesis process (smds). *Catalysis Today*, 8(3):371–394, 1991.

J Ilja Siepmann, Sami Karaborni, and Berend Smit. Simulating the critical behaviour of complex fluids. *Nature*, 365(6444):330, 1993.

Bruce E Stangeland. A kinetic model for the prediction of hydrocracker yields. *Industrial & Engineering Chemistry Process Design and Development*, 13(1):71–76, 1974.

Andre Steynberg and Mark Dry. *Fischer-Tropsch Technology*, volume 152. Elsevier, 2004.

Maria Sudiro and Alberto Bertucco. Production of synthetic gasoline and diesel fuel by alternative processes using natural gas and coal: Process simulation and optimization. *Energy*, 34(12):2206 – 2214, 2009. ISSN 0360-5442. doi: http://dx.doi.org/10.1016/j.energy.2008.12.009. URL http://www.sciencedirect.com/science/article/pii/S0360544208003186. {ECOS} 2007.

Michiel J.A. Tijmensen, Andrae P.C. Faaij, Carlo N. Hamelinck, and Martijn R.M. van Hardeveld. Exploration of the possibilities for production of fischer tropsch liquids and power via biomass gasification. *Biomass and Bioenergy*, 23(2):129 – 152, 2002. ISSN 0961-9534. doi: http://dx.doi.org/10.1016/S0961-9534(02)00037-5. URL http://www.sciencedirect.com/science/article/pii/S0961953402000375.

Chorng H Twu, John E Coon, and John R Cunningham. A generalized vapor pressure equation for heavy hydrocarbons. *Fluid Phase Equilibria*, 96:19–31, 1994.

Chorng H Twu, John E Coon, and John R Cunningham. A new generalized alpha function for a cubic equation of state part 1. peng-robinson equation. *Fluid Phase Equilibria*, 105(1):49–59, 1995.

Chorng H Twu, John E Coon, and David Bluck. Equations of state using an extended twu-coon mixing rule incorporating unifac for high temperature and high pressure phase equilibrium predictions. *Fluid Phase Equilibria*, 139(1-2):1–13, 1997.

Gerald Peter van der Laan. *Kinetics, selectivity and scale up of the Fischer-Tropsch synthesis*. [University Library Groningen][Host], 1999.

Gerard P van der Laan, Antonie ACM Beenackers, and Rajamani Krishna. Multicomponent reaction engineering model for fe-catalyzed fischer–tropsch synthesis in commercial scale slurry bubble column reactors. *Chemical Engineering Science*, 54(21):5013–5019, 1999.

Eric van Steen and Hans Schulz. Polymerisation kinetics of the fischer-tropsch {CO} hydrogenation using iron and cobalt based catalysts. *Applied Catalysis A: General*, 186(1-2):309 – 320, 1999. ISSN 0926-860X. doi: http://dx.doi.org/10.1016/S0926-860X(99)00151-9. URL http://www.sciencedirect.com/science/article/pii/S0926860X99001519.

Oscar P.R. van Vliet, Andrae P.C. Faaij, and Wim C. Turkenburg. Fischer-tropsch diesel production in a well-to-wheel perspective: A carbon, energy flow and cost analysis. *Energy Conversion and Management*, 50(4):855 – 876, 2009. ISSN 0196-8904. doi: http://dx.doi.org/10.1016/j.enconman.2009.01.008. URL http://www.sciencedirect.com/science/article/pii/S0196890409000041.

Alessandro Vetere. New correlations for predicting vaporization enthalpies of pure compounds. *The Chemical Engineering Journal*, 17(2):157–162, 1979.

Alessandro Vetere. Methods to predict the vaporization enthalpies at the normal boiling temperature of pure compounds revisited. *Fluid Phase Equilibria*, 106(1-2):1–10, 1995.

Carlo Giorgio Visconti. Vapor–liquid equilibria in the low-temperature fischer–tropsch synthesis. *Industrial & Engineering Chemistry Research*, 53(5):1727–1734, 2013.

Carlo Giorgio Visconti, Enrico Tronconi, Luca Lietti, Roberto Zennaro, and Pio Forzatti. Development of a complete kinetic model for the fischer–tropsch synthesis over co/al 2 o 3 catalysts. *Chemical Engineering Science*, 62(18):5338–5343, 2007.

Yi-Ning Wang, Yuan-Yuan Xu, Yong-Wang Li, Yu-Long Zhao, and Bi-Jiang Zhang. Heterogeneous modeling for fixed-bed fischer–tropsch synthesis: Reactor model and its applications. *Chemical Engineering Science*, 58(3):867–875, 2003.

Yu Wang, Wei Fan, Ying Liu, Zhiyong Zeng, Xu Hao, Ming Chang, Chenghua Zhang, Yuanyuan Xu, Hongwei Xiang, and Yongwang Li. Modeling of the fischer–tropsch synthesis in slurry bubble column reactors. *Chemical Engineering and Processing: Process Intensification*, 47(2):222–228, 2008.

Kwang-Jae Woo, Suk-Hwan Kang, Seung-Moon Kim, Jong-Wook Bae, and Ki-Won Jun. Performance of a slurry bubble column reactor for fischer–tropsch synthesis: determination of optimum condition. *Fuel processing technology*, 91(4):434–439, 2010.

Jianguo Xu and Gilbert F Froment. Methane steam reforming, methanation and water-gas shift: I. intrinsic kinetics. *AIChE Journal*, 35(1):88–96, 1989.

Yali Yao, Xinying Liu, Diane Hildebrandt, and David Glasser. Fischer–tropsch synthesis using h 2/co/co 2 syngas mixtures: a comparison of paraffin to olefin ratios for iron and cobalt based catalysts. *Applied Catalysis A: General*, 433:58–68, 2012.

Marcelo S Zabaloy and Juan H Vera. The peng- robinson sequel. an analysis of the particulars of the second and third generations. *Industrial & engineering chemistry research*, 37(5):1591–1597, 1998.

9. Appendices

9.1. ThermoPhysical Properties

Table 9.1: First-order groups used in the property estimation (Constantinou and Gani, 1994)

Group	t_{c1i}	p_{c1i} $bar^{-0.5}$	v_{c1i} $m^3/kmol$	t_{b1i}	t_{m1i}	h_{1i} kJ/mol	g_{1i} kJ/mol	h_{v1i} kJ/mol
CH_3	1.6781	0.019904	0.07504	0.8894	0.4640	-45.947	-8.030	4.116
CH_2	3.4920	0.010558	0.05576	0.9225	0.9246	-20.763	8.231	4.650

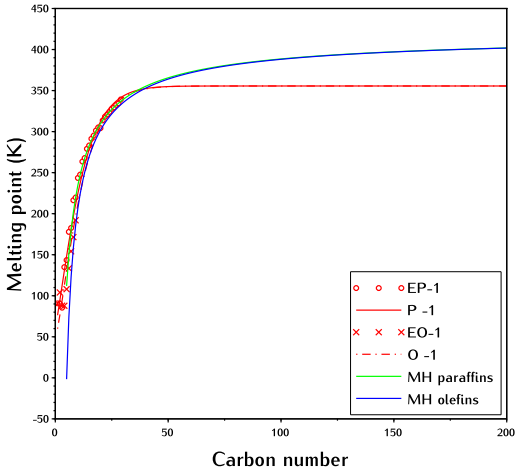

Figure 9.1: Melting point

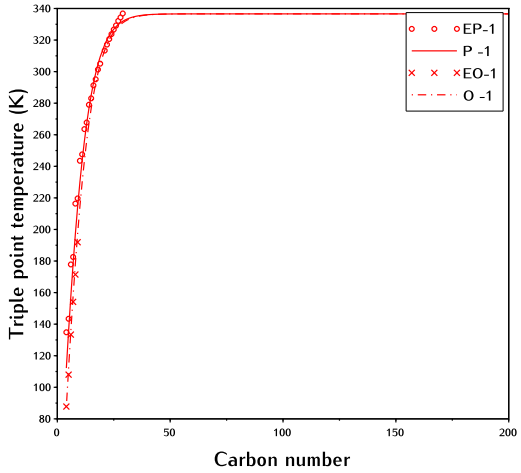

Figure 9.2: Triple point temperature

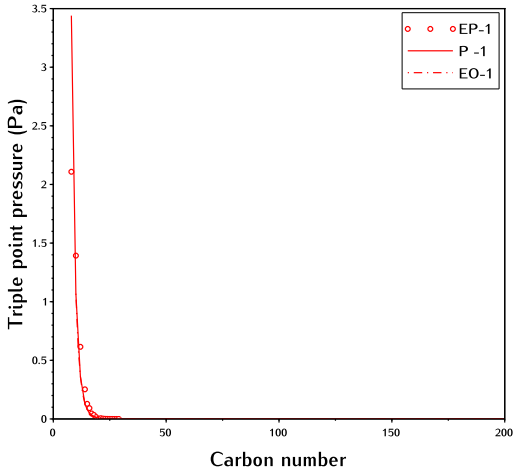

Figure 9.3: Triple Point Pressure

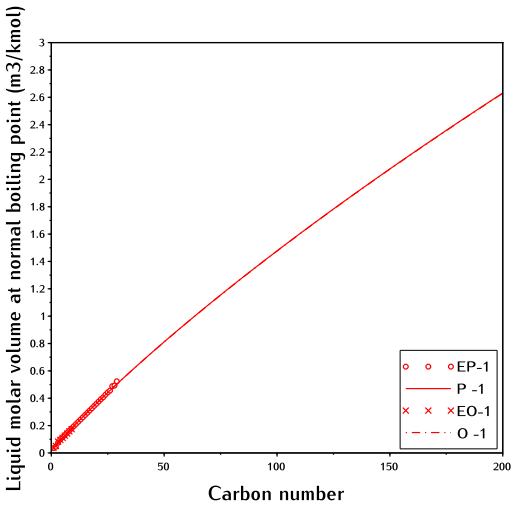

Figure 9.4: Liquid molar volume at normal boiling point

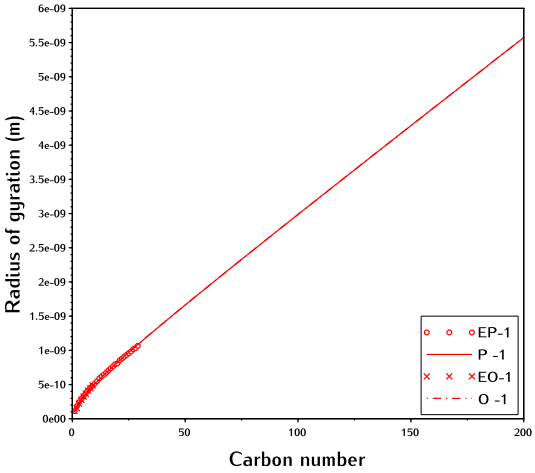

Figure 9.5: Radius of gyration

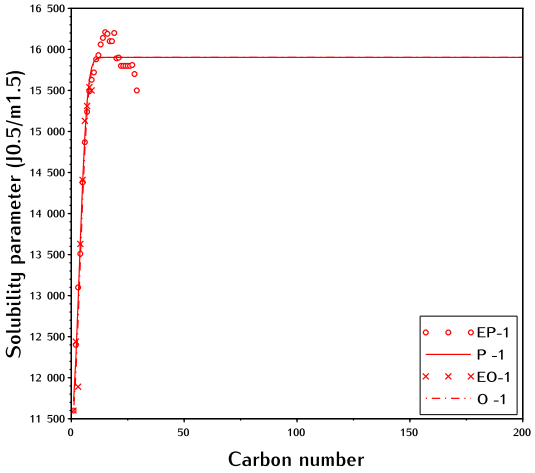

Figure 9.6: Solubility parameter

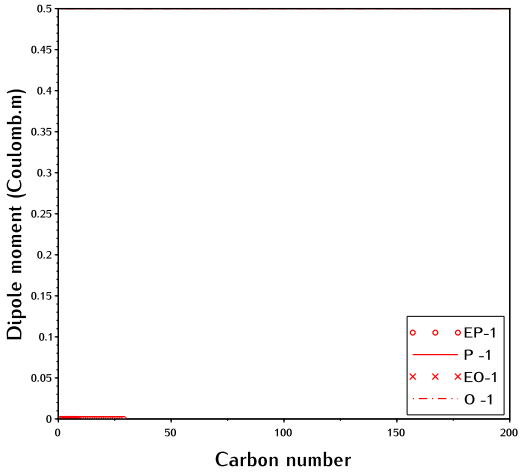

Figure 9.7: Dipole moment

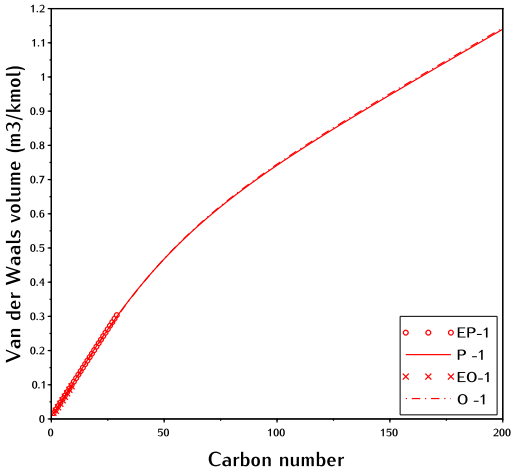

Figure 9.8: Van der Waals volume

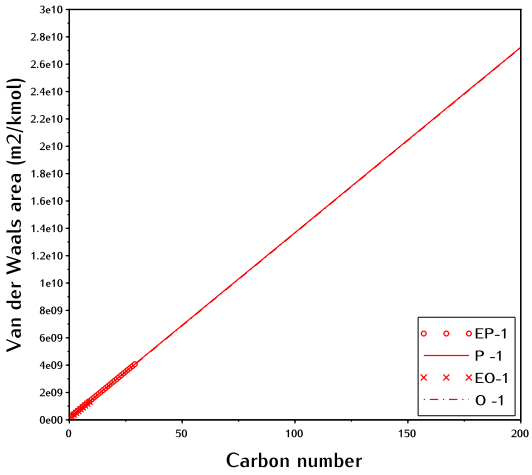

Figure 9.9: Van der Waals area

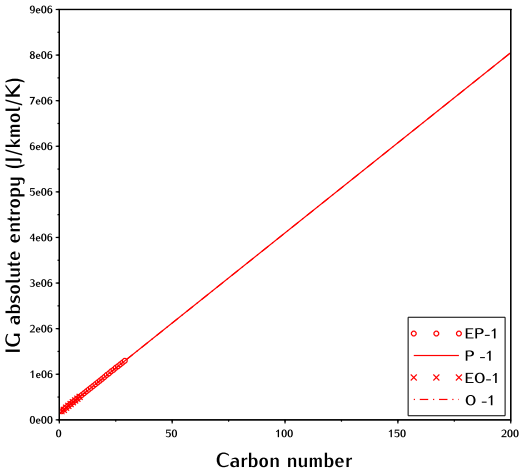

Figure 9.10: Ideal Gas absolute entropy

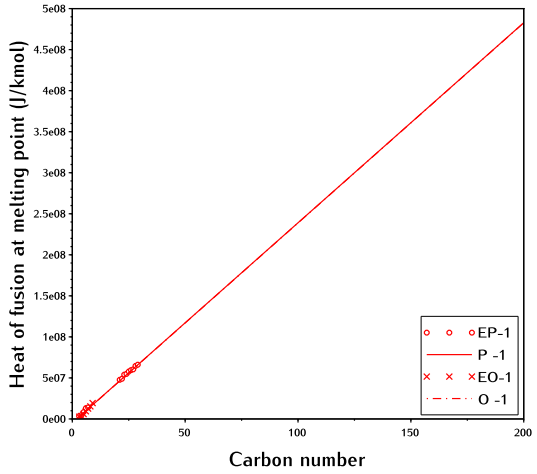

Figure 9.11: Heat of fusion at melting point

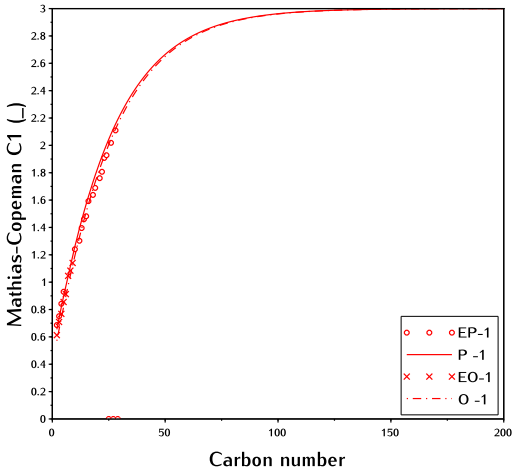

Figure 9.12: Mathias-Copeman C1

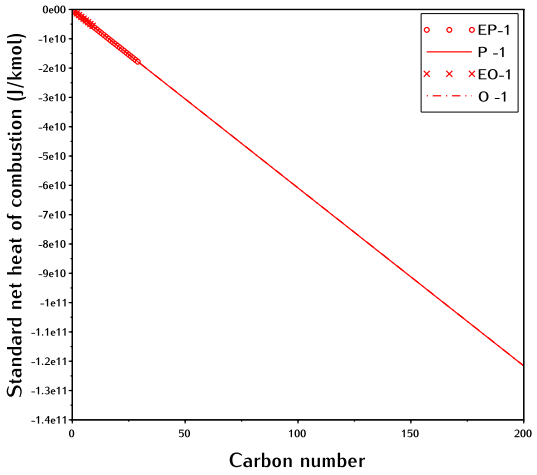

Figure 9.13: Standard net heat of combustion

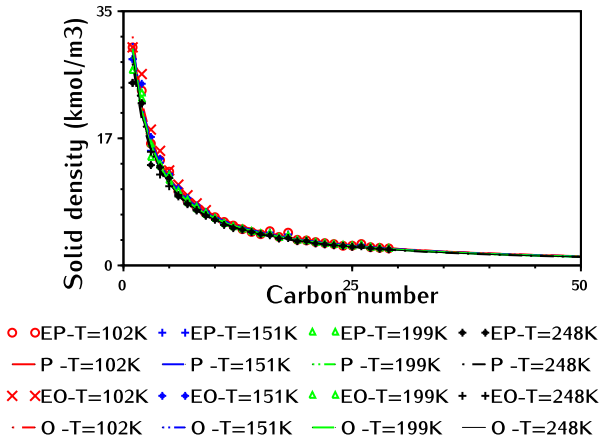

Figure 9.14: Solid density

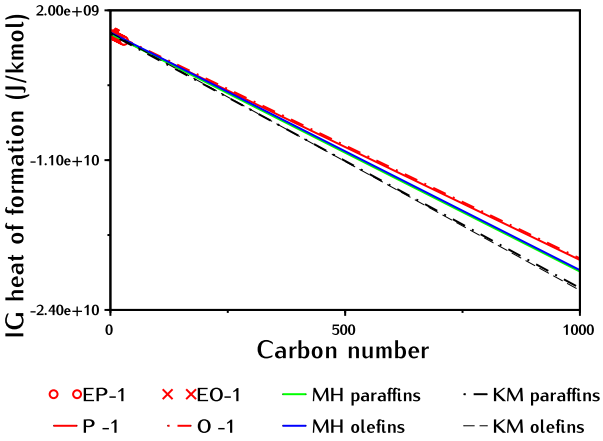

Figure 9.15: Ideal Gas heat of formation

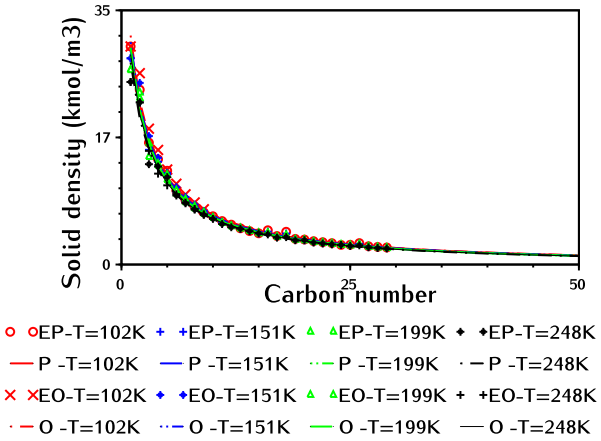

Figure 9.16: Solid density

9.2. Peng Robinson Equation Of State Parameters

$$a_i(T) = 0.45724 \frac{R^2 T_{c,i}^2}{P_{c,i}} \alpha_i(T) \tag{9.1}$$

$$b_i = 0.07790 \frac{R T_{c,i}}{P_{c,i}} \tag{9.2}$$

$$B_i = b_i \frac{P}{RT} \tag{9.3}$$

$$a_{ij} = \sqrt{a_{ii} a_{jj}} \tag{9.4}$$

$$A_{mix}^{\Omega} = z_i^T a_{ij} z_i \tag{9.5}$$

$$B_{mix}^{\Omega} = z_i^T b_i \tag{9.6}$$

$$\alpha_{mix}^{\Omega} = -1 + B_{mix}^{\Omega} \tag{9.7}$$

$$\beta_{mix}^{\Omega} = A_{mix}^{\Omega} - 3\left(B_{mix}^{\Omega}\right)^2 - 2B_{mix}^{\Omega} \tag{9.8}$$

$$\gamma_{mix}^{\Omega} = -A_{mix}^{\Omega} B_{mix}^{\Omega} + \left(B_{mix}^{\Omega}\right)^2 + \left(B_{mix}^{\Omega}\right)^3 \tag{9.9}$$

9.3. EOS Correlation

This sections presents the results of the correlations of the separation factors of all species using the Peng Robinson and Universal Mixing Rule PR-UMR EOS with data being generated by ChemSep. This correlation is used for initial guess for K_i in both FTS and Hydrocracking and used to determine the separation factor in FTS. Subsequent K_i calculations for the FTS and hydrocracking are done according to the procedure defined in Sections 3.4 and 3.5. In both reactors the activity is defined according to 3.27.

Figure 9.17 shows the variation of the separation factor with carbon number and temperature for a model stream for a pressure of 40 bar. The graph only shows the separation factors for the FTS products with carbon numbers greater than 2 (ethane/ethene onward). The model stream contains all the light gases and methane and the Ki values shown here are calculated from the mole fractions in that stream. These results have been generated using ChemSep to flash the model stream at different temperatures. The datapoints (KiCSP,KiCSO) represent the ChemSep data and the KiPSM are a linear fit of the Ki values and are regarded as equal for paraffins and olefins.

In terms of the first guess to the FT reactor the simulated separation factors shown in Figure 9.17 are only used for compounds not present in the ChemSep PCD so as to preserve the nonlinear trends seen for low carbon number compounds.

$$ln\left(\frac{K_{i,j}}{K_{i,0}}\right) = a_i\left(\frac{1}{T_j^3} - \frac{1}{T_0^3}\right) \tag{9.10}$$

$$\begin{bmatrix} \frac{1}{T_{j=1}^3} - \frac{1}{T_0^3} \\ \frac{1}{T_2^3} - \frac{1}{T_0^3} \\ \vdots \\ \frac{1}{T_n^3} - \frac{1}{T_0^3} \end{bmatrix} [a_{i=1},\ a_2,\ \dots\ a_n] = ln\left(\begin{bmatrix} K_{i=1,,j=1} & K_{2,1} & \dots & K_{n,1} \\ K_{1,2} & K_{2,2} & \dots & K_{n,2} \\ \vdots & \vdots & \ddots & \vdots \\ K_{1,n} & K_{2,n} & \dots & K_{n,n} \end{bmatrix}\right) - ln\left(K_{i,0}\right) \tag{9.11}$$

$$\boldsymbol{T'} \setminus \left(ln\left(\boldsymbol{K'}\right) - ln\left(K_{i,0}\right)\right) = \boldsymbol{a'} \tag{9.12}$$

The separation factors vary linearly with carbon number and an increase in temperature will produce a higher separation factor. Equation 9.10which is a modification of the van't Hoff equation has been found to describe the aforementioned temperature dependence accurately. In the Equation the iterator i steps through the carbon numbers from 2 to 200 and j steps through the temperatures from T_1 to T_n. The separation factor at some temperature T_j is defined in relation to the separation factor at a reference temperature T_0. The a parameter is expected to be a function of the heat of vaporization; however, this relationship has not been implemented. Equation 9.11 shows the vectorized version of Equation 9.10. This formulation is advantageous because it allows the least squares fit to be carried out in Scilab using the backslash operator as shown in equation 9.12. The

results of fitting Equation 9.10 to the temperature data are shown in Figure 9.17 by (T corr) and seem to fit the datapoints produced by ChemSep well.

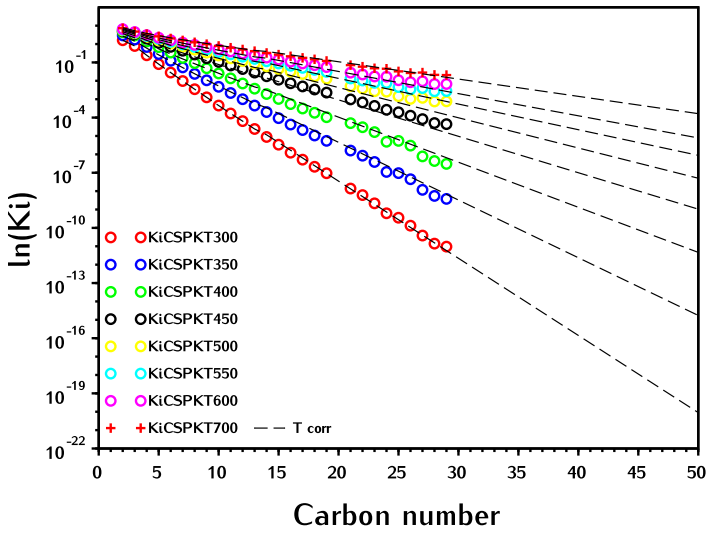

Figure 9.17: Separation factor vs carbon number for changing temperature

Figure 9.18 shows the effect of varying pressure on the separation factor of the paraffins and olefins. Figure 9.21 illustrates a complication with fitting the separation factor in the same way as for the temperature variation: the lines resulting from linear regressions through the separation factors intersect at different points. In other words for some pressure P_1 there will be some hypothetical carbon number (non-integer most likely) where the separation factor will be the same as for some other pressure P_2. Upon further inspection it was noted that the intercept followed a linear trend with changing reciprocal pressure difference $(P - P_0)^{-1}$. Choosing $10\,bar$ as the reference pressure allowed for the intercepts to be determined accurately using this linear model.

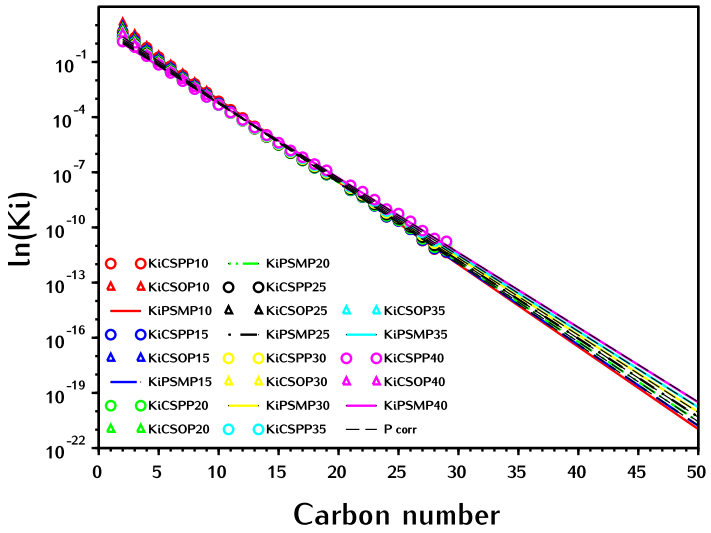

Figure 9.18: Separation factor vs carbon number for changing pressure

Figure 9.19 shows the effect of changing FT α from 0.7 to 0.99 on the separation factors of the paraffins and olefins. Figure 9.23 shows the same data plotted against the chain growth probability for ethane to heptane. This relationship is difficult to fit using the standard models so a fourth order polynomial was employed, shown in Figure 9.23 by 'poly'. This polynomial is not suitable for extrapolation beyond the range of $0.7 < \alpha < 0.99$. The steps taken in the polynomial regression are shown in Equations 9.14 and 9.15. For the missing carbon numbers (i.e. olefins C9 to CN and paraffins C29 to CN) the polynomial is fitted against the linear regression through the datapoints. In contrast to the other regressions the polynomial correlations in Equation 9.13 are defined for all species except olefins larger than C8 which are assumed to be equal the paraffins. Equation 9.13 gives the absolute separation factor; however, it is more useful to have the separation factor in relation to some reference chain growth probability. Using $\alpha = 0.7$ as a reference, a relative definition of the separation factor is obtained by elimination of the coefficient e_i using Equation 9.13 at the reference point and an undefined chain growth probability α_j resulting in Equation 9.16.

$$K_{i,j} = a_i \alpha_j^4 + b_i \alpha_j^3 + c_i \alpha_j^2 + d_i \alpha_j + e_i \tag{9.13}$$

$$\begin{bmatrix} \alpha_1^4 & \alpha_1^3 & \alpha_1^2 & \alpha_1 & 1 \\ \alpha_2^4 & \alpha_2^3 & \alpha_2^2 & \alpha_2 & 1 \\ \vdots & \vdots & \vdots & \vdots & \vdots \\ \alpha_n^4 & \alpha_n^3 & \alpha_n^2 & \alpha_n^1 & 1 \end{bmatrix} \begin{bmatrix} a_1 & a_2 & \cdots & a_n \\ b_1 & b_2 & \cdots & b_n \\ c_1 & c_2 & \cdots & c_n \\ d_1 & d_2 & \cdots & d_n \\ e_1 & e_2 & \cdots & e_n \end{bmatrix} = \begin{bmatrix} K_{i=1,,j=1} & K_{2,1} & \dots & K_{n,1} \\ K_{1,2} & K_{2,2} & \dots & K_{n,2} \\ \vdots & \vdots & \ddots & \vdots \\ K_{1,n} & K_{2,n} & \cdots & K_{n,n} \end{bmatrix} \tag{9.14}$$

$$\boldsymbol{\alpha' \setminus K' = abcde'} \tag{9.15}$$

$$K_{i,j} = K_{i,0} + a_i \left(\alpha_j - \alpha_0\right)^4 + b_i \left(\alpha_j - \alpha_0\right)^3 + c_i \left(\alpha_j - \alpha_0\right)^2 + d_i \left(\alpha_j - \alpha_0\right) \tag{9.16}$$

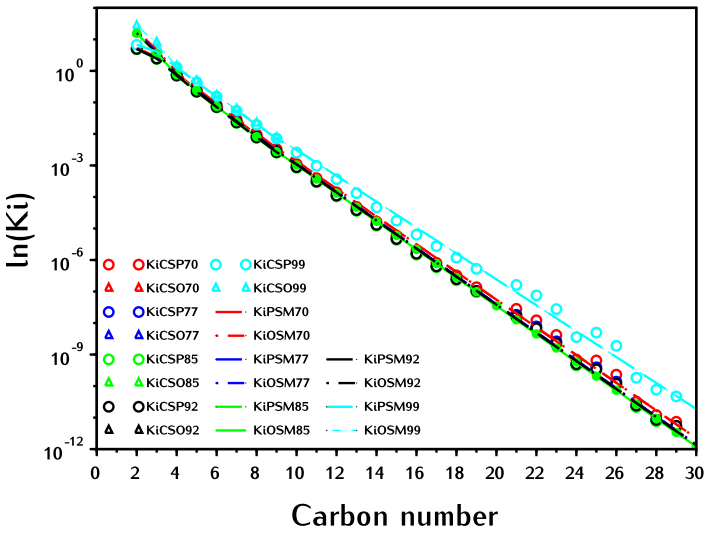

Figure 9.19: Separation factor vs carbon number for changing alpha%

Figure 9.20 shows the effect of varying nitrogen mole fraction on the separation factors of the paraffins and olefins. As before the olefins and paraffin separation factors are assumed to be equal beyond C8. The mole fraction of nitrogen in the feed has been varied from 7.02×10^{-5} to 0.41 and does not appear to have a strong effect on the separation factors of the FT compounds. The maximum difference occurs between nitrogen mole fractions of7.02×10^{-5} to 0.41 for ethane and is equal to 0.246. It is therefore assumed that the nitrogen concentration does not affect the separation factors of the FT products. Figure 9.22 shows the variation of the separation factor with nitrogen mole fraction for the light compounds. Here the maximum difference is for hydrogen with a value of 18.9. The light compounds have a greater sensitivity to the Nitrogen mole fraction; therefore, the linear model shown in Equation 9.17was fitted through through the datapoints for each component indicated by the dotted lines in Figure 9.22. The regression was achieved by a least squares fit using the backslash operator in Scilab, the steps are shown in Equations 9.18 and 9.19. Equation 9.17 gives the absolute separation factor; however, it is more useful to have the separation factor in relation to the that at some specific nitrogen concentration. Using an arbitrarily chosen nitrogen concentration, 7.02×10^{-5} in this case, a relative definition of the separation factor is obtained by elimination of the intercept c_i using Equation 9.17 at a reference mole fraction $z^0_{N_2}$ and an undefined mole fraction z_{N_2} resulting in Equation 9.20.

$$K_{i,z_{N_2}} = m_i z_{N_2} + c_i \tag{9.17}$$

$$\begin{bmatrix} z_{N_2,1} & 1 \\ z_{N_2,2} & 1 \\ \vdots & \vdots \\ z_{N_2},n & 1 \end{bmatrix} \begin{bmatrix} m_i \\ c_i \end{bmatrix} = \begin{bmatrix} K_{i,z_{N_2,1}} \\ K_{i,z_{N_2,2}} \\ \vdots \\ K_{i,z_{N_2,n}} \end{bmatrix} \tag{9.18}$$

$$z_i' \setminus K_i' = mc_i' \tag{9.19}$$

$$K_{i,z_{N_2}} = m_i \left(z_{N_2} - z_{N_2}^0\right) + K_{i,z_{N_2}}^0 \tag{9.20}$$

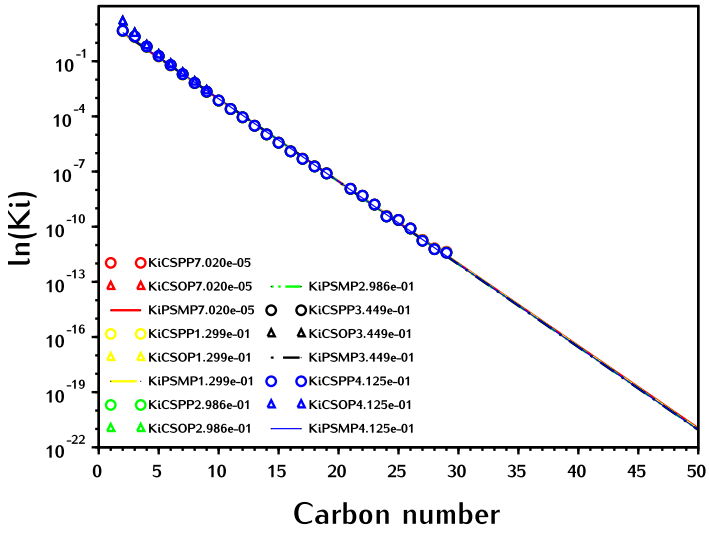

Figure 9.20: Separation factor vs carbon number for changing Nitrogen mole fraction

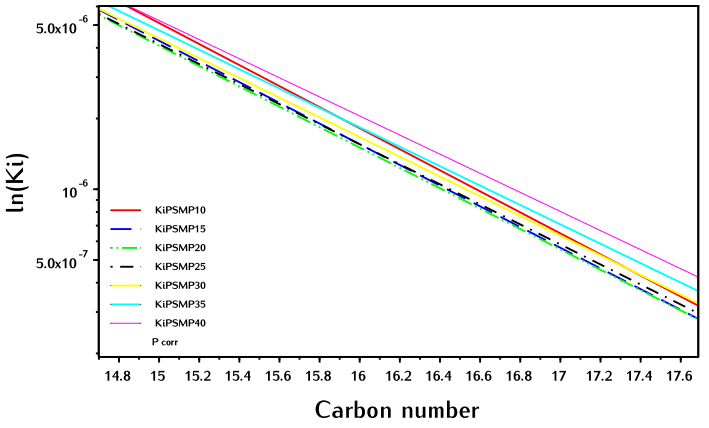

Figure 9.21: Effect of pressure on the separation factor of the paraffins and olefins.

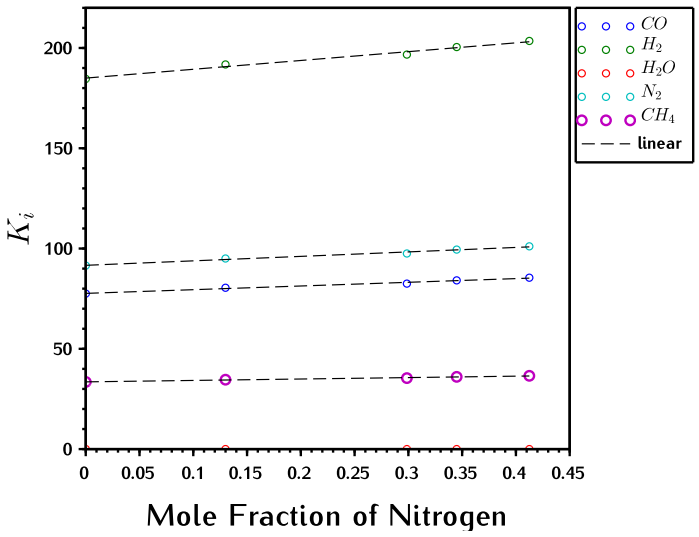

Figure 9.22: Effect of the mole fraction of Nitrogen on the separation factor of the light gases.

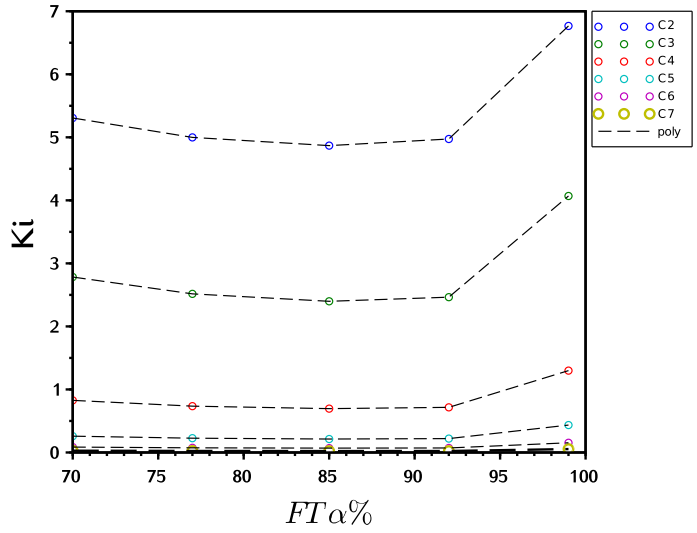

Figure 9.23: Effect of FT α on the separation factor of ethane to heptane.

9.4. Fischer-Tropsch Synthesis

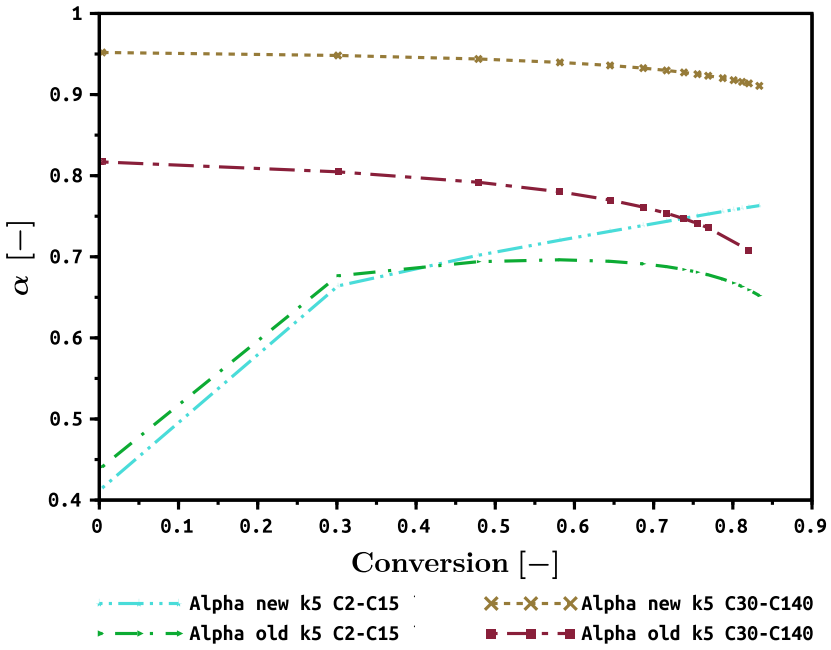

Figure 9.24: Fischer-Tropsch Synthesis chain growth probability (α) versus conversion for the $(k_5)_{old} = 1.56 \times 10^3$ and $(k_5)_{new} = 22\,(k_5)_{old}$ $H_2 : CO = 1.92$, $N = 140$, $xN_2 = 0$, $T_{FTS} = 230^oC$, $P_{FTS} = 35$ bar.

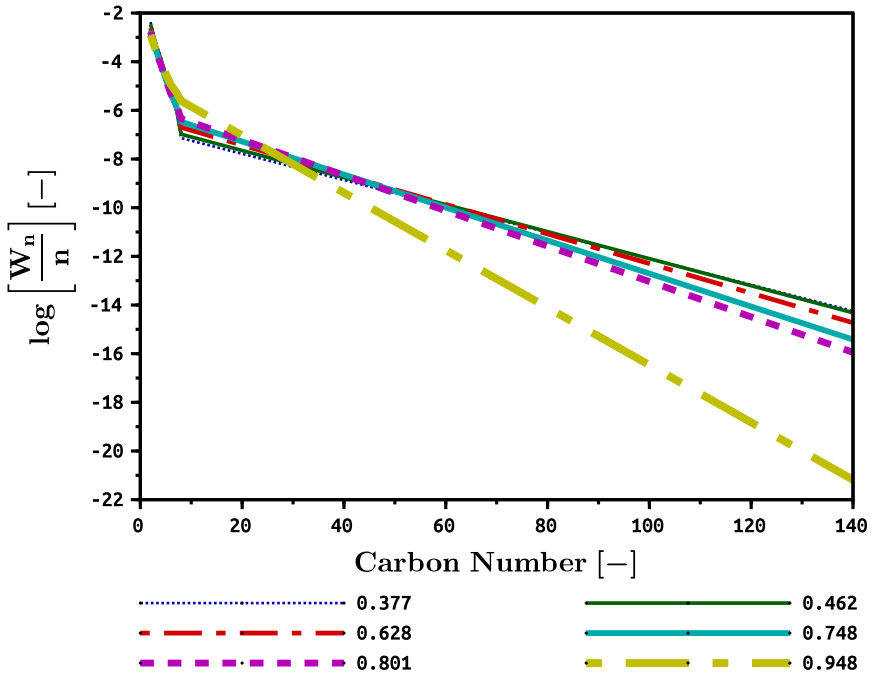

Figure 9.25: Fischer-Tropsch Synthesis syncrude ASF distribution for various carbon monoxide conversions, where $H_2 : CO = 1.92$, $N = 140$, $xN_2 = 0$, $T_{FTS} = 230^oC$ and $P_{FTS} = 35$ bar.

9.5. Hydrocracking

9.5.1. Optimal Value of FT α

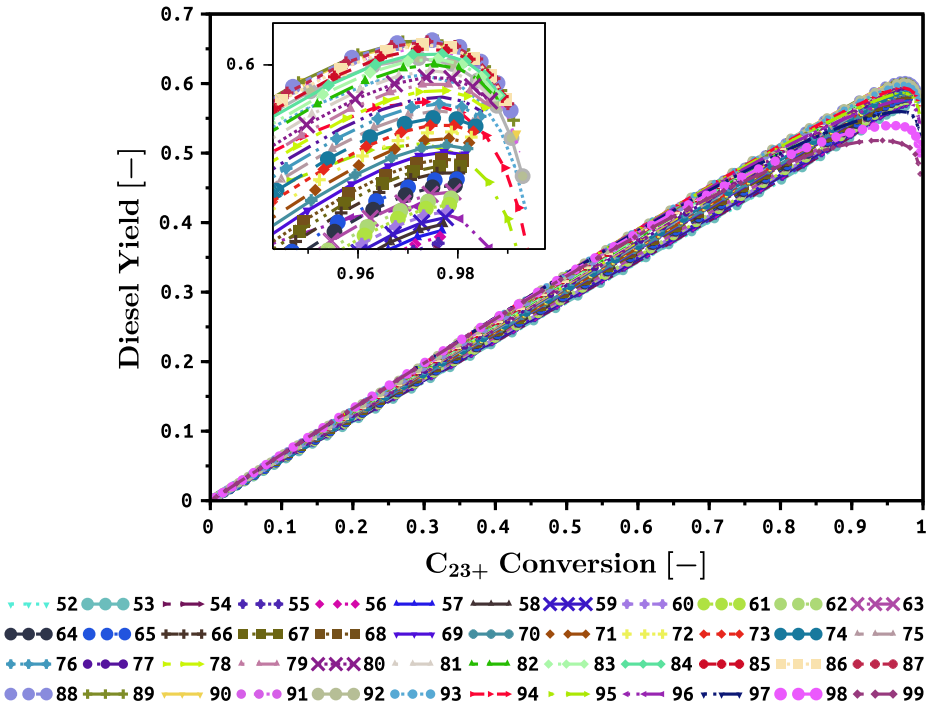

Figure 9.26: Once through hydrocracking of Fischer-Tropsch Synthesis C_{23+} wax $\alpha = 0.94$, $T = 350^{o}C$, $P = 35\,bar$, $H_2 : Hydrocarbons = 15 : 1$ showing the sensitivity of the diesel yield to C_{23+} conversion and Fischer-Tropsch Synthesis α

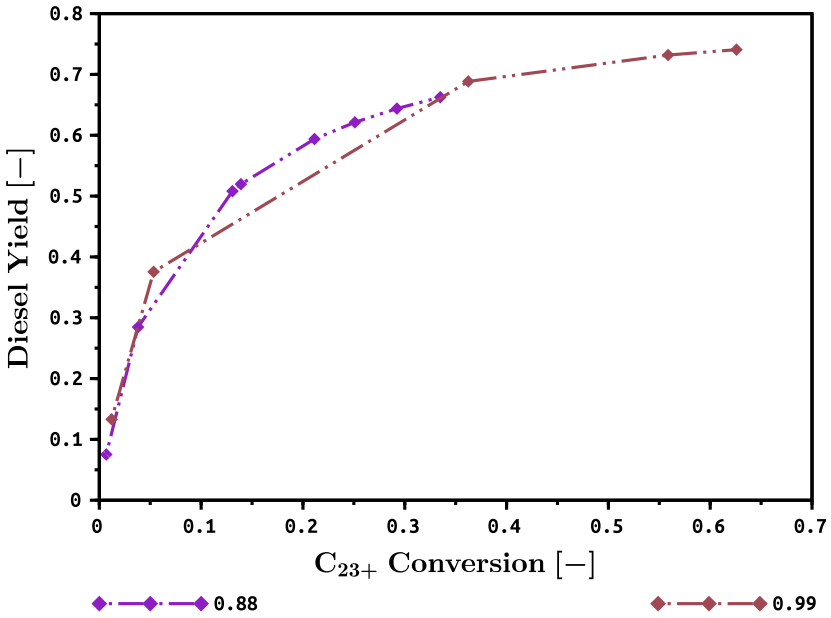

Figure 9.27: Once through hydrocracking of Fischer-Tropsch Synthesis C_{21+} wax $T = 350^{o}C$, $P = 35\,bar$, $H_2 : Hydrocarbons = 45 : 1$ showing the sensitivity of the diesel yield to C_{21+} conversion and Fischer-Tropsch Synthesis α with the heavy wax recycle active where the purge ratio is 5%

9.6. Scripts

The directory structure of various modules and data is given below. The files which run the configurations are under the process synthesis folder. Within this folder folders ending in -streams contain stream cache files (e.g. save the internalRecycle.csv). The grayed out folders contain files that are not included in the program listings in this appendix.

/
- processsynthesis
  - OOT80.sce
  - A25OT.
  - A50OT.
  - OIR40.
  - OIR60.
  - OER40.
  - OER60
  - OOT80-streams.
  - A25OT-streams.
  - A50OT-streams.
  - OIR40-streams.
  - OIR60-streams.
  - OER40-streams.
  - OER60-streams.
- sensitivities
- FTS-X-alpha-syngas.csv.
- internalRecycle.csv.
- externalRecycle.csv.
- hydrocrackerRecycle.csv.
- properties.xls
- getfilename.sci.
- streamIO.sci.
- correlationsT.sci
- propertieslights.sci
- properties.sci
- Kicorr.sce
- Ki.sce
- PREOS.sci
- flashRR.sci
- feed.sce
- POODEreactor.sci
- SMRreactor.sci
- FTreactor.sci
- PreHydrocrackerreactor.sci
- Hydrocrackerreactor.sci
- ebal.sci
- checks.sci
- FZERO.sci.

```
function dF=fbr_comments(Mcat,F)
    global psi Kiold
    F = clean(F)
    zi = F./sum(F)
    tol=1E-2
    Bloop = 0
    Cloop = 0.999
    RE = 1e-6
    AE = 1e-6
    for jloop = 1:100
        Rloop = psi
        IFLAG = 0

        psi0 = flashRR(0)
        psi1 = flashRR(0.999999)
        if psi1<=0 then
            psi = 1
        elseif psi0>=0 then
            psi = 0
        else
            [psi,iter,iflag] = FZERO(flashRR,Bloop,Cloop,Rloop,RE,AE,IFLAG)
            if psi>1 then
                psi=fsolve(0.99999,flashRR)
            end
        end
        xi = zi ./(1+psi .*(Ki-1))
        yi = Ki .*xi
        xi = xi./sum(xi)
        yi = yi./sum(yi)
        [fpv,fpl,Ki] = PR_EOS(yi,xi,P0,T0,%t,%t)
        ferr = sum(((Kiold-Ki)./(Kiold+%eps)) .^(2))

        if (ferr<=tol) then
            break
        else
            Kiold = Ki
        end
    end

    fl = xi.*P.*fpl
    ai=fl./fipureHYD

    R=Rinit
    R(7)=K1*sum(ai(11:N+4))+2*kC*ai(10)
    R(8:N)=((2*K2*ai(12:N+4)')*tril(ones(N-7,N-7)))'
    R(8:N+1)=R(8:N+1)+K1.*ai(11:N+4)
    R(10)=R(10)-kC*ai(10)
    R(11)=R(11)-K1*ai(11)
    R(12:N+4)=R(12:N+4)-([1:N-7]'.*K2+K1).*ai(12:N+4)
    R(7:N+4) = R(7:N+4)*kCH2V*(1 ./ai(2))
```

```
51
52      dF=R*Mcat
53  endfunction
54  function dF=fbr(Mcat,F)
55      global psi Kiold
56      F = clean(F)
57      zi = F./sum(F)
58      tol=1E-2
59      Bloop = 0
60      Cloop = 0.999
61      RE = 1e-6
62      AE = 1e-6
63      for jloop = 1:100
64          Rloop = psi
65          IFLAG = 0
66          psi0 = flashRR(0)
67          psi1 = flashRR(0.999999)
68          if psi1<=0 then
69              psi = 1
70          elseif psi0>=0 then
71              psi = 0
72          else
73              [psi,iter,iflag] = FZERO(flashRR,Bloop,Cloop,Rloop,RE,AE,IFLAG)
74              if psi>1 then
75                  psi=fsolve(0.99999,flashRR)
76              end
77          end
78          xi = zi ./(1+psi .*(Ki-1))
79          yi = Ki .*xi
80          xi = xi./sum(xi)
81          yi = yi./sum(yi)
82          [fpv,fpl,Ki] = PR_EOS(yi,xi,P0,T0,%t,%t)
83          ferr = sum(((Kiold-Ki)./(Kiold+%eps)) .^(2))
84          if (ferr<=tol) then
85              break
86          else
87              Kiold = Ki
88          end
89      end
90      fl = xi.*P.*fpl
91      ai=fl./fipureHYD
92      R=Rinit
93      R(7)=K1*sum(ai(11:N+4))+2*kC*ai(10)
94      R(8:N)=((2*K2*ai(12:N+4)')*tril(ones(N-7,N-7)))'
95      R(8:N+1)=R(8:N+1)+K1.*ai(11:N+4)
96      R(10)=R(10)-kC*ai(10)
97      R(11)=R(11)-K1*ai(11)
98      R(12:N+4)=R(12:N+4)-([1:N-7]'.*K2+K1).*ai(12:N+4)
99      R(7:N+4) = R(7:N+4)*kCH2V*(1 ./ai(2))
100     R(2)=-sum(R(7:N+4))

101 endfunction
```

Program listing 9.1: Hydrocrackerreactor.sci

```
function dF=PO_ODE(Mcat,FTP)
    FR = FTP(1:$-2)
    TR = FTP($-1)
    PR = FTP($)
    zi = FR./sum(FR)

    Eta = [1;1;1]

    A = [1.03E-1; 4.19E-9; 2.42E-9]
    E = [92; 29E3; 23.7E3]
    k = A .* exp( -1*E ./ (Rg*TR) )
    k(1) = A(1)*exp((-1*E(1)./Rg)*(1/TR-1/873))

    kAd = [3.901E2]
    EAd = [-16]
    kA = kAd(1)*exp((-1*EAd(1)./Rg)*(1/TR-1/873))

    nu =[  0  1  2;
           0  3  2;
           2 -1  0;
           1  0 -1;
           0  0  0;
          -2  0  0;
          -1 -1 -1;
           zeros(2*N-2,3)]


    p = zi * PR
    p_CO  = p(1)
    p_H2  = p(2)+%eps
    p_H2O = p(3)+%eps
    p_CO2 = p(4)+%eps
    p_N2  = p(5)
    p_O2  = p(6)
    p_CH4 = p(7)+%eps

    KE(2) = equilibriumConstant(viPO2,TR)
    KE(3) = equilibriumConstant(viPO3,TR)

    R1 = k(1)*(p_CH4./101325)*((p_O2./101325)./((p_O2./101325)+10^-6))./(1+
        ↪ kA(1)*(p_H2O./101325))
    R2 = k(2)*p_CH4*p_H2O*(1-(p_CO*p_H2^3)./(KE(2)*p_CH4*p_H2O))
    R3 = k(3)*p_CH4*p_CO2*(1-((p_CO^2)*p_H2^2)./(KE(3)*p_CH4*p_CO2))

    r = Eta.*[R1;R2;R3]*Mcat
    dF=nu*r
    dF($+1) = (-r'*[dHRxnPO1;dHRxnPO2;dHRxnPO3])./(FR'*Cp(TR))
    dF($+1) = 0
endfunction
```

Program listing 9.2: POODEreactor.sci

```
function f=initialize_data()
  sheets = readxls('properties.xls')
  parameters = sheets(1)
  parameter_values = sheets(2)
  number_properties = size(parameters,1)
  data.init = %t
  for iPROP = 1:number_properties-1
    key = string(parameters(iPROP+1,1))
    data(key).name = parameters(iPROP+1,2)
    data(key).units.numerator   = parameters(iPROP+1,3)
    data(key).units.denominator = parameters(iPROP+1,4)
    data(key).correlation_id    = parameters(iPROP+1,5)
    num_parms = parameters(iPROP+1,6)
    if ~(num_parms==[]) then
      parameter_names = parameters(iPROP+1,7:7+num_parms-1)
      for iPARM = 1:num_parms
        parameter_name = parameter_names(iPARM)
        data(key)('parameters')(parameter_name) = parameter_values(iPROP+1,
            ↪ iPARM+1)
      end
    end
  end
  f = data
endfunction
function Y=properties(index,nv,T)
  strind = string(index)
  correlation = data(strind).correlation_id
  select correlation,
   case 'MH1' then
    p = data(strind).parameters
    p.Sign = +1
    Y(:,:,1) = p.Yinf - p.delY0*exp(-p.Beta*(nv'+p.Sign*p.n0P).^p.Gama)
    Y(:,:,2) = p.Yinf - p.delY0*exp(-p.Beta*(nv'+p.Sign*p.n0O).^p.Gama)
    ,
   case 'MH2' then
    p = data(strind).parameters
    p.Sign = +1
    Y(:,:,1) = p.Yinf0 - p.delYinf*(nv'-p.n0P) - p.delY0*exp(-p.Beta*(nv'+p
        ↪ .Sign*p.n0P).^p.Gama)
    Y(:,:,2) = p.Yinf0 - p.delYinf*(nv'-p.n0O) - p.delY0*exp(-p.Beta*(nv'+p
        ↪ .Sign*p.n0O).^p.Gama)
    ,
   case 'MH2Vc'
    p = data(strind).parameters
    p.Sign = -1
    Y(:,:,1) = p.delYinf*(nv'-p.n0P) - p.delY0*exp(-p.Beta*(nv'+p.Sign*p.
        ↪ n0P).^p.Gama)
    Y(:,:,2) = p.delYinf*(nv'-p.n0O) - p.delY0*exp(-p.Beta*(nv'+p.Sign*p.
        ↪ n0O).^p.Gama)
    Y = ((Y./100).^(3/2))./1000
    ,
   case 'MHT' then
    p = data(strind).parameters
    p.Sign = +1
    Ainf0 = [p.Ainf01;p.Ainf02;p.Ainf03;p.Ainf04]
```

```
51      delA0 = [p.delA01;p.delA02;p.delA03;p.delA04]
52      cefOptP = Ainf0*ones(nv') + delAinf*(nv'-p.n0P) - delA0*exp(-p.Beta*(nv
            ↪ ' + p.Sign * p.n0P).^p.Gama)
53      cefOptO = Ainf0*ones(nv') + delAinf*(nv'-p.n0O) - delA0*exp(-p.Beta*(nv
            ↪ ' + p.Sign * p.n0O).^p.Gama)
54      YP = FunctionsMod(%t,4,T',cefOptP)
55      YO = FunctionsMod(%t,4,T',cefOptO)
56      Y(:,:,1) = YP
57      Y(:,:,2) = YO
58      ,
59     case 'K1' then
60      nvMat = [ones(nv) nv exp(-1*nv)]'
61      Tn = (T - 298) ./ 298
62      TMat = [ones(Tn') Tn' Tn'.^2]
63      p = data(strind).parameters
64      abc(:,:,1) = [p.p11,p.p12,p.p13;
65                    p.p21,p.p22,p.p23;
66                    p.p31,p.p32,p.p33;]
67      abc(:,:,2) = [p.o11,p.o12,p.o13;
68                    p.o21,p.o22,p.o23;
69                    p.o31,p.o32,p.o33;]
70      Y(:,:,1) = TMat*(abc(:,:,1)*nvMat)
71      Y(:,:,2) = TMat*(abc(:,:,2)*nvMat)
72      ,
73     case 'TwuWag' then
74      Tc = properties(1,nv,T)
75      Pc = properties(2,nv,T)
76      w = properties(11,nv,T)
77      TcP = Tc(:,:,1)
78      TcO = Tc(:,:,2)
79      PcP = Pc(:,:,1)
80      PcO = Pc(:,:,2)
81      wP = w(:,:,1)
82      wO = w(:,:,2)
83      TrP = (T'*ones(TcP)) ./ (ones(T')*TcP)
84      TrO = (T'*ones(TcO)) ./ (ones(T')*TcO)
85      tauP = 1-TrP
86      tauO = 1-TrO
87
88      p = data(strind).parameters
89      lnPr0P = (1 ./ TrP).*(p.p01*tauP+p.p02*tauP.^1.5+p.p03*tauP.^3+p.p04*
            ↪ tauP.^6)
90      lnPr1P = (1 ./ TrP).*(p.p11*tauP+p.p12*tauP.^1.5+p.p13*tauP.^3+p.p14*
            ↪ tauP.^6)
91      lnPr0O = (1 ./ TrO).*(p.p01*tauO+p.p02*tauO.^1.5+p.p03*tauO.^3+p.p04*
            ↪ tauO.^6)
92      lnPr1O = (1 ./ TrO).*(p.p11*tauO+p.p12*tauO.^1.5+p.p13*tauO.^3+p.p14*
            ↪ tauO.^6)
93
94      lnPrP = lnPr0P+(ones(T')*wP).*lnPr1P
95      lnPrO = lnPr0O+(ones(T')*wO).*lnPr1O
96
97      Y1 = (ones(T')*PcP).*exp(lnPrP)
98      Y2 = (ones(T')*PcO).*exp(lnPrO)
99
100     for row=1:max(size(T))
```

```
101         Y1(indicies) = PcP(indicies)
102         indicies = find(TrO>1)
103         Y2(indicies) = PcO(indicies)
104       end
105
106       Y(:,:,1) = Y1
107       Y(:,:,2) = Y2
108       ,
109      case 'Vet' then
110       Tc = properties(1,nv,T)
111       Pc = properties(2,nv,T)
112       Nb = properties(5,nv,T)
113
114       TcP = Tc(:,:,1)
115       TcO = Tc(:,:,2)
116
117       PcP = Pc(:,:,1) ./ 1E5
118       PcO = Pc(:,:,2) ./ 1E5
119
120       NbP = Nb(:,:,1)
121       NbO = Nb(:,:,2)
122
123       TbrP = NbP./TcP
124       TbrO = NbO./TcO
125
126       p = data('26').parameters
127       R = Rg
128       HvapPNb = (R*NbP.*(1-TbrP).^p.pow1).*(log(PcP)+p.np1+p.np2./(PcP.*TbrP
              ↪ .^2))./(1-TbrP+(1-(1-TbrP).^p.dpow1).*log(TbrP))
129       HvapONb = (R*NbO.*(1-TbrO).^p.pow1).*(log(PcO)+p.np1+p.np2./(PcO.*TbrO
              ↪ .^2))./(1-TbrO+(1-(1-TbrO).^p.dpow1).*log(TbrO))
130
131       TrP = (T'*ones(nv')) ./ (ones(T')*TcP)
132       TrO = (T'*ones(nv')) ./ (ones(T')*TcO)
133
134       Y(:,:,1) = ones(T')*HvapPNb.*((1-TrP)./(1-ones(T')*TbrP)).^(p.wata+p.
              ↪ watb*(1-TrP))
135       Y(:,:,2) = ones(T')*HvapONb.*((1-TrO)./(1-ones(T')*TbrO)).^(p.wata+p.
              ↪ watb*(1-TrO))
136       ,
137     end
138 endfunction
```

Program listing 9.3: properties.sci

```
1 function f = flashRR(psi)
2     f = (zi .* (1-Ki))' * (1 ./(1+psi.*(Ki-1)))
3 endfunction
```

Program listing 9.4: flashRR.sci

```
function Y=properties_lights(index,TPROP)
    select index
    case 29,
    a = [29100;3994.325;33200;28933;29103.63;29061.62]
    bcde = [-1979.753,10.58274,-0.0000790406,-1.996850E-07;
            -48.69006,10.36209,-0.0003401440,+1.960333E-07;
            -878.9001,8.436956,+0.0020762700,-6.467085E-07;
            -494.2800,10.65800,-0.0000273750,+3.326800E-09;
            -2305.946,11.31935,-0.0010055700,+1.706099E-07;
            -1470.897,11.10778,-0.0012848400,+3.183122E-07]
    Y = a*ones(TPROP) + exp(bcde*[(1 ./TPROP') ones(TPROP') TPROP' TPROP
        ↪ '.^2]')
    Y = Y ./ 1000
    end
endfunction
```

Program listing 9.5: propertieslights.sci

```
function [FOUT,FH2] = preHydrocracker(FIN)
    FH2 = sum(FIN(N+5:2*N+3))
    FOUT(6:N+4) = FIN(6:N+4) + FIN(N+5:2*N+3)
    FOUT(N+5:2*N+3) = 0
    FOUT(2) = FIN(2)-FH2
endfunction
```

Program listing 9.6: PreHydrocrackerreactor.sci

```
function f=SScstr(y,FSScstr)
    y=sqrt(y.^2)
    yi=y(1:nFS);
    xi=y(nFS+1:2*nFS);
    V=y(2*nFS+1);
    L=y(2*nFS+2)
    thetai=y((2*nFS+3):(2*nFS+2+mSS)-1)
    Tv = y($)
    fi=xi.*Ki*P0
    ai=fi./fipureFTS

    aCO = ai(1)
    aH2 = ai(2)
    apar = ai(5:N+4)
    aole = [0;ai(N+5:nFS)]

    TH = thetai(1)
    TCH2 = thetai(2)
    TCH3 = thetai(3)
    TCi = [TCH3;thetai(4:N+2)]

    r1 = k1*aCO*TH
    r2 = k2 .*aH2 .*Tv .^(2)
    r3 = k3 .*TCH2 .*TH
    r4 = k4 .*TCH3 .*TH
    r5 = k5 .*TCH2 .*TCi
    r6 = ((k6f .*TCi)-(k6r .*aole .*TH))
    r7 = k7 .*TCi .*TH

    Rr=[etaLF*[r1;r2;r3;r4];r7(2:N);r6(2:N)]

    f1=FSScstr-V*yi-L*xi+Rr(1:nFS)*McatFTS
    f2=sum(FSScstr)-V-L+sum(Rr(1:nFS)*McatFTS)
    f3=yi-Ki.*xi
    f4=sum(xi-yi)
    r567 = [[0;r5(1:N-1)] -1*r5 -1*r6 -1*r7]
    r567(1,:) = 0
    r567(N,2) = 0


    rH = (-4*r1+2*r2-r3-r4+sum(r6(2:N))-sum(r7(2:N)))
    rCH2 = (r1-r3-sum(r5(1:N-1)))
    rCH3 = (r3-r4-r5(1))
    rCi = (r567*[1;1;1;1])

    f5 = [rH;rCH2;rCH3;rCi(2:N)]
    f5($+1) = 1-sum(thetai)-Tv
    f=[f1;f2;f3;f4;f5]
endfunction
```

Program listing 9.7: FTreactor.sci

```
function [Vam,Vbm,Lam,Lbm] = mixprop(yi,xi,a,b)
    Vam = yi'*aij*yi
    Vbm = yi'*b
    Lam = xi'*aij*xi
    Lbm = xi'*b
endfunction
function [fpv,fpl,Ki] = PR_EOS_comments(yi,xi,P,T,isothermal,isobaric)


    Vam = yi'*aij*yi
    Vbm = yi'*b
    Lam = xi'*aij*xi
    Lbm = xi'*b

    Aij = aij*PoRT2
    VAm = Vam*PoRT2
    VBm = Vbm*PoRT
    VBm2 = VBm.^2
    vGama = (-1*VAm*VBm+VBm2+VBm2.*VBm)
    vBeta = (VAm-3*VBm2-2*VBm)
    vAlfa = (-1+VBm)
    VZ = roots([1,vAlfa,vBeta,vGama])


    VZ(imag(sqrt(VZ))<>0) = []
    Zv = max(real(VZ))

    LAm = Lam*PoRT2
    LBm = Lbm*PoRT
    LBm2 = LBm.^2
    lGama = (-1*LAm*LBm+LBm2+LBm2*LBm)
    lBeta = (LAm-3*LBm2-2*LBm)
    lAlfa = (-1+LBm)
    LZ = roots([1,lAlfa,lBeta,lGama])


    LZ(imag(sqrt(LZ))<>0) = []
    Zl = min(real(LZ))

    BoVBm = B./VBm
    sqrt2TVBm = sqrt2*VBm
    ZvpVBm = Zv+VBm
    cv1 = BoVBm*(Zv-1)
    cv2 = -(log(Zv-VBm))
    cv3 = -(VAm./(2*sqrt2TVBm))
    cv4 = (2*(yi'*Aij)./VAm)'-BoVBm
    cv5 = log((ZvpVBm+sqrt2TVBm)/(ZvpVBm-sqrt2TVBm))
    fpv = exp(cv1+cv2+cv3.*cv4.*cv5)

    BoLBm = B./LBm
```

```
51      ZlpLBm = Zl+LBm
52      cl1 = BoLBm*(Zl-1)
53      cl2 = -(log(Zl-LBm))
54      cl3 = -(LAm/(2*sqrt2TLBm))
55      cl4 = (2*(xi'*Aij)/LAm)'-BoLBm
56      cl5 = log((ZlpLBm+sqrt2TLBm)/(ZlpLBm-sqrt2TLBm))
57      fpl = exp(cl1+cl2+cl3.*cl4.*cl5)
58
59      Ki = fpl./fpv
60
61      if sum(imag(Ki))<>0 then
62          error('Ki imaginary')
63      end
64  endfunction
65  function fippr = Pure_preos(Tsppr)
66      Psppr = 101325
67      TrPure = Tsppr./Tc
68      alf0Pure(2) = (TrPure(2)^-0.792615)*exp(0.40129*(1-TrPure(2)^-0.992615)
            ↪ )
69      alf1Pure(2) = (TrPure(2)^-1.98471)*exp(0.024955*(1-TrPure(2)^-9.98471))
70      alf0Pure(5) = (TrPure(5)^-0.792615)*exp(0.40129*(1-TrPure(5)^-0.992615)
            ↪ )
71      alf1Pure(5) = (TrPure(5)^-1.98471)*exp(0.024955*(1-TrPure(5)^-9.98471))
72      alf0Pure(6:N+4) = (TrPure(6:N+4).^-0.17183).*exp(0.125283*(1-TrPure(6:N
            ↪ +4).^1.77634))
73      alf1Pure(6:N+4) = (TrPure(6:N+4).^-0.607352).*exp(0.511614*(1-TrPure(6:
            ↪ N+4).^2.20517))
74
75      alf0Pure(N+5:2*N+3) = (TrPure(N+5:2*N+3).^-0.17183).*exp(0.125283*(1-
            ↪ TrPure(N+5:2*N+3).^1.77634))
76      alf1Pure(N+5:2*N+3) = (TrPure(N+5:2*N+3).^-0.607352).*exp(0.511614*(1-
            ↪ TrPure(N+5:2*N+3).^2.20517))
77
78      alfPure = alf0Pure + Af.*(alf1Pure - alf0Pure)
79
80      kappa = 0.37464 + 1.54226*Af(1:4) - 0.26992*Af(1:4).^2
81      alfLightsPure = (1 + kappa.*(1 - sqrt(TrPure(1:4)))).^2
82
83      alfPure(1:4) = alfLightsPure(1:4)
84      RTppr = Rg*Tsppr
85      RTcppr = Rg*Tc
86      RT2ppr = RTppr^2
87      sqrt2 = sqrt(2)
88      Trppr = Tsppr./Tc
89
90      appr = ((0.45724*(RTcppr).^2)./Pc).*alfPure
91      bppr = 0.07780*RTcppr./Pc
92      Appr = appr*Psppr/(RT2ppr)
93      Bppr = bppr*Psppr/(RTppr)
94
95      bcoef = -1+Bppr
96      ccoef = Appr-3*(Bppr.^2)-2*Bppr
97      dcoef = -1*Appr.*Bppr + Bppr.^2 + Bppr.^3
98      acoef = ones(bcoef)
99      bSQ = (bcoef.^2)
100     _3ac = 3*acoef.*ccoef
```

```
101     _9abc = 3*_3ac.*bcoef
102     _27aSQd = 27*dcoef.*acoef.^2
103     determinants = 2*_9abc.*dcoef - 2*_2bCB.*dcoef + bSQ.*(ccoef.^2) - 4*
            ↪ acoef.*ccoef.^3 - _27aSQd.*dcoef
104     d0 = bSQ - _3ac
105     d1 = _2bCB - _9abc + _27aSQd
106     Ccubic1 = (0.5*(d1 + sqrt(d1.^2 -4*d0.^3))).^(1/3)
107     Ccubic2 = (0.5*(d1 - sqrt(d1.^2 -4*d0.^3))).^(1/3)
108     Ccubic3 = 0.5*(-1+sqrt(3)*%i)*Ccubic1
109     Ccubic4 = 0.5*(-1-sqrt(3)*%i)*Ccubic1
110     root1 = -(1 ./(3*acoef)).*(bcoef+Ccubic1+d0./Ccubic1)
111     root2 = -(1 ./(3*acoef)).*(bcoef+Ccubic2+d0./Ccubic2)
112     root3 = -(1 ./(3*acoef)).*(bcoef+Ccubic3+d0./Ccubic3)
113     root4 = -(1 ./(3*acoef)).*(bcoef+Ccubic4+d0./Ccubic4)
114     iml = determinants>0
115     root1(iml)=real(root1(iml))
116     root2(iml)=real(root2(iml))
117     root3(iml)=real(root3(iml))
118     root4(iml)=real(root4(iml))
119     root1(find(imag(root1)<>0)) = 1
120     root2(find(imag(root2)<>0)) = 1
121     root3(find(imag(root3)<>0)) = 1
122     root4(find(imag(root4)<>0)) = 1
123     root1 = real(root1)
124     root2 = real(root2)
125     root3 = real(root3)
126     root4 = real(root4)
127     root1(find(root1<0)) = 1
128     root2(find(root2<0)) = 1
129     root3(find(root3<0)) = 1
130     root4(find(root4<0)) = 1
131     ZlFast = min([root1 root2 root3 root4],'c')
132     Zlppr = ZlFast
133
134
135     Zlppr(1:12)=1
136     Zlppr(N+5:N+11)=1
137
138     numppr = Zlppr+(1+sqrt(2)) .*Bppr
139     denppr = Zlppr+(1-sqrt(2)) .*Bppr
140     ln_phippr = -log(Zlppr-Bppr)- (Appr ./(Bppr .*sqrt(8))) .*log(numppr ./
            ↪ denppr) +Zlppr -1
141     fippr = Psppr .*exp(ln_phippr)
142     if sum(imag(fippr))>0 then
143         error('Error imaginary fugacities in pure PREOS: Function
                ↪ excecution paused')
144     end
145 endfunction
146 function [fpv,fpl,Ki] = PR_EOS(yi,xi,P,T,isothermal,isobaric)
147     Vam = yi'*aij*yi
148     Vbm = yi'*b
149     Lam = xi'*aij*xi
150     Lbm = xi'*b
```

```
151     VAm = Vam*PoRT2
152     VBm = Vbm*PoRT
153     VBm2 = VBm.^2
154     vGama = (-1*VAm*VBm+VBm2+VBm2.*VBm)
155     vBeta = (VAm-3*VBm2-2*VBm)
156     vAlfa = (-1+VBm)
157     VZ = roots([1,vAlfa,vBeta,vGama])
158     VZ(imag(sqrt(VZ))<>0) = []
159     Zv = max(real(VZ))
160     LAm = Lam*PoRT2
161     LBm = Lbm*PoRT
162     LBm2 = LBm.^2
163     lGama = (-1*LAm*LBm+LBm2+LBm2*LBm)
164     lBeta = (LAm-3*LBm2-2*LBm)
165     lAlfa = (-1+LBm)
166     LZ = roots([1,lAlfa,lBeta,lGama])
167     LZ(imag(sqrt(LZ))<>0) = []
168     Zl = min(real(LZ))
169     BoVBm = B./VBm
170     sqrt2TVBm = sqrt2*VBm
171     ZvpVBm = Zv+VBm
172     cv1 = BoVBm*(Zv-1)
173     cv2 = -(log(Zv-VBm))
174     cv3 = -(VAm./(2*sqrt2TVBm))
175     cv4 = (2*(yi'*Aij)./VAm)'-BoVBm
176     cv5 = log((ZvpVBm+sqrt2TVBm)/(ZvpVBm-sqrt2TVBm))
177     fpv = exp(cv1+cv2+cv3.*cv4.*cv5)
178     BoLBm = B./LBm
179     sqrt2TLBm = sqrt2*LBm
180     ZlpLBm = Zl+LBm
181     cl1 = BoLBm*(Zl-1)
182     cl2 = -(log(Zl-LBm))
183     cl3 = -(LAm/(2*sqrt2TLBm))
184     cl4 = (2*(xi'*Aij)/LAm)'-BoLBm
185     cl5 = log((ZlpLBm+sqrt2TLBm)/(ZlpLBm-sqrt2TLBm))
186     fpl = exp(cl1+cl2+cl3.*cl4.*cl5)
187     Ki = fpl./fpv
188     if sum(imag(Ki))<>0 then
189         error('Ki imaginary')
190     end
191 endfunction
```

Program listing 9.8: PREOS.sci

```
function y = Functions(vcsc?,eqn,T,cef)
  select vcsc?
   case %t then
    select eqn
     case   2 then y = cef(:,1) + cef(:,2)*T;
     case   4 then y = cef(:,1) + cef(:,2)*T + cef(:,3)*T.^2 + cef(:,4)*T
        ↪ .^3
     case  10 then y = exp( cef(:,1) - cef(:,2)./( T + cef(:,3) ) )
     case  12 then y = exp( cef(:,1) - cef(:,2)*T)
     case  13 then y = exp( cef(:,1) + cef(:,2)*T + cef(:,3)*(T.^2) )
     case  16 then y = cef(:,1) + exp( (cef(:,2) ./ T) + cef(:,3) + (cef
        ↪ (:,4) .* T) ...
... + cef(:,5).*T.^2 )
     case 100 then y = cef(:,1) + cef(:,2)*T + cef(:,3)*T.^2 + cef(:,4)*T
        ↪ .^3 ...
... + cef(:,5)*T.^4
     case 101 then y = exp( cef(:,1) + (cef(:,2) ./ T) + (cef(:,3) * log(T)
        ↪ ) ...
... + cef(:,4).*T.^cef(:,5) )
     case 102 then y = ( cef(:,1).*T.^(cef(:,2)) ) ./ ( 1 + (cef(:,3) ./ T)
        ↪  ...
... + ( cef(:,4) ./ (T.^2) ) )
     case 104 then y = cef(:,1) + (cef(:,2) ./ T) + (cef(:,3) ./ (T.^3))
        ↪ ...
... + (cef(:,4) ./ (T.^8)) + (cef(:,5) ./ (T.^9))
     case 105 then y = cef(:,1) ./ ( cef(:,2).^( 1 + ( 1 - (T ./ cef(:,3))
        ↪ .^cef(:,4) ) ) )
     case 106 then y = cef(:,1).*(1-T./Tc).^( cef(:,2) + cef(:,3).*(T./Tc)
        ↪ ...
... + cef(:,4).*((T./Tc).^2) + cef(:,5).*((T./Tc).^3) )
     case 120 then y = cef(:,1) - cef(:,2) ./ ( T + cef(:,3) )
    end
   case %f then
    select eqn
     case   2 then y = cef(1) + cef(2)*T;
     case   4 then y = cef(1) + cef(2)*T + cef(3)*T^2 + cef(4)*T^3
     case  10 then y = exp( cef(1) - cef(2)./( T + cef(3) ) )
     case  12 then y = exp( cef(1) - cef(2)*T)
     case  13 then y = exp( cef(1) + cef(2)*T + cef(3)*(T.^2) )
     case  16 then y = cef(1) + exp( (cef(2) ./ T) + cef(3) + (cef(4) .* T)
        ↪  ...
... + cef(5).*T.^2 )
     case 100 then y = cef(1) + cef(2)*T + cef(3)*T.^2 + cef(4)*T.^3 ...
... + cef(5)*T.^4
     case 101 then y = exp( cef(1) + (cef(2) ./ T) + (cef(3) * log(T)) ...
... + cef(4).*T.^cef(5) )
     case 102 then y = ( cef(1).*T.^(cef(2)) ) ./ ( 1 + (cef(3) ./ T) ...
... + ( cef(4) ./ (T.^2) ) )
     case 104 then y = cef(1) + (cef(2) ./ T) + (cef(3) ./ (T.^3)) ...
... + (cef(4) ./ (T.^8)) + (cef(5) ./ (T.^9))
     case 105 then y = cef(1) ./ ( cef(2).^( 1 + ( 1 - (T ./ cef(3)).^cef
        ↪ (4) ) ) )
     case 106 then y = cef(1).*(1-T./Tc).^( cef(2) + cef(3).*T./Tc ...
... + cef(4).*((T./Tc).^2) + cef(5).*((T./Tc).^3) )
     case 120 then y = cef(1) - cef(2) ./ ( T + cef(3) )
    end
  end
endfunction
function y = FunctionsMod(vcsc?,eqn,T,cef)
  row1s = ones(cef(1,:))
```

```
51    select vcsc?
52     case %t then
53      select eqn
54      case   2  then y = [ones(T) T]*cef;
55       case   4 then y = [ones(T) T T.^2 T.^3]*cef
56       case  10 then y = exp( T1s*cef(1,:) - (T1s*cef(2,:))./(T*row1s) + T1s*
           ↪ cef(3,:))
57       case  12 then y = exp( [ones(T) T]*cef )
58       case  13 then y = exp( [ones(T) T T.^2]*cef )
59       case  16 then y = T1s*cef(1,:) + exp( (T1s*cef(2,:))./(T*row1s) + T1s*
           ↪ cef(3,:) ...
60  ... + (T1s*cef(4,:)).*(T*row1s) + ((T1s*cef(5,:)).*(T*row1s)).^2 )
61       case 100 then y = [ones(T) T T.^2 T.^3 T.^4]*cef
62       case 101 then y = exp( T1s*cef(1,:) + (T1s*cef(2,:))./(T*row1s) ...
63  ... + (T1s*cef(3,:)).*log(T*row1s) + (T1s*cef(4,:)).*(T*row1s).^(T1s*cef
    ↪ (5,:)) )
64       case 102 then y = ( (T1s*cef(1,:)).*(T*row1s).^(T1s*cef(2,:)) ) ./ ...
65  ... ( 1 + ((T1s*cef(3,:)) ./ (T*row1s)) + ( (T1s*cef(4,:)) ./ ((T*row1s)
    ↪ .^2) ) )
66       case 104 then y = [ones(T) 1 ./T 1 ./(T.^3) 1 ./(T.^8) 1 ./(T.^9)]*cef
67       case 105 then y = (T1s*cef(1,:)) ./ ( (T1s*cef(2,:)).^( 1 + ...
68  ... ( 1 - ((T*row1s)./(T1s*cef(3,:))).^(T1s*cef(4,:)) ) ) )
69       case 106 then y = ((T1s./Tc)*cef(1,:)).*(1-(T./Tc)*row1s).^( (T1s./Tc)
           ↪ *cef(2,:) + ...
70  ... ((T1s./Tc)*cef(3,:)).*((T./Tc)*row1s) + ((T1s./Tc)*cef(4,:)).*(((T./Tc)
    ↪ *row1s).^2) + ...
71  ... ((T1s./Tc)*cef(5,:)).*(((T./Tc)*row1s).^3) )
72       case 120 then y = T1s*cef(1,:) - T1s*cef(2,:) ./ ( T*row1s + T1s*cef
           ↪ (3,:) )
73      end
74     case %f then
75      select eqn
76       case   2 then y = cef(1) + cef(2).*T;
77       case   4 then y = cef(1) + cef(2).*T + cef(3).*T.^2 + cef(4).*T.^3
78       case  10 then y = exp( cef(1) - cef(2)./( T + cef(3) ) )
79       case  12 then y = exp( cef(1) - cef(2)*T)
80       case  13 then y = exp( cef(1) + cef(2)*T + cef(3)*(T.^2) )
81       case  16 then y = cef(1) + exp( (cef(2) ./ T) + cef(3) + (cef(4) .* T)
           ↪  ...
82  ... + cef(5).*T.^2 )
83       case 100 then y = cef(1) + cef(2)*T + cef(3)*T.^2 + cef(4)*T.^3 ...
84  ... + cef(5)*T.^4
85       case 101 then y = exp( cef(1) + (cef(2) ./ T) + (cef(3) .* log(T)) ...
86  ... + cef(4).*T.^cef(5) )
87       case 102 then y = ( cef(1).*T.^(cef(2)) ) ./ ( 1 + (cef(3) ./ T) ...
88  ... + ( cef(4) ./ (T.^2) ) )
89       case 104 then y = cef(1) + (cef(2) ./ T) + (cef(3) ./ (T.^3)) ...
90  ... + (cef(4) ./ (T.^8)) + (cef(5) ./ (T.^9))
91       case 105 then y = cef(1) ./ ( cef(2).^( 1 + ( 1 - (T ./ cef(3)).^cef
           ↪ (4) ) ) )
92       case 106 then y = cef(1).*(1-T./Tc).^( cef(2) + cef(3).*T./Tc + cef(4)
           ↪ .* ...
93  ... ((T./Tc).^2) + cef(5).*((T./Tc).^3) )
94       case 120 then y = cef(1) - cef(2) ./ ( T + cef(3) )
95      end
96    end
97  endfunction
```

Program listing 9.9: correlationsT.sci

```
function dF=SMR(Mcat,FTP)
    FR = FTP(1:$-2)
    TR = FTP($-1)
    PR = FTP($)
    zi = FR./sum(FR)
    Eta = [1;1;1]
    k0 = [ 1.955E6; 1.020E15; 5.852E17 ]
    E =  [ 67130  ; 243900  ; 204000    ]
    k = k0 .* exp( -E ./ (Rg*TR) ) ./ 3600
    KE0 = [ 5.75E12; 1.26E-2; 7.24E10 ]
    dHE = [-11476  ; 4639   ; -21646  ]
    KE = KE0 .* exp( dHE ./ TR )
    KA0  = [ 6.65E-4; 8.23E-5; 6.12E-9; 1.77E5]
    dHA = [-38280  ;-70650  ;-82900  ; 88680 ]
    KA = KA0 .* exp( -dHA ./ (Rg*TR) )
    K_CH4 = KA(1)
    K_CO  = KA(2)
    K_H2  = KA(3)
    K_H2O = KA(4)
    nu =[  1 -1  0 ;
           3  1  4 ;
          -1 -1 -2 ;
           0  1  1 ;
           0  0  0 ;
           0  0  0 ;
          -1  0 -1 ;
          zeros(2*N-2,3)]
    p = zi * P0./1E5
    p_CO  = p(1)
    p_H2  = p(2) + %eps
    p_H2O = p(3)
    p_CO2 = p(4)
    p_N2  = p(5)
    p_O2  = p(6)
    p_CH4 = p(7)
    R=zeros(nFS,1)
    DEN = 1 + K_CO*p_CO + K_H2*p_H2 + K_CH4*p_CH4 + K_H2O*p_H2O / p_H2
    R1 = k(1) * (p_H2^-2.5 ) * ( p_CH4 * p_H2O   - p_CO  * p_H2^3 / KE(1) )
        ↪  * DEN^-2
    R2 = k(2) * (p_H2^-1   ) * ( p_CO * p_H2O    - p_CO2 * p_H2   / KE(2) )
        ↪  * DEN^-2
    R3 = k(3) * (p_H2^-3.5 ) * ( p_CH4 * p_H2O^2 - p_CO2 * p_H2^4 / KE(3) )
        ↪  * DEN^-2
    r = Eta.*[R1;R2;R3]*Mcat
    dF=nu*r
    dF($+1) = 0
endfunction
```

Program listing 9.10: SMRreactor.sci

```
function Y=Cp(T)
    a = [29100;3994.325;33200;28933;29103.63;29061.62;33151.9]
    bcde = [-1979.753,10.58274,-0.0000790406,-1.996850E-07;
            -48.69006,10.36209,-0.0003401440,+1.960333E-07;
            -878.9001,8.436956,+0.0020762700,-6.467085E-07;
            -494.2800,10.65800,-0.0000273750,+3.326800E-09;
            -2305.946,11.31935,-0.0010055700,+1.706099E-07;
            -1470.897,11.10778,-0.0012848400,+3.183122E-07;
            -1220.001,12.09070,-0.0003847910,+9.896403E-08]
    CpLgt = a*ones(T) + exp(bcde*[(1 ./T') ones(T') T' T'.^2]')
    CpLgt = CpLgt ./ 1000

    CpHyd = properties(29,nv,T)
    P_Cp = CpHyd(1,:,1)'
    O_Cp = CpHyd(1,2:$,2)'
    Y = [CpLgt(1:$-1);P_Cp;O_Cp]
endfunction
function Y=intCP(T1,T2)
    function Z = cp2(Tz,ind,PO)
        Z = properties(29,nv,Tz)
        Z = Z(1,ind,PO)'
    endfunction
    for icp=1:N
        Y(1,icp,1) = intg(T1,T2,list(cp2,icp,1))
    end
    for icp=1:N
        Y(1,icp,2) = intg(T1,T2,list(cp2,icp,2))
    end
endfunction
function Y=intCpLgt(T1,T2)
    aiCPLGT = [29100;3994.325;33200;28933;29103.63;29061.62;33151.9]
    bcdeiCPLGT = [-1979.753,10.58274,-0.0000790406,-1.996850E-07;
            -48.69006,10.36209,-0.0003401440,+1.960333E-07;
            -878.9001,8.436956,+0.0020762700,-6.467085E-07;
            -494.2800,10.65800,-0.0000273750,+3.326800E-09;
            -2305.946,11.31935,-0.0010055700,+1.706099E-07;
            -1470.897,11.10778,-0.0012848400,+3.183122E-07;
            -1220.001,12.09070,-0.0003847910,+9.896403E-08]
    function Z = cplgt(Tz)
        Z = aiCPLGT*ones(Tz) + exp(bcdeiCPLGT*[(1 ./Tz') ones(Tz') Tz' Tz
            ↪ '.^2]')
        Z = Z ./ 1000
    endfunction

    function Z = cplgt2(Tz,ind)
        Z = (aiCPLGT(ind) + [(1 ./Tz) 1 Tz Tz.^2]*bcdeiCPLGT(ind,:)') ./
            ↪ 1000
    endfunction
    for icp=1:6
        Y(icp) = intg(T1,T2,list(cplgt2,icp))
    end
endfunction
```

```
51      ICPLT = intCpLgt(Ts,T)
52      icp = intCP(Ts,T)
53      P_ICP = icp(1,:,1)'
54      O_ICP = icp(1,2:$,2)'
55      ICP = [ICPLT;P_ICP;O_ICP]
56
57      hvapeb = properties(26,nv,T)
58      hvapeb(find(imag(hvapeb)~=0))=0
59      P_HvapEB = hvapeb(1,:,1)'
60      O_HvapEB = hvapeb(1,2:$,2)'
61      HvapEB = [0;0;0;0;0;0;P_HvapEB;O_HvapEB]
62
63      Hv = (Hf + ICP).*yi.*VH
64      Hl = (Hv - HvapEB).*xi.*LH
65  endfunction
66  function HR = heatOfReaction(vi)
67      HR = vi'*Hf
68  endfunction
69  function KE = equilibriumConstant(vi,T)
70      KE = exp(-1*(vi'*Gf)./(Rg*T))
71  endfunction
72  function [HvIN,HlIN,HvOUT,HlOUT]=ebal(F0,F,T0,T)
73      [HvIN,HlIN] = streamH(F0./sum(F0),zeros(F0),sum(F0),0,T0)
74      [HvOUT,HlOUT] = streamH(F./sum(F),zeros(F),sum(F),0,T)
75      if prnt then, printf('Energy     IN - OUT = %.2e',sum(HvIN)+sum(HlIN)-
            ↪ sum(HvOUT)-sum(HlOUT)), end
76  endfunction
```

Program listing 9.11: ebal.sci

```
function [Mbal,Cbal,Hbal,Obal]=checks(FIN,FOUT,Mr,rctr,overide)
    if sum(real(FIN)<0)>0 then
        printf('\nNegative flows in feed of %s:',rctr)
        ind = find(real(FIN)<0)
        printf('\n    %s = %e',nms(ind),FIN(ind))
    end
    if sum(real(FOUT)<0)>0 then
        printf('\nNegative flows in product of %s',rctr)
        ind = find(real(FOUT)<0)
        printf('\n    %s = %e',nms(ind),FOUT(ind))
    end

    if sum(imag(FIN))>0 then
        printf('\nImaginary flows in feed of %s',rctr)
        ind = find(imag(FIN))
        printf('\n    %s = %s',nms(ind),string(FIN(ind)))
    end
    if sum(imag(FOUT))>0 then
        printf('\nImaginary flows in product of %s',rctr)
        ind = find(imag(FOUT))
        printf('\n    %s = %s',nms(ind),string(FOUT(ind)))
    end

    if sum(isnan(FIN))>0 then
        printf('\nNAN flows in feed of %s',rctr)
        ind = find(isnan(FIN))
        printf('\n    %s = %e',nms(ind),FIN(ind))
    end
    if sum(isnan(FOUT))>0 then
        printf('\nNAN flows in product of %s',rctr)
        ind = find(isnan(FOUT))
        printf('\n    %s = %e',nms(ind),FOUT(ind))
    end

    if round(sum(FIN ./ sum(FIN)))~=1 then
        printf('\nFeed stream mole balance does not sum to 1 of %s',rctr)
    end
    if round(sum(FOUT ./ sum(FOUT)))~=1 then
        printf('\nProduct stream mole balance does not sum to 1 of %s',rctr
            ↪ )
    end

    Mbal=sum(FIN.*Mr)-sum(FOUT.*Mr)
    CarbonIN = FIN(1)+FIN(4)+FIN(7)+sum(FIN(8:N+6).*[2:N]')+sum(FIN(N+7:2*N
        ↪ +5).*[2:N]')
    CarbonOUT = FOUT(1)+FOUT(4)+FOUT(7)+sum(FOUT(8:N+6).*[2:N]')+sum(FOUT(N
        ↪ +7:2*N+5).*[2:N]')
    Cbal=CarbonIN-CarbonOUT
    HydrogenIN = 2*FIN(2)+2*FIN(3)+4*FIN(7)+sum(FIN(8:N+6).*(2*[2:N]'+2))+
        ↪ sum(FIN(N+7:2*N+5).*(2*[2:N]'))
    HydrogenOUT = 2*FOUT(2)+2*FOUT(3)+4*FOUT(7)+sum(FOUT(8:N+6).*(2*[2:N
        ↪ ]'+2))+sum(FOUT(N+7:2*N+5).*(2*[2:N]'))
    Hbal=HydrogenIN-HydrogenOUT
    OxygenIN = FIN(1)+FIN(3)+2*FIN(4)+2*FIN(6)
    OxygenOUT = FOUT(1)+FOUT(3)+2*FOUT(4)+2*FOUT(6)
```

```
51      if prnt | overide then
52          printf('\nMass       IN - OUT = %.2e\n',clean(Mbal))
53          printf('Carbon     IN - OUT = %.2e\n',clean(Cbal))
54          printf('Hydrogen   IN - OUT = %.2e\n',clean(Hbal))
55          printf('Oxygen     IN - OUT = %.2e\n',clean(Obal))
56      end
57  endfunction
58  function [Mbal,Cbal,Hbal,Obal]=checks2(FIN,FOUT,Mr,overide)
59      Mbal=Mr'*FIN-Mr'*FOUT
60      CarbonIN = FIN(1)+FIN(5)+[2:N]*FIN(6:N+4)+[2:N]*FIN(N+5:2*N+3)
61      CarbonOUT = FOUT(1)+FOUT(5)+[2:N]*FOUT(6:N+4)+[2:N]*FOUT(N+5:2*N+3)
62      Cbal=CarbonIN-CarbonOUT
63      HydrogenIN = 2*FIN(2)+2*FIN(3)+4*FIN(5)+sum(FIN(6:N+4).*(2*[2:N]'+2))+
            ↪ sum(FIN(N+5:2*N+3).*(2*[2:N]'))
64      HydrogenOUT = 2*FOUT(2)+2*FOUT(3)+4*FOUT(5)+sum(FOUT(6:N+4).*(2*[2:N
            ↪ ]'+2))+sum(FOUT(N+5:2*N+3).*(2*[2:N]'))
65      Hbal=HydrogenIN-HydrogenOUT
66      if prnt | overide then
67          printf('\nMass       IN - OUT = %.2e\n',clean(Mbal))
68          printf('Carbon     IN - OUT = %.2e\n',clean(Cbal))
69          printf('Hydrogen   IN - OUT = %.2e\n',clean(Hbal))
70      end
71  endfunction
```

Program listing 9.12: checks.sci

```
clear;clc
clearglobal('Kiold')
clearglobal('psi')
chdir('/home/ash/Documents/Plant/process_synthesis')
DIR=pwd()
chdir('..')
PARENTDIR=pwd()
stacksize('max')
prnt=%t
prntOveride = %t
exec('get_filename.sci',-1)
exec('FZERO.sci',-1)
exec('checks.sci',-1)
exec('correlationsT.sci',-1)
exec('properties.sci',-1)
exec('properties_lights.sci',-1)
exec('streamIO.sci',-1)
exec('ebal.sci',-1)
exec('format_plot.sci',-1)
exec('Kicorr.sce',-1)
exec('flashRR.sci',-1)
exec('PREOS.sci',-1)
exec('Ki.sce',-1)
exec('feed.sce',-1)
exec('PO_ODE_reactor.sci',-1)
exec('SMR_reactor.sci',-1)
exec('FT_reactor.sci',-1)
exec('PreHydrocracker_reactor.sci',-1)
exec('Hydrocracker_reactor.sci',-1)
RUNFILENAME = getFilename()
Rg = 8.31
Ps = 101325
Ts = 298
N = 141
nv = [1:N]'
nvPO = nv(2:N)
data = initialize_data()
nms = ['CO';'H2';'H2O';'CO2';'N2';'O2';'CH4']
for inms=2:N
    nms($+1) = 'C'+string(inms)+'H'+string(2*inms+2)
end
for inms=2:N
    nms($+1) = 'C'+string(inms)+'H'+string(2*inms)
end
clear(['inms'])
ConvertDex2 = [
find(nms=='CO');
find(nms=='H2');
find(nms=='H2O');
find(nms=='N2');
```

```
(find(nms=='C2H4'):find(nms==msprintf('C%iH%i',N,2*N)))']
nms2 = nms(ConvertDex2)
maxChars = max(length(nms))
for iNMS=1:size(nms,1)
    repetitions = maxChars - length(nms(iNMS))
    spaces = ''
    for jREP=1:repetitions
        spaces = spaces+' '
    end
    nmsSpaces(iNMS) = spaces
end
shunt = ''
for iCHARS =1:maxChars
    shunt = shunt+' '
end
clear(['iNMS','maxChars','jREP','repetitions','spaces','iCHARS'])
ltXdex = [1:find(nms=='CH4')-1]'
ltIdex = [1:find(nms=='CH4')]'
pIdex  = [find(nms=='CH4'):find(nms==msprintf('C%iH%i',N,2*N+2))]'
pXdex  = pIdex(nvPO)
oXdex  = [find(nms=='C2H4'):find(nms==msprintf('C%iH%i',N,2*N))]'
ltXdex2 = [1:find(nms2=='CH4')-1]'
ltIdex2 = [1:find(nms2=='CH4')]'
pIdex2  = [find(nms2=='CH4'):find(nms2==msprintf('C%iH%i',N,2*N+2))]'
pXdex2  = pIdex2(nvPO)
oXdex2  = [find(nms2=='C2H4'):find(nms2==msprintf('C%iH%i',N,2*N))]'
Mr = [28;2;18;44;28;32;16;12*nvPO+2*nvPO+2;12*nvPO+2*nvPO]
Mr2= Mr(ConvertDex2)
Tc = properties(1,nv,298)
Pc = properties(2,nv,298).*1E5
Vc = properties(3,nv,298) ./ 1000
nb = properties(5,nv,298)
Af = properties(11,nv,298)
hf = properties(17,nv,298)*1000
gf = properties(18,nv,298) ./ 1000
P_Tc = Tc(1,nv,1)'
P_Pc = Pc(1,nv,1)'
P_Vc = Vc(1,nv,1)'
P_Nb = nb(1,nv,1)'
P_Af = Af(1,nv,1)'
P_Hf = hf(1,nv,1)'
P_Gf = gf(1,nv,1)'
O_Tc = Tc(1,nvPO,2)'
O_Pc = Pc(1,nvPO,2)'
O_Vc = Vc(1,nvPO,2)'
O_Nb = nb(1,nvPO,2)'
O_Af = Af(1,nvPO,2)'
O_Hf = hf(1,nvPO,2)'
O_Gf = gf(1,nvPO,2)'
P_Gf(1) = -5.04900E+07 / 1000
```

```
P_Gf(3) = -2.43900E+07 / 1000
P_Gf(4) = -1.67000E+07 / 1000
P_Gf(5) = -8.81300E+06 / 1000
O_Gf(1) = 6.84400E+07 / 1000
O_Gf(2) = 6.26400E+07 / 1000
O_Gf(3) = 7.04100E+07 / 1000
O_Gf(4) = 7.83700E+07 / 1000
clear(['Tc','Pc','Vc','nb','Af','Pvap','rhoL','hf','gf'])
CO_Tc = 132.9
CO_Pc = 3.496*1000000
CO_Vc = 0.0931/1000
CO_Nb = 81.6600
CO_Af = 0.049
CO_Hf = -1.10530E+08 ./1000
CO_Gf = -1.37150E+08 ./ 1000
H2_Tc = 33.2
H2_Pc = 1.297*1000000
H2_Vc = 0.065/1000
H2_Nb = 20.3900
H2_Af = -0.22
H2_Hf = 0
H2_Gf = 0
W_Tc = 647.3
W_Pc = 22.048*1000000
W_Vc = 0.056/1000
W_Nb = 373.150
W_Af = 0.344
W_Hf = -2.41814E+08 ./1000
W_Gf = -2.28590E+08 ./1000
CO2_Tc = 304.210
CO2_Pc = 7.38300E+06
CO2_Vc = 0.0940000/1000
CO2_Nb = 0
CO2_Af = 0.223621
CO2_Hf = -3.935E+8 ./ 1000
CO2_Gf = -3.94370E+08 ./ 1000
N2_Tc = 126.2
N2_Pc = 3.394*1000000
N2_Vc = 0.0895/1000
N2_Nb = 77.3500
N2_Af = 0.040
N2_Hf = 0
N2_Gf = 0
O2_Tc = 154.580
O2_Pc = 5.04300E+06
O2_Vc = 0.0733700/1000
O2_Nb = 90.1700
O2_Af = 0.0220000
O2_Hf = 0
O2_Gf = 0
```

```
Pc=[CO_Pc; H2_Pc; W_Pc; N2_Pc; P_Pc; O_Pc]
Af=[CO_Af; H2_Af; W_Af; N2_Af; P_Af; O_Af]
Vm=[CO_Vc; H2_Vc; W_Vc; N2_Vc; P_Vc; O_Vc]
Hf=[CO_Hf; H2_Hf; W_Hf; CO2_Hf; N2_Hf; O2_Hf; P_Hf; O_Hf]
Gf=[CO_Gf; H2_Gf; W_Gf; CO2_Gf; N2_Gf; O2_Gf; P_Gf; O_Gf]
Nb = [CO_Nb; H2_Nb; W_Nb; CO2_Nb; N2_Nb; O2_Nb; P_Nb; O_Nb]
clear(['CO_Tc','H2_Tc','H2O_Tc','CO2_Tc','N2_Tc','O2_Tc','P_Tc','O_Tc'])
clear(['CO_Pc','H2_Pc','H2O_Pc','CO2_Pc','N2_Pc','O2_Pc','P_Pc','O_Pc'])
clear(['CO_Vc','H2_Vc','H2O_Vc','CO2_Vc','N2_Vc','O2_Vc','P_Vc','O_Vc'])
clear(['CO_Nb','H2_Nb','H2O_Nb','CO2_Nb','N2_Nb','O2_Nb','P_Nb','O_Nb'])
clear(['CO_Af','H2_Af','H2O_Af','CO2_Af','N2_Af','O2_Af','P_Af','O_Af'])
clear(['CO_Hf','H2_Hf','H2O_Hf','CO2_Hf','N2_Hf','O2_Hf','P_Hf','O_Hf'])
clear(['CO_Gf','H2_Gf','H2O_Gf','CO2_Gf','N2_Gf','O2_Gf','P_Gf','O_Gf'])
sqrt2 = sqrt(2)
kappa = 0.37464 + 1.54226*Af(ltXdex2) - 0.26992*Af(ltXdex2).^2
RTc = Rg*Tc
b = 0.07780*RTc./Pc
viPO1 = zeros(Hf)
viPO1(find(nms=='CH4')) = -1
viPO1(find(nms=='O2')) = -2
viPO1(find(nms=='H2O')) = 2
viPO1(find(nms=='CO2')) = 1
dHRxnPO1 = heatOfReaction(viPO1)
viPO2 = zeros(Hf)
viPO2(find(nms=='CH4')) = -1
viPO2(find(nms=='H2O')) = -1
viPO2(find(nms=='CO')) = 1
viPO2(find(nms=='H2')) = 3
dHRxnPO2 = heatOfReaction(viPO2)
viPO3 = zeros(Hf)
viPO3(find(nms=='CH4')) = -1
viPO3(find(nms=='CO2')) = -1
viPO3(find(nms=='CO')) = 2
viPO3(find(nms=='H2')) = 2
dHRxnPO3 = heatOfReaction(viPO3)
viSMR1 = zeros(Hf)
viSMR1(find(nms=='CH4')) = -1
viSMR1(find(nms=='H2O')) = -1
viSMR1(find(nms=='CO')) = 1
viSMR1(find(nms=='H2')) = 3
dHRxnSMR1 = heatOfReaction(viSMR1)
viSMR2 = zeros(Hf)
viSMR2(find(nms=='CO')) = -1;
viSMR2(find(nms=='H2O')) = -1
viSMR2(find(nms=='CO2')) = 1
viSMR2(find(nms=='H2')) = 1
dHRxnSMR2 = heatOfReaction(viSMR2)
viSMR3 = zeros(Hf)
viSMR3(find(nms=='CH4')) = -1
viSMR3(find(nms=='H2O')) = -2
```

```
viSMR3(find(nms=='H2')) = 4
dHRxnSMR3 = heatOfReaction(viSMR3)
k1 = 1
k2 = k1/70
k3 = k1*2.42e02
k4 = k1*2.18e03
k5 = k1*1.56e03*22
k6f = k1*4
k6r = k1*6.7e-07
k7 = k1*9.71e01
kCH2V = 3
kA= 1.17E4
kB1= 1.56E2
kB2 = 55.4
kC= 1
K1=kB1+kB2+2*kC
K2=kA+kB1+kB2+kC
etaLF=[-1   0   0   0;
        0  -1   0   0;
        1   0   0   0;
        0   0   0   0;
        0   0   0   1]
TFTS = 230+273.15
THYD = 350+273.15
PATR = 10E5
PFTS = 40E5
PHYD = 35 * 1E5
McatPOLAST = 100
McatPOSTEPS = 1000
McatPORANGE = linspace(0,McatPOLAST,McatPOSTEPS)
McatSMRLAST = 1*0.8
McatSMRSTEPS = 1000
McatSMRRANGE = linspace(0,McatSMRLAST,McatSMRSTEPS)
McatFTSLAST = 95
McatFTSSTEPS = 20
McatFTSRANGE = linspace(0.1,McatFTSLAST,McatFTSSTEPS)
McatHYDLAST = 0.00045*9.63
McatHYDSTEPS = 50
McatHYDRANGE = linspace(0,McatHYDLAST,McatHYDSTEPS)
internalRecycle = %f
externalRecycle = %f
hydrocrackerRecycle = %t
tolERC=1E-3
tolkiloop=1E-6
tolIRC=1E-3
tolWHCRC=1E-3
iRyMaxERC=1000
iRyMaxIRC=2000
iRyMaxWHCRC=3000
jKiloopMax = 100
```

```
PURFTS = 0.02
PURHYD = 0.05
POalfa = 0.6
POgama = 0
H2COTarget = 2.15
nFS=2*(N-1)+7
mSS=N+3
alpha1Range = [2:15]
alpha2Range = [80:120]
FTSRClightsRange = [1:find(nms2=='C4H10'),...
                    ...find(nms2=='C2H4'):find(nms2=='C4H8')]
H2HYD = 10
CNpX = 21
diesel=[10:20]
dieselC1= diesel(1)
dieselCN = diesel($)
dieselPDex = [find(nms2==msprintf('C%iH%i',dieselC1,2*dieselC1+2)):...
              ...find(nms2==msprintf('C%iH%i',dieselCN,2*dieselCN+2))]'
dieselODex = [find(nms2==msprintf('C%iH%i',dieselC1,2*dieselC1)):...
              ...find(nms2==msprintf('C%iH%i',dieselCN,2*dieselCN))]'
finalProducts = [1:dieselC1-1,diesel]'
clear(['dieselC1','dieselCN'])
liquidsPDex = [find(nms2=='C5H12'):pXdex2($)]'
liquidsODex = [find(nms2=='C5H10'):oXdex2($)]'
FeedstockFlow = 10
pcntAir=0
T0 = 400+273.15
P0 = 25 * 1E5
XFeedstock = [0;0;0;0;0;0;0.864;0.0647;0.0287;0.0154;
              0.0072;0.0031;0.0015;zeros(14:nFS)']
XFeedstock = XFeedstock ./ sum(XFeedstock)
F0 = XFeedstock*FeedstockFlow
FlowsToCarbonFlow = [1,0,0,1,0,0,nv',nvPO']
FlowsToCarbonFlow1 = FlowsToCarbonFlow(ConvertDex2)
FProcessCarbon0 = FlowsToCarbonFlow*F0
function [FSteamAir,FCleaning,FAqueous,FPURFTS,FTailGas,...
          ...FTLiquids,FAllXceptWax,FHYDIN,FPURHYD,FPRODUCTS] = plant(F0,T0
              ↪ ,P0)
    if internalRecycle & externalRecycle then
        FoldEXT=F0
        FnewEXT=FoldEXT*2
        FREXT=csvRead('externalRecycle.csv')
        for iRyEXT=1:iRyMaxERC
            if prntOveride|prnt then
                printf('\nEXTERNAL RECYCLE Flow convergence test:"+...
                       ..." %f',abs(sum(FoldEXT-FnewEXT)))
            end
            if abs(sum(FoldEXT-FnewEXT))<tolERC then
                if prntOveride|prnt then
                  printf('\nEXTERNAL RECYCLE Elemental balance convergence
                      ↪ test')
                end
```

```
301     ...F+FPURFTS+FAllXceptWax+FCleaning+FTailGas+FAqueous,Mr,...
302     ...'External Recycle',prntOveride)
303                     if abs(Mbal)<tolERC & abs(Cbal)<tolERC &...
304     ... abs(Hbal)<tolERC then
305                     if prntOveride|prnt then
306      printf('\nEXTERNAL RECYCLE loop converged in %i iterations',iRyEXT)
307         end
308                     csvWrite(FREXT,'externalRecycle.csv')
309                     csvWrite(FREXT,DIR+'/'+RUNFILENAME+'-streams/'+...
310         ...'externalRecycle.csv')
311                     F = [F(1:3);F(5);F(7:$)]
312                     break
313                 end
314             end
315             FoldEXT = FnewEXT
316             F0_FREXT = F0+FREXT
317             [F,T,P,FSteamAir,FCleaning,FAqueous,FREXT,FPURFTS,FTailGas,
                    ↪ FTLiquids,...
318     ...FAllXceptWax]= plant_ATR_FTS(F0_FREXT,T0,P0)
319             FREXT = [FREXT(1:3);0;FREXT(4);0;FREXT(5:2*N+3)]
320             F = [F(1:3);0;F(4);0;F(5:2*N+3)]
321             FPURFTS = [FPURFTS(1:3);0;FPURFTS(4);0;FPURFTS(5:2*N+3)]
322             FAllXceptWax = [FAllXceptWax(1:3);0;FAllXceptWax(4);0;
                    ↪ FAllXceptWax(5:2*N+3)]
323             FTailGas = [FTailGas(1:3);0;FTailGas(4);0;FTailGas(5:2*N+3)]
324             FTLiquids = [FTLiquids(1:3);0;FTLiquids(4);0;FTLiquids(5:2*N+3)
                    ↪ ]
325             FAqueous = [FAqueous(1:3);0;FAqueous(4);0;FAqueous(5:2*N+3)]
326             FnewEXT = F0+FREXT
327             csvWrite(FREXT,'externalRecycle.csv')
328             if iRyEXT==iRyMaxERC then
329                 printf('\n\nExternal Recycle loop did not converge after %i
                        ↪ iterations',iRyEXT)
330             end
331         end
332      else
333         FREXT=zeros(nms2)
334         FTailGas=zeros(nms2)
335         [F,T,P,FSteamAir,FCleaning,FAqueous,FREXT,FPURFTS,FTailGas,...
336   ...FTLiquids,FAllXceptWax] = plant_ATR_FTS(F0,T0,P0)
337         FPURFTS = [FPURFTS(1:3);0;FPURFTS(4);0;FPURFTS(5:2*N+3)]
338         FAllXceptWax = [FAllXceptWax(1:3);0;FAllXceptWax(4);0;FAllXceptWax
                ↪ (5:2*N+3)]
339         FTailGas = [FTailGas(1:3);0;FTailGas(4);0;FTailGas(5:2*N+3)]
340         FTLiquids = [FTLiquids(1:3);0;FTLiquids(4);0;FTLiquids(5:2*N+3)]
341         FAqueous = [FAqueous(1:3);0;FAqueous(4);0;FAqueous(5:2*N+3)]
342      end
343      csvWrite(F,'syncrude.csv')
344      csvWrite(F,DIR+'/'+RUNFILENAME+'-streams/'+'syncrude.csv')
345      [FPRODUCTS,FPURHYD,FHYDIN] = plant_WHC(F,T,P)
346      FPRODUCTS = [FPRODUCTS(1:3);0;FPRODUCTS(4);0;FPRODUCTS(5:2*N+3)]
347      FPURHYD = [FPURHYD(1:3);0;FPURHYD(4);0;FPURHYD(5:2*N+3)]
348      FHYDIN = [FHYDIN(1:3);0;FHYDIN(4);0;FHYDIN(5:2*N+3)]
349  endfunction
350  function [Ki,psi,yikiloop,xikiloop] = Kiloop(psikiloop,T0kiloop,P0kiloop
        ↪ ,...
```

```
351     if usecorr then
352         Ki = KiCorrelation(T0kiloop,P0kiloop,%f,Fkiloop(4)./sum(Fkiloop),
                ↪ nvPO)
353     end
354     Kiold = 1
355     for jKiloop = 1:jKiloopMax
356         B = 0
357         C = 0.999
358         R = psikiloop
359         RE = 1e-6
360         AE = 1e-6
361         IFLAG = 0
362         psi0 = flashRR(0)
363         psi1 = flashRR(0.999999)
364         if (psi1<=0) then
365             psikiloop = 1
366         elseif (psi0>=0) then
367             psikiloop = 0
368         else
369             [psikiloop, iter, iflag] = FZERO(flashRR, B, C, R, RE, AE,
                    ↪ IFLAG)
370             if psikiloop>1 then
371                 psikiloop=fsolve(0.99999,flashRR)
372             end
373         end
374         xikiloop = zi ./(1+psikiloop .*(Ki-1)+%eps)
375         yikiloop = Ki .*xikiloop
376         xikiloop = xikiloop/sum(xikiloop)
377         yikiloop = yikiloop/sum(yikiloop)
378         [fpv,fpl,Ki] = PR_EOS(yikiloop,xikiloop,P0,T0,%t,%t)
379         ferr = sum(((Kiold-Ki)./(Kiold+1E-15)) .^(2))
380         if (ferr<=tolkiloop) then
381             break
382         else
383             Kiold = Ki
384         end
385     end
386 endfunction
387 function [y0cat,Ki,psi,Finit] = FTinit(F0init,Tinit,Pinit)
388     McatFTS=0
389     Finit = feed( sum(F0init), 0.94 , N , F0init(4)./sum(F0init), F0init
            ↪ (2)./F0init(1) ,...
390     ... F0init(1) , F0init(3) , 0.5 )
391     zi = Finit ./ sum(Finit)
392     psi=0.5
393     [Ki,psi,yiinit,xiinit] = Kiloop(psi,Tinit,Pinit,Finit,%t)
394     thetaiinit = ones(N+2,1).*0.0005469999999999999602
395     thetaiinit($+1) = 0.5
396     y0init = [yiinit;xiinit;0.5*sum(Finit);0.5*sum(Finit);thetaiinit]
397     [y0cat,v0cat,info0cat]=fsolve(y0init,list(SScstr,Finit))
398     y0cat=abs(y0cat)
399     if prnt then, printf('\nFsolve FTS with no catalyst INFO=====>%i',
            ↪ info0cat), end
400 endfunction
```

```
401     ...FAllXceptWax] = plant_ATR_FTS(F0,T0,P0)
402     if prnt then, printf('\nPartial oxidation'), end
403     P0 = PATR
404     T0PO = T0
405     Fcarbon0 = F0(7)
406     FMethane0 = F0(7)
407     FSteamAir = zeros(F0)
408     FSteamAir(3) = POgama*Fcarbon0
409     FSteamAir(6) = POalfa*Fcarbon0
410     FSteamAir(5) = pcntAir*0.79*(FSteamAir(6)./0.21)
411     F0 = F0 + FSteamAir
412     fpo = ode([F0;T0;P0],0,McatPORANGE,PO_ODE)
413     P = fpo($,$)
414     T = fpo($-1,$)
415     F = clean(fpo(1:$-2,$))
416     checks(F0,F,Mr,'PO',%f)
417     ebal(F0,F,T0,T)
418     TPO = T
419     H2COPO = F(2)./F(1)
420     XMPO = (F0(7)-F(7))./F0(7)
421     if prnt then, printf('\nTemperature into partial oxidation is %.2f K [
            ↪ %.2f C ]',...
422     ...T0,T0-273.15), end
423     if prnt then, printf('\nTemperature out of partial oxidation is %.2f K
            ↪ [ %.2f C ]',...
424     ...TPO,TPO-273.15), end
425     if prnt then, printf('\nMethane conversion in partial oxidation is %.2f
            ↪ ',XMPO), end
426     if prnt then, printf('\nH2:CO ratio out of PO is %.2f',H2COPO), end
427     if prnt then, printf('\nOxygen required in ATR = %f',F(6)), end
428     if prnt then, printf('\nSteam required in ATR = %f',F(3)), end
429     if prnt then, printf('\n\nSteam reforming'), end
430     T0=T
431     P0=P
432     F0=F
433     fsmr = ode([F0;T0;P0],0,McatSMRRANGE,SMR)
434     P = fsmr($,$)
435     T = fsmr($-1,$)
436     F = clean(fsmr(1:$-2,$))
437     checks(F0,F,Mr,'SMR',%f)
438     ebal(F0,F,T0,T)
439     TSMR = T
440     H2COATR = F(2)./F(1)
441     XMSMR = (F0(7)-F(7))./F0(7)
442     XMATR = (FMethane0-F(7))./FMethane0
443     extraHYD = F(2)-H2COTarget*F(1)
444     if prnt then, printf('\nTemperature out of partial oxidation is %.2f K
            ↪ [ %.2f C ]',...
445     ...TSMR,TSMR-273.15), end
446     if prnt then, printf('\nMethane conversion in steam reformer is %.2f',
            ↪ XMSMR), end
447     if prnt then, printf('\nTotal methane conversion in reformer is %.4f',
            ↪ XMATR), end
448     if prnt then, printf('\nH2:CO ratio out of SMR is %.2f',H2COATR), end
449     if prnt then, printf('\nNitrogen fraction in syngas is %.4f',F(5)./sum(
            ↪ F)), end
450     if prnt then, printf('\nExtra H2 available is %.4f',extraHYD), end
```

```
451     if extraHYD>0 then
452     if prnt then, printf('\nExtra H2 removed from Syngas'), end
453     FCleaning(2) = extraHYD
454     end
455     if prnt then, printf('\nCO2 removed from Syngas is %f',F0(4)), end
456     FCleaning(4) = F(4)
457     if prnt then, printf('\nWater removed from Syngas is %f',F0(3)), end
458     FCleaning(3) = F(3)
459     if prnt then, printf('\nN2 removed from Syngas is %f',F0(5)), end
460     FCleaning(5) = F(5)
461     if prnt then, printf('\nO2 removed from Syngas is %f',F0(6)), end
462     FCleaning(6) = F(6)
463     F = F - FCleaning
464     csvWrite(F,'FTS-X-alpha-syngas.csv')
465     csvWrite(F,DIR+'/'+RUNFILENAME+'-streams/'+'FTS-X-alpha-syngas.csv')
466     if prnt then, printf('\n\nFischer-Tropsch Synthesis'), end
467     T0=TFTS
468     P0=PFTS
469     F0=F
470     if prnt then, printf('\nEnergy to bring feed to FTS temperature'), end
471     ebal(F0,F0,T0,TFTS)
472     F0 = F0(ConvertDex2)
473     FCOFT0 = F0(1)
474     nFS=2*(N-1)+5
475     fipureFTS = Pure_preos(TFTS)
476     Tr = T0./Tc
477     alf0(2) = (Tr(2)^-0.792615)*exp(0.40129*(1-Tr(2)^-0.992615))
478     alf1(2) = (Tr(2)^-1.98471)*exp(0.024955*(1-Tr(2)^-9.98471))
479     alf0(5) = (Tr(5)^-0.792615)*exp(0.40129*(1-Tr(5)^-0.992615))
480     alf1(5) = (Tr(5)^-1.98471)*exp(0.024955*(1-Tr(5)^-9.98471))
481     alf0(6:N+4) = (Tr(6:N+4).^-0.17183).*exp(0.125283*(1-Tr(6:N+4)
            ↪ .^1.77634))
482     alf1(6:N+4) = (Tr(6:N+4).^-0.607352).*exp(0.511614*(1-Tr(6:N+4)
            ↪ .^2.20517))
483     alf0(N+5:2*N+3) = (Tr(N+5:2*N+3).^-0.17183).*exp(0.125283*(1-Tr(N+5:2*N
            ↪ +3).^1.77634))
484     alf1(N+5:2*N+3) = (Tr(N+5:2*N+3).^-0.607352).*exp(0.511614*(1-Tr(N+5:2*
            ↪ N+3).^2.20517))
485     alf = alf0 + Af.*(alf1 - alf0)
486     alfLights = (1 + kappa.*(1 - sqrt(Tr(1:4)))).^2
487     alf(1:4) = alfLights(1:4)
488     RT = Rg*T0
489     RT2 = RT^2
490     a = ((0.45724*(RTc).^2)./Pc).*alf
491     aij = sqrt(a*a')
492     PoRT2 = P0./(RT2)
493     PoRT = P0./(RT)
494     B = b*PoRT
495     if internalRecycle then
496         Fold=F0
497         Fnew=Fold*2
498         FRINT=csvRead('internalRecycle.csv')
499         for iRy=1:iRyMaxIRC
500             if prntOveride|prnt then
```

```
501       end
502               if abs(sum(Fold-Fnew))<tolIRC then
503                   if prntOveride|prnt then
504           printf('\nINTERNAL Elemental balance convergence test')
505       end
506                   [Mbal,Cbal,Hbal]=checks2(F0,F+FAqueous+FPURFTS+FREXT+
                          ↪ FTailGas,Mr2,prntOveride)
507                   if abs(Mbal)<tolIRC & abs(Cbal)<tolIRC & abs(Hbal)<tolIRC
                          ↪ then
508                       if prntOveride|prnt then
509        printf('\nINTERNAL Recycle loop converged in %i iterations',iRy)
510           end
511                       csvWrite(FRINT,'internalRecycle.csv')
512                       csvWrite(FRINT,DIR+'/'+RUNFILENAME+'-streams/'+'
                              ↪ internalRecycle.csv')
513                       XCOFTS = (F0_FR(1)-F(1))./F0_FR(1)
514                       break
515                   end
516               end
517               Fold=Fnew
518               F0_FR = F0+FRINT
519               if prnt then
520         printf('\nEffective H2:CO ratio into FTS is %.2f',F0_FR(2)./F0_FR(1))
521         end
522               [y0cat,Ki,psi,F] = FTinit(F0_FR,T0,P0)
523               zi = F0_FR./sum(F0_FR)
524               yg = y0cat
525               newX = 0
526               for iMcat=length(McatFTSRANGE)
527                   McatFTS=McatFTSRANGE(iMcat)
528                   [y,v,info]=fsolve(yg,list(SScstr,F0_FR))
529                   if prnt then
530        printf('\nFsolve FTS with catalyst INFO=========>%i for iMcat=%i',info,
             ↪ iMcat)
531       end
532                   y=sqrt(y.^2)
533                   ySi=y(1:nFS)
534                   xSi=y(nFS+1:2*nFS)
535                   VS=y(2*nFS+1)
536                   LS=y(2*nFS+2)
537                   thetaSi=y((2*nFS+3):(2*nFS+2+mSS)-1)
538                   F = ySi.*VS + xSi.*LS
539                   FTLiquids = F
540                   lastX = newX
541                   newX = (F0_FR(1)-F(1))./F0_FR(1)
542                   if prnt then
543         printf(' Carbon monoxide conversion per pass in FTS is %.2f%%', 100*
                ↪ newX)
544       end
545               end
546               FAqueous = zeros(F)
547               FAqueous(3) = F(3)
548               F = F - FAqueous
549               FRINT = zeros(F)
550               FRINT(FTSRClightsRange) = F(FTSRClightsRange)
```

```
551             FPURFTS = FRINT*PURFTS
552             FRINT = FRINT-FPURFTS
553             if externalRecycle then
554                 FREXT = RCEXTFTS*FRINT
555                 FRINT = FRINT - FREXT
556                 FTailGas = zeros(FREXT)
557                 FTailGas([find(nms2=='CO'),find(nms2=='H2'),find(nms2=='
                        ↪ C2H6'):...
558 ...find(nms2=='C4H10'),find(nms2=='C2H4'):find(nms2=='C4H8')]') =...
559                 FREXT([find(nms2=='CO'),find(nms2=='H2'),find(nms2=='C2H6')
                        ↪ :...
560 ...find(nms2=='C4H10'),find(nms2=='C2H4'):find(nms2=='C4H8')]')
561                 FREXT = FREXT - FTailGas
562             end
563             Fnew = F
564             if iRy==iRyMaxIRC then
565                 printf('\nINTERNAL Recycle loop did not converge after %i
                        ↪ iterations',iRy)
566             end
567         end
568     else
569         FREXT = zeros(F0)
570         FPURFTS = zeros(F0)
571         FTailGas = zeros(F0)
572         [y0cat,Ki,psi,F] = FTinit(F0,T0,P0)
573         zi = F0./sum(F0)
574         yg=y0cat
575         lastSolveYg = yg
576         for iMcat=1:length(McatFTSRANGE)
577             McatFTS=McatFTSRANGE(iMcat)
578             [y,v,info]=fsolve(yg,list(SScstr,F0))
579             y=sqrt(y.^2)
580             if prnt then
581 printf('\nFsolve FTS with catalyst INFO=========>%i for i=%i',info,iMcat)
582     end
583             if info==1 then
584                 lastSolveYg = yg
585                 yg = y
586             else
587                 yg = lastSolveYg
588             end
589             ySi=y(1:nFS)
590             xSi=y(nFS+1:2*nFS)
591             VS=y(2*nFS+1)
592             LS=y(2*nFS+2)
593             thetaSi=y((2*nFS+3):(2*nFS+2+mSS)-1)
594             F = ySi.*VS + xSi.*LS
595             FTLiquids = F
596             [Mbal,Cbal,Hbal] = checks2(F0,F,Mr2,%f)
597             if iMcat>2 then
598                 zi = F./sum(F)
599                 psi = VS / (VS+LS)
600                 [Ki,psi,tmp,tmp] = Kiloop(psi,T0,P0,F0,%f)
```

```
601           end
602           XCOFTS = (F0(1)-F(1))./F0(1)
603           FAqueous = zeros(F)
604           FAqueous(3) = F(3)
605           F = F - FAqueous
606       end
607       WP = F(pXdex2).*Mr2(pXdex2)
608       WO = F(oXdex2).*Mr2(oXdex2)
609       WM = F(5,:).*Mr2(7)
610       wf= [WM;(WP+WO)]+%eps
611       lwf = log(wf./nv)
612       scf(0);clf
613       plot(nv,lwf)
614       A = [nv(alpha1Range) ones(nv(alpha1Range))]
615       b = lwf(alpha1Range)
616       alpha1=A\b
617       alpha1=exp(alpha1(1))
618       A = [nv(alpha2Range) ones(nv(alpha2Range))]
619       b = lwf(alpha2Range)
620       alpha2=A\b
621       alpha2 = exp(alpha2(1))
622       FAllXceptWax = zeros(F)
623       FAllXceptWax([...
624       1:find(nms2=='C20H42'),...
625       find(nms2=='C2H4'):find(nms2=='C20H40')]) = F([...
626       1:find(nms2=='C20H42'),...
627       find(nms2=='C2H4'):find(nms2=='C20H40')])
628       F = F - FAllXceptWax
629       if prnt then
630    printf('Carbon monoxide conversion in FTS is %f\n', XCOFTS)
631       end
632       if prnt then
633    printf('\nAlpha C%i-C%i = %.2f',alpha1Range(1),alpha1Range($),alpha1)
634       end
635       if prnt then
636    printf('\nAlpha C%i-C%i = %.2f',alpha2Range(1),alpha2Range($),alpha2)
637     end
638  endfunction
639  function [FPRODUCTS,FPURHYD,FHYDIN] = plant_WHC(F0,T0,P0)
640       if prnt then, printf('\n\nHydrocracker'), end
641       T0 = THYD; T = THYD
642       P0 = PHYD; P = PHYD
643       fipureHYD = Pure_preos(THYD)
644       FHYDIN = zeros(F0)
645       FHYDIN(2) = H2HYD*sum(F0(pIdex2(1):$)) - F0(2)
646       F0(2)= FHYDIN(2)
647       if prnt then
648    printf('\nHydrogen required for WHC feed = %f',FHYDIN(2))
649       end
650       [F0,PreHYDH2] = preHydrocracker(F0)
```

```
651   printf('\nHydrogen required for preWHC = %f',PreHYDH2)
652      end
653      if F0(2)<=0 then
654   error('No hydrogen left after pre hydrocracking')
655      end
656      FT0 = sum(F0)
657      zi=F0./FT0
658      Ki = KiCorrelation(T0,P0,%f,%f,nvPO)
659      psi1 = 0.9
660      [psi2,v,info] = fsolve(psi1,flashRR)
661      V2 = psi2*sum(F0)
662      L2 = sum(F0)-V2
663      xi2 = zi ./ (1+psi2*(Ki-1))
664      yi2 = (Ki.*zi) ./ (1+psi2*(Ki-1))
665      global psi Kiold
666      Kiold = Ki
667      psi = psi2
668      FC0 = nv'*F0(pIdex2)
669      FC0 = FC0 + nvPO'*F0(oXdex2)
670      FCD0 = nv(diesel)'*F0(dieselPDex)
671      FCD0 = FCD0 + nv(diesel)'*F0(dieselODex)
672      Dfrac0 = FCD0./FC0
673      FCNp00 = nv(CNpX:N)'*F0(pIdex2(CNpX:N))
674      FCNp00 = FCNp00 + nv(CNpX:N)'*F0(oXdex2(CNpX-1:N-1))
675      FCpotnD0 = nv(diesel($)+1:N)'*F0(diesel($)+5:pXdex2($))
676      FCpotnD0 = FCpotnD0 + nv(diesel($)+1:N)'*F0(N+diesel($)+4:oXdex2($))
677      Tr = T0./Tc
678      alf0(2) = (Tr(2)^-0.792615)*exp(0.40129*(1-Tr(2)^-0.992615))
679      alf1(2) = (Tr(2)^-1.98471)*exp(0.024955*(1-Tr(2)^-9.98471))
680      alf0(5) = (Tr(5)^-0.792615)*exp(0.40129*(1-Tr(5)^-0.992615))
681      alf1(5) = (Tr(5)^-1.98471)*exp(0.024955*(1-Tr(5)^-9.98471))
682      alf0(6:N+4) = (Tr(6:N+4).^-0.17183).*exp(0.125283*(1-Tr(6:N+4)
           ↪ .^1.77634))
683      alf1(6:N+4) = (Tr(6:N+4).^-0.607352).*exp(0.511614*(1-Tr(6:N+4)
           ↪ .^2.20517))
684      alf0(N+5:2*N+3) = (Tr(N+5:2*N+3).^-0.17183).*exp(0.125283*(1-Tr(N+5:2*N
           ↪ +3).^1.77634))
685      alf1(N+5:2*N+3) = (Tr(N+5:2*N+3).^-0.607352).*exp(0.511614*(1-Tr(N+5:2*
           ↪ N+3).^2.20517))
686      alf = alf0 + Af.*(alf1 - alf0)
687      alfLights = (1 + kappa.*(1 - sqrt(Tr(1:4)))).^2
688      alf(1:4) = alfLights(1:4)
689      RT = Rg*T0
690      RT2 = RT^2
691      a = ((0.45724*(RTc).^2)./Pc).*alf
692      aij = sqrt(a*a')
693      PoRT2 = P0./(RT2)
694      PoRT = P0./(RT)
695      B = b*PoRT
696      Rinit = zeros(2*N+3,1)
697      if hydrocrackerRecycle then
698          Fold=F0
699          Fnew=Fold*2
700          FRHYD=csvRead('hydrocrackerRecycle.csv')
```

```
701 if prnt then, printf('\nIteration %i for WHC-RC',iRy), end
702 if prntOveride|prnt then, printf('\nFlow convergence test: %f',abs(sum(Fold
    ↪ -Fnew))), end
703 if abs(sum(Fold-Fnew))<tolWHCRC then
704 if prntOveride|prnt then, printf('\nElemental balance convergence test'),
    ↪ end
705 [Mbal,Cbal,Hbal]=checks2(F0,FPHYD+FPURHYD,Mr2,prntOveride)
706 if abs(Mbal)<tolWHCRC & abs(Cbal)<tolWHCRC & abs(Hbal)<tolWHCRC then
707     if prntOveride|prnt then
708  printf('\nHydrocracker Recycle loop converged in %i iterations',iRy)
709     end
710     csvWrite(FRHYD,'hydrocrackerRecycle.csv')
711     csvWrite(FRHYD,DIR+'/'+RUNFILENAME+'-streams/'+'hydrocrackerRecycle.csv
        ↪ ')
712     FTPROD = FPHYD+FPURHYD
713     FC = nv'*FTPROD(pIdex2)
714     FC = FC + nvPO'*FTPROD(oXdex2)
715     FCD = nv(diesel)'*FPHYD(dieselPDex)
716     FCD = FCD + nv(diesel)'*FPHYD(dieselODex)
717     FCL = FlowsToCarbonFlow1(liquidsPDex)*FPHYD(liquidsPDex)
718     FCL = FCL + FlowsToCarbonFlow1(liquidsODex)*FPHYD(liquidsODex)
719     Dfrac = FCD./FC
720     if prnt then, printf('\nDiesel Fraction in over feed is %f',Dfrac0),
        ↪ end
721     if prnt then, printf('\nDiesel Fraction in over all product is %f',
        ↪ Dfrac($)), end
722     FCNp = nv(CNpX:N)'*FHYDMAT(pIdex2(CNpX:N),:)
723     FCNp = FCNp + nv(CNpX:N)'*FHYDMAT(oXdex2(CNpX-1:N-1),:)
724     XCNp = (FCNp0-FCNp)./(FCNp0)
725     if prnt then, printf('\nC%i+ conversion per pass is %.2f%%',CNpX,XCNp($
        ↪ )*100), end
726     YieldD = (FCD - FCD0) ./ FCpotnD0
727     if prnt then, printf('\nDiesel yield to product is %.2f%%',YieldD*100),
        ↪  end
728     nDiesel = (FCD+diesel*(FAllXceptWax(dieselPDex)+FAllXceptWax(dieselODex
        ↪ )+...
729     ....FPURHYD(dieselPDex)+FPURHYD(dieselODex))) ./ FProcessCarbon0
730     if prnt then
731  printf('\nPlantwide carbon efficiency to diesel is %.2f%%',nDiesel*100)
732     end
733     nLiquids = (...
734     FCL+FlowsToCarbonFlow1(liquidsPDex)*(FAllXceptWax(liquidsPDex)+...
735     FAllXceptWax(liquidsODex)+...
736     FPURHYD(liquidsPDex)+...
737     FPURHYD(liquidsODex))) ./ FProcessCarbon0
738     if prnt then
739  printf('\nPlantwide carbon efficiency to liquids is %.2f%%',nLiquids*100)
740     end
741     FPRODUCTS = FPHYD
742     break
743 end
744 end
745 Fold=Fnew
746 F0_FR = F0+FRHYD
747 FCNp0 = nv(CNpX:N)'*F0_FR(pIdex2(CNpX:N))
748 FCNp0 = FCNp0 + nv(CNpX:N)'*F0_FR(oXdex2(CNpX-1:N-1))
749 FHYDMAT = ode(F0_FR,0,McatHYDRANGE,fbr)
750 F=FHYDMAT(:,$)
```

```
751             FPHYD(finalProducts+4) = F(finalProducts+4)
752             FPHYD(N+finalProducts(2:$)+3) = F(N+finalProducts(2:$)+3)
753             FRHYD = F - FPHYD
754             FPURHYD = FRHYD*PURHYD
755             FRHYD = FRHYD - FPURHYD
756             Fnew = FRHYD
757             if iRy==iRyMaxWHCRC then
758                 printf('\n\nHydrocracker recycle loop did not converge
                        ↪ after %i iterations',iRy)
759                 csvWrite(FRHYD,'hydrocrackerRecycleNoConverge.csv')
760             end
761         end
762     else
763         for iMcat=1:length(McatHYDRANGE)
764             if prnt then, printf('\niMcat = %i',iMcat), end
765             try
766                 if iMcat==1 then
767                     FHYDMAT(:,iMcat) = ode(F0,0,McatHYDRANGE(1),fbr)
768                 else
769                         [FHYD_out,w_opt_out,iw_opt_out] = ...
770     ...ode(FHYDMAT(:,iMcat-1),McatHYDRANGE(iMcat-1),McatHYDRANGE(iMcat),fbr)
771                         FHY_out(FHYD_out<1) = 0
772                         FHYDMAT(:,iMcat) = clean(FHYD_out)
773                         if w_opt_out(13)<McatHYDRANGE(iMcat) then
774                             if prnt then, printf('\n'), end
775                             if prnt then
776     printf('\nIterative solution of the Hydrocracker ODE failed before the
            ↪ last timestep. Breaking out of loop')
777         end
778                             break
779                         end
780                 end
781             catch
782                 [err_msg,err_code] = lasterror(%t)
783                 if err_msg == 'Ki imaginary' then
784                     if prnt then, printf('\n'), end
785                     if prnt then
786     printf('Liquid has run out and Ki is now imaginary. Breaking out of loop
            ↪ ')
787         end
788                     break
789                 end
790             end
791         end
792         [Mbal,Cbal,Hbal]=checks2(F0,FHYDMAT(:,$),Mr2,%f)
793         FC = nv'*FHYDMAT(pIdex2,$)
794         FC = FC + nvPO'*FHYDMAT(oXdex2,$)
795         FCD = nv(diesel)'*FHYDMAT(dieselPDex,$)
796         FCD = FCD + nv(diesel)'*FHYDMAT(dieselODex,$)
797         FCL = FlowsToCarbonFlow1(liquidsPDex)*FHYDMAT(liquidsPDex)
798         FCL = FCL + FlowsToCarbonFlow1(liquidsODex)*FHYDMAT(liquidsODex)
799         Dfrac = FCD./FC
800         if prnt then, printf('\nDiesel Fraction in feed is %f',Dfrac0), end
```

```
801         FCNp = nv(CNpX:N)'*FHYDMAT(pIdex2(CNpX:N),$)
802         FCNp = FCNp + nv(CNpX:N)'*FHYDMAT(oXdex2(CNpX-1:N-1),$)
803         XCNp = (FCNp00-FCNp)./(FCNp00)
804         if prnt then, printf('\nC%i+ conversion once through is %.2f%%',
                ↪ CNpX,XCNp*100), end
805         YieldD = (FCD - FCD0) ./ FCpotnD0
806         if prnt then, printf('\nDiesel yield to product is %.2f%%',YieldD
                ↪ *100), end
807         nDiesel = (FCD+diesel*(FAllXceptWax(dieselPDex)+FAllXceptWax(
                ↪ dieselODex)+...
808  ...FPURHYD(dieselPDex)+FPURHYD(dieselODex))) ./ FProcessCarbon0
809         if prnt then
810   printf('\nPlantwide carbon efficiency to diesel is %.2f%%',nDiesel*100)
811  end
812         nLiquids = (...
813         FCL+FlowsToCarbonFlow1(liquidsPDex)*(FAllXceptWax(liquidsPDex)+...
814         FAllXceptWax(liquidsODex)+...
815         FPURHYD(liquidsPDex)+...
816         FPURHYD(liquidsODex))) ./ FProcessCarbon0
817         if prnt then
818   printf('\nPlantwide carbon efficiency to liquids is %.2f%%',nLiquids*100)
819  end
820         FPURHYD = zeros(F0)
821         FPRODUCTS = FHYDMAT(:,$)
822     end
823     clearglobal('Kiold')
824     clearglobal('psi')
825 endfunction
826 [FSteamAir,FCleaning,FAqueous,FPURFTS,FTailGas,FTLiquids,FAllXceptWax,...
827 ...FHYDIN,FPURHYD,FPRODUCTS] = plant(F0,T0,P0)
828 tmp1 = (FPURFTS+FTailGas+FAllXceptWax+FPRODUCTS).*FlowsToCarbonFlow'
829 tmp2 = FPURHYD.*FlowsToCarbonFlow'
830 tmp3 = FCleaning(find(nms=='CO2'))
831 nC1 = tmp1(find(nms=='CH4'))./FProcessCarbon0
832 nC2_C4 = sum(tmp1(find(nms=='C2H6'):find(nms=='C4H10'))+...
833 ...tmp1(find(nms=='C2H4'):find(nms=='C4H8')))./FProcessCarbon0
834 nC5_C9 = sum(tmp1(find(nms=='C5H12'):find(nms=='C9H20'))+...
835 ...tmp1(find(nms=='C5H10'):find(nms=='C9H18')))./FProcessCarbon0
836 nWax = sum(tmp2((find(nms=='C21H44'):N+6))+...
837 ...tmp2((find(nms=='C21H42'):2*N+5)))./FProcessCarbon0
838 nCO2 = tmp3./FProcessCarbon0
839 nCO = tmp1(find(nms=='CO'))./FProcessCarbon0
840 Sliquids = (FlowsToCarbonFlow(liquidsPDex)*FTLiquids(liquidsPDex)...
841 ... + FlowsToCarbonFlow(liquidsODex)*FTLiquids(liquidsODex))./(
        ↪ FlowsToCarbonFlow*FTLiquids)
842 printf('\nFTS carbon C10+ selectivity = %.2f%%',Sliquids*100)
843 printf('\nPlantwide carbon efficiency to C1 = %.2f%%',nC1*100)
844 printf('\nPlantwide carbon efficiency to C2-C4 = %.2f%%',nC2_C4*100)
845 printf('\nPlantwide carbon efficiency to C5-C9 = %.2f%%',nC5_C9*100)
846 printf('\nPlantwide carbon efficiency to purged wax = %.2f%%',nWax*100)
847 printf('\nPlantwide carbon efficiency to CO2 = %.2f%%',nCO2*100)
848 printf('\nPlantwide carbon efficiency to unused CO = %.2f%%',nCO*100)
849 Plant_mass_in = Mr'*(F0+FSteamAir+FHYDIN)
850 Plant_mass_out = Mr'*(FCleaning+FTailGas+FPURFTS+FAllXceptWax+FAqueous+
        ↪ FPURHYD+FPRODUCTS)
```

```
851 printf('\nMass out of GTL plant = %f',Plant_mass_out)
852 printf('\nPlantwide mass balance = %f',Plant_mass_in-Plant_mass_out)
853 carbonStreams = list(FCleaning,FTailGas,FPURFTS,FAllXceptWax,FPURHYD,
    ↪ FPRODUCTS)
854 carbonStreamNames= ['Fcleaning','FTailGas','FPURFTS','FAllXceptWax','
    ↪ FPURHYD','FPRODUCTS']
855 for i=1:6
856     printf('\nCarbon out of %s = %f',carbonStreamNames(i),FlowsToCarbonFlow
        ↪ *carbonStreams(i))
857 end
858 mclose()
```

Program listing 9.13: OOT80.sce

Table 9.2: properties.xls Sheet 1

Prop	Name	Num	Den	Corr ID	No. pars	p1	p2	p3	p4	p5	p6	p7	p8	p9	p10	p11	p12	p13	p14	p15	p16	p17	p18
1	Critical temperature	K		MH1	7	Yinf	Y0	n0P	n0O	Gama	Beta	delY0											
2	Critical pressure	Pa		MH1	7	Yinf	Y0	n0P	n0O	Gama	Beta	delY0											
3	Critical volume	m3	kmol	MH2Vc	7	delYinf	Yinf0	n0P	n0O	Gama	Beta	delY0											
4	Critical compressibility factor																						
5	Normal boiling point	K		MH1	7	Yinf	Y0	n0P	n0O	Gama	Beta	delY0											
6	Melting point																						
7	Triple point temperature																						
8	Triple point pressure																						
9	Molecular weight																						
10	Liquid molar volume at normal boiling point																						
11	Acentric factor			MH1	7	Yinf	Y0	n0P	n0O	Gama	Beta	delY0											
12	Radius of gyration																						
13	Solubility parameter																						
14	Dipole moment																						
15	Van der Waals volume																						
16	Van der Waals area																						
17	IG heat of formation	kJ	mol	K1	18	p11	p12	p13	p21	p22	p23	p31	p32	p33	o11	o12	o13	o21	o22	o23	o31	o32	o33
18	IG Gibbs energy of formation	J	kmol	MH2	18	delYinf	Yinf0	n0P	n0O	Gama	Beta	delY0											
19	IG absolute entropy																						
20	Heat of fusion at melting point																						
21	Mathias-Copeman C1																						
22	Standard net heat of combustion																						
23	Solid density																						
24	Liquid density	kmol	m3	MHT	16	Ainf01	Ainf02	Ainf03	Ainf04	delAinf1	delAinf2	delAinf3	delAinf4	delA01	delA02	delA03	delA04	Beta	Gama	n0P	n0O		
25	Vapour pressure	Pa		TwuWag	8	p01	p02	p03	p04	p11	p12	p13	p14										
26	Heat of vaporization	J	mol	Vet	6	pow1	np1	np2	dpow1	wata	watb												
27	Solid heat capacity																						
28	Liquid heat capacity																						
29	Ideal gas heat capacity	J	mol K	K1	18	p11	p12	p13	p21	p22	p23	p31	p32	p33	o11	o12	o13	o21	o22	o23	o31	o32	o33
30	Second virial coefficient																						
31	Liquid viscosity																						
32	Vapour viscosity																						
33	Liquid thermal conductivity																						
34	Vapour thermal conductivity																						
35	Surface tension																						
36	Ideal gas heat capacity (RPP)																						
37	Relative static permittivity																						
38	Antoine																						
39	Liquid viscosity																						
40	COSTLD characteristic volume																						
41	Lennard Jones diameter																						
42	Lennard Jones energy																						
43	Rackett parameter																						
44	Fuller et al. diffusion volume																						
45	Mathias-Copeman C2																						
46	Parachor																						
47	Specific gravity																						
48	Charge																						
49	SRK acentric factor																						
50	Wilson volume																						
51	UNIQUAC r																						
52	UNIQUAC q																						
53	UNIQUAC q'																						
54	API-SRK s1																						
55	API-SRK s2																						
56	Mathias-Copeman C3																						
57	Chao-Seader acentric factor																						
58	Chao-Seader solubility parameter																						
59	Chao-Seader liquid volume																						
60	IG entropy of formation	J	mol K	K1	18	p11	p12	p13	p21	p22	p23	p31	p32	p33	o11	o12	o13	o21	o22	o23	o31	o32	o33

Table 9.3: properties.xls Sheet 2

Property	1	2	3	4	5	6	7	8	9	10	11	12	13	14	15	16	17	18
1	1.06e03	1.50e02	-8.49e-01	-9.06e-01	6.46e-01	1.71e-01	9.11e02											
2	0.00e00	1.72e03	2.99e00	2.49e00	2.21e-01	2.50e00	-1.72e03											
3	2.38e00	0.00e00	-5.35e01	-5.31e01	2.15e00	1.37e-04	2.19e02											
4																		
5	1.06e03	2.86e01	1.59e-01	0.00e00	7.22e-01	9.66e-02	1.03e03											
6																		
7																		
8																		
9																		
10																		
11	2.03e01	-8.63e-02	7.50e-04	0.00e00	7.79e-01	4.79e-03	2.04e01											
12																		
13																		
14																		
15																		
16																		
17	-4.05e01	-2.21e01	-2.79e01	-6.59e00	-3.64e00	9.92e-01	7.84e-01	8.01e-01	-8.36e-01	7.13e01	-2.24e01	2.05e02	-2.54e00	-3.50e00	1.40e00	1.82e-01	8.34e-01	-4.92e00
18	-8.00e06	4.00e07	1.10e01	0.00e00	0.00e00	0.00e00	0.00e00											
19																		
20																		
21																		
22																		
23																		
24	1.07e00	-1.48e-03	1.60e-05	-7.23e-10	0.00e00	0.00e00	0.00e00	0.00e00	-1.25e01	2.15e-02	-2.42e-05	1.12e-08	1.95e-01	1.03e00	1.75e-10	8.73e-10		
25	-5.96e00	1.18e00	-5.60e-01	-1.32e00	-4.79e00	4.14e-01	-8.91e00	-4.99e00										
26	3.80e-01	-5.13e-01	5.07e-01	3.80e-01	3.83e-01	2.03e-01												
27																		
28																		
29	5.05e00	2.49e01	9.64e00	1.08e01	1.63e01	-2.60e01	-2.92e00	-1.84e00	1.30e01	-8.69e00	2.51e01	1.36e01	3.66e00	1.72e01	-7.17e01	-2.48e00	-2.25e00	2.97e01
30																		
31																		
32																		
33																		
34																		
35																		
36																		
37																		
38																		
39																		
40																		
41																		
42																		
43																		
44																		
45																		
46																		
47																		
48																		
49																		
50																		
51																		
52																		
53																		
54																		
55																		
56																		
57																		
58																		
59																		
60	1.51e02	3.76e01	4.69e01	5.40e00	2.37e01	7.60e00	2.85e-01	-1.92e00	-4.06e00	1.54e02	3.66e01	-4.34e01	-1.12e01	2.39e01	4.83e01	1.93e00	-1.78e00	-1.69e01

Application for Approval of Ethics in Research (EiR) Projects
Faculty of Engineering and the Built Environment, University of Cape Town

APPLICATION FORM

Please Note:
Any person planning to undertake research in the Faculty of Engineering and the Built Environment (EBE) at the University of Cape Town is required to complete this form **before** collecting or analysing data.The objective of submitting this application *prior* to embarking on research is to ensure that the highest ethical standards in research, conducted under the auspices of the EBE Faculty, are met. Please ensure that you have read, and understood the **EBE Ethics in Research Handbook**(available from the UCT EBE, Research Ethics website) prior to completing this application form: http://www.ebe.uct.ac.za/usr/ebe/research/ethics.pdf

APPLICANT'S DETAILS		
Name of principal researcher, student or external applicant		Ashcaan Tendo Khazali
Department		Chemical Engineering
Preferred email address of applicant:		khzash001@myuct.ac.za
If a Student	Your Degree: e.g., MSc, PhD, etc.,	MSc
	Name of Supervisor (if supervised):	Professor Klaus Moller
If this is a research contract, indicate the source of funding/sponsorship		
Project Title		Optimisation of configurational alternatives of a Gas To Liquids process based on Fischer-Tropsch technology

I hereby undertake to carry out my research in such a way that:

- there is no apparent legal objection to the nature or the method of research; and
- the research will not compromise staff or students or the other responsibilities of the University;
- the stated objective will be achieved, and the findings will have a high degree of validity;
- limitations and alternative interpretations will be considered;
- the findings could be subject to peer review and publicly available; and
- I will comply with the conventions of copyright and avoid any practice that would constitute plagiarism.

SIGNED BY	Full name	Signature	Date
Principal Researcher/ Student/External applicant	Ashcaan Tendo Khazali	Signed by candidate	16/08/2017

APPLICATION APPROVED BY	Full name	Signature	Date
Supervisor (where applicable)	Klaus Moller		16/08/2017
HOD (or delegated nominee) Final authority for all applicants who have answered NO to all questions in Section1; and for all Undergraduate research (Including Honours).	J. Petersen		24-8-2017
Chair : Faculty EIR Committee For applicants other than undergraduate students who have answered YES to any of the above questions.			